Harnessing Microbially-mediated Redox Processes for Sustainable Water Treatment

Margaret L White

A thesis submitted to Newcastle University in partial fulfilment of the requirements for the degree of Doctor of Philosophy within the Faculty of Science, Agriculture and Engineering

School of Engineering

June 2025

Declaration

I hereby declare that the work presented in this thesis has not been submitted for any other degree or professional qualification, and that it is the result of my own independent work.

Margaret L White

June 2025

Acknowledgements

My supervisors – Dr Anke Neumann, Dr James Kitson and latterly but so importantly, Dr Joe Weaver, Dr Elizabeth Heidrich and Dr Jordan Cuff. Thank you all for the opportunity to complete this PhD with you and for teaching me so much. Anke and James, sorry that we had to weather the worst of Covid-19 together.

Anke – during the course of the PhD you have helped me to unearth organisational skills that I never knew I had, thank you! (although I do still need to finish reading 'Getting Things Done: The Art of Stress-free Productivity'!). Thank you also for your patience, support and time in reviewing all manner of documents and spreadsheets for me, and for appreciating my efforts at artwork. My outputs are better for it and I will take a lot away with me, thank you so much. Thank you also for making such pretty biscuits at Christmas time.

James – thank you for sharing your expertise, creativity and patience around molecular methods with me. Your high standards were always appreciated and I am very grateful.

Joe, Liz and Jordan – I am so very grateful for the time you made for me during these last 9 months – a huge thank you. I am indebted to you all, as you made the last part of this journey so much more manageable for me.

Liz – no-one can get things done like you can. Thank you for your motivational chats and good humour during my time in Environmental Engineering. I always appreciated our catch-ups and I have no doubt that you will continue to lead with positivity and strength in the future.

Joe – I have never met anyone as organised and as knowledgeable when it comes to coding and bioinformatics, as you! Thank you so much for your time, for imparting your wisdom and guiding me towards some really great coding habits and lastly, thank you for your calm and patience - it really helped.

Jordan – I always felt better after a meeting with you and remain in awe of your positivity. A massive thanks for helping to streamline my molecular work during the final stretches of my PhD. It made a big difference to me practically and psychologically. Please continue to shine bright as you lead your own research group, I know you will be awesome.

To my amazing lab mates past and present – Jim, Harry, Mat, Leaf, Sam, Hannah, Katie, Ben A, Malvika, Andy, Kyle, Tom and Ben SH. Thank you all for being great company, for laughing with me, listening to me chat and for making me feel more positive about lab work when I felt overwhelmed. Andy, I hope you continue to enjoy your writing and Malvika, I really enjoyed learning how to take better selfies! I wish you all every success in the future.

My sponsor and funders – EPSRC for funding my PhD, for allowing me a really great internship opportunity and also for awarding me an Enhancement Fund to present my research in Australia, which was an amazing experience.

I would also like to thank the Clay Minerals Society of America and for my travel awards and the Clay Minerals Group within the Mineralogical Society of the UK and Ireland. Both of these learned societies provided me with very positive conference experiences within clay science research, and with great colleagues. My particular gratitude goes to Mary Gray at the CMS for finding solutions to almost everything and for being a really generous person, and to

Mr Kevin Murphy at the Min Soc, for being a great colleague, informal mentor and for highlighting opportunities to me. Thank you both.

To my friends close to home – thank you for always caring, being great company and making me laugh so much. I couldn't have asked for a better group of people to hang out with – thank you, you good-looking bunch.

Lastly my family – Col, Isla and Nick. No words express my gratitude for your strength, support and humour over the last few years when I've needed cheering up, and for understanding when I needed to work. You were all the best motivation for me to complete this PhD – thank you. Rose, Treds, Ted, James, Mum, Dad, Marie and Steve – thank you for always being on the end of a phone for a chat and for great company when we could all get together.

Abstract

Water and wastewater treatment are essential for ensuring environmental and human health and identifying sustainable low carbon technologies for water treatment is now critical. However, the incomplete removal of organic micropollutants during conventional wastewater treatment continues to pose an emerging threat to our water resources. Encouragingly, AOPs, which rely mainly on the production of reactive oxidizing species such as OH radicals (•OH), have successfully been applied to degrade micropollutants during water treatment although currently applied AOPs are energetically expensive with high carbon footprints. Recent studies have shown that •OH can be effectively generated and degrade micropollutants during the oxygenation of natural ferrous iron-bearing clay minerals. To contribute to this research field, this PhD research provides the proof-of-concept for a sustainable clay-based advanced oxidation process (AOP) for water treatment through generation of hydroxyl radicals. Using mesocosm column experiments, this study has demonstrated that clay mineral iron can be effectively and sustainably 'activated' by microbial communities from local pond water, through microbial iron reduction, in the first essential step of this novel AOP. The introduction of oxygenated water produced hydroxyl radicals (•OH) in-situ as reduced clay mineral iron was oxidised and subsequently led to the degradation of a surrogate micropollutant, benzoic acid. Treatment efficiency and •OH production were measured during two time-series experiments and three activation-treatment cycles in microbially-activated columns. Chemical activation of the same clay mineral was tested in a separate experiment and yielded comparable results for treatment efficiency and •OH production. Analysis of 16S rRNA sequencing data indicated that although microbial community diversity narrowed and species numbers decreased over time with increasing treatment cycles, known iron-reducing microbes appeared to be resilient to •OH exposure over three treatment cycles. Implications of this research include promise for this novel clay-based AOP although the long-term impact of microbial iron reduction on clay mineral integrity requires further study.

List of Figures

List of Tables

1. Introduction

1.1 Introduction

The provision of clean water and sanitation is an increasingly pressing global challenge. In 2006 it was reported that around one-fifth of the global population did not have access to safe drinking water and two-fifths had unacceptable sanitary conditions (Schwarzenbach et al., 2006), highlighting the need for better wastewater treatment (WWT) in much of the developing world. Achieving universal access to clean water and basic sanitation is the general theme of the United Nation's Sustainable Development Goal 6 (UN SDG6). In July 2019, the UN reported progress towards achieving the six targets of the 'Global Indicator Framework' (Inter-Agency and Expert Group on SDG Indicators, 2016). It concluded that, in order to provide clean water and basic sanitation facilities for the global population by 2030, current work efforts would need to be doubled (United Nations, 2019). This will require both the widespread deployment of conventional technologies but also the development of new passive, low energy technologies to meet the polarising demands of providing water whilst attaining Net Zero.

In addition to basic water treatment needs, the number of emerging pollutants is growing exponentially worldwide (Llanos et al., 2019), outpacing all other agents of global change (Bernhardt et al., 2017). It is estimated that every year over 10 million new compounds are produced, with unknown effects to the environment. Over the last two decades, considerable attention has been given to treatment options for micropollutants, and emerging and legacy contaminants due to their harmful and unknown nature. Advanced Oxidation Processes (AOP) have been identified as being among the most effective treatment technologies available; however, they are not affordable for many low-to-middle-income nations due to the chemical and energetic inputs required. The profuse nature of micropollutants in urbanised watercourses, due to daily domestic activities, means that water quality remains an issue.

Conventional WWT plants are currently listed by the Intergovernmental Panel on Climate Change (IPCC) as being measurable emitters of greenhouse gases (GHGs) in their report 'Refinement to the 2006 IPCC Guidelines for National Greenhouse Gas Inventories' published in 2019 (Intergovernmental Panel on Climate Change, 2019). With reduction of GHG emissions considered a priority globally (Intergovernmental Panel on Climate Change, 2018),

research is urgently required into the development of low-carbon footprint and sustainable WWT systems as alternatives to current high (input) energy WWT plants if the ongoing effects of climate change are to be mitigated. Humanity requires clean water to survive and thrive, thus if the UN SDG6 is to be successfully met and the contribution that WWT makes to GHG emissions minimised, new solutions must be found for WWT by leveraging recent advances in biological and chemical research.

1.2 Project Aim

The aim of this interdisciplinary project is to provide proof of concept for a novel low energy input, self-sustaining and effective WWT system targeting oxidizable organics via an AOP. The treatment system should operate at scale and use only water flow, oxygenation saturation extent and the natural redox-activity of iron-bearing clay minerals alongside microbially-mediated Fe-reduction to catalyse hydroxyl radical (•OH) production. To address this aim, objectives were formulated within several research themes, and these are outlined below.

1.2.1 Outline of research themes and objectives

- **Theme 1:** Wastewater treatment efficiency and sustainability

Theme 1 concerns monitoring the performance of the wastewater (WW) treatment over time and over several treatment (redox) cycles at mesocosm scale, using the oxygen saturation level of the water to cycle between reducing and oxidising environments. The objectives for this theme are:

1. Design and test an appropriate treatment system with the capacity to upscale;
2. Build and test a larger system under realistic conditions;
3. Monitor the chemical and biological activity of the treatment system over time and through at least three treatment cycles;
4. Analyse the results to determine whether hydroxyl radicals generated during clay mineral iron oxygenation can efficiently remove target pollutants from a synthetic WW under flow (treatment) conditions, and to what extent;
5. Determine how many cycles can be achieved before target pollutants are no longer removed.

- **Theme 2:** Characterisation of microbial community

Theme 2 develops a deeper understanding of the microbial community and its dynamics, responsible for driving iron reduction during the treatment process. The objectives within this theme are:

1. Develop a methodology for effective microbiology sampling and monitoring of treatment mesocosms;
2. Use and develop nucleic acid extraction protocols for microbiological communities from different sample types related to the mesocosms;
3. Use high-throughput sequencing-based microbial community profiling to characterise the active microbial community within mesocosms;
4. Determine which communities are active and driving iron reduction during the treatment process;
5. Analyse microbial community structure and attempt to elucidate how the microbiology in the treatment system is changing over time with treatment cycles.

1.3 Thesis outline

Chapter 1 – provides an introduction to the research and presents the project aim and objectives.

Chapter 2 – is a critical review of literature in the subject area, which is supported by further citations and critical discussion in the subsequent chapters.

Chapter 3 – presents the final design and design tests involved in developing the mesocosm (column) experiments that were used in the biological experimental section of the research, to provide proof-of-concept for the novel Advanced Oxidation Process (AOP).

Chapter 4 – presents the results of the chemical (mesocosm) column experiments that were used to inform the research, ahead of the biological column experiments, and critically discusses this work.

Chapter 5 – presents the results of the biological (mesocosm) column experiments, designed to provide proof-of-concept for a sustainable AOP that effectively removes micropollutants from water. Chemical and microbiology data sets are presented and discussed alongside relevant literature in order to analyse how successful the proof-of-concept treatment system has been.

Chapter 6 – concludes the research, provides recommendation for further work discusses several engineering challenges of taking this research to the next level.

2. Literature Review

2.1 Introduction

The following chapter critically reviews literature relevant to this proof of concept PhD thesis and places the research in the context of other relevant works. Additional literature is discussed and referenced in the following results chapters.

2.2 Current water treatment methods and pollutants of today

Wastewater treatment (WWT) plants in developed countries involve sophisticated multi-stage treatment processes to disinfect municipal wastewater (WW) effluents (Figure 2.1). WWT plants are costly to operate both financially and energetically (Gandiglio et al., 2017), making them often unaffordable in developing countries. Through processes of primary screening, sedimentation (including sludge formation) and secondary biological aeration and sedimentation, WWT plants are designed to remove macropollutants (e.g. nitrite and ammonia (Margot et al., 2013)) and pathogens in the form of solid wastes, suspended solids and biodegradable dissolved organic matter (DOM) from wastewater effluents (Margot et al., 2015). An overview of these treatment steps is shown in Figure 2.1.

While WWT plants were designed for WW disinfection, i.e. the removal of pathogenic organisms, they also degrade a diverse range of inorganic and organic contaminants. Many of these contaminants are anthropogenic in origin and comprise synthetic compounds that are used for industrial, agricultural and domestic purposes (Schwarzenbach et al., 2006). Since World War II, the global production and use of synthetic compounds has increased from 1 to 400 million tonnes annually (Anjum et al., 2017), leading to an increased burden on WWT plants to remove these compounds alongside the intended target compounds and organisms.

WWT plants can remove greater than 70% of pollutants such as surfactants, persistent organic pollutants (POPs), volatile organic compounds (VOCs), polycyclic aromatic hydrocarbons (PAHs), a considerable number of hormone group compounds and heavy metals, certain personal care products and pharmaceuticals and some household chemicals (Figures 2.2a-b). Many of these chemical groups are partially biodegradable and can be

transformed or degraded by sewage sludge sorption, volatilisation or abiotic degradation (Margot et al., 2015).

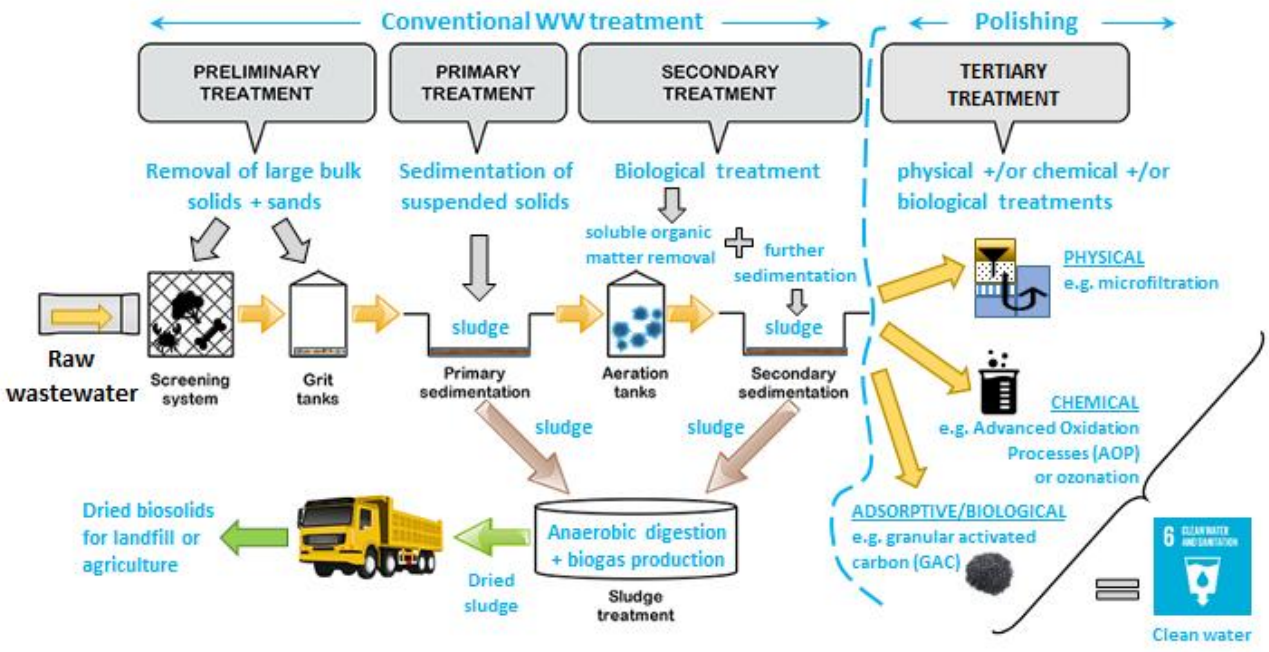

Figure 2. 1. *Schematic showing conventional primary, secondary and tertiary (polishing) processes in conventional WWT plants, from wastewater influent to treatment of dried sludge and clean water effluent. Adapted from Gandiglio et al (2017).*

The most recalcitrant of these chemical groups are termed micropollutants (Stamm et al., 2016) as they are either not removed at all during primary, secondary and (some) tertiary WWT processes or are only partially removed. Examples of micropollutant groups include large numbers of pharmaceutical compounds and certain illicit drugs (Figure 2.2a), certain heavy metals, large numbers of pesticides, e.g. DDT (Schwarzenbach et al., 2006) and many household chemicals (Figure 2.2b), (Schwarzenbach et al., 2006; Margot et al., 2015). These persistent chemicals can remain in WWT plant effluents in detectable quantities up to ~100000 ng/l (Figure 2.2b), sometimes with no clear treatment route. In fact, effluents from WWT plants have been identified as major point sources of micropollutants (Lee & von Gunten, 2010).

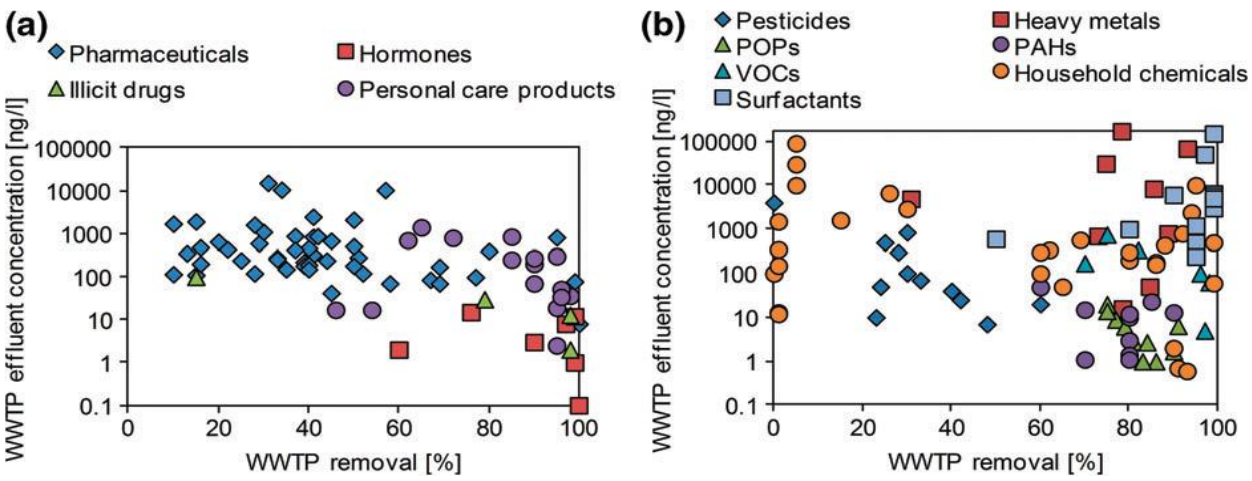

Figure 2. 2. *Annotated plots showing range of removal extents for two groups of common MPs, including* ***(a)*** *pharmaceuticals, hormones, illicit drugs, personal care products and* ***(b)*** *pesticides, heavy metals, persistent organic pollutants (POPs), polycyclic aromatic hydrocarbons (PAHs), volatile organic compounds (VOCs), household chemicals and surfactants, from WWT plant effluents. Data based on average removal efficiencies and effluent concentrations from European and American WWT plants after conventional primary and secondary WWT (from Margot et al, 2015).*

Micropollutants (MPs) are defined as environmental pollutants that exist in low concentrations, usually within the picogram to microgram per litre range (Stamm et al., 2016; Murray et al., 2010). MPs that have been chemically characterised and believed to be potentially harmful to human health or the environment are termed Emerging Contaminants (EMs) (Murray et al., 2010). Due to the continual development and production of new anthropogenic chemicals, it has been difficult to generate an exhaustive list of current ECs (Murray et al., 2010), thus, their identification, classification and management in the environment is an ongoing process.

The thousands of chemicals that fall into the categories of MPs and EMs (Schwarzenbach et al., 2006) are already broadly described above. More specifically they include the poorly biodegradable and hydrophilic polluting fraction of WW effluents, e.g. certain antibiotics and pharmaceuticals residues (Figure 2.2a), pesticides, biocides and household chemicals such as corrosion inhibitors, sweeteners, chelating agents and phosphorus flame retardants (Figure 2.2b) (Margot et al., 2015). Even at trace levels in the environment, many MPs are highly toxic to the aquatic food web, terrestrial ecological networks and food safety (Rastogi et al., 2018; Baresel et al., 2019). Pharmaceutical and antibiotic MPs in the aquatic environment are of particular concern due to their contribution to antibiotic resistant gene development in bacteria, which is considered a global-scale threat in humanity's endeavours to eradicate

life-threatening diseases (WHO 2014; (Baresel et al., 2019)). It is suggested that their biological reactivity in nature, combined with continual release into the environment, renders MPs and EMs both significant and problematic for humanity (Anjum et al., 2017) and therefore removal of these chemicals through effective treatment technologies is critical.

2.2.1 Introduction to Advanced Oxidation Processes

Micropollutants can be affected by conventional primary and secondary physical, chemical, and biological WWT processes, although they are only considered to be effectively removed from WW effluents using chemical treatments and Advanced Oxidation Processes (AOPs), such as ozonation, combined O_3/H_2O_2, UV/H_2O_2 or other combinations of AOPs with adsorptive and/or biological methods such as sorption onto granular activated carbon (GAC) filters (Margot et al., 2015; Baresel et al., 2019; Myers et al., 2018). If implemented, these can form either a combined secondary/tertiary step or a discrete tertiary polishing process (Figure 2.1). AOPs are defined as a series of water treatment processes involving the generation of hydroxyl radicals (·OH) in enough quantity to affect water purification (Glaze et al., 1987). Usually, AOPs are intended to remove organic (and occasionally inorganic) chemicals in WWs by utilising ·OH, due to its extremely high oxidising potential (E° = +2.73 Volts; (Pignatello et al., 2006)) and ability to react unselectively at near diffusion-controlled rates with most organic substrates (Page et al., 2012).

Over at least the last decade numerous studies have reported the successful treatment by AOPs of a broad range of MPs from WW effluents containing herbicides such as atrazine, pesticides, antibiotics, azo dyes to industrial solvents such as dioxane, e.g. Balmer & Sulzberger (1999); Vione et al. (2006); Chitra et al. (2012); Kwon et al. (2012); Wang et al. (2012); Zuorro et al. (2014); Zuorro & Lavecchia (2014); Hao et al. (2014); Zeng et al. (2017); Khan et al. (2019); Yan et al. (2019); Romero et al. (2020). The success of AOPs is suggested to be due to their significant oxidant power, moderate cost, simplicity of operation (as the chemical inputs are not complex) and in many cases, the manageability of the disinfection by-products produced (von Gunten, 2018; Romero et al., 2020). AOPs are consequently considered as the most promising WWT technologies of today (von Gunten, 2018; Mierzwa et al., 2018) for the effective removal of MPs from WW effluents and polishing treatment to drinking water standard. However, successful implementation at full-scale is currently reported only in some higher income countered, e.g. Switzerland (Hollender et al., 2009) and

others described in Schwarzenbach et al. (2010), in the form of tertiary polishing treatments (e.g. Figure 2.1).

Operational costs of AOPs, such as ozonation, are often considered feasible in higher income countries (Hollender et al., 2009), although in relative terms, the high energy consumption levels required for AOPs and overall chemical costs can present issues of affordability for many lower income nations. For example, following ozonation, subsequent biological polishing is required to remove the potential for toxic by-product formation (Baresel et al., 2019). Combined with issues of poor infrastructure, these are likely to be major barriers to the successful implementation of AOPs for WW treatment in densely populated areas of low- to middle income countries, where MP concentrations in drinking water may be of concern due to poor water management strategies. Thus, affordable, sustainable and effective strategies must continue to be sort.

Hydroxyl radicals (·OH) and other Reactive Oxygen Species (ROS) such as peroxides (e.g. H_2O_2) and superoxides (e.g. $\cdot O_2^-$) occur naturally in aqueous environments, the atmosphere and in biological systems (Gligorovski et al., 2015). Hence, these species are potentially available for rapid pollutant degradation in the natural environment and the (natural) processes forming ROS offer a potentially sustainable source of ·OH, if harnessed appropriately. For example, (Liao et al., 2019), suggests that although ·OH is highly influential in the cycling of redox-active elements, cycling of global carbon and the global emissions of CO_2, the abiotic production of ·OH in the dark (aphotically), has only recently started to attract attention due to its potential as a powerful oxidant in WWT.

Tong et al. (2016) were some of the earliest researchers to report the significant production of ·OH from subsurface sediments containing iron (Fe) in oxidative decontamination processes and they further suggest that this natural ·OH source is much more significant than previously considered. The research of (Tong et al., 2016) highlighted the occurrence of the Fenton reaction in Fe-bearing subsurface sediments, where ·OH is produced via a relatively simple abiotic reaction pathway involving the catalytic decomposition of hydrogen peroxide (H_2O_2) in the presence of ferrous iron (Fe^{2+}) (Romero et al., 2020), as shown in Equation 1:

$$Fe^{2+} + H_2O_2 \rightarrow Fe^{3+} + OH^- + \cdot OH \quad [1]$$

The Fenton AOP has recently become popular in WWT applications for treatment of MPs as supplying Fe for ·OH production (usually in the form of iron chlorides, sulphates or oxides) is

relatively straight forward. However, this does require financial resource and maintenance and thus is not an operationally sustainable option.

Furthermore, to ensure the availability of ferrous Fe (Fe^{2+}) for reaction with H_2O_2 in solution (Romero et al., 2020), Fenton AOPs operated as an entirely chemical process may have a high dependency on pH, if successful oxidation of MPs is to be achieved (Romero et al., 2020). To remedy this, the addition of chelating agents are usually required (Clarizia et al., 2017), otherwise, insoluble ferric oxides may precipitate as a product of the Fenton process (Pignatello et al., 2006). This would mean Fe was no longer available within the system as an electron donor, during the oxidation of H_2O_2 and production of ·OH. The precipitation of ferric oxides would further contribute to the waste loading of the treatment plant and would require landfilling. Also, the presence of organic compounds, e.g. those present in WW effluents, can modify the reactivity of Fenton AOPs, either by improving the efficiency (Romero et al., 2020; Zeng et al., 2019) or retarding it, e.g. Zeng et al. (2017), and this needs to be considered.

Besides the research of Tong et al. (2016), other studies have described occurrences of subsurface Fenton reactions, the related biogeochemical conditions and sources of Fe^{2+} in natural waters and sediments, all which lead to the production of ·OH. Although not currently exploited on a large-scale, the ubiquity of Fe-bearing minerals in soils and sediments could make them an extremely valuable source of renewable Fe, potentially for use in environmental decontamination processes (such as the Fenton AOP described above). This area of research is key given the global challenges of today related to climate change and reducing carbon emissions from energetically expensive environmental disinfection and decontamination processes, especially in developing nations where infrastructure and cost may be limiting factors and decentralised WWT systems are more popular (von Gunten, 2018; Lee & von Gunten, 2010).

2.3 Reactive oxidising species in natural sediments

Fe is highly available in the natural environment and by weight is the fourth most abundant element in the earth's crust (Remucal & Sedlak, 2011). However, Fe is a redox-active element and if in aqueous form, the speciation of Fe^{2+}_{aq} and Fe^{3+}_{aq} depends on pH and the presence of complexing ligands (Remucal & Sedlak, 2011); and also as discussed in the context of AOPs

by (Lee et al., 2014; Zhang & Yuan, 2017). As previously stated, this can limit the sustainability of Fenton AOPs at WWT plants.

Around a decade ago, several groups of researchers reported on the production of elevated concentration of ·OH in natural surface waters, aquifers and soils, e.g. (Allen et al., 1996; Vione et al., 2006; Page et al., 2012, 2013). These studies focussed on the role of dissolved organic matter (DOM) and reduced humic acids (HAs) in the dark (aphotic zone) of aqueous environments and did not investigate the source of Fe^{2+} in their studied systems. Moreover they acknowledged the role of Fe^{2+} as the key electron donor in the Fenton Reaction and potential for pollutant degradation.

A more recent study in 2015 (Minella et al., 2015) reported significant aphotic production of ·OH from anoxic lake sediments and noted the potential for local pollutant degradation, given that Fe^{2+} was present in local sediments. Reduced HA moieties were also noted by the authors as potentially being available to trigger the Fenton or Fenton-type reactions. These and several other studies provided early insight into pathways of ·OH production via the Fenton reaction in dark aquatic (frequently aphotic) environments.

More specific to Fe-bearing minerals was work reporting the degradative oxidation of the industrial solvent trichloroethylene (TCE), a recognised MP, by ·OH during the abiotic oxidation of the ferrous sulphide mineral pyrite (FeS_2) (Pham et al., 2008). Although the mechanisms of ·OH production by pyrite oxidation have been probed and the Fenton reaction found to be a likely pathway for ·OH production (Zhang et al., 2016), MP degradation via this abiotic chemical pathway (without additives) occurs at low pH of around 2.5-3 and thus is highly unsuitable for most WWT processes. Later work (Zhang & Yuan, 2017) showed that it was possible for ·OH to be produced via FeS_2 oxidation in neutral pH environments, although only in the presence of low-molecular-weight organic acids (LMWOAs, which the authors suggest may be present in certain natural environments such as salt marches and estuarine settings) was the yield of ·OH significant, due to increased availability of Fe^{2+} following complexation with the LMWOAs.

Limitations of using pyrite as a sustainable source of Fe^{2+} during ·OH production via the Fenton reaction are (i) the compromise on yield of ·OH at neutral or near pH in the absence of LMWOAs, (ii) the variability of ·OH yield which is dependent on the ratio of the Fe^{2+} sites on the pyrite surface compared to the aqueous Fe^{2+} concentration (Zhang et al., 2018) and

(iii) the reported precipitation of soluble Fe^{3+} as ferric hydroxide (Zhang & Yuan, 2017) which may act as a sink for Fe, permanently immobilising it causing ·OH production to cease.

2.4 Using iron-bearing clay minerals as a sustainable source of reactive oxidising species

Following oxygenation of subsurface sediments collected from oxic-anoxic interface environments, a very high •OH yield (123 μmol/g Fe^{2+}) was reported (Tong et al., 2016) with the •OH production level orders of magnitude greater than any previously reported from surface water environments, e.g. (Vione et al., 2006; Page et al., 2012; Minella et al., 2015). In the context of these findings, it was suggested that the oxygenation of structurally-coordinated Fe^{2+} in clay minerals was likely to be responsible for the majority of •OH production in subsurface environments, followed probably by Fe in other mineral forms (e.g. Fe oxy(hydroxides) and sulphides), adsorbed Fe and then organic carbon (Tong et al., 2016).

The majority of clay minerals that exist in the shallow subsurface contain both Fe^{2+} and Fe^{3+} in their structure. Fe-bearing clay minerals, such as the dioctahedral smectite mineral nontronite, are known to be able to accommodate multiple Fe redox cycles without suffering significant structural changes (Zhao et al., 2015; Zeng et al., 2017; Yuan et al., 2018) except some modification of layer charge, swelling capacity and/or cation-exchange capacity (Finck et al., 2015; Gates et al., 1996). To date, studies of smectite redox chemistry have focussed on the Fe-rich smectite nontronite, specifically NAu-2 as it contains 23% structural Fe (Keeling et al., 2000) and has previously been well-characterised in terms of its structure and Fe redox chemistry (Komadel et al., 2006; Stucki, 2011; Neumann et al., 2011, 2011; Zhao et al., 2013; Liu et al., 2017; Zeng et al., 2017).

The reduction of structural Fe^{3+} to Fe^{2+} in nontronite and other ferruginous smectites can be achieved by chemical methods, e.g. dithionite (Komadel et al., 2006) and also by microbially-mediated processes, e.g. (Kostka et al., 1999, 2002; Jaisi et al., 2005; O'Reilly et al., 2006; Jaisi et al., 2007, 2007; Kashefi et al., 2008; Zhao et al., 2015; Zeng et al., 2016, 2017; Wang et al., 2017; Li et al., 2019), and reduced ferruginous smectites have been applied in various environmental decontamination processes. For example, the reductive transformation of nitroaromatic compounds by (abiotically-reduced) structural Fe^{2+} in the montmorillonite and nontronite by (Neumann et al., 2008), of chlorinated solvents by (Neumann et al., 2009),

(Fialips et al., 2010; Entwistle et al., 2019) and the reduction of certain heavy metals such as chromium (Cr^{6+} to Cr^{4+}) by (Zhuang et al., 2012).

Oxidation of structural Fe^{2+} to Fe^{3+} in smectite minerals is easily achieved if molecular oxygen (O_2) is present and proceeds by a series of one-electron transfer reactions (Haber & Weiss, 1932) where Reaction 3 is the rate limiting step, due to the availability of O_2 and pH (Equation 2):

$$Fe^{2+} + O_2 \leftrightarrow Fe^{3+} + O_2^{-\cdot} \quad [2]$$

Following formation of the superoxide radical ($O_2^{-\cdot}$; Equation 3) equilibration occurs according to pH with the hydroperoxyl radical ($HO_2^{\cdot}$), as shown in Equation 3:

$$HO_2^{\cdot} \leftrightarrow H^+ + O_2^{-\cdot} \qquad K_a = 10^{-4.8} \quad [3]$$

The speciation of Fe^{2+}_{aq} and Fe^{3+}_{aq} depends on pH and any complexing ligands present, e.g. (Remucal & Sedlak, 2011; Lee et al., 2014; Zhang & Yuan, 2017) and others. Assuming that Fe^{2+} and Fe^{3+} represent all dissolved ferrous and ferric species, a further one-electron transfer process occurs during the reaction of the superoxide ($O_2^{-\cdot}$) and the hydroperoxyl radicals ($HO_2^{\cdot}$) with Fe^{2+}, to produce HO_2^-/O_2^{2-}, which following protonation, transforms to H_2O_2 (Equations 4 and 5, respectively; (Remucal & Sedlak, 2011)):

$$Fe^{2+} + HO_2^{\cdot} \rightarrow Fe^{3+} + HO_2^- \xrightarrow{H+} Fe^{3+} + H_2O_2 \quad [4]$$

$$Fe^{2+} + O_2^{-\cdot} \rightarrow Fe^{3+} + O_2^{2-} \xrightarrow{2H+} Fe^{3+} + H_2O_2 \quad [5]$$

Once H_2O_2 is generated, the Fenton reaction (Equation 1) can occur where Fe^{2+} is oxidised and ·OH produced. However, if no other scavengers of ·OH are present, e.g. other organic compounds or bicarbonate (Remucal & Sedlak, 2011), any remaining Fe^{2+} will scavenge ·OH during oxidation to Fe^{3+} and produce the hydroxide ion (OH^-) as shown in Equation 6:

$$Fe^{2+} + \cdot OH \rightarrow Fe^{3+} + OH^- \quad [6]$$

Following the findings of (Tong et al., 2016), a number of lab-based studies investigated the feasibility of Fe-bearing clay minerals as potential renewable sources of Fe with which to catalyse the Fenton reaction for production of ·OH and then oxidise a specific organic probe, on the basis that structural Fe could be cycled *in-situ* between Fe^{2+} and Fe^{3+} without compromising the integrity of the clay as a catalyst, e.g. (Zeng et al., 2017, 2019). Similarly

motivated studies used Fe oxides and sulphates as sources of Fe^{2+} for oxygenation, e.g. (Jia et al., 2017; Chen et al., 2019).

These studies have shown that organic probes representative of MPs can be successfully removed from WW effluents through oxidation over time, using either the same Fe-clay catalyst to drive the Fenton reaction or non-renewable source of Fe^{2+}. However, a main limitation of these published studies has been the necessity to 'regenerate' Fe-clays by either chemically or biologically reducing them *ex-situ*, outside of mesocosm experiments, or by providing additional ferrous Fe to the system, after each treatment cycle. There is therefore an urgent need to formulate a more sustainable solution for the regeneration of structural Fe^{3+} to Fe^{2+} in otherwise promising clay catalysts.

Furthermore, no studies have investigated the structure and health of the microbial communities, as part of larger ecological networks, capable of reducing structural Fe in clays. Although the role of microbially-mediated Fe reduction (FeR) in clay minerals is widely recognised to play a key role in soil biogeochemistry and potentially bioremediation (Kostka et al., 1999, 1996), only a few studies have reported the reduction of structural Fe in clay minerals mediated by indigenous microbial communities to the clay itself (Stucki et al., 1987; Wu et al., 1988), rather than spiking clay substrates with additional pure bacterial cultures, as reported in (Mueller, 2015). Of the studies reporting successful FeR by indigenous microbial communities (Stucki et al., 1987; Wu et al., 1988), neither of these works characterise the structure, health or ecological networks associated with the communities responsible for FeR within the clay minerals.

For a sustainable microbially-mediated WW treatment system to be successful, understanding the microbiological community structure, interactions between species and resilience of the network are critical. Although the use of microbes as 'bioindicators' in WWT performance is widely recognised (Stoeck et al., 2018), it has been used little as a monitoring tool for WWT. Furthermore, although there are a number of studies investigating the robustness of terrestrial ecological networks (Evans et al., 2016; Pocock et al., 2012; Evans et al., 2013), there is no published research that characterises the microbial network ecology of WWT systems, or reported indicator tools based on these fundamentals that could be used to monitor such as system. For low-input, low energy and low cost WWT systems that rely on natural redox processes within sediments, this is a significant knowledge gap that requires urgent research.

This PhD project therefore aims to address the issue of sustainable redox cycling by exploiting microbially-mediated Fe-reduction in Fe-bearing, redox-active clays and natural sediments in order to achieve multiple cycles of MP treatment via oxidation (i.e. an AOP), with minimal energy and chemical input. Figure 2.3 is a schematic of the processes that this PhD intends to realise in developing a novel sustainable WWT system, using the approaches and methods described in the next section.

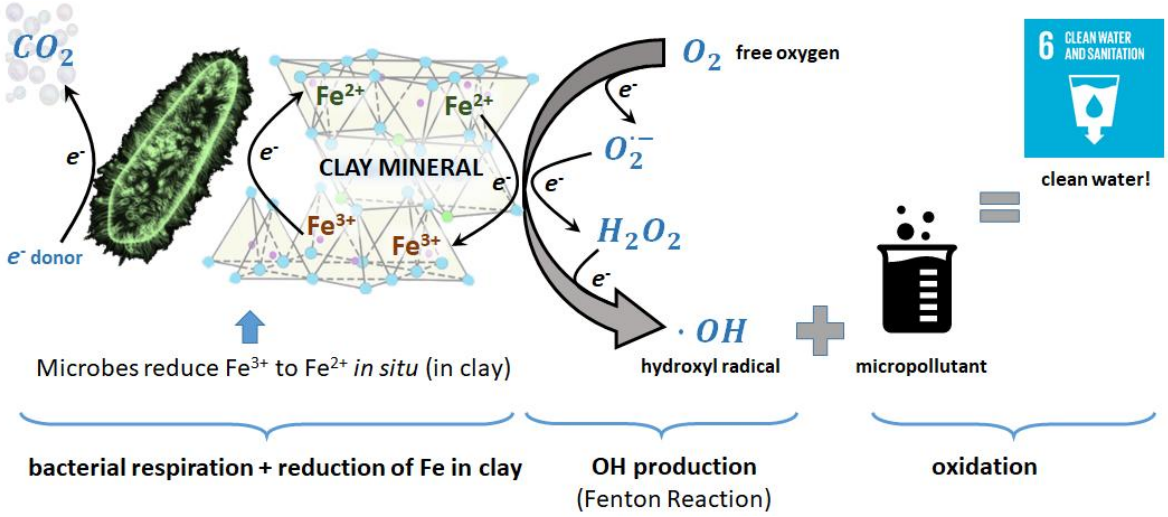

Figure 2. 3. *Schematic showing the electron transfer pathway from microbially-mediated iron reduction (left) occurring in-situ within an iron-bearing smectite clay mineral to the oxidation (via hydroxyl radicals, •OH) and consequential treatment of a micropollutant (left).*

3. Column Design

3.1 Introduction

Batch experiments have previously been used to show that hydroxyl radicals generated from the oxygenation of ferrous iron (Fe) in clay-bearing sediments can successfully degrade aqueous phase organic pollutants in the subsurface (Pearson, 2017; Ding, 2017; Chen, 2017; Liu et al., 2017; Tong et al., 2016; Zeng et al., 2017). To this end, translating the results from these batch experiments to conditions more relevant to a water treatment environment was key to providing proof-of-concept for this water treatment technology.

A literature review determined that vertically-oriented benchtop column experiments would be most appropriate for this work as they are best suited to investigating dynamic processes in fluidic environments (Banzhaf & Hebig, 2016), especially where flow and redox zones are of interest (Banzhaf & Hebig, 2016; Banzhaf et al., 2012). Column flow rate can be used to simulate different environmental settings, and physical dimensions of columns can be adapted to reflect environments with either fast or slow reaction rate phases (Banzhaf & Hebig, 2016; Banzhaf et al., 2012). For example, longer columns allow slower reactions to be observed, e.g. those involving the formation of redox zones (Banzhaf & Hebig, 2016). Hence, these were factors considered during the column design process, as maintaining low and constant flow whilst providing the opportunity for redox zone formation were both major elements in the success of the treatment system being developed.

Two column sets of different sizes were produced and used for experimental work in the thesis. Whilst the primary, large set of columns was being designed, tested and fabricated in the School of Engineering Workshops, several smaller test columns (volume of 590 mL and diameter:length ratio of 1:6) were developed using pre-existing materials. These were packed according to the regime described in Sections 3.2 and 3.3.1.3 and validated during flow tests described in Section 3.3.3. These small columns were used to develop and inform dynamic aspects of the biological treatment experiments that were to be carried out in the large columns. For example, how best to: (i) enable microbial activity inside columns, (ii) monitor redox conditions associated with microbial Fe-reduction and determine approximate timescales for redox transitions, and (iii) sample column sediments in ambient and oxygen-free conditions for measurement Fe^{2+}/Fe^{3+} ratios in oxidised clay and microbially-reduced clay. The small columns were also then used in a series of chemically-driven micropollutant

treatment trials (Chapter 4) to provide further insight into operational aspects of the microbially-driven column treatment experiments.

The small column design was the basis for a large column prototype, which on completion, was used in a microbial-reduction validation experiment to determine the volume of column porewater needed to obtain enough extractable DNA for 16S RNA and DNA sequencing. Following minor adjustments to the large column prototype (in the School of Engineering Workshops), the biological treatment experiments were completed in a set of 5 large column reactors (3,100 mL volume). These large columns ensured a greater porewater sampling capacity, which was anticipated for sufficient extraction of DNA and RNA. For example, around 250 mL of column porewater was required for successful sequencing of 16S RNA during the work of Vignola et al. (2018).

This chapter first presents the column design for the set of large benchtop columns used for the majority of PhD experiments. The rationale behind the chosen design is then described through the development process, whereby column packing materials, fluid flow rates and column dimensions were tested and optimised. This work provided the means to maximise interaction between fluid flow and Fe-bearing clay mineral inside the column, whilst minimising clay mineral loss in effluent flow. Secondly, methods to enable, monitor and control other dynamic experimental aspects, e.g. cycling of redox conditions and microbial activity levels were developed and validated using the smaller prefabricated columns. Lastly, modes of experimental sampling and time frames for column operation were established using the smaller prefabricated columns and the rationales for decisions made around these factors are presented.

3.2 Final column design

The primary (large) experimental columns were designed, fabricated and tested in-house at Newcastle University over the course of approximately 8 months, with assistance from the School of Engineering Workshop Team. The final design for these benchtop columns (Figure 3.1) included a column shaft fabricated from PN10 WP EU Food grade (2002/72/EC) clear polyvinyl chloride (U-PVC) pipe with a wall thickness of 5.3 mm, an outer bore of 110 mm and average internal diameter of 99.4 mm purchased from the Plastic Pipe Shop (https://www.plasticpipeshop.co.uk/). Screw-thread high density polyethylene (HDPE) collars were fabricated to secure the HDPE top and base of the column to the PVC shaft. Three HDPE

sampling ports were also fabricated and installed at equal distances along the vertical column shaft and circular deformable teflon spacers were used to form an airtight seal between each sampling port and the outer curved column shaft.

Food grade, low gas permeability Tygon tubing (Saint Gobain, RS Components Ltd) that was suitable for use with peristaltic pumps, was used for the influent and effluent column flows. Further details of the column plumbing and tubing connections are provided in Section 3.3.2 and Figure 3.9. When tested, the plumbed column could sustain a steady state flow of 5 mL/min across the entire column cross section and achieve full upflow saturation.

Column flow was measured by placing the tip of the column effluent tubing into a 10 mL volume measuring cylinder and whilst recording time, allowing effluent to fill the cylinder to 5 mL using a peristaltic pump. The pump rate was then calibrated by adjusting the pump speed up or down, as required, to ensure sufficient flow to the measuring cylinder to complete a 5 mL volume within 1 minute. The same steps were applied to establish flow rates for all column experiments in this research and separate peristaltic pumps attached to each column, to ensure that pump calibrations remained valid and to minimise variability and/or error in flow rates. Column flow rates were checked at the start of each experiment then monitored throughout, with minor adjustments being made if necessarily.

The optimal column packing regime (Figure 3.2) was determined following a series of packing and flow tests, to balance clay content with permeability and laminar flow. This led to a final column packing height of 400 mm, with column pore volumes of 400mL and 250 mL for nontronite or montmorillonite clay minerals, respectively, with pore volumes representing approximately 13% and 8.1% of the total column volumes, respectively. The small benchtop columns used to constrain redox transition times and for chemical treatment experiments, had column pore volumes of 250 mL which was approximately 42% of the total column volume and greater than the larger columns, due to a lower packing density in these narrower but volumetrically smaller columns.

Figure 3.1 provides a sketch representation of column dimensions, fabrication materials and location of sampling ports, and full technical drawings of the column design are provided in Appendix A.

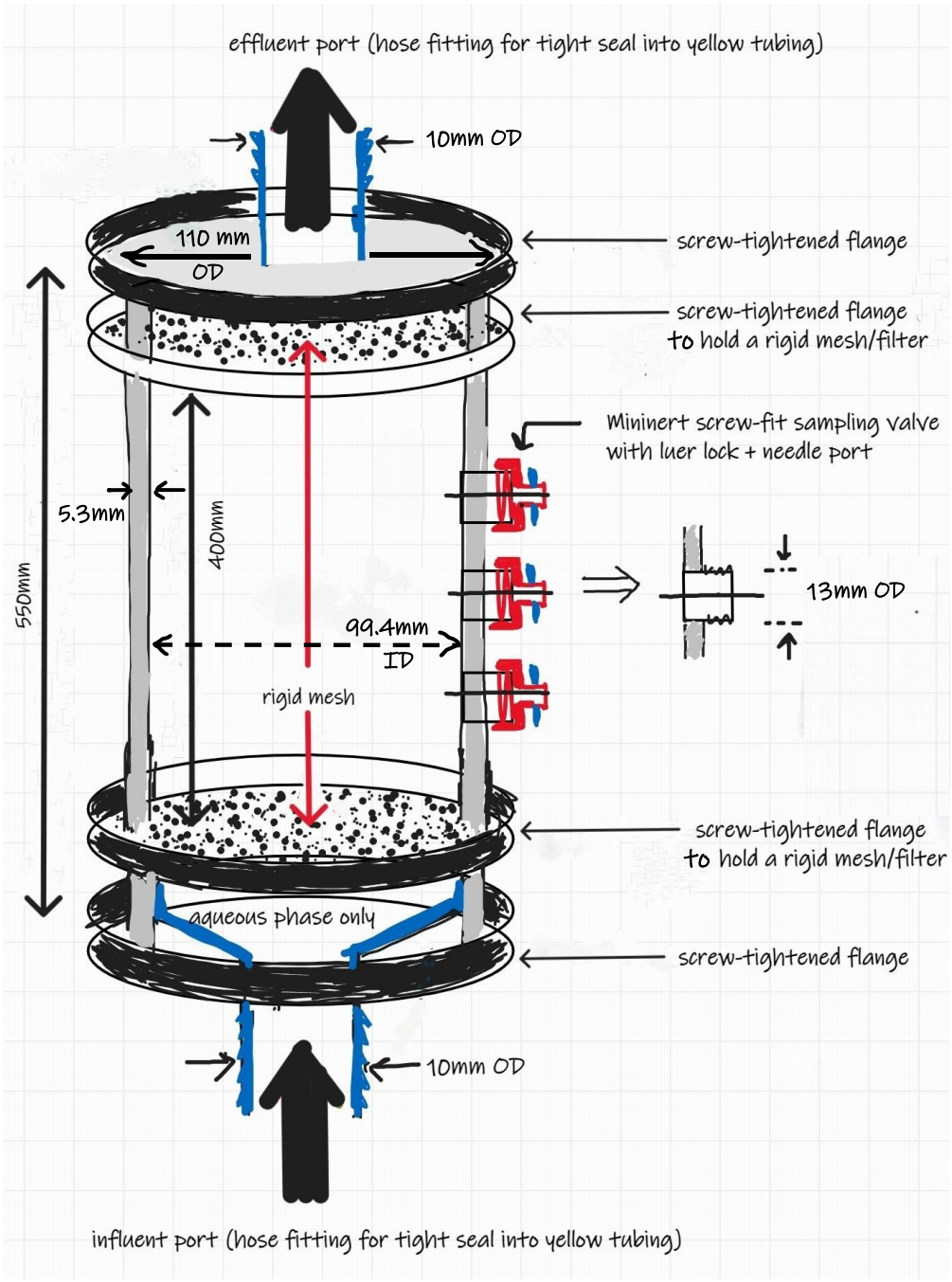

Figure 3. 1. *Sketch of the final column design showing dimensions, flow direction, internal features and location of the sampling ports of the PVC columns used in experiments.*

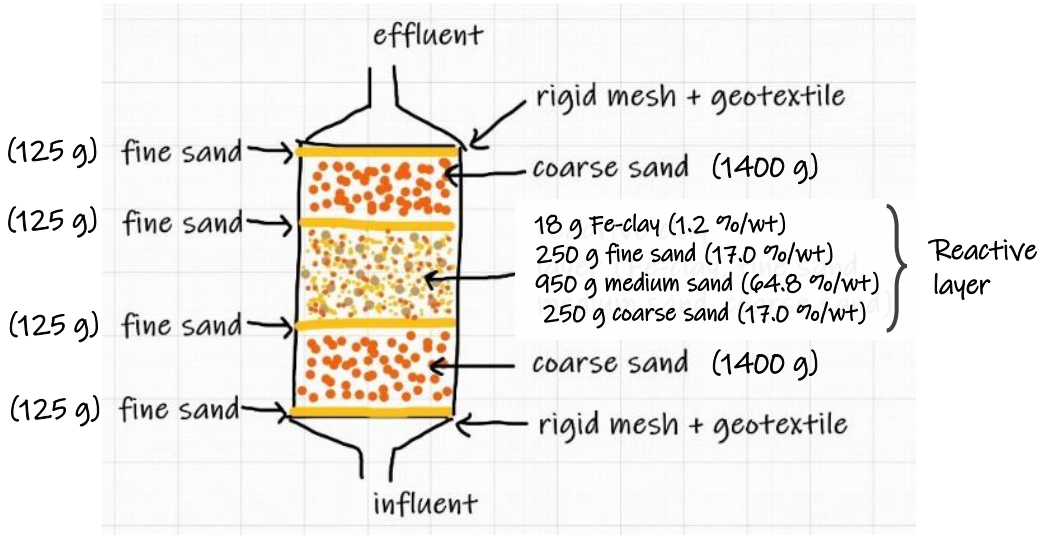

Figure 3. 1 *Sketch showing final packing regime of benchtop experimental columns. Fine and coarse sand fractions are packed in layers, vertically encapsulating a 'reactive' nontronite clay fine, medium and coarse sand layer in the column centre.*

3.3 Column development process

Five specific goals were identified in working towards successfully developing the experimental columns:

i. Determining suitable packing materials (alongside the Fe-bearing clay mineral) and a packing regime for these substrates, whilst achieving column saturation in an upflow direction;

ii. Establishing a working fluid flow rate capable of fully saturating columns whilst minimising clay mineral loss from effluent flow, in addition to measuring column volume and pore volume;

iii. Establishing optimal locations for monitoring and sampling ports;

iv. Selecting appropriate materials from which to construct the columns, and finalising working dimensions;

v. Determining the length of time required for the system to transition between one redox state and the next, i.e. successive cycles of anoxic, oxic then anoxic conditions, and so on), therefore defining the approximate time required to complete one entire treatment cycle;

3.3.1 Selection of column packing materials and initial fluid flow tests

The Fe-bearing clay mineral nontronite was chosen for use in the column experiments as it contains a high proportion of structural Fe compared to other smectite clays and is well

characterised in the literature. Nontronite (NAu-2, 23 wt% iron) was purchased from the Clay Mineral Society Source Clay Repository (Chantilly, Virginia, USA) and the bulk clay was size-fractionated following the method of Jackson (1969), to achieve a grain size of <2 microns (µm). To minimise the interlayer charge within the nontronite, the <2 µm size fraction was homo-ionised by washing with increasingly dilute concentrations of sodium chloride solution. Decreasing the layer charge of the clay mineral is beneficial as it makes the clay mineral crystal structure more flexible and allows it to accommodate the change in ionic radius between Fe^{2+} and Fe^{3+} that occurs during repeat reduction and re-oxidation cycles. The nontronite was then freeze-dried (Figure 3.3a) so that the same dry mass of clay mineral could be packed in the column experiments in a reproducible manner.

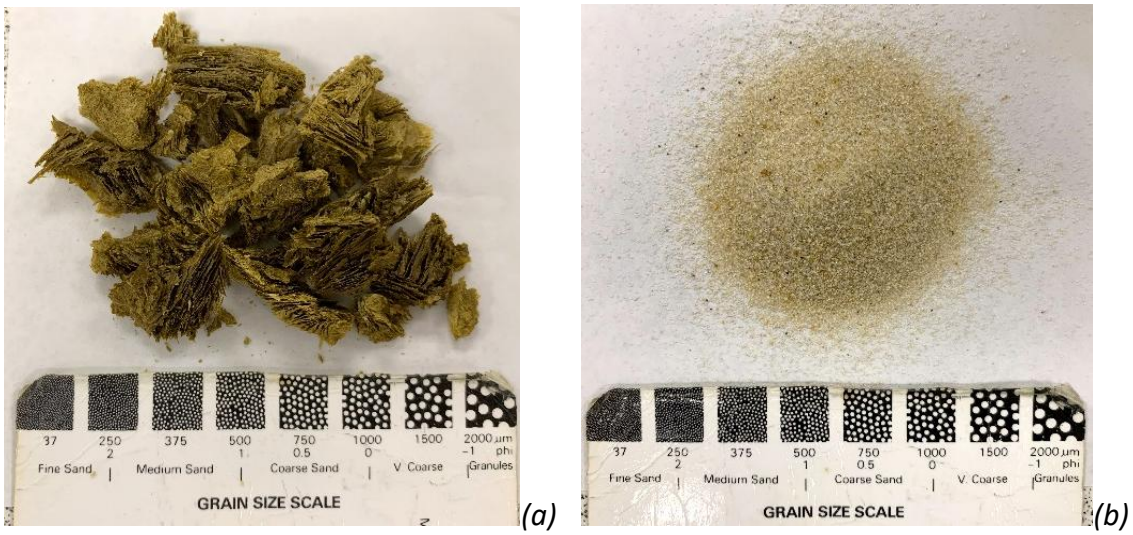

Figure 3. 3. *Images of (a) freeze-dried nontronite, <2 micron size fraction, and (b) high purity quartz sand (Supelco, Sigma Aldrich) used in the central 'reactive' layer of the test columns.*

Clay minerals are recognised to have a very low permeability, with a maximum of around 5 x 10^{-9} metres per second (m/sec) (Domenico & Schwartz, 1997). Combining clay minerals with a porous material such as sand, can improve the permeability to one desirable for a permeable system, of >10^{-5} m/sec (Zhuang et al., 2012). Furthermore, findings from previous column studies at Newcastle University (Neumann Group, (Pearson, 2017; Chen, 2017; Ding, 2017)) and communication with Newcastle University Geotechnical Laboratory staff (Patterson, 2020) suggested that limiting the clay mineral content to ≤2% of dry weight should minimise vertical dispersion transverse to the direction of fluid flow (Carey et al., 2018) and maximise laminar flow through the column substrate. Minimising changes in permeability through different column packing zones is also recognised to improve laminar flow through column substrates (Patterson, 2020).

3.3.1.1. Testing packing regimes under upflow

The first packing regime tested included a homogenised mixture of <2 µm size nontronite (as above) and high purity quartz sand (Figure 3.3b; Supelco, Sigma Aldrich), in a clay mineral:sand ratio of 1:50 resulting in 2% dry weight content of nontronite. To confirm suitable permeability of the nontronite and sand, the homogenised mixture was packed into a small glass column permeameter (Figure 3.4a; after (Zhuang et al., 2012)) with an approximate total column volume of 100 mL and substrate volume of 70 mL. A peristaltic pump was used to flow tap water in a upflow direction at rates of approximately 20 mL/min, 10 mL/min and 5 mL/minute, yet little to no effluent flow was observed. The lack of flow was attributed to swelling of the nontronite inside the column, severely limiting the overall permeability of the column packing materials by blocking available pore spaces and thus, hindering flow. Furthermore, the introduction of flow to the column sediments was not uniform at the base.

(a)

(b)

Figure 3. 4 (a) *Small glass column packed with <2 µm nontronite clay and high purity quartz sand (in a 1:50 ratio).* ***(b)*** *Open-topped large glass columns being packed with either pea gravel, coarse or medium sand above and below the clay and sand 'reactive layer'.*

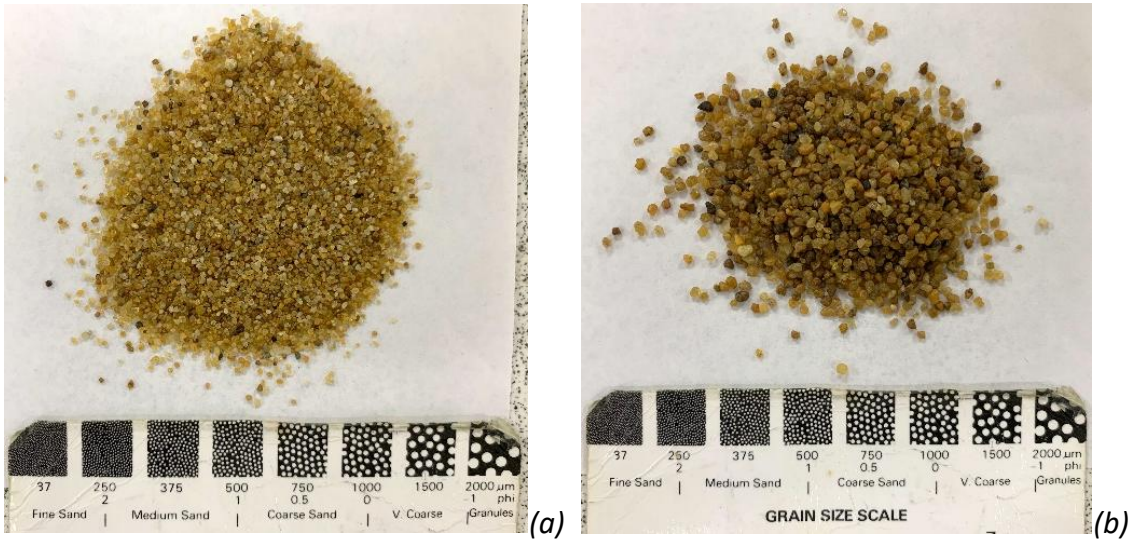

(a) *(b)*

Figure 3. 5. *Images of* ***(a)*** *medium sand and* ***(b)*** *coarse sand from the Woburn Beds, Lower Greensand Formation (Bedfordshire UK), used to increase permeability in the test columns.*

To improve several column design aspects including fluid flow, several large, open-topped glass test columns with stopped sampling ports were used to assess different nontronite:sand ratios and further packing combinations. The large test columns were 480 mm high with diameters of 90 mm and internal (column) volumes of approximately 3 litres (L). Geotextile discs cut from drainage geomembrane (Naue Secudran, Geo-Coastal Engineering Ltd, Ireland) were placed above P16 sintered glass frits (porosity grade 4, <10>4 µm) at the base of each column shaft, to minimise loss of sand grains and fines through the influent feed and also to evenly distribute flow as fluid entered the column (Figure 3.4b).

During testing, the columns were sealed with a tightly fitting rubber bung and the uppermost side sampling port was used as the effluent drain, packed with geotextile to minimise loss of fines during saturated upflow tests. Layers of pea gravel, coarse and medium sand (Figure 3.5a-b; from Woburn Sands, Lower Greensand, Bedfordshire UK (Bedfordshire Geology Group, 2011) were packed into the columns during three separate tests, to form higher permeability zones above and below a central zone of 1.5% (dry weight) nontronite combined with approximately equal weights of high purity quartz sand, medium sand and coarse sand, named the 'reactive layer'. Figure 3.6 shows a sketch of the generic packing regime used in these tests and shows the experimental set-up including flow direction (and pump), influent and effluent ports, and column support structure.

The proportions of clay and sand in the reactive layer were adjusted to increase the permeability of this central zone by decreasing the clay:sand ratio to 1:66 (equivalent to 1.5% nontronite) and then to 1:77 (equivalent to 1.2% nontronite). The addition of gravel or sand

layers above and below the reactive layer allowed a greater resident pore volume inside the column appropriate for geochemical and microbiological porewater sampling (e.g. DNA/RNA). These higher permeability layers also promoted laminar flow and the formation of a uniform fluid horizon across the column.

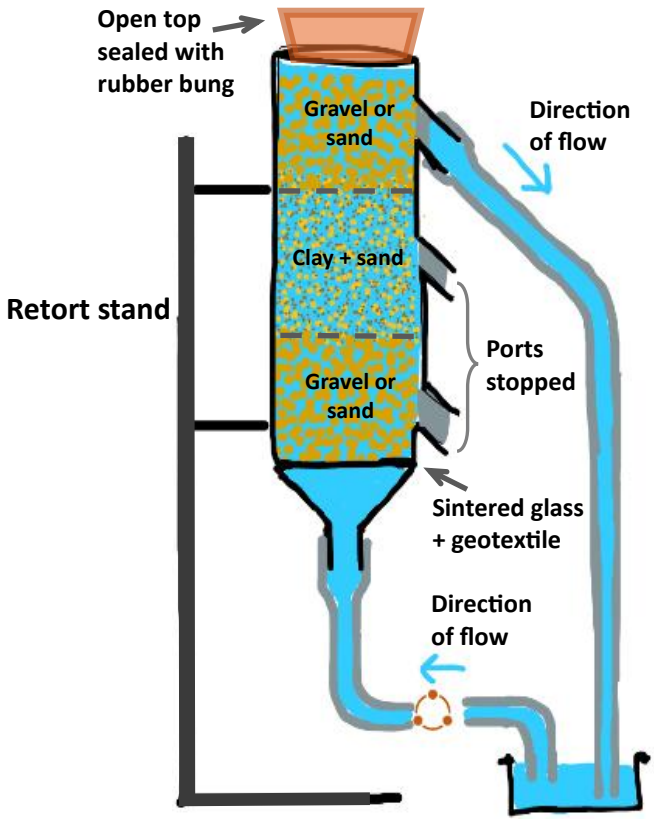

Figure 3. 6. *Schematic of large glass test columns, with high permeability gravel or sand layers above and beneath nontronite and sand 'reactive layer'. The influent is at the base of the column and effluent port at the side. Flow direction is upwards for saturation.*

Steady state upflow was achieved with all packing combinations tested at flow rates of 20, 10 and 5 mL/min. For all flow rates trialled, using pea gravel above and below the reactive layer consistently gave rise to the shortest hydraulic retention times measured (~20 minutes at 5 mL/min) and using medium sand (only), the longest retention time (~125 minutes at 5 mL/min). These results are summarised in Table 3.1.

Table 3. 1. *Flow rate trials results summary showing hydraulic retention times when different sediments were packed above and below the column reactive layer.*

	Flow rate (mL/min)		
Sediment above/below reactive layer	**5**	**10**	**20**
Fine sand	no flow	232 mins	140 mins
Medium sand	125 mins	70 mins	42 mins
Pea gravel	20.3 mins	10.8 mins	6.2 mins

3.3.1.2. Controlling fines migration

Despite the measures taken to prevent loss of fines during the column packing and flow tests, light brown colouration of the effluent water (Figure 3.7) indicated that clay-size fines were passing through the geotextile packed in the effluent port. Maintaining a consistent concentration of clay within the test columns was key to the success of the treatment process, as Fe within the clay structure would also have been lost through fines migration. Subsequent column tests using different flow rates determined that a linear relationship existed between increasing flow and dry mass of fines lost. Using the same packing configuration as before, a flow rate of around 5 mL/min was found to result in negligible loss of clay-size fines, so was adopted for future column tests going forward.

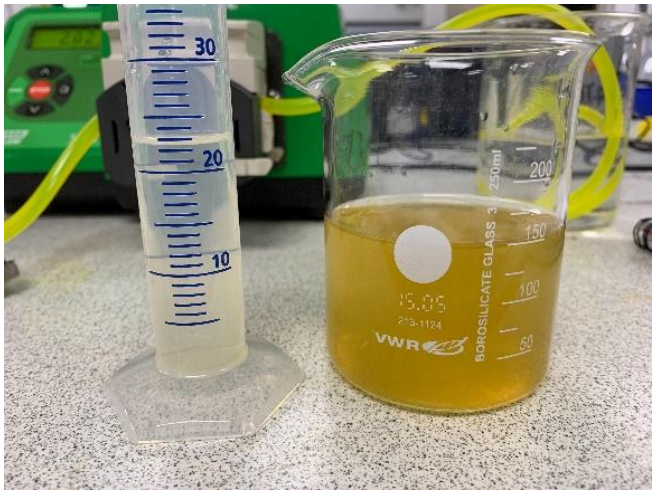

Figure 3. 7. *Brown colouration of column effluent in a collection beaker (right) indicating clay fines migration from test column, where only 1 goetextile layer was used as a filter material. Left hand cylinder contains effluent filtered by 2 geotextile layers.*

A small proportion of column fines also passed through the lower geotextile and glass frit at the column base during periods of low flow, when little or no positive hydraulic pressure was applied to the column in an upflow direction. To remedy this issue, a second geotextile disc was placed above the glass frit in the base of column shaft, to further inhibit physical loss of material through gravity. Cotton wool bungs are sometimes used in laboratory column studies test to prevent fines migration (Pearson, 2017; Chen, 2017; Ding, 2017), although this approach can lead to clogging of sampling ports and severe reduction in flow rates. Furthermore, the availability, processing costs and overall sustainability of using filter materials such a cotton wool or other synthetic composites was not considered ethical in this research project, so was not adopted. Moreover, the use of natural, unprocessed filter materials was prioritised given that this research project aims to provide proof-of-concept for

a sustainable water treatment system suitable for low to middle-income counties. Therefore, maximising clay retention inside column experiments whilst minimising fines migration was achieved using a combination of flow rate and different grain-sizes of sand. Geotextile layers were used as the only synthetic input to the experimental set-up.

Pea gravel was excluded as a column packing material for several reasons. The large void spaces between gravel grains led to poor consolidation of the central nontronite clay and sand layer along the boundary with the gravel. Secondly, clay and sand fines migrated into the gravel layers in both directions, during either positive or static hydraulic pressures. Lastly, a perched water layer formed between the lower gravel and the central clay/sand layers, suggesting that the hydraulic gradient between these different column layers was too high. Minimising the difference in permeability of column packing materials can improve fluid flow dynamics (Patterson, 2020) and this aspect was the focus of final column packing tests.

3.3.1.3. Final column packing regime/method

A number of final measures were adopted to maximise sediment packing success, reduce the hydraulic gradient between different column layers, mitigate issues with column flow and reduce migration of clay-fines:

i. the reactive layer containing nontronite, high purity quartz sand, medium sand and coarse sand was adjusted to the proportions shown in Figure 3.2, to further increase permeability whilst minimising migration of clay fines;
ii. coarse sand only was used above and below the reactive layer;
iii. high purity quartz sand was used as a natural permeable barrier to minimise fines migration at the top and base of the experimental column, also above and below the reactive layer (Figure 3.2);
iv. HDPE mesh grids (example shown in Figure 3.8) were fabricated in-house to fit inside the large benchtop test columns, to provide rigidity for the geotextile layers, facilitate material packing and also to prevent migration of the coarsest sediment from the column;
v. column sediments were moistened with a fine mist of reverse-osmosis de-ionised water to minimise the formation of air pockets during packing.

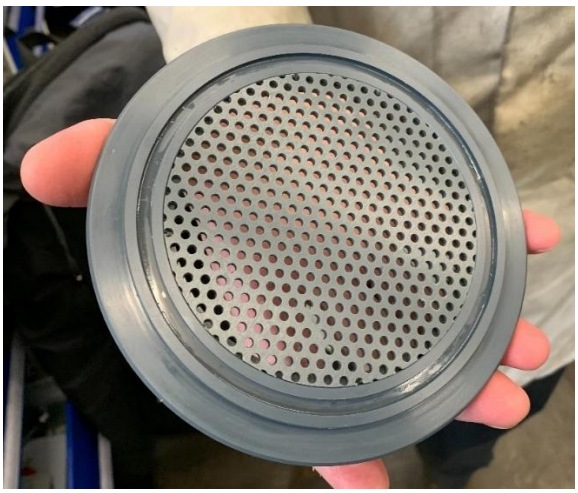

Figure 3. 8. *A rigid HDPE mesh grid fabricated in-house to fit inside the large benchtop test columns to provide support for the geotextile layer and to prevent coarse sediment migration.*

3.3.2 Column dimensions and construction

The final design for the large experimental columns included a working internal cylinder length of 400 mm and an internal diameter of 99.4 mm (Figure 3.1), as Lewis and Sjöstrom (2010) suggested that a diameter to length ratio of 1:4 is optimal in maintaining laminar flow through a column. These dimensions were considered suitable for the formation of redox zones, as Banzhaf and Hebig (2016) suggest that longer columns allow a greater number of smaller reactions to be differentiated from each other, e.g. redox reactions, compared to shorter columns. The overall column length (from the influent base to the effluent port at the top) was 600 mm to enable the entire column to be transferred to an oxygen-free glovebox for sampling (and to fit inside the antechamber).

Priorities for column fabrication material were strength, chemical compatibility, hermetic sealing, safety and ease of working (should modifications be needed once the column was constructed). Colour and transparency of the column shaft was also considered, to allow visual inspections during experiments. Discussions with the School of Engineering workshop team were key to the material selection process as all columns were engineered in-house.

Clear and colourless materials such as PVC and Perspex, were considered for the column shaft as they met almost all design criteria. PVC was found to be more chemically-resistant than Perspex and more durable compared to polycarbonate, so only PVC was carried forward in the column design process. Disrupted supply chains during the Covid-19 Pandemic meant that availability of PVC tubing was limited and the only available PVC tube in suitable

dimensions was transparent, although blueish in colour. Following testing, the colouration of the PVC was found not to be problematic although to prevent excessive algal growth inside the columns, sleeving the exterior of the column shafts with aluminium foil was used to provide light shielding during experiments. Visual inspection of column packing and flow progress was also possible with this approach and monitoring of certain physico-chemical parameters during column experiments, e.g. oxygen saturation, was achieved using *in-situ* DO probes (Section 3.3.4.2).

HDPE was used for all other column parts, e.g. top and base fittings and sampling ports, due to ease of in-house machining, material durability, cost, ease of repair, safety and ideal chemical compatibility.

Two different sizes of Tygon tubing were used to supply influent and effluent flows. A 500 mm length of 9.5 mm bore tubing was attached to a hose fitting machined into the column effluent, at the top of the column (Figure 3.9). An in-line Teflon 2-way directional tap 100 mm above the column effluent port provided a means to completely seal the top of column from ambient laboratory conditions. The column influent, at the base of the column, was also fed by a 100 mm length of 9.5 mm bore tubing, which was attached to an in-line Teflon 3-way directional tap (Figure 3.9). One tap port was connected to approximately 500 mm of 4.8mm bore Tygon tubing and the influent flow pumped from the influent reservoir using an in-line peristaltic pump (Figure 3.9). The other tap port was connected to 300 mm length of 9.5 mm bore tubing and provided a bleed valve and drain to prevent air entering the column influent, which was critical for achieving column saturation. Hose adapters, secured with stainless steel hose clips, were used to form secure connections between the Tygon tubing and influent, effluent and tap ports.

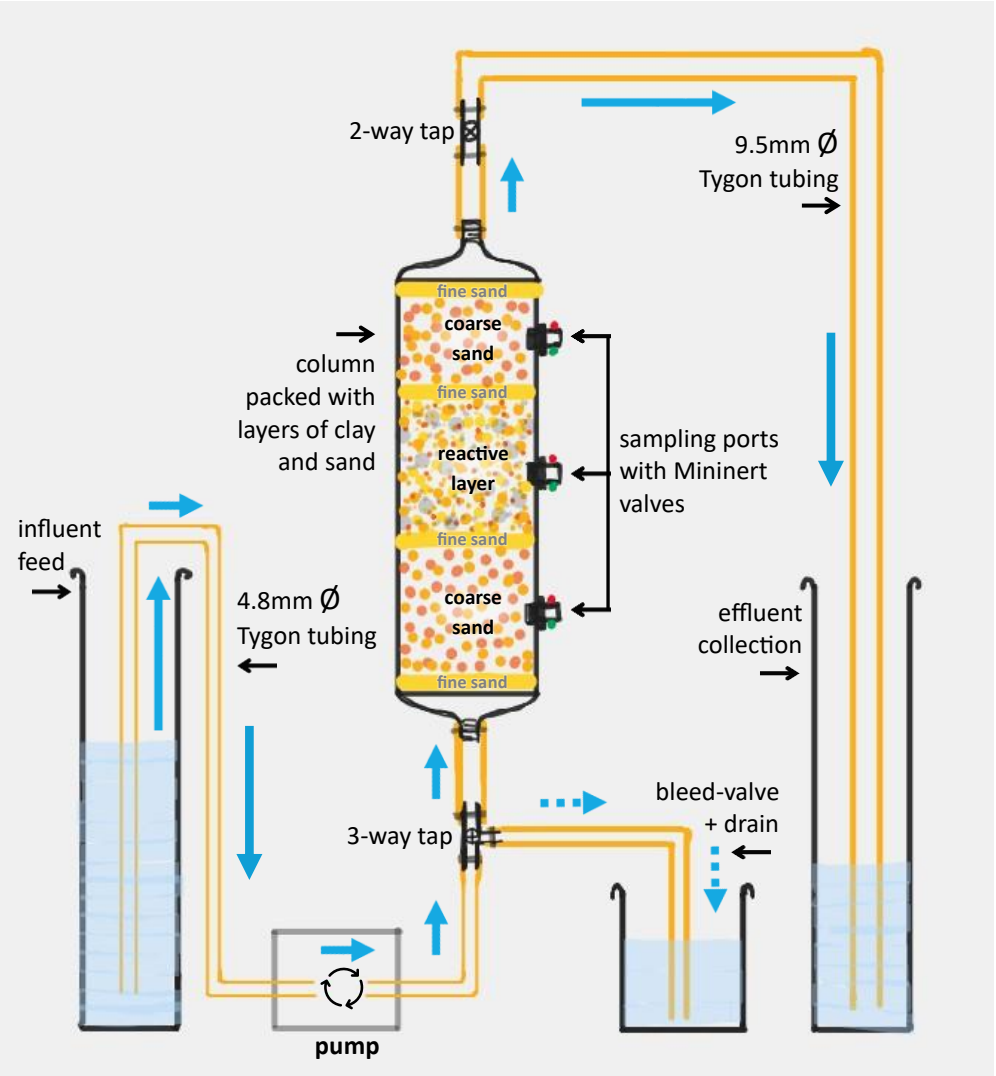

Figure 3. 9. *Sketch of column set-up showing flow direction (yellow arrows), influent feed, effluent collection and drain (yellow dashed arrows). Inline 2- and 3-way tubing taps control exposure to ambient conditions.*

3.3.3 Volumetric flow tests

Saturated and unsaturated conditions in columns can be achieved by adjusting flow to either an upwards or downwards direction, respectively (Banzhaf & Hebig, 2016), however flow tests under saturated conditions were relevant for this study and are reported here.

Besides saturated column pore volume, boundary conditions such as hydraulic retention time were obtained for all experimental columns by a series of volumetric fluid displacement measurements using graduated measuring cylinders. During these measurements, test columns were packed with the columns sediments already dampened to field capacity, according to the final packing regime (Figure 3.2; Section 3.2).

3.3.3.1. Saturated pore volume measurements

Tap water was pumped from a graduated measuring cylinder into each test column influent at a rate of 5 mL/min. When flow reached the column effluent, the volume of fluid displaced from the influent measuring cylinder was noted and the tubing volume subtracted from this to give the sediment pore volume within the column (Table 3. 1).

The optimal flow rate established during testing was around 5 mL/min (Section 01). This was higher than the 0.5-2 mL/min range used in other column studies at Newcastle University (Jarvis, 2020) but was necessary to overcome the relatively low permeability of the clay and sand reactive layer within the columns designed here.

The hydraulic retention time (HRT) for each column was calculated by dividing the column pore volume by the flow rate (Table 3. 2). This aspect of column flow was key to ensuring that the correct volume and concentration of reactants passed through the column during treatment experiments.

Table 3. 2. *Results of volumetric flow tests carried out on large and small test columns, using coarse sand as packing material above and below the reactive layer (containing nontronite clay).*

	Column volume (mL)	**Pore volume (mL)**	**HRT @ 5 mL/min**
Large column	3,100	400	80 mins
Small column	590	250	50 mins

3.3.4 Sampling and monitoring

Samples were collected from the influent feed reservoir and the effluent outlet before, during and after experiments for geochemical and microbiological analysis (Figure 3.9). To capture the geochemical and microbiological dynamics in the reactive layer sediments, all experimental columns were designed with HDPE screw-sealed sampling ports in the centre of the vertical column shaft, next to the reactive layer. The large columns had two further sampling ports installed 100 mm above and below the central port (Figure 3.9) to allow sampling of column sediments and measurement of porewater geochemistry from the upper and lower coarse sand layers. Microbiology samples were also taken from the sampling ports in the large columns to measure variation in microbial abundance related to sediment type.

3.3.4.1. Sampling

Leak-proof, airtight, screw-thread (ID = 13 mm) PTFE Mininert needle valves (Merck, UK) with self-sealing rubber septa were fitted to each column sampling port (Figure 3.9). Porewater

could be extracted through the Mininert valves in ambient conditions during experiments, without perturbing the column redox environment. The Mininert valves accommodated (sterile) 0.8mm bore hyperdermic needles and were compatible with any sterile luer-lock plastic syringe, depending on the sample volume required.

For sediment sampling, experimental columns were sealed using the influent and effluent taps and then transferred to an oxygen-free glovebox. Small quantities of sediment were extracted from the columns via the sampling ports, by unscrewing the Mininert valves and using blunted 1 mL sterile plastic syringe to remove small cores of sediment. For large sediment samples, the entire column was dismantled in the glovebox and sediment collected from the main packed column core. Sediment samples were then sealed in sterile plastic containers and either stored in the glovebox for later analysis or removed and stored in the -80^{o}C freezer.

3.3.4.2. Monitoring

The dissolved oxygen concentrations inside the columns were measured during experiments to indicate redox environment and stage of the treatment process reached. *In-situ* fibre-optic dissolved oxygen (DO) probes (OXROB10, Pyroscience, QCL Scientific Ltd) were sealed inside the central sampling ports of each large experimental column. The DO probes were slowly pushed through a pre-made hole in a 4 mm diameter suba-seal bung, and the bung secured to the outer wall of the sampling port using a hose clip to form an airtight seal with the column (Figure 3.10). The end of each DO probe was attached to a multi-channel Pyroscience FireSting logging unit with a compatible temperature probe attached, and real-time DO data from the column interior were collected and transferred to a PC using Pyro Oxygen Logger software.

Figure 3. 10. *An in-situ dissolved oxygen (DO) probe is sealed inside the central sampling port of large packed experimental column. A suba-seal bung and hose clip are used to form an airtight seal between the probe and the column sampling port.*

During sampling events, physico-chemical parameters of column influents and effluents were monitored (e.g. pH, temperature, DO and conductivity) using a ExStik II (ExTech, EC500) and fluid samples collected taken for determination of metals, inorganic anions and total organic carbon, in order to build up time-series data sets of the column geochemistry.

3.4 Timescale for iron-reduction

The time required for microbial Fe-reduction of the reactive layer nontronite to occur was measured in test experiments using the small column, packed according to the final design regime (Figure 3.2). The small column was saturated with live pondwater (Leazes Park Pond, Richardson Road, Newcastle upon Tyne, NE2 4BJ) that had been supplemented with the nitrogen-phosphorus-potassium (NPK) seaweed-based Green Future Organic Tomato Fertiliser (Growth Technology Ltd, UK) at 1/8 of the recommended strength, equivalent to 0.003125% potassium loading. The pondwater-NPK fertiliser mix was used as an inoculum for microbial Fe-reduction of the nontronite, and to ensure saturation, three column pore volumes (Table 3.2) of the pondwater-NPK fertiliser mix were pumped through the column and the fourth volume allowed to reside. The NPK fertiliser was used as it provided a range

of carbon sources (as electron donors) suitable for the Leazes Park pondwater microbial community to metabolise and thrive on.

Following saturation, the influent and effluent ports of the column were sealed and the column allowed to stagnate for 23 days. After this time, the sealed column was transferred to an oxygen-free glovebox and once inside, the column was unsealed and opened. Approximately 1.5 grams of the reactive layer was removed during destructive column sampling, sealed in a sterile 2 mL vial and temporarily stored in the glovebox.

After this 3-week period, the reactive layer was noticeably green in colour (Figure 3.11), having changed from brown. Following combined sulphuric and hydrofluoric acid digestion of sediment samples and Fe^{2+}/Fe^{TOT} determinations using 1,10 phenanthroline (adapted from Stucki et al. (1984); Amonette & Charles Templeton (1998)), the average microbial reduction extent of Fe within the clay was measured as 23.5% (n=2; Fe^{2+}/Fe^{TOT}) which is typical for the microbial Fe-reduction extent achievable for nontronite and other Fe smectites (Stucki et al., 1987; Ernstsen et al., 1998; Kostka et al., 1996). As no chemical reductants were added to the column, Fe-respiring microbes in the pondwater community are suggested to be responsible for mediating the following redox reactions in the reactive layer of the column:

(i) the oxidation of carbon compounds in the pondwater-NPK fertiliser mix;
(ii) the transfer of electrons (e^-; from the carbon compounds) into the nontronite, as the terminal e^- acceptor;
(iii) the reduction of Fe^{3+} to Fe^{2+} through e^- transfer into the clay mineral structure.

These key findings provided proof-of-concept for the first part of the novel water treatment process proposed here; where microbially-mediated processes alone can activate a Fe-bearing clay mineral, through microbial Fe-reduction in approximately 3 weeks.

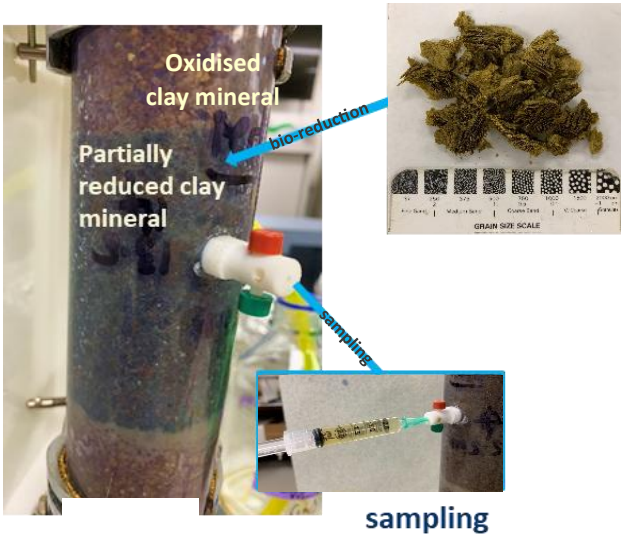

Figure 3. 11. *Microbially-mediated iron reduction evident as a green band in the middle of the small PVC column. The reduction extent of nontronite clay was 23.5% Fe^{2+}/Fe^{TOT} after 23 days.*

3.5 DNA collection from porewater

Porewater sampling protocols (Section 3.3.4.1) were first validated on the small column (Figure 3.11) to ensure reproducibility before being applied to the large prototype column.

Using the sampling approach described in Section 3.3.4.1, the large prototype column was packed according to the final design (Figure 3.2) and used to determine the minimum volume of porewater required for successful DNA sequencing of column microbial communities. Results from this part of the study are provided in Table 3.3 below. This section of work also provided the opportunity for reproducibility tests of the large column pore volume.

Time-series porewater sampling for geochemical analysis during treatment experiments (Chapters 4 and 5) required volumes of up to 100 mL per column flush or pore volume, so ensuring that an adequate volume was available to sample during these times was key.

The large column was saturated as above (Section 3.3.5) and different volumes of porewater (3 mL to 30 mL) were collected through the Mininert needle valves (Figures 3.9, 3.10) during the 3-week stagnation period. Hypodermic needles attached to sterile plastic luer-lock syringes were used to remove porewaters, before then passing them through sterile 0.22 µm Sterivex filter cartridges (Millipore® Sterivex™ Pressure Filter, Merck) with polyethersulfone membranes (Figure 3.12a). The filter cartridges were capped at either end with sterile luer-lock caps (Figure 3.12b) and stored at -80°C for DNA extraction and purification (using

approaches adapted from (Oberacker et al., 2019; Wong et al., 2020)). Providing the DNA quality was sufficient, 16S sequencing using the Illumina MiSeq platfom was then performed.

Table 3.3. *DNA quantities in column porewater and pondwaters extracted from different volume samples. Also shown are DNA concentrations post-PCR to confirm that all sample types and volumes tested would likely amplify sufficiently for Illumina MiSeq sequencing.*

		DNA extracts from lysate (ng/µl)		PCR products (amplified DNA)
Sample tested	**Volume filtered**	**Measured DNA in sample**	**Normalised DNA to 10ml volume**	**Measured DNA (ng/µl) in sample**
Column day 8	3.5	6.56	18.743	58.2
Column Day 15	6	7.56	12.600	62.4
Pondwater	10	0.548	0.548	64.8
Pondwater	30	0.984	0.328	43.2
Pondwater + NPK feed	10	5.56	5.56	65.8
Pondwater + NPK feed	25	6.64	2.656	56.4
NPK feed alone	10	4.16	4.16	54.2

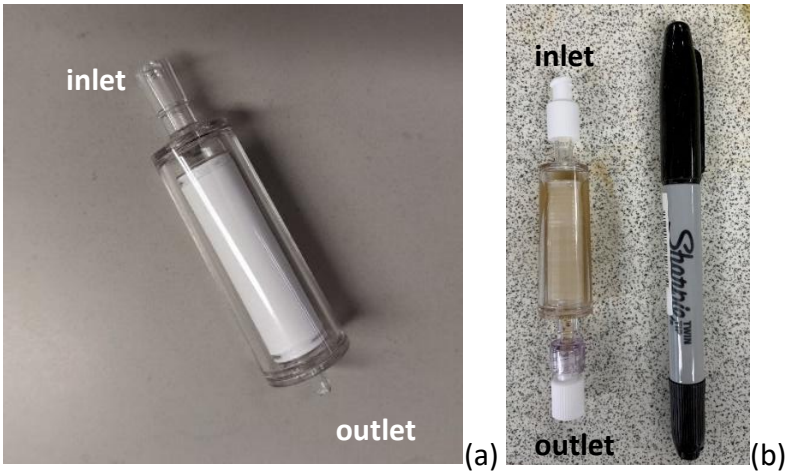

(a) (b)

Figure 3. 12. a) *Empty sterile 0.22 um Sterivex filter cartridge used to filter and preserve DNA from column porewater samples and* ***b)*** *sterivex filter cartridge containing DNA from column porewaters, sealed with sterile luer-lock caps at either end.*

Gel electrophoresis of polymerase chain reaction (PCR) products extracted and purified from the large prototype column over the 3-week stagnation period showed the presence of bacterial DNA in all of the column porewater samples collected (Figure 3.13). Results indicated that as little as 3 mL of porewater from the reactive clay later contained enough viable DNA for meaningful extractions and further sample purification.

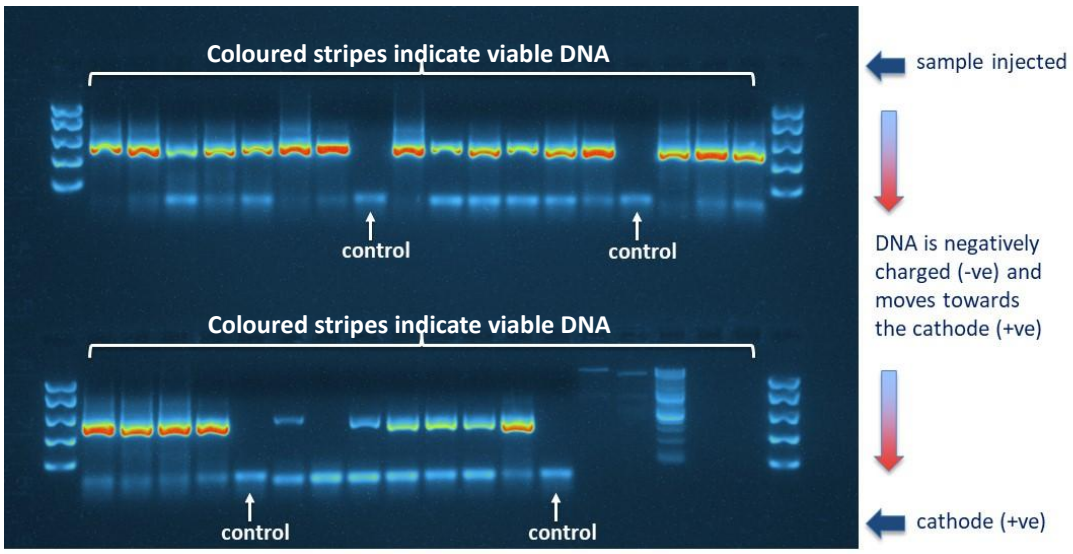

Figure 3. 13. *Gel electrophoresis showed the presence of measurable quantities of bacterial DNA, compared to a negative control, in the large prototype column.*

Porewater samples collected from the large prototype columns were also used to acquire baseline concentrations for metals (using ICP-OES) and inorganic anions (ion chromatography). Total organic carbon measurements of the pondwater inoculum and column extracts were initially measured to check compositional variation over time, but these data are not reported in detail in the thesis.

3.6 Conclusions

The final column design was reached by considering four main aspects of column development. These were:

(i) column packing materials;

(ii) fluid flow;

(iii) column dimensions and construction, and

(iv) design of sampling and monitoring ports.

The two other areas of experimental development work were considered key to adequately being able to test the proof-of-concept water treatment system that this thesis presents.

Firstly, ascertaining the timescale for microbial Fe-reduction, as the first stage of the treatment process, is important in ensuring that the second treatment step can occur at the correct point: once the content of ferrous Fe is at a maximum and oxygen saturation is low. The work described in Chapter 4 will test the second stage of the treatment, where

oxygenation of ferrous Fe should lead to the generation of hydroxyl radicals and an organic probe is used to test treatment success.

Secondly, confirming the viability of DNA extracted from porewater samples is critical to assessing the sustainability of the treatment process. If the column environment cannot sustain a microbial community through successive treatment cycles then treatment system may not offer a feasible low-carbon water treatment solution. Chapter 5 presents the results of biological column experiments designed to test the feasibility of a self-sustaining water treatment system and describes the microbial community composition alongside the water treatment efficiency (Figure 3.14).

Figure 3. 14. *Outline of biological column experiment designed to test the efficiency of water treatment alongside microbial community compositional analysis.*

4. Chemical Column Experiments

4.1 Introduction

It is now well known that micropollutants, e.g. pharmaceutical residues, pesticides and other organic contaminants, remain in conventionally treated wastewater effluents as these pollutants are not completely removed by most common treatment methods (Margot et al., 2015; Rekhate & Srivastava, 2020; Zhang et al., 2023; Lee & von Gunten, 2010; Margot et al., 2013; Schwarzenbach et al., 2010). These recalcitrant compounds pose an emerging threat to our water resources due to their detrimental effects on human and aquatic health (Schwarzenbach et al., 2010). However, the degradation of these (primarily) organic pollutants can be effectively achieved using advanced oxidation processes (AOPs). Advanced oxidation relies mainly on the production of reactive oxidizing species such as OH radicals (•OH) (Oturan & Aaron, 2014; Rekhate & Srivastava, 2020; Chitra et al., 2012; Pandis et al., 2022), sulphate radicals (SO_4^-•) (Deng & Zhao, 2015; Mezyk et al., 2011), or more generally reactive oxygen species (ROS), which include •OH, hydrogen peroxide, superoxide radical and ozone.

Currently applied AOPs in water treatment, e.g. ozonation and UV irradiation (or combinations of these), are energetically and chemically expensive with a high-carbon footprint. The water industry is under considerable pressure to reduce carbon emissions arising from water treatment processes (Intergovernmental Panel on Climate Change, 2019) and sustainable, low-carbon, low-cost and low-input treatment alternatives are urgently required. One such alternative could be to harness naturally occurring processes for the effective and sustainable production of •OH.

Recent studies have shown that •OH can be effectively generated during the oxygenation of natural ferrous iron-bearing clay minerals, e.g. nontronite (Xie et al., 2020; Liu et al., 2017; Tong et al., 2016; Zeng et al., 2017). The 'activation' of iron-bearing clay minerals, through reduction of clay mineral structural iron from ferric (Fe^{3+}) to ferrous iron (Fe^{2+}) has previously been reported in laboratory studies using either chemical agents (Stucki et al., 1984; Ribeiro et al., 2009; Pham et al., 2012; Komadel et al., 2006; Gates et al., 1996; Zeng et al., 2016; Joe-Wong et al., 2017) or microbial respiration (Wang et al., 2017; Zhao et al., 2015; Zeng et al., 2017; Ernstsen et al., 1998; Gates et al., 1996; Stucki et al., 1987; Kostka et al., 1996; Bishop et al., 2014; Ribeiro et al., 2009; Wu et al., 1988). It is not known at present whether and

how these two processes, so far studied mostly in isolation, can be combined in one (treatment) system for the sustained removal of micropollutants during repeated treatment cycles.

This thesis chapter aims to address this knowledge and technological gap by conducting column experiments, in which the same Fe-bearing clay mineral will be activated by Fe reduction and used for oxidative degradation of a surrogate micropollutant in repeated treatment cycles. In this proof-of-concept study, the overall AOP treatment will be simplified from a system using microbial activity for clay activation (Chapter 2, Figure 2.3) to one using the chemical reducing agent, sodium dithionite (Komadel et al., 2006, 1990) (Figure 4.1).

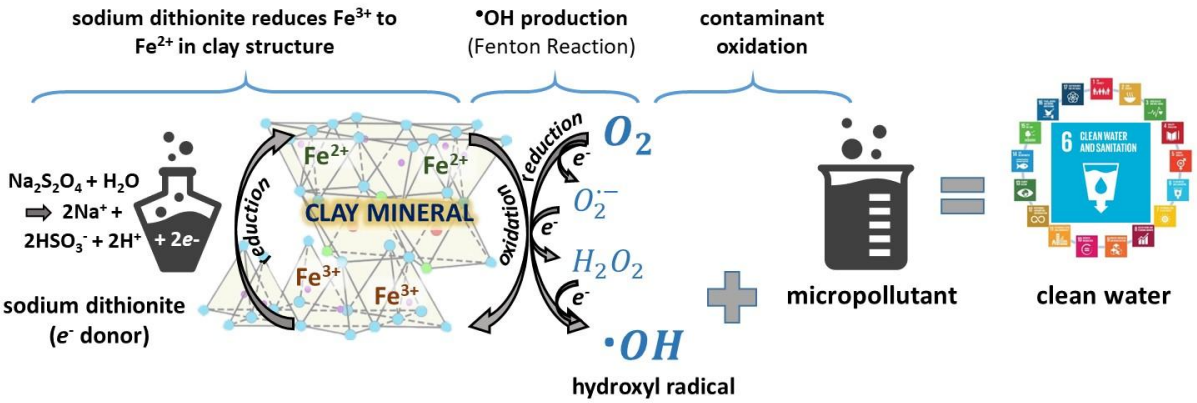

Figure 4. 1. *Schematic showing the simplified AOP relying on clay mineral activation via reduction of clay mineral structural iron through transfer of two electrons from the chemical reductant sodium dithionite ($Na_2S_2O_4$). The treatment portion of the AOP remains the same with stepwise reduction of dissolved oxygen by clay mineral Fe^{2+} to yield the reactive oxygen species hydroxyl radical (•OH) for the degradation of micropollutants.*

The chapter will address the following specific objectives:

(i) verify that the Fe-bearing clay mineral nontronite can be activated using a chemical reducing agent over repeated treatment cycles and in flow-through, benchtop column experiments;

(ii) determine whether •OH can be generated *in situ* through oxygenation of the activated nontronite within the same column experiment and if so, to quantify the yield of •OH, using benzoic acid as a quantitative scavenger;

(iii) identify whether the sustained activation of nontronite and the treatment of benzoic acid within the same column experiment is possible over repeated treatment cycles, quantifying the loss of Fe and/or clay during the experiments.

Sodium dithionite ($Na_2S_2O_4$; Sigma UK) was used to activate the nontronite as it is still considered the most effective method of reducing structural Fe^{3+} to Fe^{2+} in nontronites (Figure 4.1, left and centre) (Komadel et al., 2006, 1990). To perform each treatment cycle, the production of •OH *in-situ* (Figure 4.1 centre) was stimulated by flowing an oxygenated synthetic wastewater spiked with the chemical probe benzoic acid (BA) through the column (see Chapter 2, Section X for redox reaction scheme). Treatment effect was determined by measuring 4-hydrobenzoic acid (4-HBA) in the column effluent, as a product of BA dehydroxylation by •OH (Figure 4.1 centre, Figure 4.2). Benzoic acid was selected over other •OH scavengers due to its elevated reaction rate with •OH in ambient conditions (Buxton et al., 1988; Zhang et al., 2019) and its use in comparable research studies (Zhang & Yuan, 2017; Wu et al., 2017; Zhang et al., 2016; Liu et al., 2020).

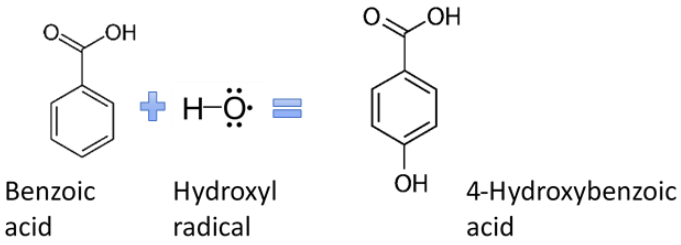

Figure 4. 2. *Transformation of benzoic acid to 4-hydroxybenzoic acid through hydroxylation with a hydroxyl radical.*

The following sections of this chapter describe results from the chemical treatment experiments, notes lessons learnt from this work and places the results in the context of other relevant studies reported in the literature.

4.2 Methods

4.2.1 Experimental set-up

Two small PVC benchtop columns were used for the chemical activation and treatment experiments. These small columns had the same generic design to that described in Chapter 3 (Section 3.2) for the large biological test columns. Small adaptations to the overall dimensions (50 mm diameter, 300 mm packing height) yielded a smaller total column volume of 589 mL and a smaller column pore volume of 250 mL (Chapter 3, Table 3.2). The small columns also had only one sampling port midway along the vertical length of the column shaft. One of the chemical test columns was used to perform repeat treatment experiments

and the second test column was used as a control. The packing configuration for the chemical columns is described in Section 4.2.3.

4.2.2 Design modifications to chemical column experiments

Some modifications to the overall experimental set-up were necessary to accommodate the transfer of oxygen-free solutions into the chemical columns. An oxygen-free reservoir bottle with gas-tight cap was set-up to allow oxygen-free (de-oxygenated) solutions to be supplied to the column experiment via the influent port (Figures 4.3 and 4.4a-b). This was necessary to prevent oxygen (O_2) from entering the column experiment and to ensure that once the chemical reducing agent (sodium dithionite) was flushed through the column sediments, clay activation could successfully be achieved (Figure 4.1, left side) through reduction of clay mineral structural Fe (from Fe^{3+} to Fe^{2+}). Using this approach, it was assumed that the reaction of sodium dithionite with any residual O_2 trapped inside the column sediments would be negligible.

To effectively supply each of the de-oxygenated influent solutions (these specified in Table 4.4) to the column experiments, two modified 1 mL sterile plastic syringes were inserted through the red rubber septum in the cap of each DURAN bottle and fitted to lengths of Tygon tubing with in-line 2-way HDPE directional taps attached, to form gas-tight inlet and outlets ports (Figure 4.4a-b). A suitable length of Tygon tubing was also fitted to the lower end of outlet port, so that the de-oxygenated solution inside the DURAN bottle could be drawn up into the tubing during pumping (Figure 4.4b). Before removing the de-oxygenated solutions from the glovebox, the in-line tubing taps on the inlet and outlet ports of each DURAN bottle were closed to prevent solution leakage and ensure that the bottle was gas-tight.

At the start of all chemical column experiments, Tygon tubing attached to the inlet tap of the DURAN bottle was securely fitted to an oxygen-free nitrogen (N_2) gas supply (Figure 4.3). A steady state flow of N_2 was established and adjusted so that the pumping rate used during chemical column experiments was equivalent to the N_2 flow rate. This ensured that changes in headspace-to-solution ratios during the pumping of de-oxygenated solutions from the DURAN bottle could be accommodated during experiments and prevent a vacuum forming inside the bottle.

Using the 2:1 stoichiometry reported in the literature (Stucki et al., 1984; Ribeiro et al., 2009; Pham et al., 2012; Komadel et al., 2006; Gates et al., 1996; Zeng et al., 2016; Joe-Wong et al., 2017), sodium dithionite was used to achieve specific Fe reduction levels, i.e. Fe^{2+}/Fe^{TOT} ratios, in the clay mineral[17–23]. For the first chemical treatment cycle, a target reduction level of 19% (Fe^{2+}/Fe^{TOT}) was used to represent an achievable microbial Fe reduction level. This target was based on the mean Fe^{2+}/Fe^{TOT} reduction level of 23.5% obtained in biological column reduction tests after 23 days (Chapter 3, Section 3.3.5). Calculations relevant to solution composition used in the chemical column experiments are provided in Appendix B.

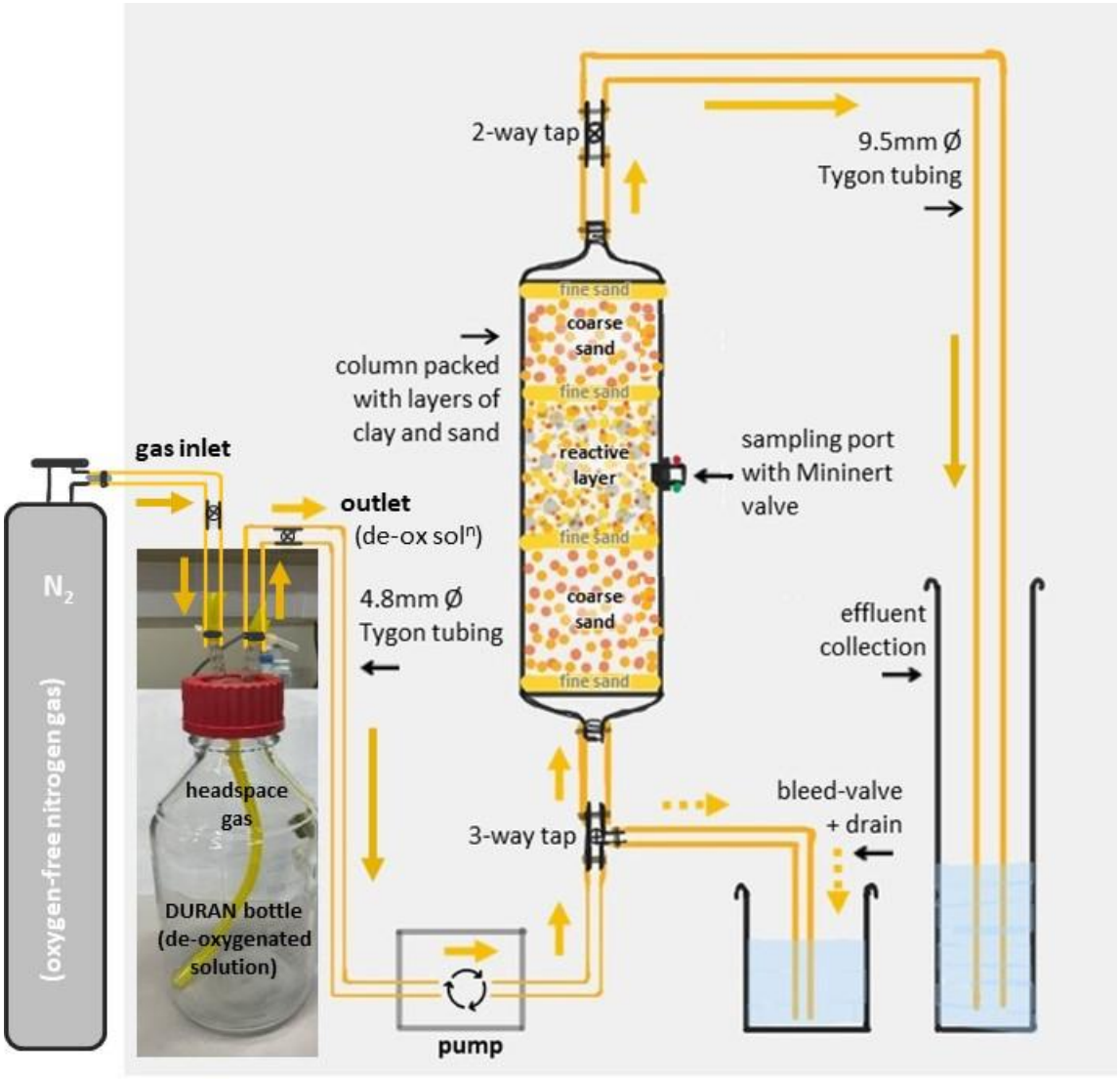

Figure 4. 3. *Chemical column experiment schematic showing the gas-tight influent reservoir (1 L DURAN bottle, lower left) supplying the column influent feed, via Tygon tubing. A nitrogen gas supply was used to add gas to the headspace in the gas-tight DURAN bottle as de-oxygenated influent solutions were supplied to the chemical column via a peristaltic pump. Also shown are flow direction (yellow arrows), the chemical column (packed according to the method previously specified; Chapter 3, Section 3.3.2) and effluent collection into a measuring cylinder.*

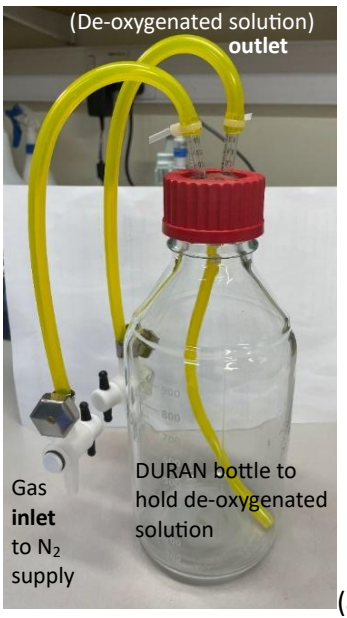

(a)

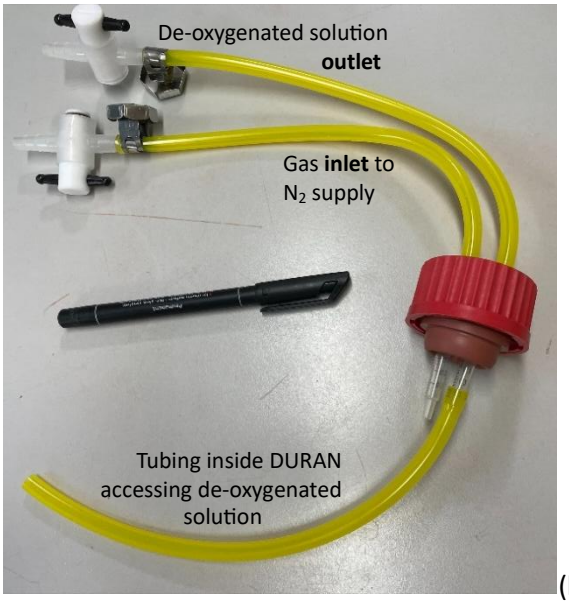

(b)

Figure 4. 4. (a) *Borosilicate glass 1 L DURAN bottle used to supply de-oxygenated influent solutions to the chemical column experiments. Two modified 1 mL sterile plastic syringes were inserted into the GL 45 red rubber septa to form inlet and outlet ports* ***(a, b)****. Each inlet and outlet port was attached to Tygon tubing fitted with in-line 2-way directional gas-tight taps* ***(b)*** *to allow: (i) de-oxygenated solutions to remain oxygen-free once removed from the glovebox and during supply to the chemical column experiment; and (ii) nitrogen (N_2) gas to enter the DURAN bottle to replace lost headspace during removal of de-oxygenated solutions through pumping to the chemical column influent port during experiments.*

4.2.3 Column packing

The chemical columns were assembled using the same methodology and packing configuration as described in Chapter 3 (Figure 3.2 and Section 3.3.1), with adjusted sediment proportions to reflect the smaller column volume. Briefly, this involved combining 4.2 g nontronite clay (< 2 µm size fraction, freeze-dried; Chapter 3, Section 3.3.1) by thorough mixing with fine, medium and coarse sand grades in the masses specified in Table 4.1 and dampened to field capacity. Separate layers of fine sand and coarse sand were weighed out (Table 4.1) and packed into the chemical treatment experiment column, above and below the 'reactive layer' (Figure 4.3), which occupied the central section of the column to an equivalent dry weight of 1.5% nontronite. Geotextile discs saturated with 15 MΩ/cm reverse osmosis (RO) water were placed inside each end of the column shaft at the outer bounds of the sediment, and the column was sealed using 6 hand-tightened screw-nuts. The sand-only chemical control column was packed using the same methodology but the nontronite clay was omitted from the reactive layer and the sand proportions adjusted to ensure that the same total mass of sediment was packed within the column (Table 4.1). All columns were then inverted before the start of the experiments, to aid flow dynamics.

***Table 4. 1**. Inventory of sediments packed in chemical column experiments, where repeat chemical treatment experiments used clay and sand (a) and control experiments used sand-only columns (b).*

(a)	**Clay + sand column**				
	Nontronite clay (<2 µm)	Very fine + fine sand (0.063-250 µm)	Medium sand (250-500 µm)	Coarse sand (0.5-2 mm)	Totals
Mass reactive layer (g)	4.2	75	150	50	279.2
% reactive layer	1.5	26.9	53.7	17.9	100
Mass in column (g)	4.2	140	150	610	904.2

(b)	**Sand only column**				
	Nontronite clay (<2 µm)	Very fine + fine sand (0.063-250 µm)	Medium sand (250-500 µm)	Coarse sand (0.5-2 mm)	Totals
Mass reactive layer (g)	-	76.3	152.2	50.7	279.2
% reactive layer	-	27.3	54.5	18.2	100
Mass in column (g)	-	142.1	152.2	609.9	904.2

Using the same tubing configuration described in Chapter 3, Section 3.2, lengths of food-grade Tygon tubing (ID = 0.9 mm) supplied by Saint Gobain (RS Components Ltd) were attached to hose fittings at the top and base of the columns and used as influent and effluent ports, respectively (Figure 4.3).

4.2.4 Preparation of reactant solutions

Oxygen-free solutions ('de-oxygenated') were used during the initial 'activation' phase of the chemical column experiments (Figure 4.1, left side) and prepared inside an oxygen-free glovebox (N_2: 100%, O_2 < 1ppm; GS Glovebox Systemtechnik GmbH, Germany). De-ionised water (18 MΩ/cm) was de-oxygenated by bubbling with a steady flow of oxygen-free nitrogen (N_2) for 2 hours per litre before transfer to the glovebox and combination with anhydrous salts to generate the required solutions. De-oxygenated solutions were then transferred to acid-washed, 1 L borosilicate glass bottles fitted with gas-tight GL 45 DURAN plastic caps with compatible red rubber septa, attached to Tygon tubing and gas tight taps (Section 4.2.2; Figures 4.4a-b). Before removal from the glovebox, all gas-tight taps attached to tubing and bottles were securely closed.

Oxygenated solutions for the treatment phase of the experiment were prepared outside the glovebox under normal laboratory conditions. Open bottles of solution were equilibrated for 2 hours with the atmosphere or until the solutions reached a dissolved oxygen concentration of ≥10 mg/L O_2.

To prevent mobilisation of clay fines from the column (Cihan et al., 2022), and to minimise ionic gradients between the clay mineral and column porewaters, the ionic strength (IS) of all

solutions were adjusted to values similar to that of secondary clarifier effluent from a wastewater treatment plant in the North East of England. The IS was estimated from mean measured values (n = 3) for total dissolved solids (TDS) of 630 mg/L and using a conversion factor (Equation 4.1), yielded a target IS of 0.0158.

$$2.5 \times 10^{-5} \times TDS\ (mg/L) = IS_{estimate} \qquad \textit{Equation 4.1}$$

The concentrations of all reactant solutions, except that of BA, were adjusted to approximate the target IS, making use of *Equation 4.2* and considering the charge Z of each ionic species '*i*':

$$IS = 0.5 \times \Sigma(C_i Z_i^2) \qquad \textit{Equation 4.2}$$

Solutions of sodium dithionite were prepared following the method of (Stucki et al., 1984) and concentrations were calculated using the known 1:2 stoichiometry of Fe^{2+} formed per Fe^{3+}. Molar amounts of sodium dithionite were calculated by multiplying clay mineral Fe^{TOT} by 0.19 and 0.38 to obtain clay mineral Fe^{2+} at 19% and 39% reduction, respectively, then multiplying these values by 0.5 (Table 4.2).

Benzoic acid (BA) was chosen as chemical probe to determine •OH formation rates and yields because its hydroxylation products (Zepp et al., 1987; Lee & von Gunten, 2010; Zhang & Yuan, 2017; Zhang et al., 2019; Liu et al., 2020; Tong et al., 2016), most notably the OH-adduct 4-hydroxy benzoic acid (4-HBA), can easily be monitored and quantified. Complete scavenging of •OH by BA was achieved through excess loading of BA (Table 4.2), using greater than three times the BA concentration needed to quantitatively scavenge the maximum possible amount of •OH. The maximum possible yield of •OH was calculated from the clay mineral Fe^{2+} content and the known 1:3 stoichiometry of •OH formed per Fe^{2+} oxidised (Table 4.2).

Table 4. 2. *Calculations and assumptions made to determine an appropriate concentration of benzoic acid (BA) to use in chemical column experiments.*

Target reduction level	19%	38% *
Fe^{2+} in 4.2 g nontronite	3.3 mmol	6.7 mmol
sodium dithionite needed for target reduction (stoichiometry: 1:2 moles Fe^{2+})	1.6 mmol	3.4 mmol
•OH generated (stoichiometry: 1:3 moles Fe^{2+})	1.08 mmol	2.2 mmol
BA needed for quantitative reaction with •OH	1.08 mmol	2.2 mmol
provide BA in >x3 excess to outcompete •OH reaction with other species	7.5 mmol	7.5 mmol
BA in total pore volume of 500 mL (column flush 4; Table 4.4)	15 mM	15mM

* calculations for 38% target reduction assumes 4 g nontronite, to account for sediment removal during solid sampling after 1st treatment cycle.

4.2.5 Validation batch experiments

To establish whether the target reduction levels of 19% and 38% (Fe^{2+}/Fe^{TOT}) had been achieved during activation of the chemical column experiments, batch experiments were set up in 120 mL serum bottle inside the oxygen-free glovebox and run in triplicate.

Serum bottles were each filled with 26.6 g sediment comprising either 400 mg nontronite clay and sand (representing the column reactive layer), or sand-only (as controls), and then moved into the glovebox. Before capping, microcosms were reduced using de-oxygenated solutions of sodium dithionite in concentrations appropriate to achieve either 19% or 38% (Fe^{2+}/Fe^{TOT}) reduction (Table 4.3), to represent activation of the chemical column reactive layer.

All serum bottles were sealed with butyl rubber stoppers, crimp-capped and placed on a shaking table at 100 rpm for 3 h, to represent the equivalent time of reduction in the column experiments. Then, sediments were allowed to settle for at least 24 h inside the glovebox before sediment samples were extracted under oxygen-free conditions (Section 4.2.7).

Table 4. 3. *Concentrations of reagents used to achieve clay activation in iron reduction batch experiments, with 100 mL total volume, 400mg of nontronite clay and associated sand proportions, as used for the chemical column experiments.*

Reagents	Target reduction	Sediment combination + replicates	
0.16 mM sodium dithionite in 1:8 1N sodium citrate : 1M sodium bicarbonate	19%	clay + sand X3	sand only X3
0.31 mM sodium dithionite in 1:8 1N sodium citrate : 1M sodium bicarbonate	38%	clay + sand X3	sand only X3

4.2.6 Column operation

Four treatment cycles were completed using the clay and sand chemical column, where each treatment cycle comprised five sets of column flush, each with different influent solutions

(these are detailed in Table 4.4). The first treatment cycle had a target nontronite reduction level of 19% and the subsequent 3 three treatment cycles had reduction targets of 38%; this scheme is illustrated below in Figure 4.5, to supplement Table 4.4. The sand-only control column was operated through one complete treatment cycle only. All columns were operated in an upflow direction at 5 mL/min.

Table 4. 4. *Summary of influent solutions associated with each column flush (within each treatment cycle) and concentrations of reagents used to achieve clay activation and oxidative treatment. A target nontronite Fe reduction of 19% was set for the first treatment cycle and 38% thereafter.*

	Column flush				
Treatment cycle	**1. De-ox wash**	**2. Activation by reduction ***	**3. De-ox wash**	**4. Ox + BA**	**5. Ox wash**
1: target 19% reduced nontronite	16.4 mM sodium bicarbonate	2.2 mM sodium dithionite** in 1:8 1N sodium citrate : 1M sodium bicarbonate	16.4 mM sodium bicarbonate	15 mM BA in 4.1mM sodium bicarbonate	16.4 mM sodium bicarbonate
2, 3 & 4: target 38% reduced nontronite	16.4 mM sodium bicarbonate	4.3 mM sodium dithionite** in 1:8 1N sodium citrate : 1M sodium bicarbonate	16.4 mM sodium bicarbonate	15 mM BA in 4.1mM sodium bicarbonate	16.4 mM sodium bicarbonate
No. flushes	2	3	3	2	3
Pore volume	500mL	750mL	750mL	500mL	750mL
Redox state	Anoxic	Anoxic	anoxic	Oxic	Oxic

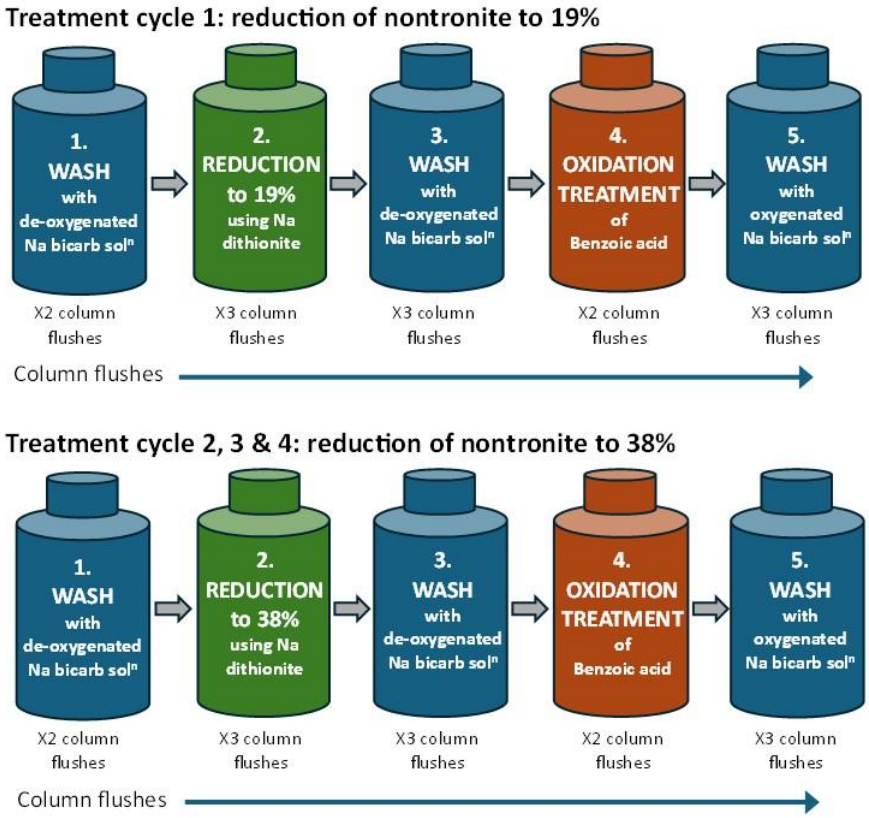

Figure 4. 5. *Schematic showing the difference between treatment cycle 1 and treatment cycles 2, 3 and 4 in the chemical column experiments. The target nontronite reduction level for treatment cycle 1 was 19% whereas the target reduction levels for treatment cycles 2, 3 and 4 was 38%.*

First, to remove any O_2 trapped within column sediments before activating the nontronite (Table 4.4, '1. De-ox wash'), two column pore volumes (500 mL) of deoxygenated sodium bicarbonate buffer (16.4 mM) were flushed through the chemical columns. Secondly, nontronite Fe was activated by reduction with 3 pore volumes of 2.2 mM or 4.3 mM sodium dithionite in citrate-bicarbonate buffer, depending on the target nontronite reduction level (Table 4.4, '2. Activation by reduction'). Third, unreacted and/or remaining sodium dithionite solution was washed out of the chemical columns using three pore volumes of de-oxygenated 16.4 mM sodium bicarbonate buffer (Table 4.4, '3. De-ox wash'). Fourth, Fe^{2+} oxidation was initiated by flushing the column with oxygenated sodium bicarbonate buffer (4.1 mM) and •OH produced were quantitatively scavenged by the chemical probe BA (15 mM), contained in two column pore volumes (Table 4.4, 4. 'Ox + BA'). Lastly, three column pore volumes of oxygenated sodium bicarbonate buffer solution were used to wash any remaining BA probe out of the columns and completely oxidise nontronite Fe (Table 4.4, 5. 'Ox wash').

During all treatment experiments, Tygon tubing attached to the top of the column drained effluent flow directly into a collection measuring cylinder (Figure 4.3).

4.2.7 Sampling and geochemical analysis

All aqueous samples were collected directly from effluent flow tubing, before reaching the collection measuring cylinder (Figure 4.3). Aqueous sample handling and analysis are described below in Sections 4.2.7.1-3 and were used to determine clay mineral dissolution, •OH production and success of BA treatment.

During experiments, small sediment samples (~200 mg) were extracted for Mössbauer analysis (Section 4.2.7.6) from treatment and control columns to assess any mineralogical changes that had occurred following the experiments. Samples were only extracted twice: after the first cycle of clay activation and after the last BA treatment cycle, in order to avoid compromising the integrity of the column sediments and adversely affecting flow dynamics. Column sampling was carried out inside an oxygen-free glovebox using a modified 1 mL sterile plastic syringe to extract a small sediment core from column reactive layers, via the central sampling port. To ensure sediments were representative of the column redox

environment and minimise oxidation of reduced clay or iron minerals, samples were stored securely inside the glovebox until analysis.

Sediments sampled from microcosm experiments were analysed for Fe^{2+} and Fe^{TOT} (Section 4.2.7.5) to estimate Fe reduction extent of column sediments, before and after clay activation and treatment (representing one treatment cycle). Samples were extracted from microcosm serum bottles under oxygen-free conditions using a 3 mL sterile plastic syringe with a wide nozzle, to ensure representative sediment sampling, and were stored inside the glovebox until analysis.

4.2.7.1. Aqueous sample prep for cation and anion analysis

Samples of column effluent were collected every 50 minutes during experiments (through column flushes 1-5, Table 4.4), for elemental analysis of Fe, aluminium (Al), silicon (Si), sodium (Na) and sulphur (S) by Inductively coupled plasma – optical emission spectrometry (ICP-OES; Agilent ICP-OES 5800 Series) to determine (clay) mineral dissolution during the treatment process. During the first treatment cycle, samples were only collected during and after clay oxygenation and BA treatment (through column flushes 4-5, Table 4.4), not during activation of the clay. Samples were collected throughout all subsequent treatment cycles.

Colloidal metals were determined by immediately acidifying 10 mL of effluent sample to 1% of the total sample volume with 70% nitric acid then filtering through a 0.22 µm PTFE filter after 48 h, whilst total metals were determined by filtering 10 mL effluent immediately on collection and then acidifying using the same approach. All samples were then stored at 4 ^{o}C. Reagent stock solutions (as controls) were prepared for elemental analysis by filtration and acidification (as above) and selected standards analysed five or ten times to test for ICP-OES stability. Sample and stock solutions were diluted if the TDS was found to be greater than 1000 ppm prior to analysis. ICP-OES quantification limits for metals of interest are shown in Appendix B (Table B2).

4.2.7.2. Aqueous sample prep for organics analysis

Column effluent samples were collected for organics analysis using High Performance Liquid Chromatography (HPLC; Section 4.2.7.3) before, during and after clay oxygenation and BA treatment (through column flushes 3-5, Table 4.4), at approximately 10 min intervals over 3 h. To quench •OH formation during sample storage, HPLC-grade methanol (MeOH) was

added to all samples at a 1:1 ratio immediately on collection, the samples mixed thoroughly and then filtered through 0.22 µm nylon syringe filters before being stored at 4 °C.

4.2.7.3. Organic compound quantification

HPLC (Agilent Infinity 1260) was used to quantify the probe compound benzoic acid (BA) and its degradation product 4-hydroxy benzoic acid (4-HBA) in column effluent samples. A Gemini C18 column (4.6 mm pore size, 100 mm length) was used to together with MeOH and de-ionised water as mobile phases, both amended with 0.1% formic acid to buffer pH to 2.3-2.5 and ensure that BA and 4-HBA were fully protonated during elution. Samples were analysed on a gradient program (total run time 9 min), starting at MeOH/H_2O 5/95 with a ramp to 95/5 over 5 min and hold at 95/5 for 1.5 min, followed by a 1.5 min ramp starting at 95/5 (MeOH/H_2O) and decreasing to 5/95, ahead of the next sample injection (further program details in Appendix B, Figure B.1). Combined standards of 0.3-30 µM 4-HBA and 0.2-20 mM BA were used to generate calibration curves for BA and 4-HBA which allowed the conversion of integrated peak to concentrations. The quantitative limit of detection for BA and 4-HBA was determined to be 0.1 µM (based on the analysis of replicate standards), corresponding to 0.59 µM for •OH. HPLC was selected because both BA and 4-HBA should be detectable in a single run and the technique is non-specialist and inexpensive, so potentially accessible in low- to middle-income countries.

The concentration of •OH in each sample was calculated from the concentration of 4-HBA multiplied by the known branching ratio of 5.87 (Zhou & Mopper, 1990; Mopper & Zhou, 1990; Tong et al., 2016) for the adduct formation reaction of BA with •OH (Zhou & Mopper, 1990; Mopper & Zhou, 1990; Tong et al., 2016).

4.2.7.4. Aqueous parameters monitored in situ

A calibrated Extech EC500 Waterproof ExStik® II was used to measure pH and total dissolved solids (TDS) of reagent stock solutions, to check for reproducibility at the start of each treatment experiment. Oxygen saturation of column porewater during the activation and treatment stages of the fourth treatment cycle was monitored using an *in-situ* ROB-OX-10 robust dissolved oxygen (DO) probe (Pyroscience, Germany) inserted through the sampling port of the column. A portable Hach meter with DO probe was used as a secondary measure of oxygen saturation in column effluent from the same cycle.

4.2.7.5. Elemental and speciation analysis of solids

Concentrations of Fe^{TOT} and Fe^{2+} in sediment samples were determined photometrically, using a hydrofluoric acid (HF) mineral digestion combined with a modified version of 1,10 phenanthroline method adapted from (Stucki, 1981; Amonette & Charles Templeton, 1998), described by (Neumann et al., 2011). Native (oxidised) nontronite, sand and pristine reactive layer sediments were analysed alongside reduced column sediments, extracted after the first clay activation and after the fourth complete treatment cycle using the approach described in Section 4.2.7. This techniques was also used to measure the (Fe^{2+}/Fe^{TOT}) ratio of sodium dithionite-reduced microcosm sediments (combined and sand-only), described in Section 4.2.5.

4.2.7.6. Mössbauer analysis of solids

Up to 100 mg of sediment was sealed between layers of Kapton tape to prevent oxidation during loading into the S4 Mössbauer spectrometer (SEE Co., Edina, MN, U.S.A.). During analysis, the instrument was operated in transmission mode, calibrated using a 7 µm α-Fe^0 foil and during spectra acquisition, temperature was controlled using a closed cycle cryostat (SHI-850, Janis Research Co., Wilmington, MA, U.S.A.) at 13 K or 77 K, to allow quantification of solid-phase Fe oxidation state and Fe reduction extent of the nontronite. Recoil software was used to analyse raw data, with a Voigt-based fitting routine. Credit is given to Dr Anke Neumann for assistance with interpretation of Mössbauer spectra.

4.2.7.7. X-ray diffraction analysis of solids

Mineralogical analysis was carried out to check for Fe mineral phases present within the column sediments ahead of treatment experiments. Dry sand and clay samples were powdered to <50 µm using an agate pestle and mortar and analysed on a PANalytical X'Pert Pro Multi-Purpose Diffractometer operated at 40 kV and 40 mA. Samples were scanned over a 2θ range of 2-65° with a step size of 0.0334°. Phase identification was carried using HighScore Plus in combination with the ICDD 2004 crystallographic database.

4.3 Results and discussion

4.3.1 Clay activation

Following activation with sodium dithionite, the nontronite-bearing reactive layer of the chemical column changed from its initially brown to a dark green colour (Figure 4.6). This colour change is typical of structural Fe reduction from Fe^{3+} to Fe^{2+} in the NAu-2 nontronite (Huang et al., 2018) and specifically Fe^{3+} reduction within the octahedral layer (Komadel et al., 1990).

Clay activation within the chemical column reactive layers was estimated by measuring Fe^{2+}/Fe^{TOT} ratios (Section 4.2.7) from triplicate sets of nontronite and sand microcosm batch experiments (Section 4.2.5.), using target Fe reduction extents of 19% and 38%. This approach was adopted to avoid removing too much sediment from the chemical columns or compromising the packing integrity between treatment cycles. The aim of the batch experiments was to determine how closely the target activation (reduction) level for each treatment cycle compared to the actual nontronite reduction level achieved inside the chemical column experiments.

4.3.1.1. Results from batch reduction experiments

All of the microcosm batch experiments showed some level of Fe reduction and chemically reduced nontronite in the clay + sand microcosm batches turned from brown to brown-green (Figure 4.7a, left side) or to deep-green (Figure 4.7b, left side) at the target reduction levels of 19% and 38%, respectively. Because the same ratio of reactive layer to chemical reductant was used, the results from batch experiments can be extrapolated to the reduction extent in the chemical columns. The results strongly suggest that nontronite Fe^{3+} in the reactive layer of the chemical column experiments was also reduced on exposure to sodium dithionite. The sand-only microcosms showed no clear colour change at either target reduction level (Figure 4.7a-b; right).

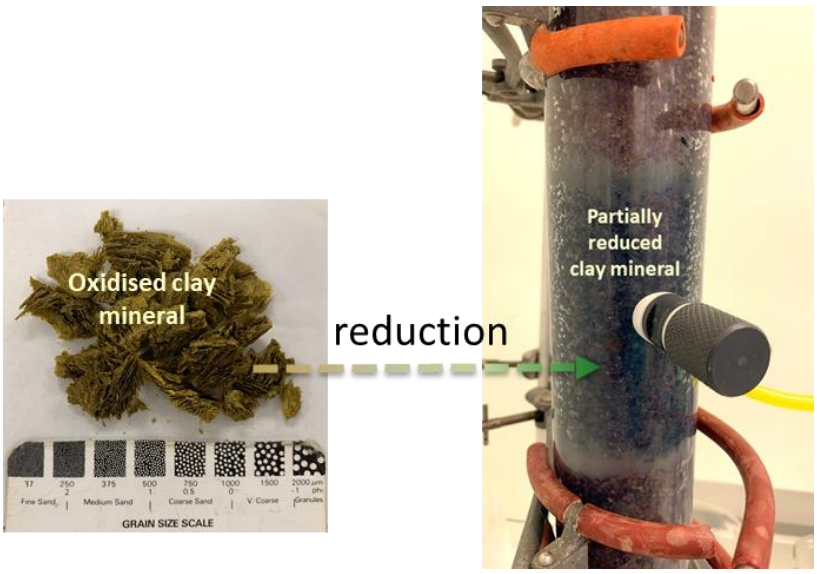

Figure 4. 6. (a) *Dry mass of native nontronite clay (NAu-2) used in chemical column experiments and* ***(b)*** *greenish-coloured reduced NAu-2 inside the reactive layer of chemical column following activation with reducing agent sodium dithionite.*

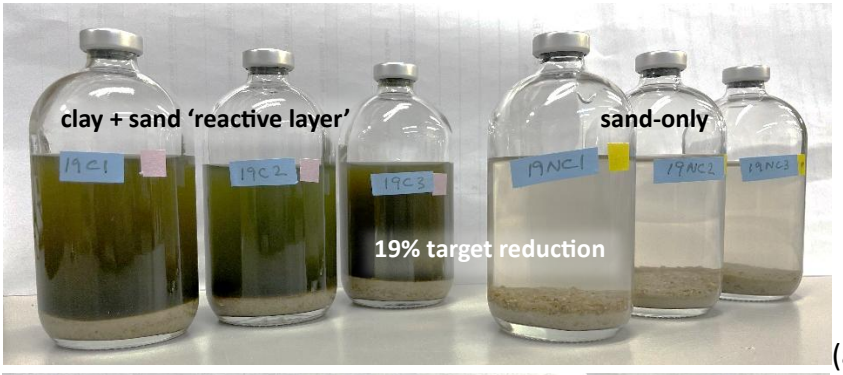

(a)

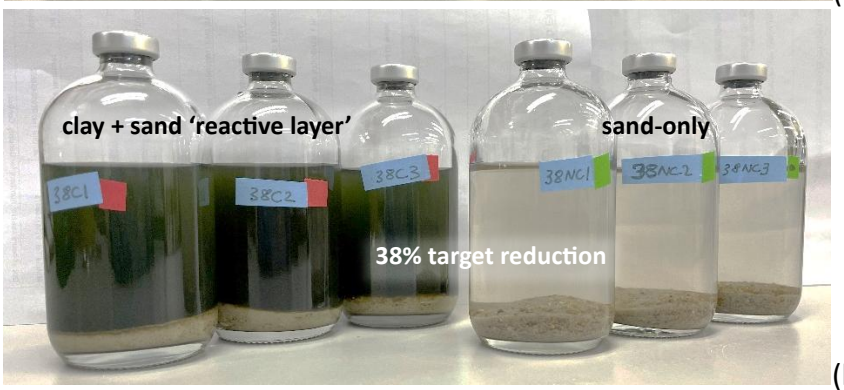

(b)

Figure 4. 7. *Microcosm batch experiments demonstrating Fe reduction in clay mineral NAu-2 using sodium dithionite and achieving different extents:* ***(a)*** *brown-green microcosms (left) containing clay + sand and sand-only (right), reduced to a target reduction level of 19% Fe^{2+}/F^{TOT};* ***(b)*** *dark-green microcosms (left) containing clay + sand and sand-only (right), reduced to a target reduction level of 38% Fe^{2+}/Fe^{TOT}.*

Quantitative results from the batch experiments are summarised in Table 4.5 and show that the percentage of Fe^{2+}/Fe^{TOT}, representing the overall reduction extent, in the combined nontronite clay and sand microcosms was consistently lower than the 19% and 38%

reduction targets set in each case (Table 4.5). Values of 8% Fe^{2+} and 16% Fe^{2+} were measured for the 19% and 38% reduction target batches, respectively. There is a plausible hypothesis for this result: the presence of additional Fe in the sand that was combined with the clay mineral in the batch (and column) experiments.

To test this hypothesis, sand-only (control) microcosms were used to measure the approximate Fe^{TOT} contribution of the sand alone (155-272 µmol), which was used to calculate the relative contribution of nontronite and sand Fe in the combined sediment microcosms (clay + sand) (Table 4.5). Calculations show that the nontronite clay consistently accounted for the majority of the total Fe (85-92% Fe^{TOT}) within the combined sediment microcosms, and Fe^{TOT} contributions by the sand ranged from 8% to 15% (Table 4.5). The latter contribution was likely due to the presence of Fe oxides associated with the sand that was used as received from the supplier.

The same type of calculation suggests that the nontronite clay accounted for 45-58% of the total Fe^{2+} in the combined reactors (Table 4.5). Due to the high sand content in the microcosm experiments (>98% dry weight; Appendix B, Table B.1), the relatively high contribution of Fe^{2+} (42%-56%; Table 4.5) by the sand (and associated Fe oxides) to the column reactive layer is not unexpected, yet much higher than what was expected based on the total Fe contribution. This result also indicates that reduction of Fe minerals associated with the sand could have accounted for the overall lower than targeted reduction extent in the clay + sand combined microcosms, which was otherwise dominated by the clay mineral Fe and its reduction extent.

Table 4.5. *Measured, target and calculated values of Fe^{2+} and Fe^{TOT} for nontronite clay and sand sediments collected from the microcosm batch experiments. All values are means (n=2).*

	Target reduction = 19%			Target reduction = 38%		
	clay + sand combined microcosm	clay in microcosm[a]	sand-only microcosm	clay + sand combined microcosm	clay in microcosm[a]	sand-only microcosm
Total Fe (Fe^{TOT})						
µmol	1931	1647 [b]	155	1839	1647 [b]	272
relative contribution	100%	92%	8.0%	100%	85.2%	14.8%
mM [c]	19.31	16.47	1.55	18.39	16.47	2.72
Fe^{2+}						
µmol	161.6	71.9	89.7	293.9	170.6	123.3
relative contribution	100%	44.5%	55.5%	100%	58.0%	42.0%
mM [c]	1.62	0.72	0.90	2.94	1.70	1.23
Reduction extent (µmol Fe^{2+}/µmol Fe^{TOT})	8.4%	4.4%	57.9%	16.0%	10.3%	45.3%

[a] calculated as the difference of results from clay + sand combined microcosm and sand-only microcosm. [b] calculated based on 0.4 g nontronite NAu-2 with 23 wt% Fe. [c] calculated based on total volume of microcosm (100 mL) and reported as mM/L.

Implications of the batch experiments are:

(i) nontronite contributed more than 85% of Fe^{TOT} in the reactive layer column sediments;

(ii) calculations suggest that the nontronite clay contributed around 50% of available Fe^{2+} to the reactive layer, although the actual extent of nontronite reduction was less (4.4% and 10.3%, respectively) than the targeted 19% and 38%;

(iii) Fe minerals associated with sand in the column experiments may have contributed around 50% of available Fe^{2+} the reactive layer during the first treatment cycle, most likely in the form of dissolved/porewater and surface sorbed Fe^{2+}. However, the availability and fate of Fe^{2+} from sand-associated Fe mineral reduction in the chemical columns is unclear after the first treatment cycle.

4.3.1.2. Mössbauer results

To expose the role of sand-associated Fe minerals in contributing Fe^{2+} to the chemical column experiments, Mössbauer spectra were obtained for the nontronite, sand and reactive layer sediments (nontronite and sand combined) before and after the first and last chemical treatments, at either room temperature (RT) or at 13 K (Figure 4.8).

Mössbauer spectra collected at RT of the individual components, sand and clay NAu-2, show the presence of Fe as only Fe^{3+} in both. While Fe^{3+} in NAu-2 is present as paramagnetic doublets with parameters consistent with those found in the literature, magnetically ordered

Fe^{3+} (sextet) in the sand sample suggests the presence of Fe (oxyhydr)oxides. The much lower relative intensity (<0.1% vs >10% absorption) of the sand vs clay sample at much higher solid loading suggests a very low total Fe content in the sand. In this context, the spectrum of combined clay and sand sample (representing column reactive layer sediments) before clay activation or any treatment show that the contribution of Fe^{3+} from the sand is minimal (<5% total Fe) and the only measurable Fe exists as structural Fe^{3+} within the nontronite clay. This is consistent with the results of the batch experiments which suggest that >85% of Fe^{TOT} in the reactive layer sediments is associated with the nontronite.

After the first treatment cycle of the chemical column, Mössbauer analysis (at 13 K) of the combined clay and sand reactive layer sediments shows a significant contribution (50% of spectral area) of a magnetically ordered Fe^{3+} phase. This is usually representative of Fe (oxyhydr)oxide mineral phases (Murad, 2006) (represented by the grey-shaded sextet in Figure 4.7d). The much higher relative proportion of this sextet compared to the reactive layer before the first cycle (Figure 4.8c) reflects the accumulation of Fe that was present in other parts of the column before the treatment cycle affected the column reactive layer. One plausible mechanism is the dissolution of sand-associated Fe^{3+} minerals during the activation flushes with dithionite, the transport and retention of the aqueous Fe^{2+} at the clay mineral with its high cation exchange capacity (697(±73) mmol/kg; (Jaisi et al., 2008) and the oxidation of this surface-bound Fe^{2+} into a new Fe^{3+}-containing phase, via either interfacial electron transfer with structural Fe^{3+} in the clay (Schaefer et al., 2011) or net oxidation during transfer and storage of the sample. Assuming that the Fe sextet was formed from external Fe and was not released from clay NAu-2, the Fe(II) contribution of overall 2% of the spectral area (green doublet) amounts to around 4% reduction extent of clay mineral NAu-2, which consistent with the low reduction extent calculated from the microcosm batch experiments (Table 4.5).

Carrying out the same analysis on a reactive layer sample collected after the fourth and final treatment cycle of the chemical column (Figure 4.8e) shows that the Fe^{3+} sextet was significantly decreased in intensity and only represented 14% of the spectral area. This suggests that throughout the course of four treatment cycles, involving reduction (and subsequent oxidation), sand-associated Fe^{3+} minerals in the reactive layer, and presumably

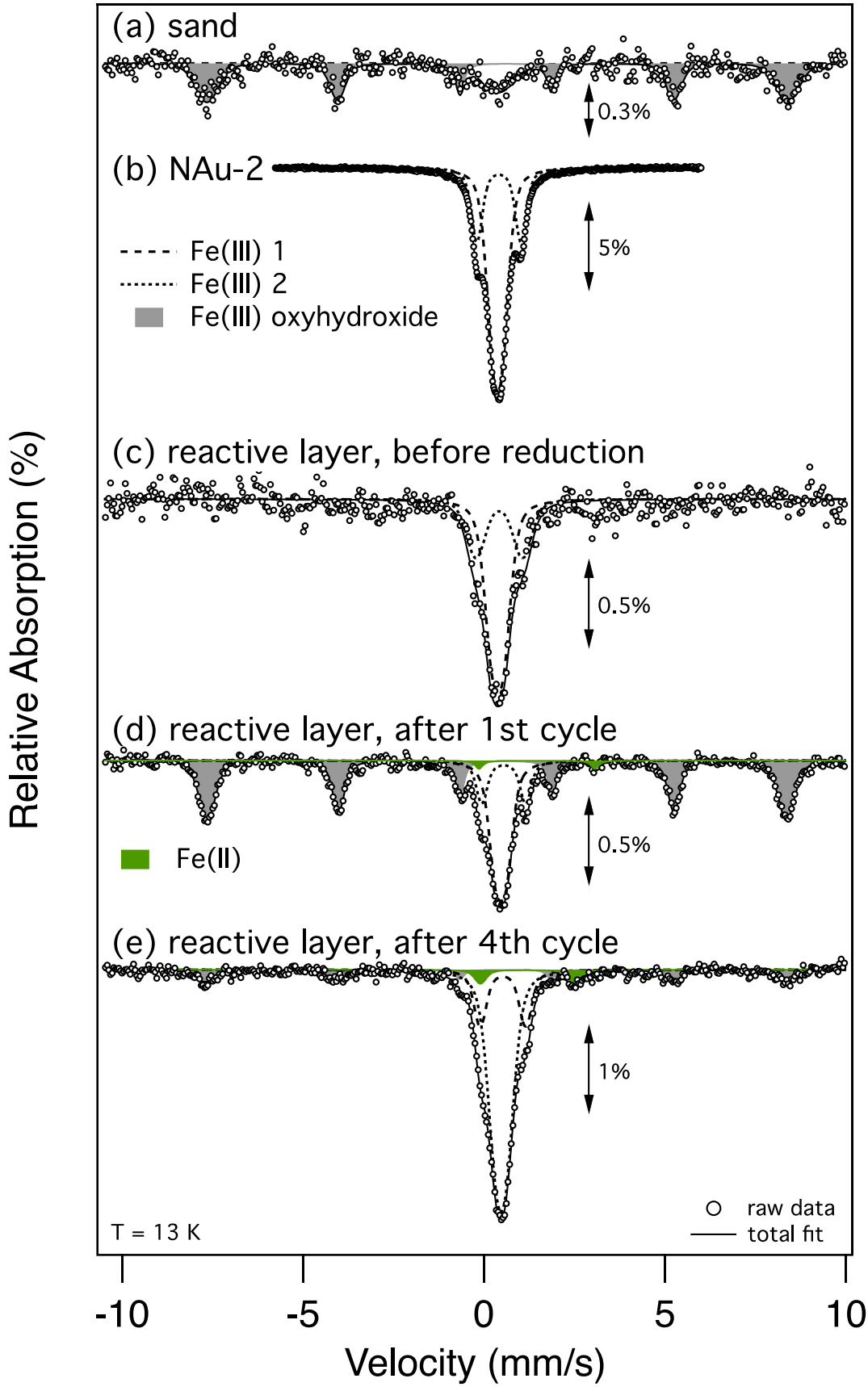

Figure 4. 8. *Mossbauer spectra of chemical column reactive layer components, combined and separately, where* ***(a)*** *shows native sand before activation;* ***(b)*** *native NAu-2 nontronite clay mineral, before activation;* ***(c)*** *column reactive layer before activation or treatment; column reactive layer after activation/reduction following the* ***(d)*** *first treatment cycle and* ***(e)*** *fourth (last) treatment cycle.*

throughout the entire column, were reductively dissolved and washed out of the column, leading to very low quantities remaining by the final treatment cycle.

4.3.2 Generation of •OH for contaminant treatment

Production of •OH from the activated, and hence Fe^{2+}-containing, reactive layer was initiated by flushes of oxygen-saturated buffer solution and quantified using the •OH scavenger benzoic acid (BA). Degradation of the model micropollutant BA occurred in all four treatment cycles carried out during the nontronite-bearing chemical column experiments. Figure 4.9 shows typical concentration profiles of BA and its degradation product, 4-hydroxy benzoic acid (4-HBA), in column effluent over ~5 h during the later oxic stages of the fourth (T4) and final chemical treatment cycle (where 1 column flush equates to ~1 h).

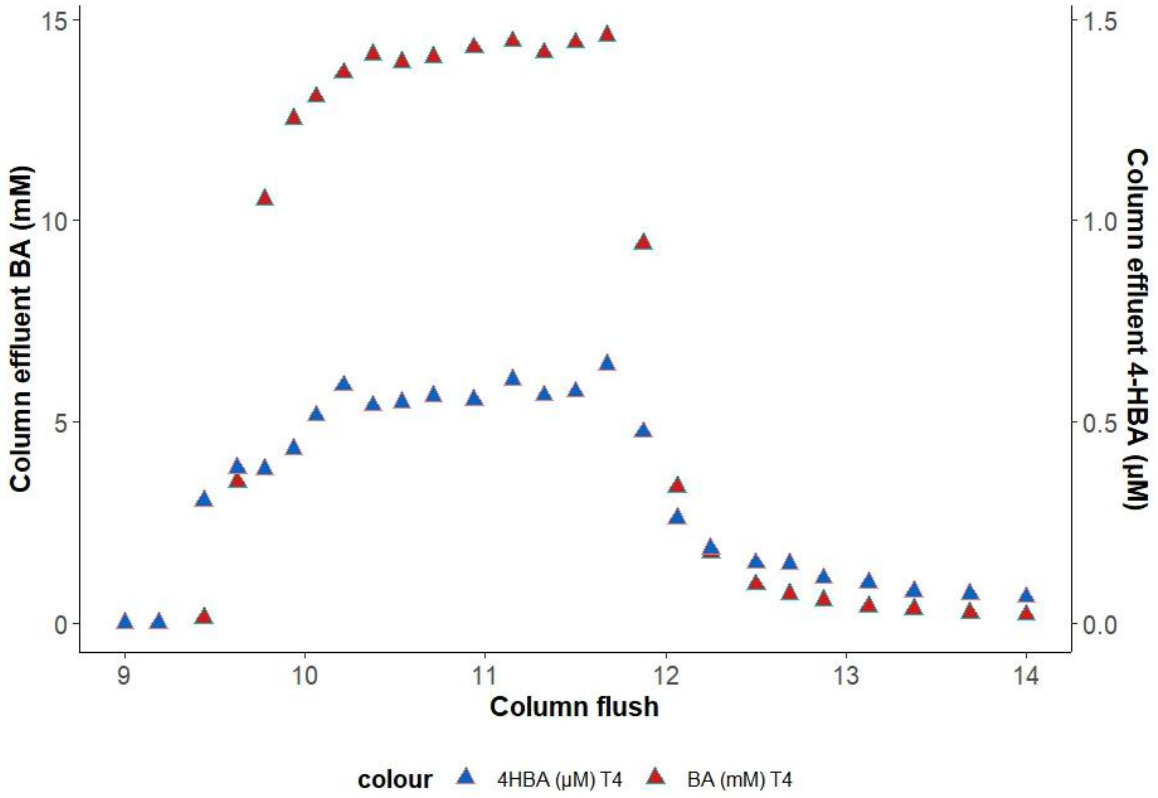

Figure 4. 9. *Typical concentration profiles of benzoic acid and 4-hydroxybenzoic acid in the effluent of nontronite-bearing chemical column experiments, over the last 5 column flushes of a typical treatment cycle. Representative data is shown from the 4th (T4) treatment cycle.*

During all four chemical treatment cycles, 4-HBA was detected in column effluents 15-20 minutes before BA, although both analytes reached concentration maxima soon after the first column flush (~250 mL) of synthetic wastewater within each treatment cycle, at a

flowrate of 5 mL/min (Figure 4.10). Both analytes typically remained at their highest concentrations in column effluents (BA: 15 mM BA, 4-HBA: 0.75 µM) until the sodium bicarbonate wash was flushed through the column (e.g. Flush '11' on Figures 4.9-4.10; also Table 4.4, 'Ox. wash' column), ahead of the next treatment cycle. Once Flush 11 was complete, the concentrations of BA, then 4-HBA, decreased rapidly towards zero during Flush 12 and onwards. The sand-only control column produced negligible 4-HBA during a single treatment cycle producing < 0.2 µM for the majority of the cycle but with a maxima of 0.29 µM 4-HBA soon after Flush 11 (Appendix B, Figure B.2).

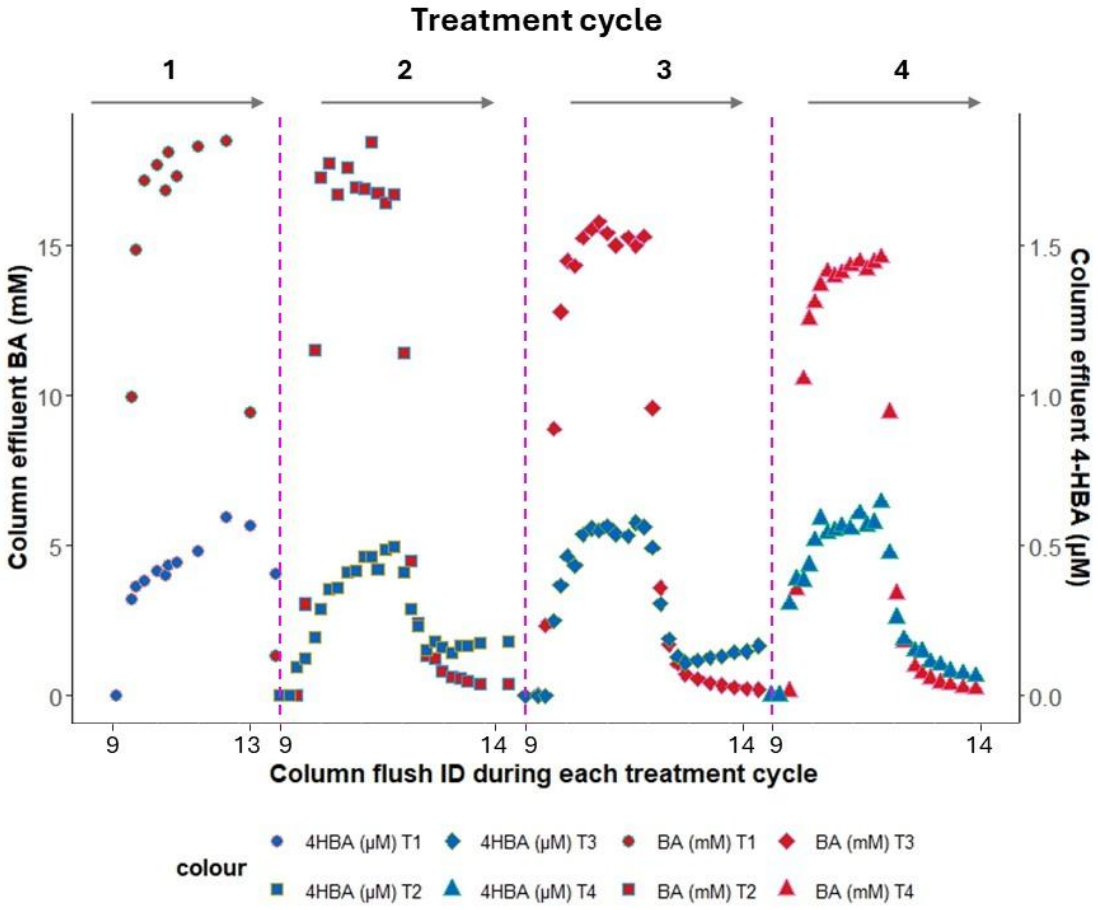

Figure 4. 10. *Concentration profiles of BA and 4-HBA measured in effluent from the chemical column experiments, during all 4 successive chemical treatment cycles. Data plotted as a function of column flush number, where column flush #9 indicates the start of the benzoic acid treatment and flush #13 or #14 indicates the end of the final sodium bicarbonate wash, at the end of each treatment cycle.*

4.3.2.1. •OH generation yield and treatment efficiency

The detection of 4-HBA in column effluents across all four treatment cycles indicates that BA became hydroxylated and hence provides evidence for the generation of •OH *in-situ* within the column experiments during the oxygenation of nontronite Fe^{2+} (and a negligible amount

of dissolved/solid-associated Fe^{2+} produced from sand-associated Fe minerals). As dissolved oxygen cannot directly oxidise BA (Jia et al., 2017), interaction of •OH with BA is considered the primary mechanism responsible for 4-HBA production during the chemical column experiments. This result is consistent with other studies reporting •OH production based on quantitative trapping with BA, during the abiotic oxygenation of Fe^{2+} in the clay mineral structure (e.g., Zhang et al., 2023; Chen et al., 2019, 2018; Liu et al., 2017, 2020; Yuan et al., 2018; Xie et al., 2020a) or associated with sand columns (Jia et al., 2017).

Support for the hypothesis that oxygenation of structurally-bound Fe^{2+}, e.g. in nontronite, and surface-adsorbed Fe^{2+}, dominates in •OH production in the column experiments here, comes from spectroscopic and wet chemical studies (Xie et al., 2020) demonstrating the minor role that aqueous Fe^{2+} (Jia et al., 2017), Fe^{2+} derived from reductive dissolution of Fe(oxy)hydroxides (Lewis et al., 2011; Han et al., 2020; Lyngsie et al., 2018) and Fe^{2+} in sulphide minerals (Zhang et al., 2016, 2017, 2018; Cheng et al., 2016) play in •OH production, following Fe^{2+} oxygenation. Furthermore, Zhang et al. (2023) used kinetic modelling to show that reactive structurally-bound Fe^{2+} contributed the most to •OH production (66–84%) and surface-adsorbed Fe^{2+} the least (16–34%).

From 4-HBA concentrations measured in column effluents, the volumes flushed through the column and the branching ratio for the hydroxylation of BA (5.87; (Mopper & Zhou, 1990; Zhou & Mopper, 1990) the cumulative •OH yield was calculated. The cumulative •OH yield was highest in the first treatment cycle (Figure 4.11) and lower for the remaining cycles, with the second treatment cycle showing the lowest yield. The higher •OH yield during the first treatment cycle can be explained by the contribution of sand-derived Fe^{2+} to the column total Fe^{2+} pool (Table 4.5), where •OH yield is the likely the product of both nontronite Fe^{2+} oxygenation and solid-associated Fe^{2+} oxygenation. In this proposed scenario, adsorption of dissolved Fe^{2+} produced during the reducing activation phase of the treatment cycle onto remaining sand-associated Fe (oxy)hydroxides and/or clay mineral is plausible. In fact, experiments with aqueous Fe^{2+} in sand columns (Jia et al., 2017) demonstrated this and subsequent oxygenation of Fe mineral-adsorbed Fe^{2+} to produce •OH, which could have occurred alongside •OH production from nontronite Fe^{2+} oxygenation here. This hypothesis is based on widely accepted published work showing that the oxygenation of free Fe^{2+}_{aq} does not produce notable •OH yields (Hug & Leupin, 2003) and that coordination of Fe^{2+} with

oxygen-containing functional groups, e.g. sorption to Fe oxides, is necessary for significant •OH production (Keenan & Sedlak, 2008).

Mössbauer spectroscopic results (Section 4.3.1.2) are consistent with this proposed scenario and indicate that sand-associated Fe minerals were present after the first cycle in column sediments but absent after the last treatment cycle (Figure 4.8). Repeated reductive dissolution over multiple treatment cycles and subsequent advective transport of the aqueous Fe^{2+} out of the column could explain these spectroscopic results. Additionally, this scenario would result in only structurally-bound clay mineral Fe remaining in column sediments after several treatment cycles (>1 and ≤4).

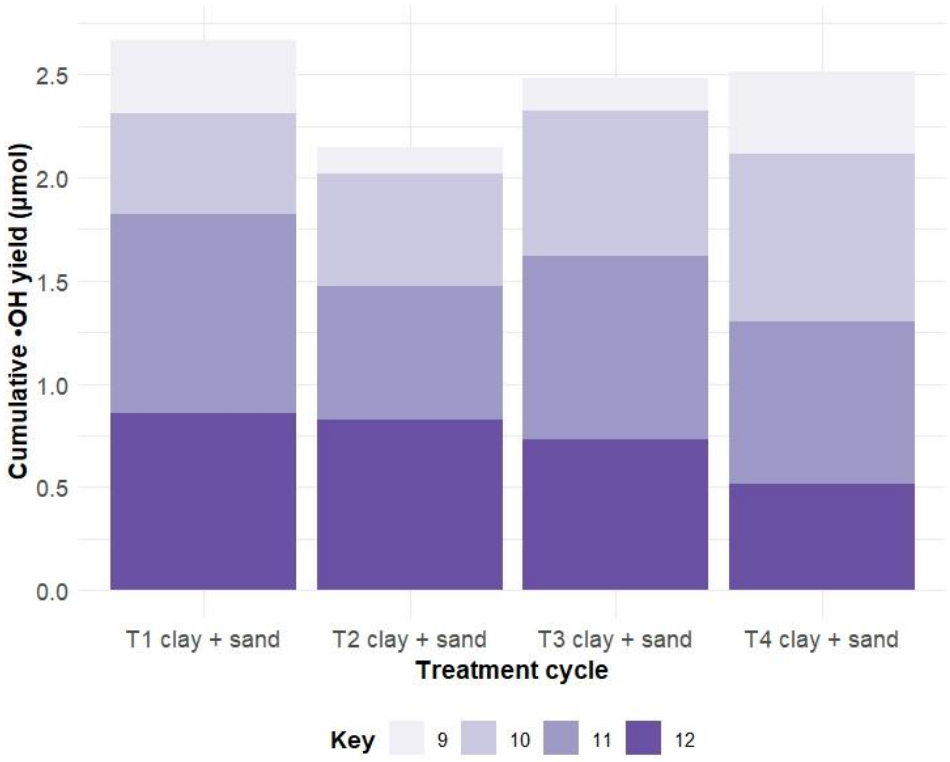

Figure 4. 11. *Cumulative •OH yield in chemical column experiments, shown for each treatment cycle and proportioned by column flush within each cycle.*

From the absolute •OH yield per treatment cycle (Figure 4.11: 2.2-2.6 µmol or 0.07-0.12 µmol/g Fe^{2+}) and the number of Fe^{2+} in the column sediments oxygenated 484.34-878.62 µmol Fe^{2+}) the efficiency of •OH production can be calculated (Figure 4.12). Assuming that all Fe^{2+} in the column sediments became oxygenated, the highest •OH production efficiency was found in cycle 1 (0.55%) and the remaining cycles were about half as efficient (0.25-0.29%). Overall, these values are much smaller than the theoretical maximum efficiency of 33%, which is based on the stoichiometry of 3:1 for the generation of •OH from the reduction of

O_2 by Fe^{2+} (Chapter 2, Section 2.4 Equations [2], [5] and [1]). In a similar type of treatment study, Jia et al. (2017a) reported a maximum •OH yield of 2.7 µM following the oxygenation of 20 mg/L Fe^{2+}_{aq} during the fourth (redox) treatment cycle in a set of sand column experiments. The work of Jia et al. (2017a) appears more efficient in generating •OH per unit of Fe^{2+} than the thesis experiments described here (Figure 4.12), however the likelihood of available Fe^{2+}_{aq} being washed away over time is high, even if associated with Fe^{3+} oxyhydroxide surfaces. Other published studies also show greater •OH production per unit of Fe^{2+} oxygenated e.g. (Liao et al., 2019; Xie et al., 2020; Zhang et al., 2023) than that measured during treatment cycles these PhD experiments (Figure 4.12) and in a treatment context, the efficiency of the chemical AOP developed here is relatively low.

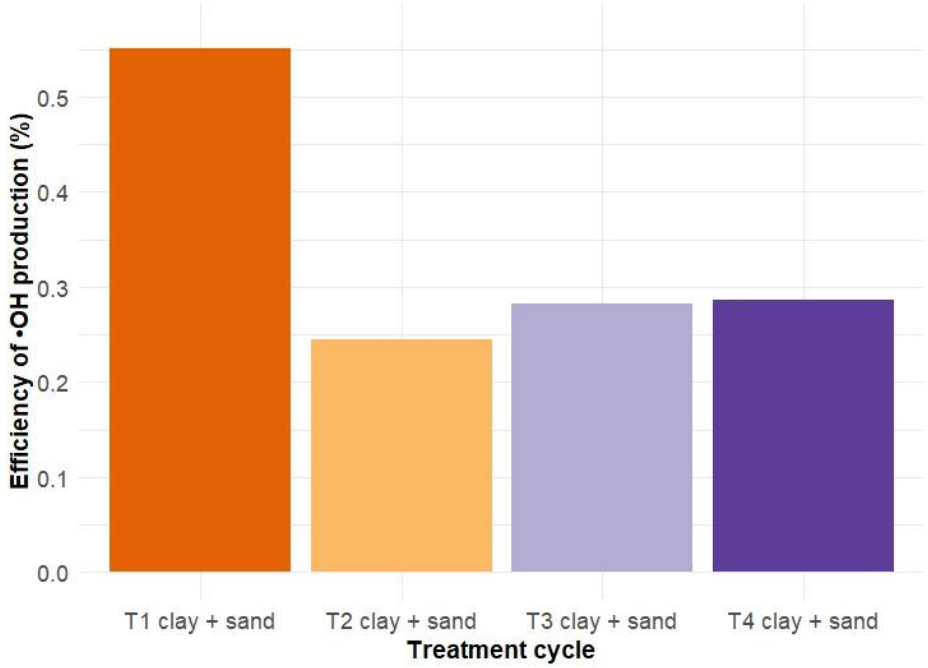

Figure 4. 12. *Efficiency of •OH generation over four cycles of treatment in the chemical column system. Note that actual measured reductions from microcosms (8.4% and 16%) are used here and not target reduction levels of 19% and 38%. Treatment efficiency was calculated by expressing the yield of •OH produced during clay oxygenation as a percentage of the maximum possible yield of •OH, if all Fe^{2+} in the column experiment was oxygenated.*

Potential causes for this low •OH production efficiency include a lack of sufficient Fe^{2+} for oxygenation, although low O_2 saturation in the chemical treatment and the control columns were both achieved (Figure 4.13) during the treatment cycle. A lack of oxygenation during the treatment phase is also possible and should be tested in further work. Disruption to flow through the column or formation of preferred flow channels is also possible, meaning the maximum clay surface area may not have been utilised for oxygenation.

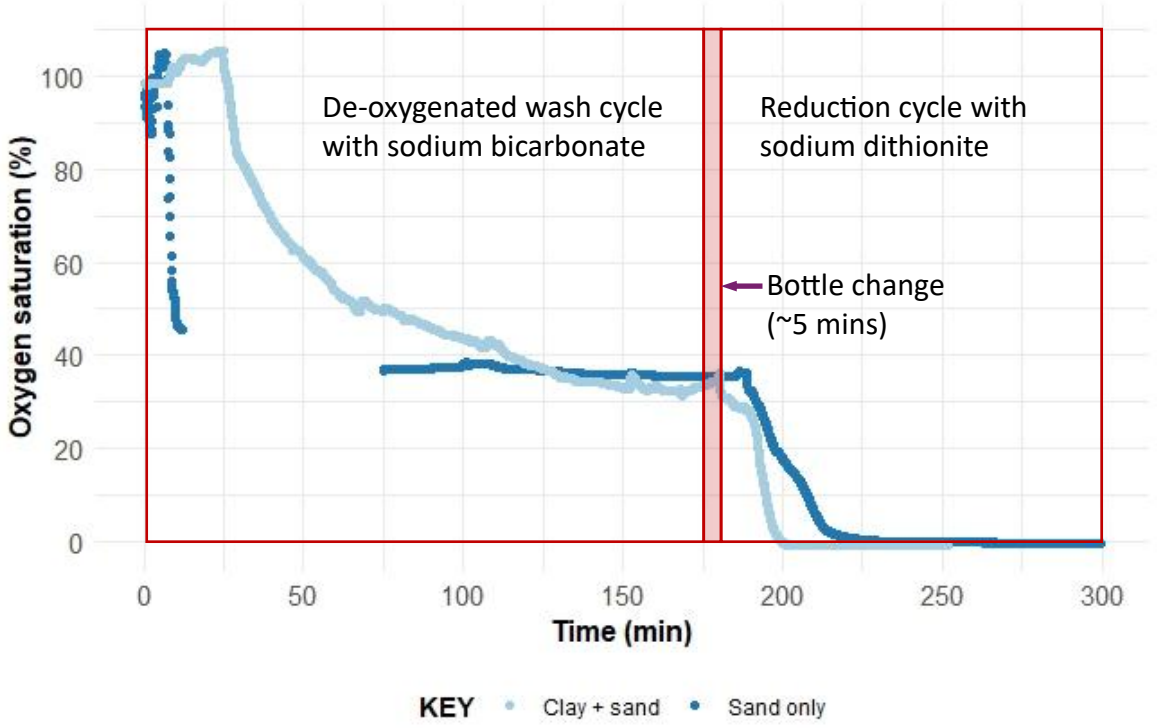

Figure 4. 13. *Oxygen saturation during the activation phase of the chemical column experiments (showing data for columns with and without clay).*

4.3.3 Sustainability of clay activation and •OH production for treatment

The potential for sustainable clay activation and •OH production over several treatment cycles depends strongly on the redox active element Fe remaining within the column sediments. Two different mechanisms could remove Fe from the column, i.e., dissolution of the clay mineral and/or physical removal of clay particles, and these are assessed here.

To assess clay stability across all four treatment cycles, the loss of Fe and other major cations was measured in column effluents. Both filtered (0.45 µm) and non-filtered column effluent samples were analysed and contained similar concentrations of Fe, suggesting only a small fraction of Fe^{TOT} transported out of the column was colloidal (difference between light and dark blue bars in Figure 4.14). This result suggests that only minor amounts of Fe-containing (clay) mineral particles were lost from the column, and hence that physical removal of clay particles was insignificant here.

The highest concentrations of Fe^{TOT} were measured in effluents during the chemical activation cycles ('3', '4' and '5' in Figure 4.15), suggesting the reductive dissolution of Fe-containing minerals. To explore whether the sand-associated Fe minerals were the source of this mobilised Fe, effluent from the control experiment (sand only) was measured. The concentrations of Fe released from column flushes 3, 4 and 5 during the activation phase of the control column were significantly lower (always <50 µM) compared to the range measured in the clay + sand column effluents over the same columns flushes (400-520 µM). This indicates that sand-associated Fe minerals were not released but rather Fe was released from the nontronite clay and sand columns during clay activation.

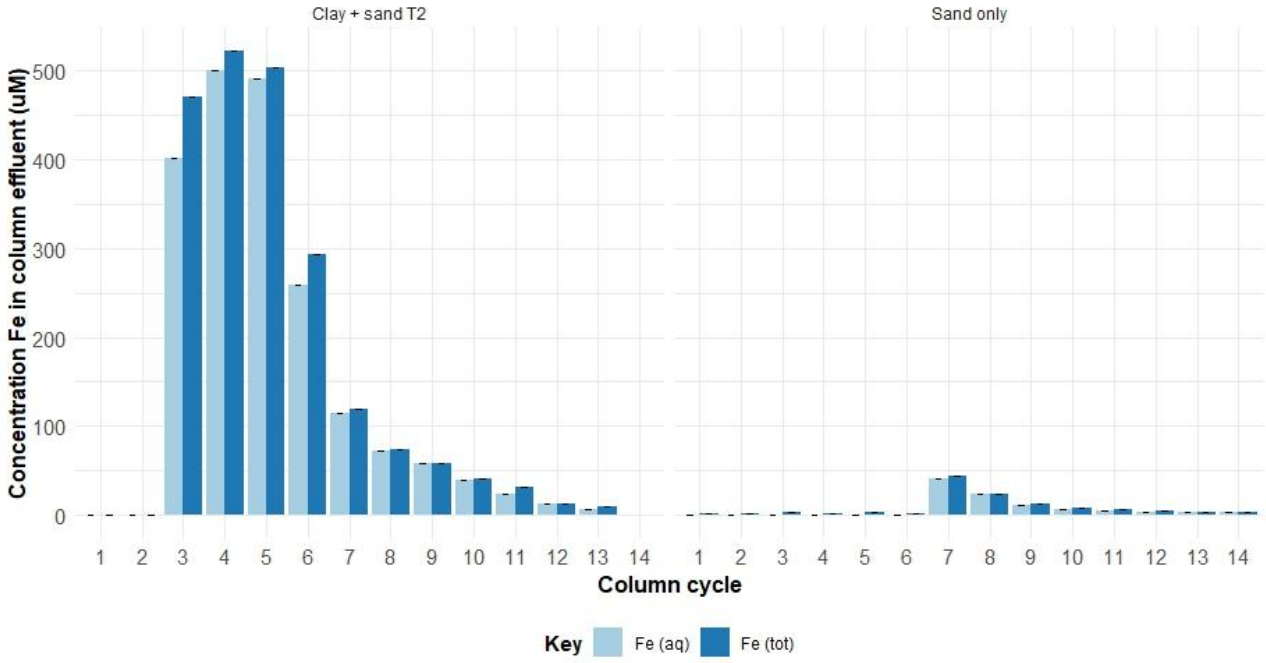

Figure 4. 14. *Proportion of Fe in filtered (aqueous Fe, light blue bars) and non-filtered (total Fe, dark blue bars) effluent samples collected during Treatment Cyle 2 (as an example) and from the sand-only control column during the first treatment cycle. The chemical reducing agent sodium dithionite was pumped through column cycles 3-6 in the chemical column experiment and through column cycles 4-6 in the control column.*

Mass balance calculations indicate that despite effluent loss, the majority of Fe remains inside both the chemical clay+sand column and the sand-only column (Table 4.6).

Table 4. 6. *Mass balance table for Fe^{TOT}, showing Fe concentration with the chemical control column and sand-only column, and total Fe lost in effluent during experiment.*

NAu-2 (mmol)			
Exp	Column	In	Out
1	N1	73.1	1.239
Sand only	N1	55.8	0.03

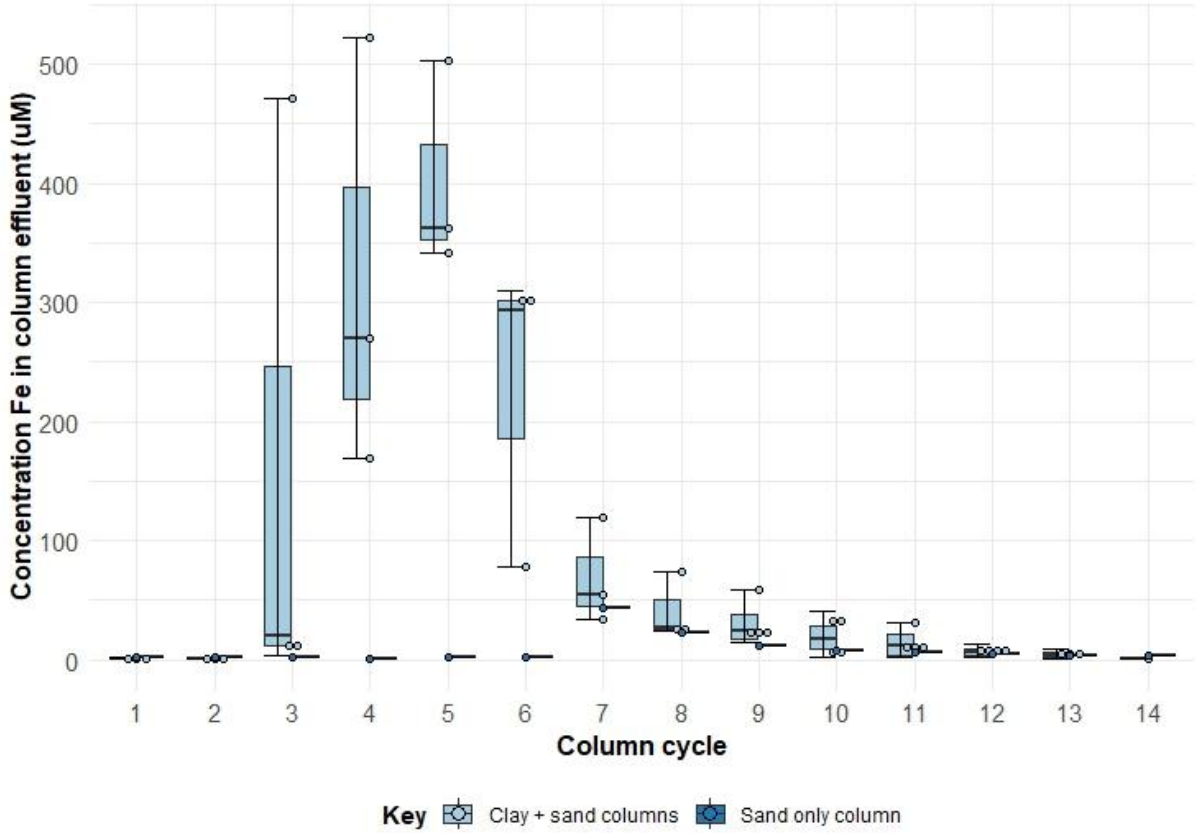

Figure 4. 15. *Box and whisker plot for Fe^{TOT} measured in effluent samples from columns flushes within all treatment cycles, for clay + sand columns and the sand-only control column. Range bars show min and max data values, dots show individual data points, top and lower bounds of boxes represent the 3rd and 1st quartile data values and the horizontal bar across the middle of each box represents the median value.*

4.3.3.1. Clay dissolution

To indicate whether other cations in the clay structure, besides Fe, were lost in column effluent, a Spearman's rank correlation test was applied to data for major cations collected from column effluents, to quantify the degree of linear relationship between the ranks of any two given cations. P values are used to indicate a positive or negative correlation and the proximity to 1, -1 or 0 indicates either a strong positive correlation, a strong negative correlation or no observed correlation, respectively. Spearman correlation matrices were generated for Fe, Si, Al, S and Na and are represented as a heatmaps in Appendix B (Figures C.4). Correlation tests were grouped according to clay type and experiment, and data for control columns were not included. The results were used to indicate potentially significant relationships for further investigation.

As a component of every buffer solution used during the chemical column experiments, Na was consistently negatively correlated with other cations due its conservative behaviour against relative increases in concentration in other metals.

Inspection of cation ratios in column effluents can elucidate the possible causes of Fe mobility alongside other cations. A modest but notable increase in the Si/Al ratio of the column effluents occurs after the chemical activation of the clay and during bicarbonate flushing (flush 6; Figure 4.16). This could indicate some level of detachment of Si tetrahedral sheets during incongruent dissolution of the clay mineral (Cama & Ganor, 2015) during clay activation and exposure to sodium dithionite. Relatively high Fe/Al ratios occur earlier during the clay activation phase (flush 3 onwards; Figure 4.17)., suggest that Fe may already be mobile during flush 3, potentially liberated through the reductive dissolution of Fe oxides and being washed through the column with silt fines. Together, these trends suggest that Fe is being lost from the chemical column through several routes during pumping: as Fe^{2+}_{aq} derived from the early reduction of Fe oxides, followed by a later and minor contribution from the clay mineral.

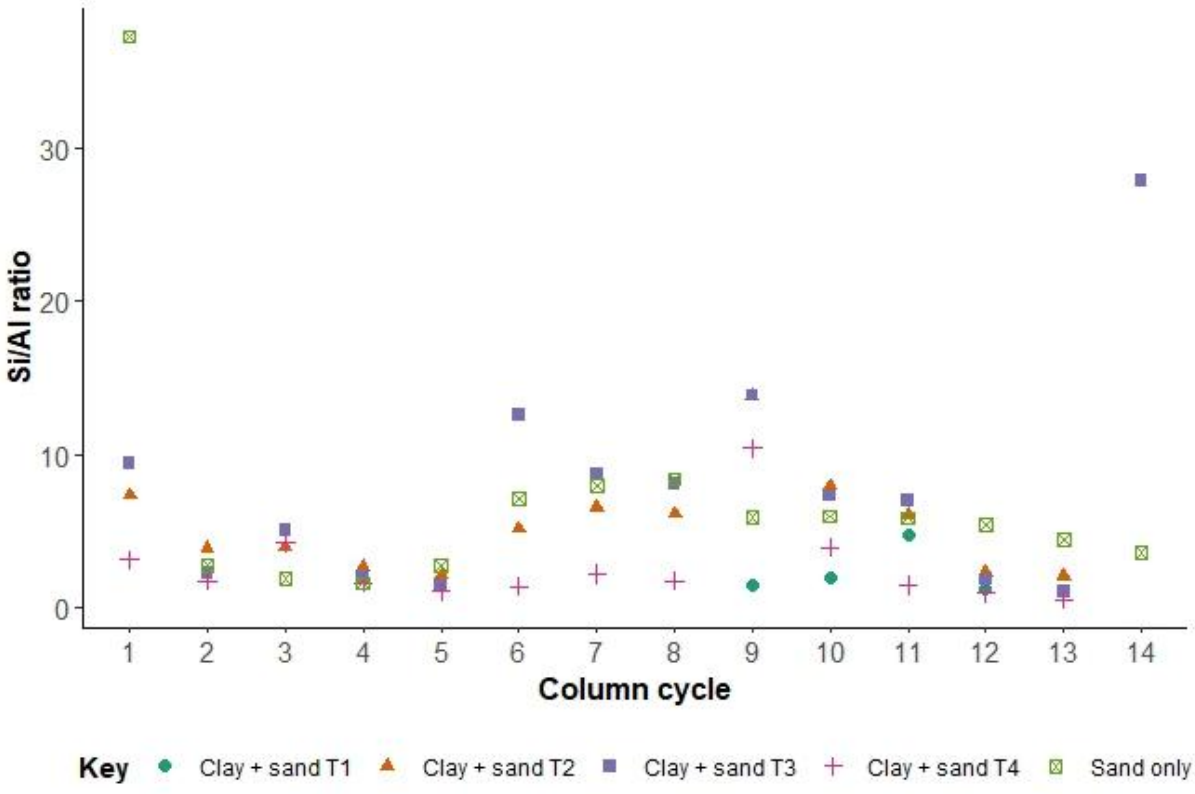

Figure 4. 16. *Fe/Al ratios in column effluents from all chemical column treatment cycles.*

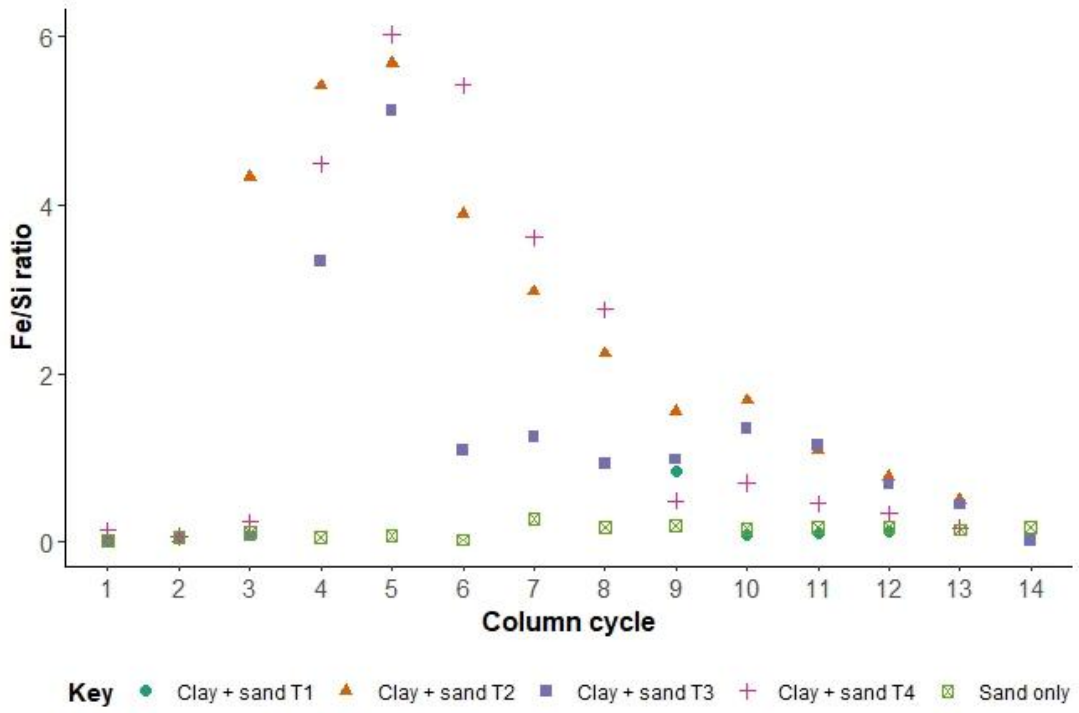

Figure 4. 17. *Fe/*Si *ratios in column effluents from all chemical column treatment cycles.*

4.4 Conclusions

Sodium dithionite is an effective reductant for clay structural Fe packed inside the column experiments and reduces the clay to approximately the target level of reduction. However, chemical reduction is also an important factor in Fe^{2+} availability as it causes a degree of Fe^{2+} dissolution during reduction. This is evidenced by high concentrations of Fe in column effluents when the column is flushed with sodium dithionite. (Descriptive statistical analysis also indicates that S is very positively correlated with both Al and Fe although the data is not discussed here). Both chemical dissolution and mechanical transport of Fe together, are key factors in the loss of Fe from the column at certain points in the treatment experiment.

Observation of Fe^{aq} and Fe^{TOT} proportions indicated that the Fe lost is as both aqueous and colloidal Fe fractions but only a small proportion of clay mineral Fe is actually lost from the column during all four treatment cycles.

The treatment experiments carried out show that •OH can be produced over at least four treatment cycles in succession. The efficiency of the treatment is low at 0.24%-0.55%, with the first cycle being the most efficient. This is consistent with the additional contribution towards •OH production from the reductive dissolution of reactive Fe(oxyhydr)oxides during the first treatment cycle, as indicated by Mossbauer results.

The loss of Fe through different mechanisms has implications for the design of sustainable advanced oxidation treatment systems where the success of the treatment is dependent on the physical stability of an intrinsic component, for example in clay mineral structural Fe. Additionally, the treatment efficiency is low using the current set-up and further work is required to develop and optimise this.

5. Biological Column Experiments

5.1 Introduction

This chapter expands on the experiments and results from Chapter 4, where nontronite Fe was reduced via chemical reduction ('activation') and subsequently induced the production of •OH during oxygenation ('treatment'). In the work described in this chapter, clay mineral Fe was activated in large column experiments, harnessing microbial activity in the absence of oxygen, and •OH were produced during the subsequent oxygenation of nontronite Fe, similarly to the work described in Chapter 4. Overall, this chapter will provide the proof-of-concept for using Fe-bearing clays minerals in a sustainable, low carbon wastewater treatment system that harnesses microbially-mediated redox processes to achieve micropollutant treatment, through advanced oxidation (Figure 5.1).

Local pondwater was used as inoculum to activate, through microbial Fe reduction, the same high Fe nontronite (NAu-2, 23 wt% Fe), as previously used in the chemical column experiments Chapter 4), and additionally a low Fe sodium montmorillonite (SWy-3, 2 wt% Fe).

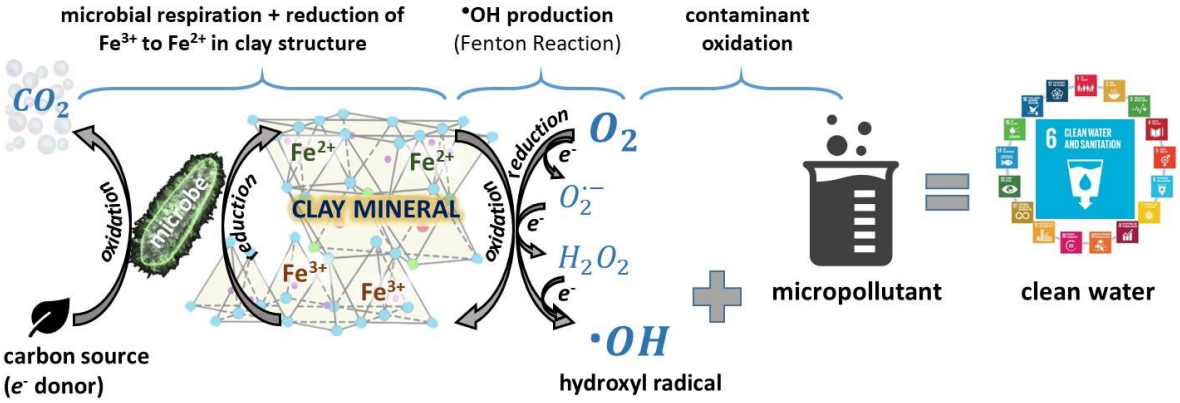

Figure 5. 1. *Schematic showing the AOP relying on clay mineral activation by microbial reduction of clay mineral structural iron through electron shuttling from an organic carbon source. The treatment portion of the AOP remains the same as the chemical AOP (Chapter 4) with stepwise reduction of dissolved oxygen by clay mineral Fe^{2+} to yield the reactive oxygen species hydroxyl radical (•OH) for the degradation of micropollutants.*

The production of •OH from the oxygenation of ferrous minerals in biologically-active sediments has been recognised for some time and reported in both mechanistic studies, e.g. Page et al., 2013; Ma et al., 2019; Xie et al., 2020; Zhang et al., 2024, and in the context of

contaminant treatment and/or degradation (Tong et al., 2016; Zeng et al., 2017; Liu et al., 2017; Liao et al., 2019). More recently, the production of •OH from other microbially-active, redoximorphic environments has been reported, e.g. riparian aquifers (Zhang et al., 2020; Zhang et al., 2024) and soils (F. Liu et al., 2024), paddy soils (J. Liu et al., 2024) and coastal sediments (Zhao et al., 2022), highlighting the potential role of Fe-bearing biologically-active subsurface environments in decontamination via naturally-occurring advanced oxidation processes (AOPs).

In these subsurface environments, including lakes, soils and aquatic sediments, a vast number of microbes are capable of dissimilatory Fe-reduction (where Fe is not assimilated by microbes during electron transfer) and it has been suggested as the most geochemically significant event that naturally takes place (Lovley, 2006). Examples of organisms isolated in these redox-active settings and used in studies to reduce Fe^{3+} in clay minerals include *Shewanella oneidensis* (from anoxic lake sediments, Lake Oneida, New York; Kostka et al., 1996) , *Geobacter metallireducens* (from freshwater sediments, Potomac River, Maryland; Kostka et al., 1999), *Pseudomonas* spp. (from wheat rhizosphere soils; Ernstsen et al., 1998), *Bacillus* spp. from source clay mineral SWa-1 and rice paddy soils in China ((Gates et al., 1998) and *Desulfitobacterium frappieri* (from subsurface smectite bedding, Twiggs Clay Formation, Georgia; Shelobolina et al., 2003).

Although the formation of oxidising species, such as •OH, from biologically reduced Fe-sediments and Fe-bearing clays has been established (Tong et al., 2016; Zeng et al., 2017), their effect on the microbial community is not as widely reported. For example, Ma et al. (2019) found that the sediment microbial community structure changed after •OH was first produced from ferrous clay but then remained stable over longer oxygenation periods. In a study investigating the interplay of Fe species and •OH production on sediments and soils, significant inactivation (74%) of *Shewanella oneidensis* MR-1 cells was initially observed during exposure to •OH (during sediment oxygenation), however inactivation of cells was found to be insignificant during subsequent redox cycles where •OH was produced, and cells increasingly survived (Zhang et al., 2020).

Even though the production of •OH from clay mineral oxygenation can be considered sustainable through microbial reduction of Fe^{3+} during redox cycles (Zeng et al., 2017), most redox cycling experiments have been carried out by re-seeding the microbial community

after oxygenation. Therefore, the effect of repeated anoxic-oxic redox cycles, and especially the •OH generation phase, on microbial community structure is still poorly understood.

To address this knowledge gap and to provide-of-concept for the novel biologically-mediated AOP proposed here, this chapter will address the following objectives:

(i) establish whether a pondwater microbial community is effective in activating clay mineral structural Fe, through microbial Fe reduction, in the Fe-bearing clay minerals nontronite and montmorillonite, using flow-through benchtop column experiments;

(ii) determine whether •OH can be generated *in situ* through oxygenation of each of the activated Fe-clay minerals, within the same column experiments and if so, to quantify the yields of •OH, using benzoic acid as a quantitative scavenger;

(iii) identify whether the sustained microbial activation of the Fe-clay minerals and the treatment of benzoic acid within the same column experiments, is possible over repeated treatment cycles, and establish whether the microbial community structure has been affected by treatment cycles during exposure to •OH;

(iv) quantify the mass balance for Fe and clay mineral during the experiments and hence assess the sustainability of this proposed AOP.

5.2 Methods

5.2.1 Experimental set-up and column packing

Two experiments were run in succession (herein Experiments 1 and 2), each using two duplicate sets of large columns and a fifth control column (Chapter 3, Section 3.2), to test the biological activation of the two clay minerals, nontronite (NAu-2; 23 wt% Fe) and montmorillonite (SWy-3; 2 wt% Fe). Both clay minerals were obtained from the Clay Mineral Society Source Clay Repository (Chantilly, Virginia, USA), size-fractionated (< 2 μm) and freeze-dried in each case (Chapter 3, Section 3.3.1) prior to use.

The production of •OH was measured using BA as a quantitative probe to trap •OH, following oxygenation of clay mineral structural Fe. The duplicate column sets (n=4) were used to test 18 g dry weight of the two clay minerals, which were combined by thorough

mixing with fine, medium and coarse sand grades (Table 5.1). Using the approach described in Chapter 4 (Section 4.2.3), fine and coarse sand fractions were weighed and packed above and below the clay mineral 'reactive layer' (Figure 5.2), according to the configuration shown in (Chapter 3, Figure 3.2). Geotextile discs cut to fit the inner diameter of the column and saturated with 15 MΩ/cm RO water, were placed inside the ends of each column shaft at the outer bounds of the sediment. These provided a secondary filter layer to minimise fines migration. The columns were then sealed using 6 hand-tightened screw-nuts, as with the chemical columns (Chapter 4, Section 4.2.3), and inverted before the start of the experiments, to aid flow dynamics.

The clay mineral NAu-2 was used together with the sand fractions in control columns due to availability, and all control sediments were sterilised twice (121 ^{o}C for 20 min) in large autoclavable mushroom spawn bags (Gourmet Woodland Mushrooms, UK). Autoclaved geotextile discs were placed inside the control columns to minimise fines migration, as above. The control columns, fixtures and tubing were all sterilised thoroughly with 70% ethanol (EtOH), air-dried in a sterile UV cabinet, then packed in the same way as the duplicate column sets (as above), using the autoclaved sediments.

For all experiments, measuring cylinders were used as influent feed reservoirs (open to the ambient laboratory conditions) and peristaltic pumps operated at a constant flow rate of 7 mL/min were used to flush influent solutions through columns, entering at the base (Figure 5.2). During the clay activation stage, no flow was applied to the columns in order for anoxia to develop and taps at the base and top of the column were closed for at least 20 days (see Section 5.2.4 for further detail).

Columns were operated under the same principal as the chemical columns (Chapter 4, Section 4.2.6) although the influent feed reservoirs in the biological experiments were open to ambient laboratory conditions during treatment cycles, except during clay activations.

Table 5. 1. *Inventory of clay and sand sediments packed in biological column experiments.*

	Column sediment				
	Clay mineral (<2 µm)	Very fine + fine sand (0.063-250 µm)	Medium sand (250-500 µm)	Coarse sand (0.5-2 mm)	**Totals (g)**
Mass reactive layer (g)	18	250	950	250	1468
% reactive layer	1.2	17	64.8	17	100
Mass in column (g)	18	750	950	3050	4768

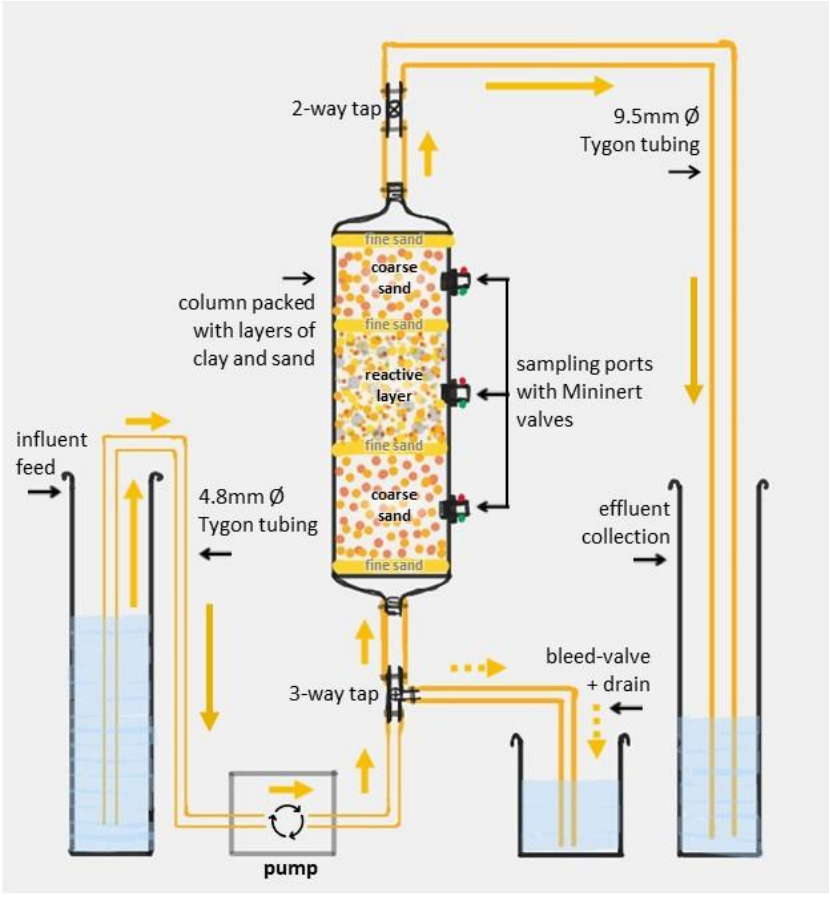

Figure 5. 2. *Schematic of biological column experiments.*

5.2.2 Preparation of inoculum and benzoic acid solution

5.2.2.1 Collection and preparation of pondwater

The duplicate column sets in Experiments 1 and 2 were inoculated using the same natural microbial community contained in pondwater, collected from Leazes Park Pond, Newcastle upon Tyne (NE2 4BJ). The pondwater was stored at 4 ^{o}C until use, which was used within 24 h of collection. To sustain the pondwater community during treatment experiments the pondwater inoculum was supplemented with twice-autoclaved (121 ^{o}C for 20 minutes, twice) seaweed-based NPK organic plant fertiliser (Green Future Organic NPK Tomato Fertiliser) up to 2 hours before column inoculation, to provide a source of carbon and electrons, for microbial metabolism. The NPK fertiliser was made to ⅛ strength of the manufacturer recommended dose, equivalent to 0.00312% potassium (K) loading and closely comparable to the K loading of a common culture broth (e.g. Terrific Broth, ThermoFisher Scientific).

Physico-chemical parameters of the pondwater, i.e. pH, temperature, conductivity, total dissolved solids (TDS), dissolved oxygen and Chemical Oxygen Demand (COD) were measured

on-site at collection, using an Extech EC500 Waterproof ExStik® II and a portable dissolved oxygen (DO) Hach meter (parameters shown in Appendix C, Table C1).

5.2.2.2 Preparation of benzoic acid solution

Benzoic acid (BA) was used as the chemical probe in the treatment stage of the experiments, to determine •OH yields through monitoring and quantification of the OH-adduct, 4-hydroxy benzoic acid (4-HBA). The rationale for this choice of probe is provided in Chapter 4 (Section 4.2.4) and, additionally, to facilitate comparisons between the chemical and biological treatment experiments.

During every treatment, autoclaved pondwater was used to make 8 L of 15 mM BA solution in a clean, ambient lab space. This concentration of BA was selected based on earlier results (Chapter 3, Section 3.4) where ~25% microbial reduction was achieved in NAu-2 test columns, generating 18.5 mM of Fe^{2+} for oxygenation (summarised in Table 5.2). The 25% microbial reduction extent measured in this PhD is within the literature reported range for NAu-2, as summarised in Dong et al. (2009). Higher microbial reduction rates (up to 69%) were reported for a similar montmorillonite (SWy-1; Gates et al., 1998) to that used in this PhD (SWy-3), although these were achieved using selected microbial cultures in growth broth and not a microbial community indigenous to a natural waterbody.

Table 5. 2. *Calculations and assumptions made to determine an appropriate concentration of benzoic acid (BA) to use in biological column experiments.*

Target reduction level	**25%**	
	NAu-2	**SWy-3**
Fe^{2+} in 18 g nontronite (NAu-2) or montmorillonite (SWy-3)	18.5 mmol	1.6 mmol
•OH generated (stoichiometry: 1:3 moles Fe^{2+})	6.2 mmol	0.54 mmol
BA needed for quantitative reaction with •OH	6.2 mmol	0.54 mmol
provide BA in excess to outcompete •OH reaction with other species	7.5 mmol	7.5 mmol
BA in total pore volume of 500 mL (column flush 3; Table 5.3)	15 mM	15 mM

* 69% SWy-3 reduction included for comparison

Once microbial activation of clay in the columns had occurred during the earlier part of the experiment, the 15 mM BA - pondwater solutions were equilibrated for 2 hours in Duran bottles with loose lids aerated using an autoclaved airstone and tubing, until solutions reached a dissolved oxygen (DO) concentration of ≥9.8 mg/L O_2.

5.2.3 Column inoculation and operation

5.2.3.1 Inoculation and clay activation

Two column pore volumes of the live pondwater-NPK fertiliser mix were pumped through the duplicate sets of columns (Experiments 1 and 2), to fully saturate column sediments (Table 5.3). To inoculate the column experiments, a third column pore volume was left to reside in the column (under stagnant conditions). Control columns for Experiments 1 and 2 were inoculated in the same way, and autoclaved (dead) pondwater-NPK fertiliser mix were used as a dead control to saturate the twice-autoclaved column sediments.

5.2.3.2 Operation

Once inoculated, the NAu-2 and SWy-3 column duplicates in Experiment 1 were operated for one complete treatment (Figure 5.3), whereas the columns in Experiment 2 were operated for three treatment cycles (Figure 5.4). In summary, following inoculation, a complete treatment cycle involved microbial-activation of the clay for at least 20 days without water flow (stagnation), to allow microbial reduction of clay mineral structural Fe^{3+} to occur and reducing conditions within the column to develop (Table 5.3; Figures 5.3 and 5.4). To measure the extent of BA treatment by the two different clay minerals (through production of •OH from Fe^{2+} oxygenation), two pore volumes of 15 mM BA in autoclaved pondwater (≥9.8 mg/L O_2) were then flushed through each column. Two flushes of autoclaved pondwater-NPK fertiliser mix (also ≥9.8 mg/L O_2) were used in the final oxic stage of each treatment cycle to wash out remaining BA and recharge the column with a carbon source for microbial metabolism (Table 5.3; Figures 5.3 and 5.4).

As Experiment 1 was run for only one complete treatment cycle (Figure 5.3), two flushes of autoclaved pondwater alone were used to wash BA out of the column in the final stage (Table 5.3). After this, the SWy-3 montmorillonite column duplicates and the NAu-2 nontronite control column were repacked, ahead of Experiment 2, but the NAu-2 nontronite treatment duplicates were not repacked due to availability of this particular source clay.

To start Experiment 2, the repacked SWy-3 montmorillonite duplicates and the original NAu-2 nontronite duplicate columns were inoculated with three column flushes of live pondwater supplemented with twice-autoclaved NPK fertiliser (121 ^{o}C for 20 minutes), as above. The experiment columns were then operated for three complete treatment cycles (Figure 5.4),

with column recharge occurring at the end of a cycle and start of the next, before clay activation (Table 5.3).

The control columns in both experiments were operated for one complete treatment cycle only, after inoculation with autoclaved pondwater-NPK fertiliser mix (as above).

Table 5. 3. *Summary of column flushes within the first two treatment cycles of the biological column experiments and reagents used to achieve oxidative treatment. Clay activation through microbial iron reduction (FeR) occurs in the middle of each cycle during a stagnation period of no flow.*

	Treatment cycle 1				Treatment cycle 2	
Treatment cycle	**1. Inoculation**	**2. Clay activation**	**3. Ox + BA**	**4./1. Wash or Recharge + wash**	**2. Clay activation**	**3. Ox + BA**
	Live pondwater + NPK fertiliser** mix	**Microbial FeR >20 days**	15 mM BA in sterile pondwater*	Sterile pondwater* ± NPK fertiliser** mix	**Microbial FeR >20 days**	15 mM BA in sterile pondwater*
No. flushes	3	-	2	2	-	2
Total pore volume	750-400 mL†	**NO FLOW**	500-800 mL†	500-800 mL†	**NO FLOW**	500-800 mL†
Redox state	Anoxic	Anoxic	Oxic		Anoxic	Oxic

* autoclaved at 121 ºC for 20 min; ** autoclaved twice at 121 ºC for 20 min before mixing with pondwater; † range represents column pore volumes for SWy-3 and NAu-2 columns, respectively.

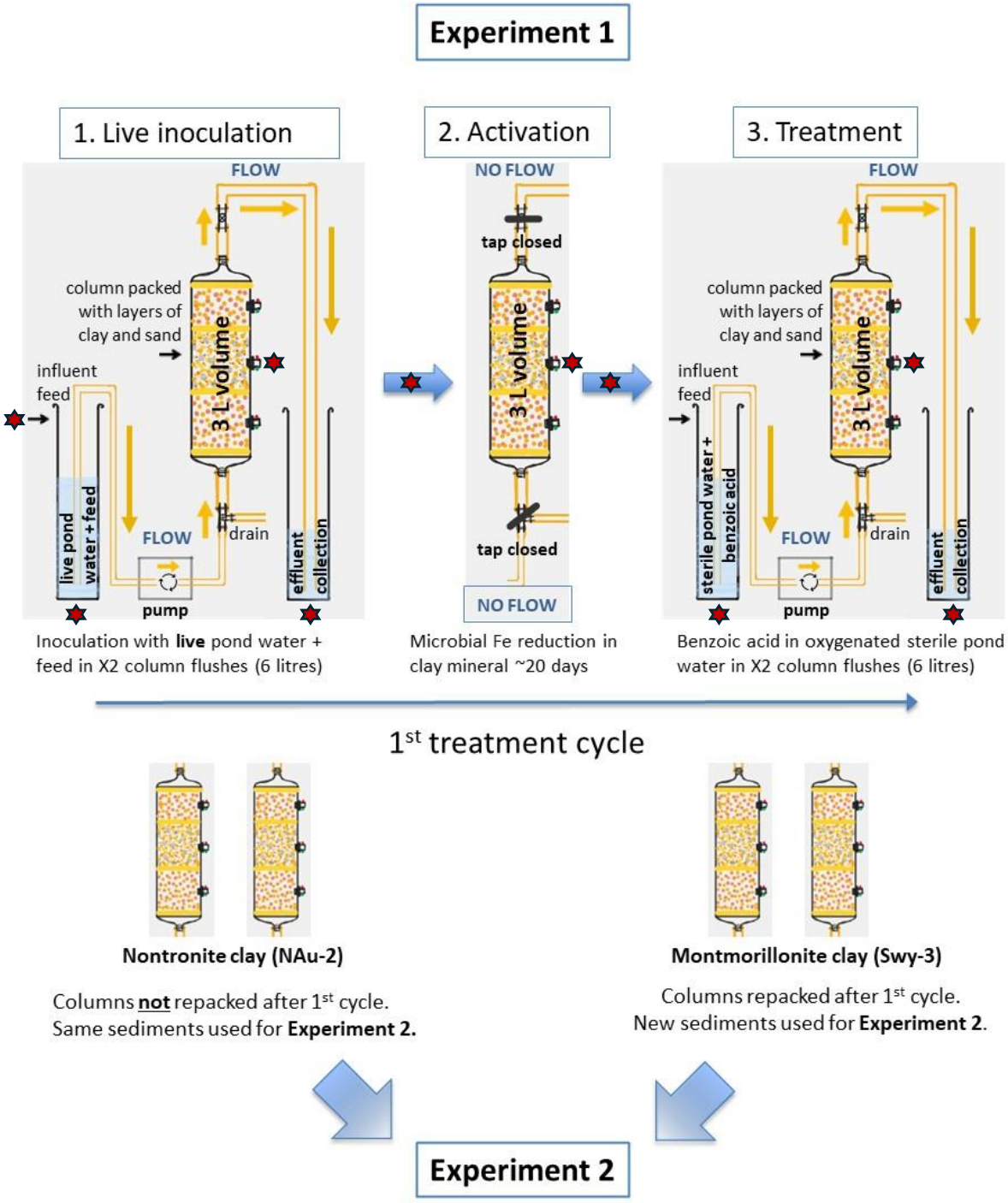

Figure 5. 3. *Diagram showing biological treatment cycle details of Experiment 1. At the start of Experiment 1, column sediments were inoculated with live pondwater to activate clay mineral structural Fe (through microbial Fe^{3+} reduction), before Fe^{2+} is oxygenated during •OH production and treatment of benzoic acid (BA). BA is flushed through the column in an autoclaved solution of pondwater, and as a surrogate micropollutant in synthetic wastewater. A further flush of autoclaved pondwater and organic plant feed is used to flush remaining BA from the column. Sterile pondwater was used to avoid introducing a new community to the column experiments at the start of each treatment cycle. 'Feed' represents the addition of the diluted seaweed-based plant feed. Red stars represent sampling points for microbiology analysis.*

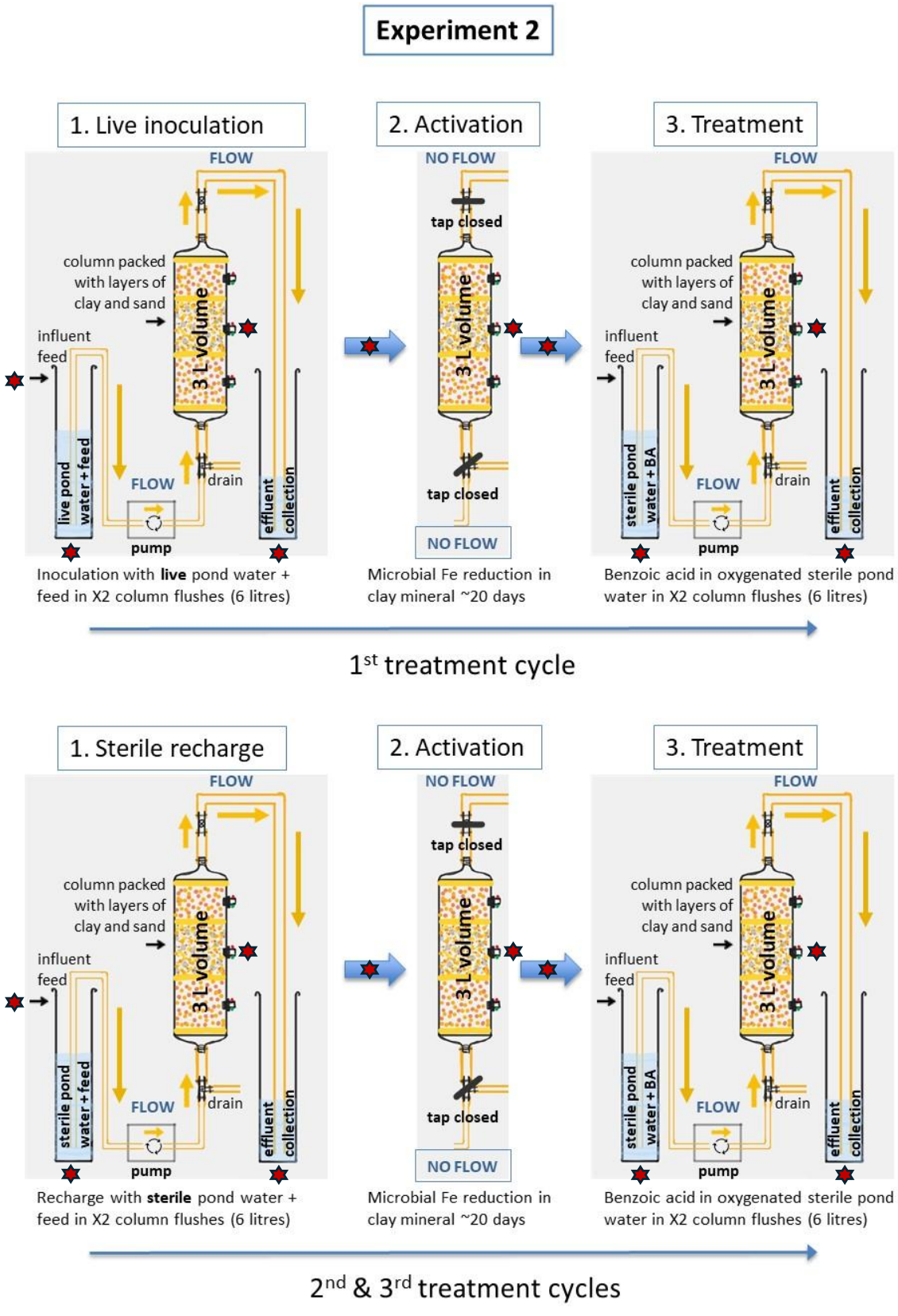

***Figure 5. 4**. Following Experiment 1, column sediments in Experiment 2 were inoculated with live pondwater to activate clay mineral structural Fe (through microbial Fe^{3+} reduction), before Fe^{2+} oxygenation during •OH production and treatment of benzoic acid (BA). BA is flushed through the column in an autoclaved solution of pond water. Further flushes of autoclaved pondwater and organic plant feed are used to both flush remaining BA from the column and prepare for the subsequent treatment cycle (activation phase) by providing a carbon source for microbial metabolism. Sterile pondwater was used to avoid introducing a new community to the column*

experiments at the start of each treatment cycle. 'Feed' represents the addition of the diluted seaweed-based plant feed. Red stars represent sampling points for microbiology analysis.

5.2.4 Sampling and monitoring

In both Experiments 1 and 2, aqueous samples for geochemical analysis were collected from effluent flow tubing before reaching the collection measuring cylinder (Figure 5.2). Similarly to the chemical column experiments, geochemical analyses of biological column samples were used to determine clay mineral dissolution, •OH production and success of BA treatment. All aqueous samples collected for cation and organic analysis were prepared using the approaches described in Chapter 4 (Sections 4.2.7.1-3) and only modifications to analysis are described briefly below (Sections 5.2.5.1).

DNA and RNA samples for 16S sequencing were collected from all inoculants, treatment recharge solutions and column effluents throughout the treatment experiments. Porewaters were extracted from the mid-column sampling ports during clay activation and before, during and after each treatment cycle, to assess changes in community structure with time. All sampling points and relative sampling times are marked on Figures 5.3 and 5.4 and further details of microbiology sampling provided in Section 5.2.5.4.

Small sediment samples (~200 mg) were extracted from the columns before and during clay activation and then after treatment, to determine the Fe reduction extent (i.e. Fe^{2+}/Fe^{TOT} ratio) using elemental analysis (Chapter 4, Section 4.2.7.5) and to characterise the column microbial communities during clay activation and treatment (Sections 5.2.5.4 and 5.2.6). For non-sterile sampling, sediments were extracted inside an oxygen-free glovebox using the approach described in Chapter 4 (Section 4.2.7). Sediment samples for nucleic acid sequence analysis were extracted via the top, middle and lower column sampling ports using EtOH-washed, modified 1 mL plastic syringes. Following extraction, samples were sealed in sterile 2 mL screw-cap vials, placed in grip-seal bags, removed from the glovebox and stored at -80 °C.

5.2.4.1 Microbiological sampling for DNA and 16s rRNA sequencing

Sterile hypodermic needles attached to sterile plastic syringes were used to extract approximately 5 mL of porewater from the central sampling ports of all columns during clay activation then before, during and after the treatment stage (Figures 5.3 and 5.4). In a clean area, samples were immediately labelled and filtered using 0.22 µm Sterivex cartridges (Chapter 3, Section 3.5; Figures 3.12 and 5.5) then flushed with 2 mL of RNA*later*

(ThermoFisher Scientific) through the filter cartridge inlets using sterile 1mL pipette tips. The Sterivex cartridges were then capped at each end with sterile Luer-lock caps and stored in individual grip-seal bags at -80 °C, until analysis.

5.2.4.2 Parameters monitored in situ

A calibrated Extech EC500 Waterproof ExStik® II and a portable Hach meter with DO probe were used to measure pH, temperature, conductivity, TDS and dissolved oxygen (DO) of all reagent stock solutions for oxic stages of the treatment cyce, to achieve a DO concentration of ≥9.8 mg/L O_2. The same physico-chemical parameters were also measured for the pondwater on collection (Section 5.2.2.1 and Appendix C, Table C1).

Before the start of Experiment 2, *in-situ* ROB-OX-10 robust DO probes (Pyroscie nce, Germany) were fixed into the central sampling ports of all columns and used to monitor oxygen (O_2) saturation of column porewaters during the 3 treatment cycles of Experiment 2.

5.2.5 Geochemical analysis

The same analytical methods detailed in Chapter 4 were used to characterise aqueous column effluent samples (HPLC, ICP-OES) with any modifications to those methods used listed below (e.g. Section 5.2.5.1). The chemical oxygen demand (COD) of Leazes Park pondwater, the pondwater-NPK fertiliser mix and the column effluents during the activation phase of experiments was also measured and used as a water quality indicator to determine relative quantities of total oxidisable carbon compounds present (Section 5.2.5.2).

5.2.5.1 High Performance Liquid Chromatography

HPLC was used to quantify BA and 4-HBA in order to calculate •OH production although the method adapted and optimised from that described in Chapter 4, to improve peak resolution of the pondwater-matrix biological column samples. The gradient run program (Appendix C, Figure C.1) was increased to 10 minutes, using mobile phases of acetonitrile (AcN) and de-ionised water (H_2O), amended with 0.5% formic acid (FA) to buffer pH to 2.2-2.4. Peak separation and organic elution were optimised using an increasing AcN/H_2O ramp (5/95 to 95/5) over 5 min with a 1.5 min hold, with a second AcN/H_2O ramp (95/5 to 5/95) over 1.5 min with a 1 min hold, to wash inorganic salts from the column before the next sample injection. Combined standards of 0.3-30 µM 4-HBA and 0.2-20 mM BA were used to generate calibration curves for BA and 4-HBA in a sterile pondwater matrix, which allowed the

conversion of integrated peak to concentrations. The quantitative limit of detection for BA and 4-HBA was determined to be 0.1 µM (based on the analysis of replicate standards), corresponding to 0.59 µM for •OH. HPLC was selected because both BA and 4-HBA should be detectable in a single run and the technique is non-specialist and inexpensive, so potentially accessible in low- to middle-income countries.

5.2.5.2 Chemical Oxygen Demand

Chemical oxygen demand (COD) was used as a water quality indicator to determine relative quantities of total oxidisable carbon compounds present in Leazes Park pondwater, in the pondwater-NPK fertiliser mix (used as a microbial metabolic supplement) and in the column effluents during experiments. Unfiltered aqueous samples of pondwater, pondwater-NPK fertiliser mix and a number of column effluents were tested using a colorimetric COD cuvette test kit (LCI400, ISO 15705, range of 0-1000 mg/L O_2, Hach) following the manufacturer's guidelines. Samples were analysed on a Spectroquant Pharo 300, set to measure absorbance at 254 nm.

5.2.6 16S rRNA gene and transcript sequencing preparation

A generalised workflow for the collection handling and preparation is provided in Figure 5.5. Many 16S surveys are based solely on DNA, however for clarity, the experiments performed here also included sequences derived from extracted RNA transcripts. The goal was to provide information that suggested which taxa were active, in addition to the usual information of which taxa were present. The following sections provide detail for sampling handling and preparation ahead of sequencing.

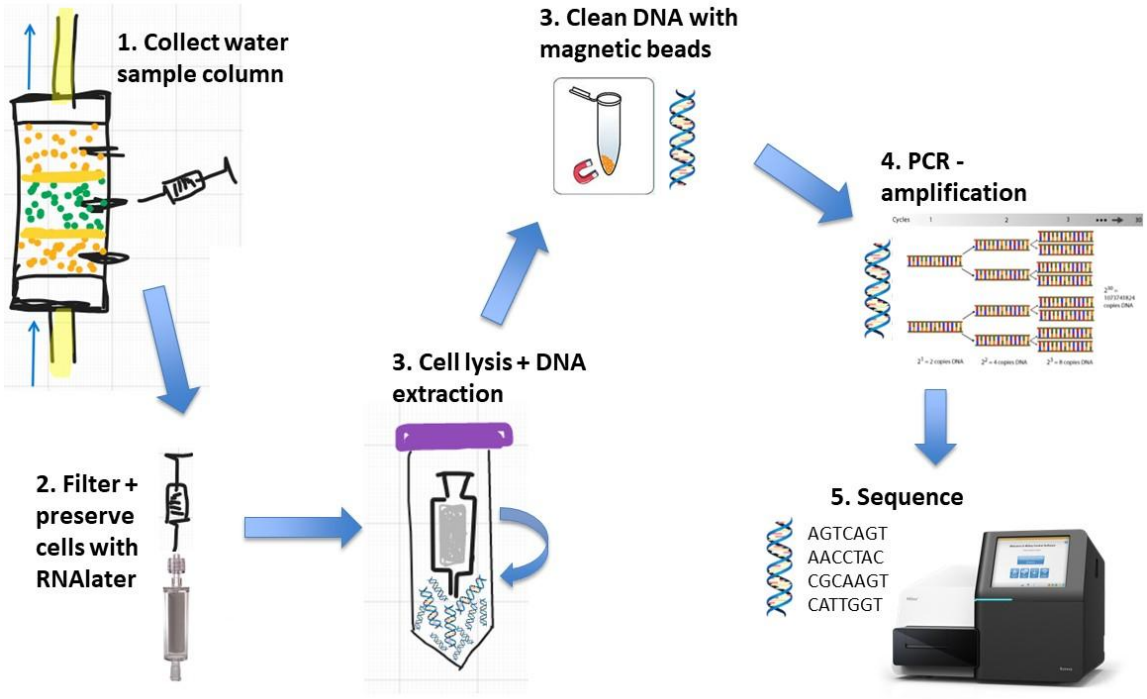

Figure 5. 5. *Diagram showing workflow used to process microbiological samples following sample collection from biological columns and ahead go sequencing using the Illumina MiSeq platform. PCR amplification encompasses all PCR operations associated with sequencing prep as well as, when relevant, reverse transcription associated with cDNA library preparation.*

5.2.6.1 DNA extraction and purification

Total nucleic acid (TNA) from column porewaters and sediments was extracted using a method based on Wong et al. (2020), developed for environmental DNA samples, followed by a TNA purification method adapted from Oberacker et al. (2019). Briefly, RNA*later* was removed from all Sterivex cartridges by centrifugation; a 2 mL screw-cap tube attached to the Sterivex outlet with sealing film and placed into a 50 mL tube, before centrifugation for 20 s at 2000x g. To extract TNA, 2 mL of lysis buffer (guanidine isothiocyanate 6 M, Tris-HCL 75 mM, Sarkosyl 3%, EDTA 30 Mm, Antifoam 0.15%) was added into Sterivex cartridge inlets using sterile 1 mL tips. The ends of each Sterivex cartridge were sealed with Luer-lock caps and incubated at 56 °C for 30 min with mild rotation (Wong et al., 2020). The lysis buffer-TNA mix was collected from each cartridge by attaching a clean 2 mL screw-cap tube to the Sterivex inlet with sealing film, placing inside a 50 mL tube and centrifuging for 20 s at 2000x g, as before.

The lysates (240 µL) were then transferred to either 96 well plates or 1.5 mL microcentrifuge tubes and TNA extracted, following a magnetic bead-based protocol for environmental samples (bomb.bio,Oberacker et al., 2019). To bind TNA to carboxyl coated magnetic beads

(SeraMag Speed Beads), isopropanol (320 µL) was added to all lysates (240 µL), sealed and shaken at RT for 5 min, then the magnetic beads added (160 µL, diluted 1:50 in Tris-EDTA buffer), sealed and shaken for a further 5 min. The bead mixtures were settled on a magnetic stand and the supernatants discarded once clear. After removal from the magnetic stand, 400 µL of isopropanol was added and the mixtures shaken at 1400 rpm for 2 min, then the 96 well plate or 1.5 mL tubes placed back on the stand, settled, and the supernatant discarded again. Using the same approach, two 80% EtOH washes were then used to wash non-target size TNA fragments from the beads. After the second EtOH wash, the supernatant was removed and the beads dried (~5 min) at RT to allow residual EtOH to evaporate. To elute the TNA off the beads, 70 µL of 10 mM Tris HCl was added and the bead mixture resuspended by shaking (and if needed centrifuging at 1000 rpm for 5 sec) before resettling on a magnetic rack. A 2 µL aliquot of each purified TNA sample was then quantified using a Qubit dsDNA HS (High Sensitivity) Assay Kit (DNA quantification range of 0.005 to 120 ng/µL and detection range of 0.1−120 ng1) with a Qubit Fluorometer, before the complete TNA-bead mixture was stored at -30 ^{o}C for up to 3 months, until further sample processing.

5.2.6.2 DNA digestion and reverse transcription

To differentiate active from inactive microbial communities within the columns, a complete subset of the extracted and purified TNA samples was used to create RNA from TNA digests, then a reverse transcription completed on the RNA to generate complimentary DNA (cDNA). An ezDNase Enzyme kit (Invitrogen, ThermoFisher Scientific) with a specificity for double-stranded DNA was used according to the manufacturer's instructions to digest DNA in the sample subset. Before reverse transcription (RT), the RNA samples (as DNA digestates) were cleaned using a magnetic bead-based protocol (Buchner, 2023) and then quantified using a Qubit™ RNA High Sensitivity (HS) Assay Kit (quantification range of 4 to 200 ng) with a Qubit Fluorometer.

Reserve transcription was carried out using LunaScript RT SuperMix (New England Biolabs) according to the manufacturer's specifications. Each reaction comprised 10 µL of cDNA sample, 3.75 µL of LunaScript RT SuperMix and 1.2 µL of random hexamers (NNNNNN oligonucleotides to facilitate random priming of reverse transcription). RT reactions comprised an initial incubation at 48 °C for 30 min, then 94 °C for 1 min, followed by 40 cycles of 94 °C for 15 s, 49 °C for 30 s and 68 °C for 1 min, and then a final extension at 68 °C for 5 min. RT products were purified using 1X solid phase reversible immobilisation (SPRI)

beads (SeraMag Speed Beads in poly-ethylene glycol-based SPRI buffer) as above for TNA isolation, but with just two 80 % EtOH washes and elution into 20 μL 10 mM Tris-HCl.

5.2.6.3 DNA and cDNA amplification

The ribosomal 16S DNA and cDNA plates were PCR-amplified using MyTaq Red Mix according to the manufacturer's instructions with forward and reverse bacterial primers. Forward and reverse bacterial primers were 515F and 806R (Caporaso et al., 2012), respectively, with 20 bp tags to facilitate demultiplexing by reference to unique tag combinations for each well of each plate of samples following sequencing, and an overhang for priming of Nextera primers for incorporation of Illumina sequencing adapters. Each PCR totalled 20 μL, containing 5 μL of template, 14.2 μL of MyTaq Red Mix and water and 0.8 μL of each PCR primer. PCRs comprised an initial denaturation at 95 °C for 5 min, then 35 cycles of 95 °C for 30 s, 50 °C for 30 s and 72 °C for 1 min, and then a final extension at 72 °C for 5 min. Successful amplification was checked using a Qiagen Qiaxcel Connect with a Fast DNA Cartridge, which generated amplicon size, concentration and molarity data. Samples were pooled into one tube per plate with sample input volumes adjusted for approximate equimolarity based on Qiaxcel molarity data. Sample pools were purified with SPRI beads as above. A second round of PCR was used to incorporate Illumina adapters using Nextera PCR primers (IDT). Each of these PCRs totalled 20 μL, containing 10 μL of template, 2 μL of MyTaq Red Mix, 3 μL of primer mix and 5 μL of water. PCRs comprised an initial denaturation at 95 °C for 5 min, then 12 cycles of 95 °C for 30 s, 60 °C for 30 s and 72 °C for 1 min, and then a final extension at 72 °C for 10 min. PCR products were purified by SPRI beads as above, their concentrations determined via Qubit dsDNA HS Assay Kit and pooled to achieve approximate equimolarity across samples. Amplicon sizes were checked via TapeStation 4200 using a D1000 tape to ensure successful incorporated of Illumina adapters, and the final library subsequently sequenced.

5.2.6.4 DNA and 16S rRNA sequencing

Sequencing of DNA and 16s rRNA was carried out on the Illumina MiSeq Platform (v3 250 bp) by the Genomics Core Facility at the International Centre for Life (Newcastle University, Central Parkway, Newcastle upon Tyne, NE1 3BZ) with assistance from the Bioinformatics Support Unit for compilation of raw sequencing read data.

5.2.7 Bioinformatics

Raw sequencing data (fastq files) were demultiplexed using the Newcastle University High Performance Computing Facility (Rocket) and sequencing data processed using the DADA2 pipeline (Callahan et al., 2016) developed for R (R Core Team, 2023) as per the DADA2 tutorial. Sequences of sufficient read quality were assigned taxa using the DECIPHER (Wright, 2016) plug-in for DADA2 and the SILVA SSU r132 (Callahan et al., 2016) training database. The PHYLOSEQ package (McMurdie & Holmes, 2013) was used to combine the OTU table with sample data and raw sequence reads and explore the data using ggplot (Wickham, 2016) through ordination and bar plots. Bacterial communities were compared using the 'manyglm' command in the R package 'mvabund' (Wang et al., 2012) with a Poisson error family and Montecarlo resampling.

5.3 Results and discussion

5.3.1 Clay activation

Following microbial activation of the biological columns, the nontronite-bearing reactive layer of the chemical column changed from brown to a dark green colour (Figure 5.6), as observed following activation of the chemical columns (Chapter 4, Figure 4.6). This colour change is typical of structural Fe^{3+} reduction to Fe^{2+} in the NAu-2 nontronite in both chemically and biologically-reduced nontronites (Huang et al., 2018). No colour change was observed in the SWy-3-bearing biological columns.

Figure 5. 6. *Image of microbially-activated NAu-2 biological column, 20 days after inoculation. Not the very dark green which is characteristic of reduced nontronite clay.*

The extent of clay activation within the biological columns was measured from Fe^{2+}/Fe^{TOT} ratios following mineral digestion of the column reactive layers, as described in Chapter 4 (Section 4.2.7.5). Taking into account the Fe^{2+}/Fe^{TOT} ratio of the column reactive layer sediments before clay activation and treatment (first column, Table 5.4), results show that over 22% microbial Fe reduction has occurred in the NAu-2 columns and < 7% in the SWy-3 columns, during activation of the clay, following inoculation. These microbial reduction extents are typical of those reported for Fe-bearing nontronite and montmorillonite clay minerals (Dong et al., 2009). Possible reasons for the differences in reduction extent may be Fe content, and therefore overall accessibility of Fe for bioreduction (Zhang et al., 2013), or that tetrahedral Fe is more susceptible to bioreduction than *cis*-octahedral Fe sites (Jaisi et al., 2005), and NAu-2 contains tetrahedral Fe whereas SWy-3 does not. The NAu-2 sterile control column showed a negligible change in the amount Fe^{2+} in the column reactive layer (increase of <1.1%) after one complete treatment cycle during Experiment 2.

Table 5. 4. *Extent of microbial Fe reduction during clay 'activation' in biological columns before experiments, after 17 days (Experiment 1) and after the third treatment cycle in Experiment 2.*

Column sediments (reactive layer)	**Before experiment**	**Day 17 – during microbial reduction, near end of 1st activation (Exp 1)**	**After last treatment (Exp 2)**
NAu-2 treatment columns	1.95 %	24.5 %	21.6 %
SWy-3 treatment columns	3.71 %	11.0 %	16.4 %
NAu-2 sterile control columns	1.95 %	-	3.01 %

5.3.2 Generation of •OH for contaminant treatment

Production of •OH from the activated, Fe^{2+}-bearing, reactive layers of the biological columns experiments was initiated by two flushes of oxygen-saturated autoclaved pondwater, spiked with 15 mM of benzoic acid (BA, as the surrogate micropollutant), and then quantified using BA as the •OH scavenger. Degradation of the BA occurred in all NAu-2 clay and SWy-3 clay biological column experiments to different extents, with the exception of the sterile NAu-2 control columns where negligible BA degradation occurred. In subsequent figures, columns containing the NAu-2 clay have prefix 'N' and those containing the SWy-3 clay have prefix 'S'.

Figure 5.7a shows typical concentration profiles of BA and its degradation product, 4-hydroxy benzoic acid (4-HBA), detected by HPLC in effluent from column 'N1', which was one of the NAu-2 clay (biological) column duplicates. Figure 5.7b shows the same data for column 'S2', one of the SWy-3 clay (biological) column duplicates. In both cases, results are shown during the oxic 'treatment' stage of the 1st treatment cycle (~6 h period) at the start of Experiment 2. Also shown on Figures 5.7a-b are BA and 4-HBA effluent concentrations from the sterile control column 'NC' (using NAu-2 clay) over the same period, where no 4-HBA was detected.

During biological treatment cycles, 4-HBA was detected in column effluents either slightly before or at approximately the same time as the BA, although both analytes usually took at least 2 pore volumes (~250 mL or 400 mL for SWy-3 and NAu-2 columns, respectively; Table 5.3) to reach concentration maxima. Both BA and 4-BHA remained at their maxima in column effluents (BA range: 10-15 mM BA, 4-HBA: 0.75-3 µM) until the pondwater + NPK fertiliser was flushed through the column (Flushes '7-8'; Figures 5.7a-b), ahead of the next treatment cycle. Figure 5.7c is an annotated plot highlighting these trends for all biological columns, including the control (NC), through one complete treatment cycle.

trends in BA and 4-HBA concentration profiles for all biological columns during the first treatment cycle in Experiment 2 (Figure C.4).

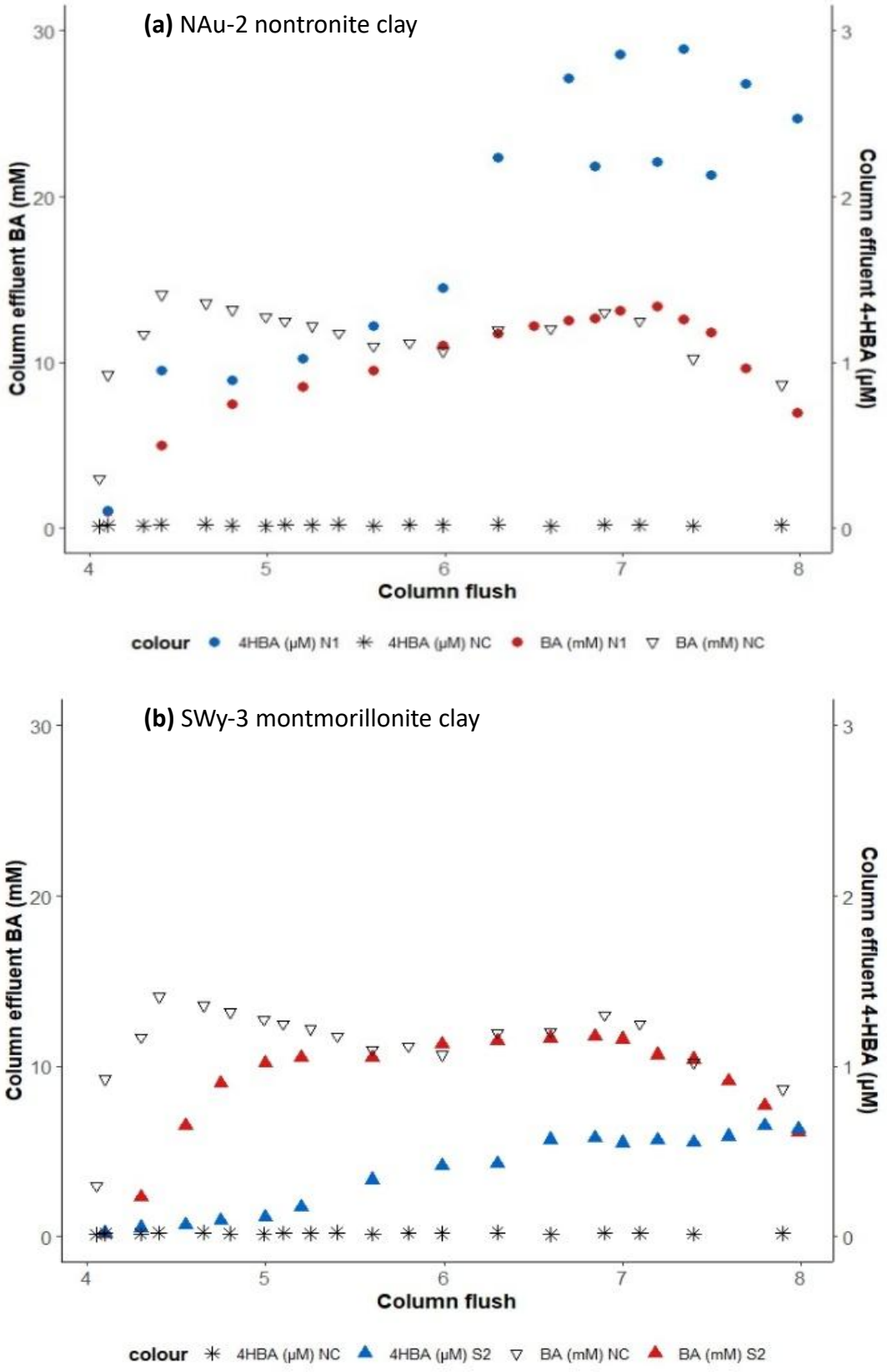

Figure 5. 7 a-b. *Typical profiles of benzoic acid (red markers) and 4-hydroxybenzoic acid (blue markers) detected in effluent from biological column experiments containing* ***(a)*** *nontronite clay (NAu-2) and* ***(b)*** *montmorillonite clay (SWy-3) during the 1st treatment cycle of Experiment 2, when BA (white triangles) is pumped through in 4 column flushes. Representative data shown are from columns* ***(a)*** *N1 (an NAu-2 clay replicate column) and* ***(b)*** *S2 (a SWy-3 clay replicate column). Data from column NC (an NAu-2 clay sterile control column) is shown on both plots for comparison - denoted by grey asterisks and triangles.*

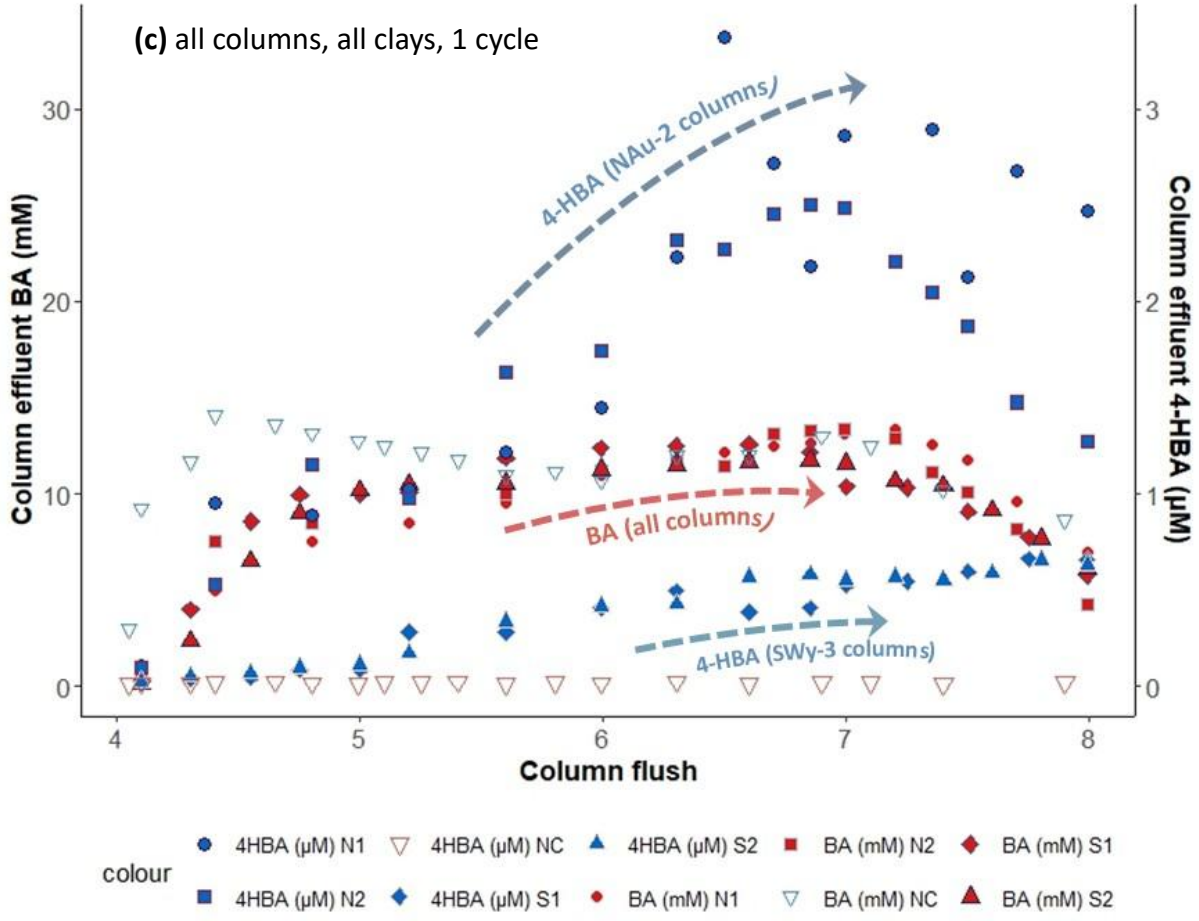

Figure 5. 7 c. *Observed trends in concentration profiles for BA and 4-HBA in effluents collected from all biological clay columns (NAu-2 clay: N1, N2 and NC (control); and SWy-3 clay: S1, S2) using data from Experiment 2, during the 1st treatment cycle, plotted as a function of column flush.*

To illustrate the cyclicity of these experiments, the profiles of BA and 4-HBA measured in column effluents across all four treatment cycles is shown in Figures 5.8a-b, for columns N1 (NAu-2 clay) and S2 (SWy-3 clay) using data from both Experiments 1 and 2. The same form of linear plot is shown in Appendix C for the biological control column (NC; NAu-2 control), and the remaining duplicate columns containing NAu-2 and SWy-3 clays (Figures C.2, C.3 and C.4, respectively).

Although a concentration of 15 mM/L BA was pumped through each of the treatment columns, it was calculated that after column flush 5, up to ~25% of BA could be unaccounted for in the column. Reasons for this could be sorption of BA onto the PVC column surface, which was not investigated in detail in this study and was not to observed as an issue in the chemical column experiments (Chapter 4). Sorption of BA to the clay surface is also a possibility, with (Kotelnikov et al., 2022) reporting that clay mineral horizons within podzolic soil could retain 0.06 to 0.15 mmol of benzoic acid per 1 kg of soil. Using this as a guide, it is

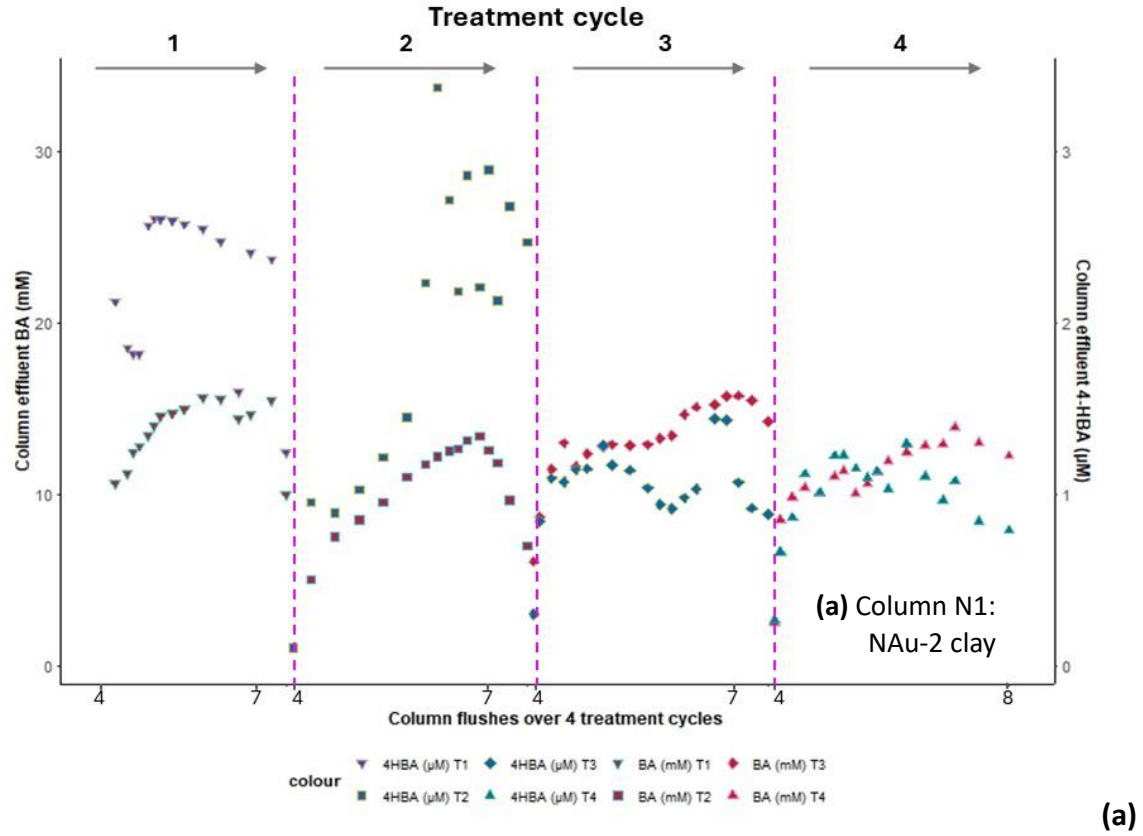

(a)

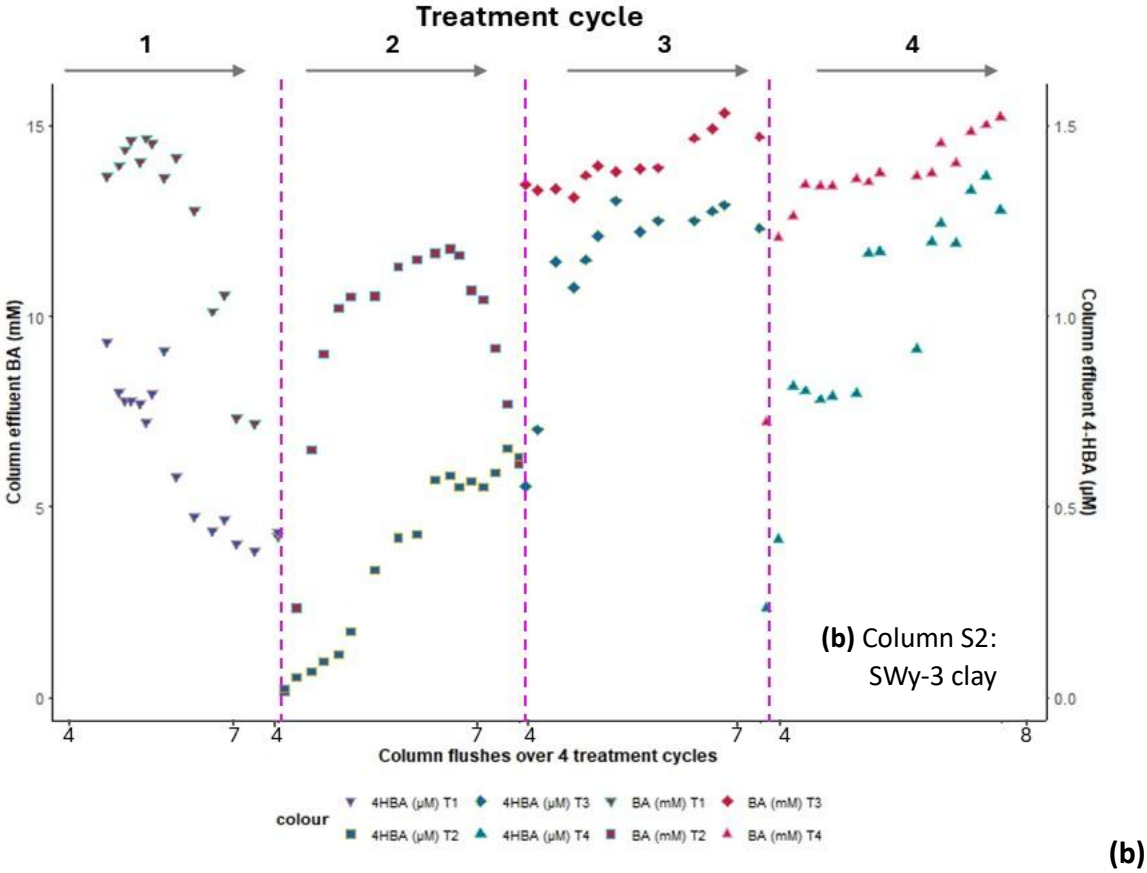

(b)

Figure 5. 8*. Concentration profiles of BA and 4-HBA measured in biological column effluents across all 4 treatment cycles, for columns* ***(a)*** *N1 (NAu-2 clay) and* ***(b)*** *S2 (SWy-3 clay), using data from both Experiments 1 and 2. Data plotted as a function of column flush, where flush #4 indicates the start of the BA treatment and flush #8 (after #7) marks the end of each treatment cycle.*

possible that ~0.18 to 0.45 mmol of benzoic could be sorbed to the clay in the test columns in this study, given the high cation exchange capacities of smectite clays. Alternatively, reaction and partial degradation of BA with pondwater constituents or micro-organisms is considered plausible. This is addressed in Section 5.3.4.

5.3.2.1 •OH generation yield and treatment efficiency

The sterile control column (Experiment 2) yields only negligible •OH (Figure 5.9). NAu-2 columns consistently yield more •OH than SWy-3 columns, with the first treatment cycle yielding the highest number of •OH in the first cycle of Experiment 1, and least in the final cycle of Experiment 2 (Figure 5.9), although these columns were not repacked between experiments. Conversely, the SWy-3 columns were repacked between experiments and show a slightly different behaviour compared to the NAu-2 columns in terms of •OH yield. The SWy-3 columns instead show an overall increase in •OH yield after the first treatment cycle in Experiment 2 (Figure 5.9).

Per unit mass of Fe^{2+} oxygenated, •OH yields calculated for the biological columns are 18-40 µmol/g Fe^{2+} (for the NAu-2 columns) and for the SWy-3 columns, 9-27 µmol/g Fe^{2+}, which are all within the range of literature values of 0.8 µmol/g Fe^{2+} (Ma et al., 2019) to 123 µmol/g Fe^{2+} (Tong et al., 2016).

The chemical column experiments (Chapter 4) provided evidence suggesting that Fe (oxy)hydroxides contribute to the generation of •OH during at least the first treatment cycle in a flowing column system. The production of OH from this pathway this likely occurred through oxygenation of sorbed and near-edge Fe^{2+}, generated through the reductive dissolution of Fe (oxy)hydroxides associated with the column sands.

Overall, the efficiency of the biological column experiments was higher than the chemical column experiments but not as high as might be expected given the biological column experiments contain approximately 6 times more clay. The efficiency of the chemical column treatment cycles ranged between 0.24-0.55% whilst the most efficient biological column treatment cycle was 0.7% in Experiment 1, in one of the NAu-2 duplicate columns (Appendix B, Figure B.5). The treatment cycles in Experiment 2 were less efficient and ranged between 0.15% and 0.45%, with the NAu-2 duplicate columns decreasing in efficiency whilst the SWy-

3 columns increased in efficiency through Experiment 2. Otherwise, there were no other trends between the two clay column sets.

A possible explanation of the low •OH yield measured in the biological experiments could be the inhibition of •OH yield by redox-active pondwater constituents, for example humic and fulvic acids. In an exploratory study of •OH production from soil organic matter-mediated microbial Fe reduction, (Han et al., 2022) showed that humic acid inhibited 30−43% of the •OH yield generated. This is a considerable proportion of •OH yield and could go some way to explaining the discrepancy in mass balance between BA and 4-HBA concentrations measured in column effluents.

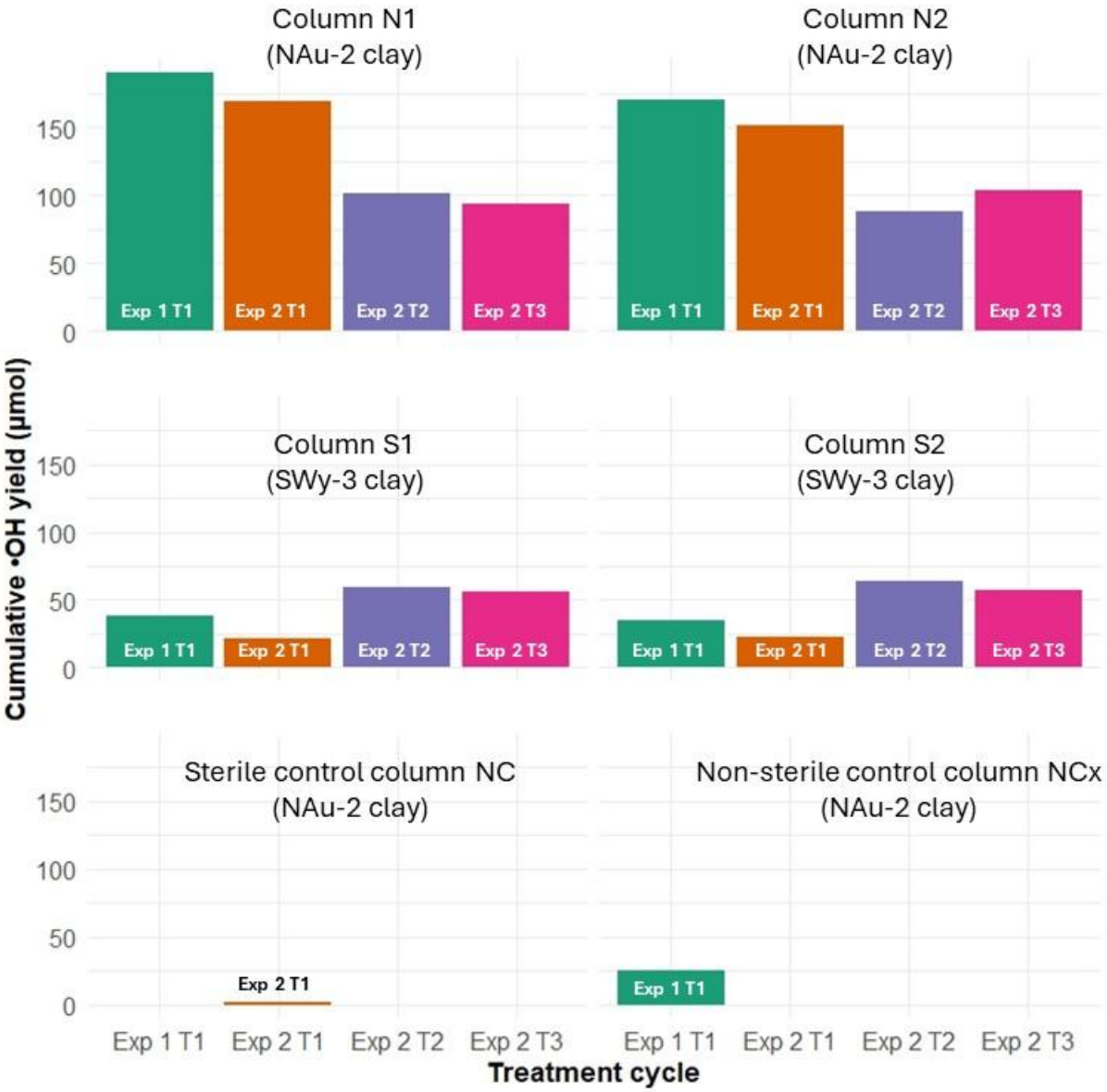

Figure 5. 9. *Cumulative •OH yield in biological experiments, shown for each treatment cycle (T1, T2, T3) in Experiments 1 and 2 (Exp 1, Exp 2). Note that the NAu-2 clay 'control column NCx' was found not to be sterile following clay activation, hence Fe^{2+} generated during microbial FeR and subsequent Fe^{2+} oxygenation during the treatment phase yielded measurable •OH.*

5.3.3 Sustainability of clay activation and •OH production for treatment

As a key component in the production of •OH in this AOP treatment system, the loss of Fe from the treatment columns was measured using the approach described in Chapter 4. Total Fe concentrations were consistently greater than filtered Fe (representing the colloidal Fe fraction) in effluents across all experiments, suggesting that like the chemical column experiment, colloidal transport of Fe out of the biological columns was not significant (Appendix C, Figures C. 5-8).

Loss of Fe from the sterile biological control (NC) was negligible at > 0.5 µM/L during one column flush through one complete treatment cycle (Appendix C, Figure C.9. However, overall, total Fe loss from the NAu-2 biological columns was considerably greater than from the SWy-3 columns and in some cases, over an order of magnitude higher (Figure 5.10). Other than Fe content of the clay (NAu-2 contained more than 10 times the amount of Fe compared to than SWy-3), it should be noted is that the NAu-2 columns were repacked between Experiments 1 and 2 and the SWy-3 columns were not. The mean (of column duplicates) loss of Fe from column effluents during both experiments highlights the difference in relative Fe loss from the NAu-2 column compared to the SWy-3 and the dead control column. It is plausible that the impact of extended exposure to biofilms was partial clay dissolution and during flow, dissolved Fe was washed out of column.

Mass balance calculations indicate that despite effluent loss, the majority of Fe remains inside both column experiments (Table 5.5).

Table 5. 5. *Mass balance table for Fe^{TOT}, showing Fe concentration (mmol) with the column and cumulative Fe lost in effluent during the entirety of each experiment. For experiment 2, the values shown for columns N1, N2, S1 and S2 are the cumulative sums of all Fe lost (mmol) during the 3 treatment cycles undertaken during that experiment.*

NAu-2 (mmol)				
Exp	Column	In	Out	%loss
1	N1	368.4	3.7	1.0
1	N1	368.4	3.2	0.87
1	NCx	368.4	0.085	0.02
2	N1	368.4	59.8	16.2
2	N2	368.4	14.97	4.06
2	Nc	368.4	9.02	2.45

SWy-3 (mmol)				
Exp	Column	In	Out	%loss
1	S1	301.4	0.39	0.13
1	S2	301.4	0.46	0.15
2	S1	301.4	43.4	14.4
2	S2	301.4	53.5	17.8

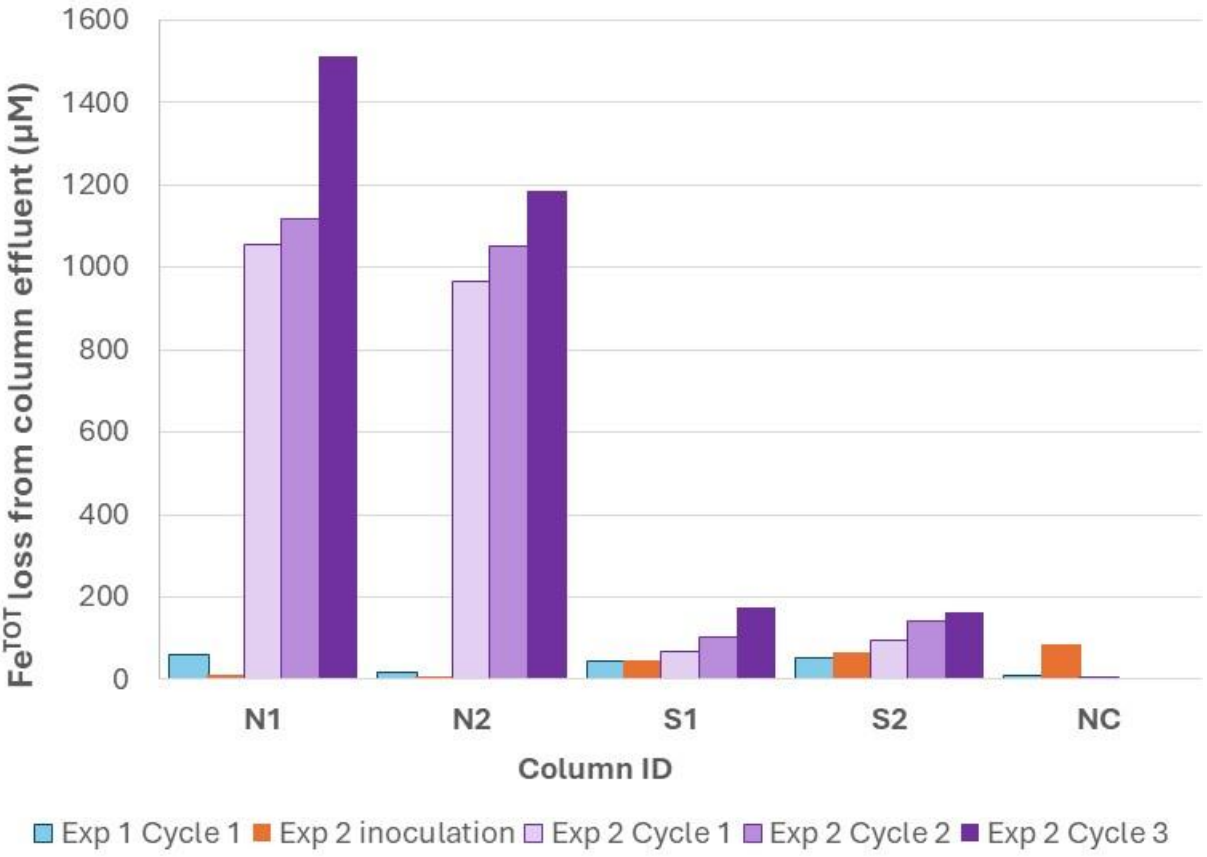

Figure 5. 10. *Absolute loss of Fe from the NAu-2 and SWy-3 biological columns after each treatment cycle and experiment.*

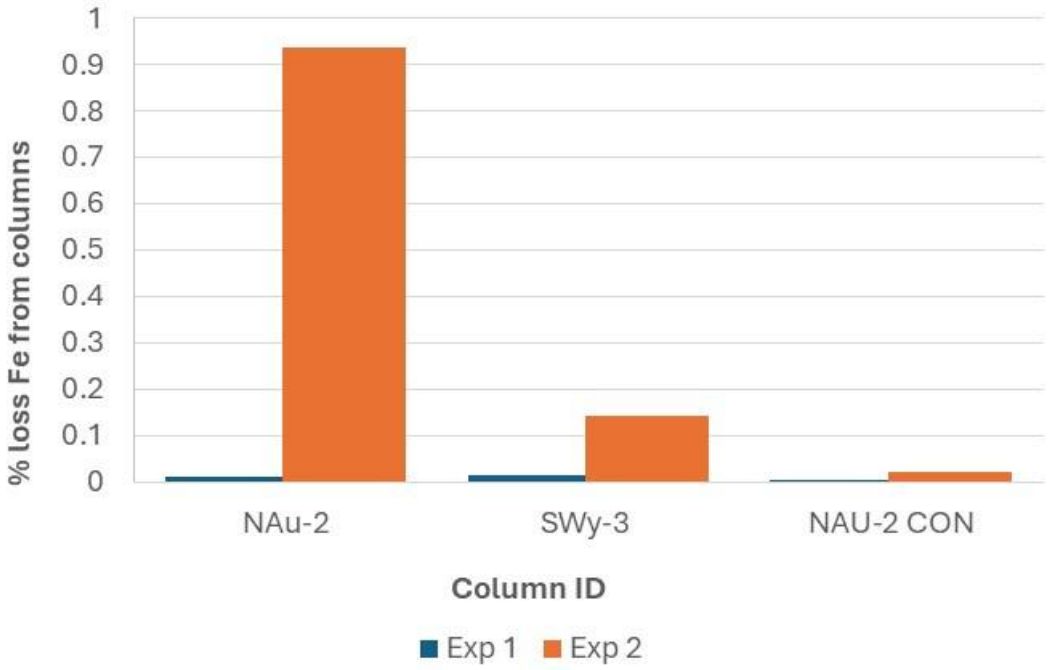

Figure 5. 11. *Combined loss of loss of Fe from NAu-2 and SWy-3 biological treatment columns and the NAu-2 control column.*

5.3.3.1 Clay dissolution

To determine whether •OH production could have been affected by availability of Fe through clay dissolution during the treatment process, a Spearman's rank correlation test was applied to data for major cations collected from column effluents, as described in Chapter 4. Spearman correlation matrices were generated for Fe, Si, Al, S, Ca, Mg, K and Na and are represented as heatmaps in Appendix C (Figures C.10 a-d). Correlation tests were grouped according to clay type and experiment, and data for control columns were not included. The results were used to indicate potentially significant relationships for further investigation.

Spearman's rank P values showed highly positive correlation between Ca and Mg (*P=0.9-1*) in all column effluents tested. This is likely attributable to the conservative behaviour of both Ca^{2+} and Mg^{2+} as major cations within the Leazes Park pondwater and suggests that pondwater chemistry has a consistently strong chemical signature in column effluents throughout experiments (e.g. Appendix C, Figure C.9). Ca and Mg are also both positively correlated with Fe (0.7) and to a lesser extent with Si (0.5 and 0.4, respectively).

In Experiment 1, a large number of cations are positively correlated (Appendix C, Figure C.10a), suggesting that these cations may be similarly mobile within column effluents in this experiment. Some issues with column plumbing were experienced in Experiment 1 causing periods of higher flow rate to occur, so it is possible that more elements were mobilised through this. In Experiment 2, Si and Al are highly positively correlated for the SWy-3 columns, which could indicate clay dissolution through loss of Si and Al from the phyllosilicate structure. Refer to (Zhang et al., 2013) for cation ratios representative of smectite dissolution due to microbially-mediated Fe reduction.

Inspection of cation ratios in column effluents can elucidate the possible causes of Fe mobility alongside other cations. An increase in the Fe/Si ratio in NAu-2 column effluents during the first treatment cycle in Experiment 2 (Figure 5.12) is coincident with the introduction of BA to the columns (during column flush 3). This suggests that Fe being lost at this stage may previously have been partially or fully solubilised from the column sediment and is easily washed out of the column as Fe_{aq}^{2+}, during BA pumping.

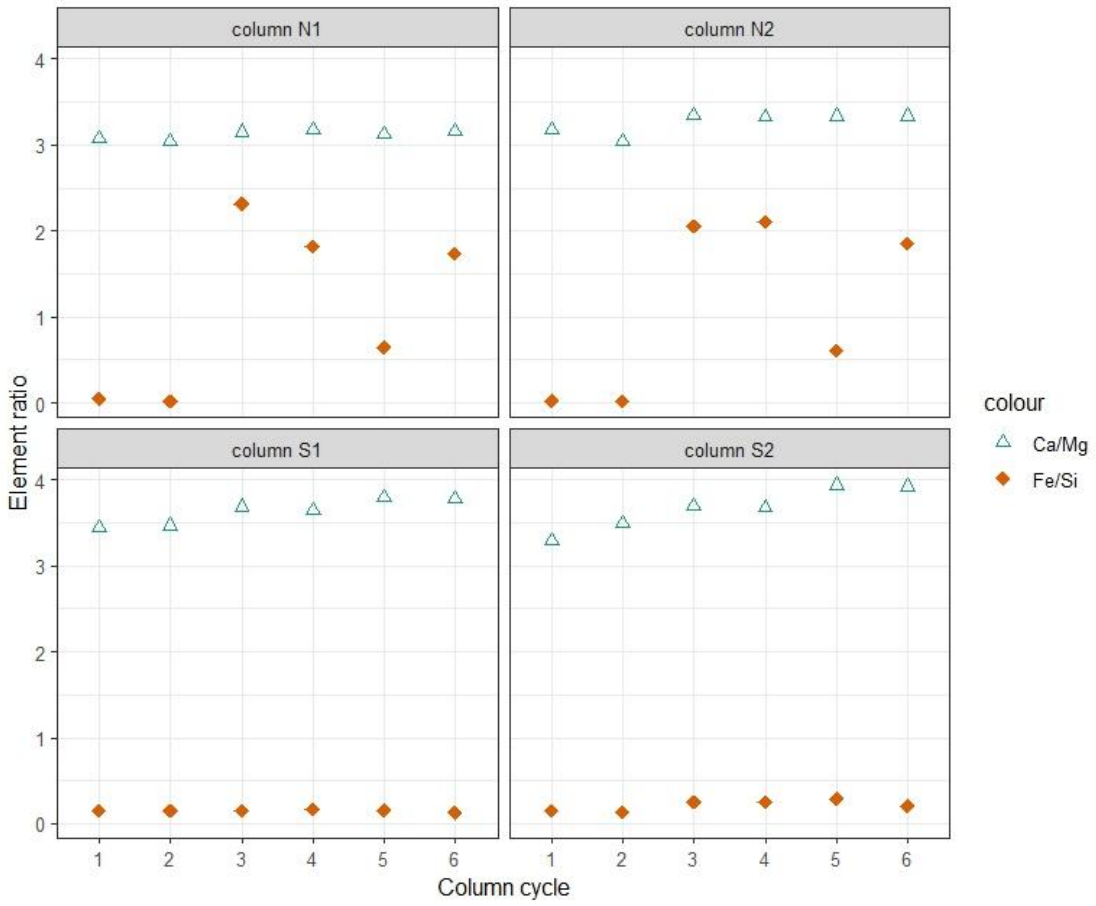

Figure 5. 12. *Ratios of Ca and Mg from effluent concentrations over time from the NAu-2 and SWy-3 biological columns in Experiment 2, treatment cycle 1.*

Fe/Al and Al/Si ratios for the same experiments (Figure 5.13), are very high in effluents for the NAu-2 columns but not the SWy-3 columns, at the point which BA is introduced (during column flush 3). The coincident loss of Al and Si with Fe suggests that clay mineral dissolution may be occurring through break down of the aluminosilicate structure, although the magnitude of the ratio indicates that the majority of loss in these effluents is Fe. The same trend in Fe/Al and Al/Si ratios is seen in all NAu-2 biological column experiments but not for the SWy-3 columns, suggesting that that Fe mobilisation and subsequent Fe washout may not be occurring to the same extent in the SWy-3 columns (if at all), compared to the NAu-2 columns. These findings are reflected in the total Fe loss reported for all of the column experiments (Figure 5.10).

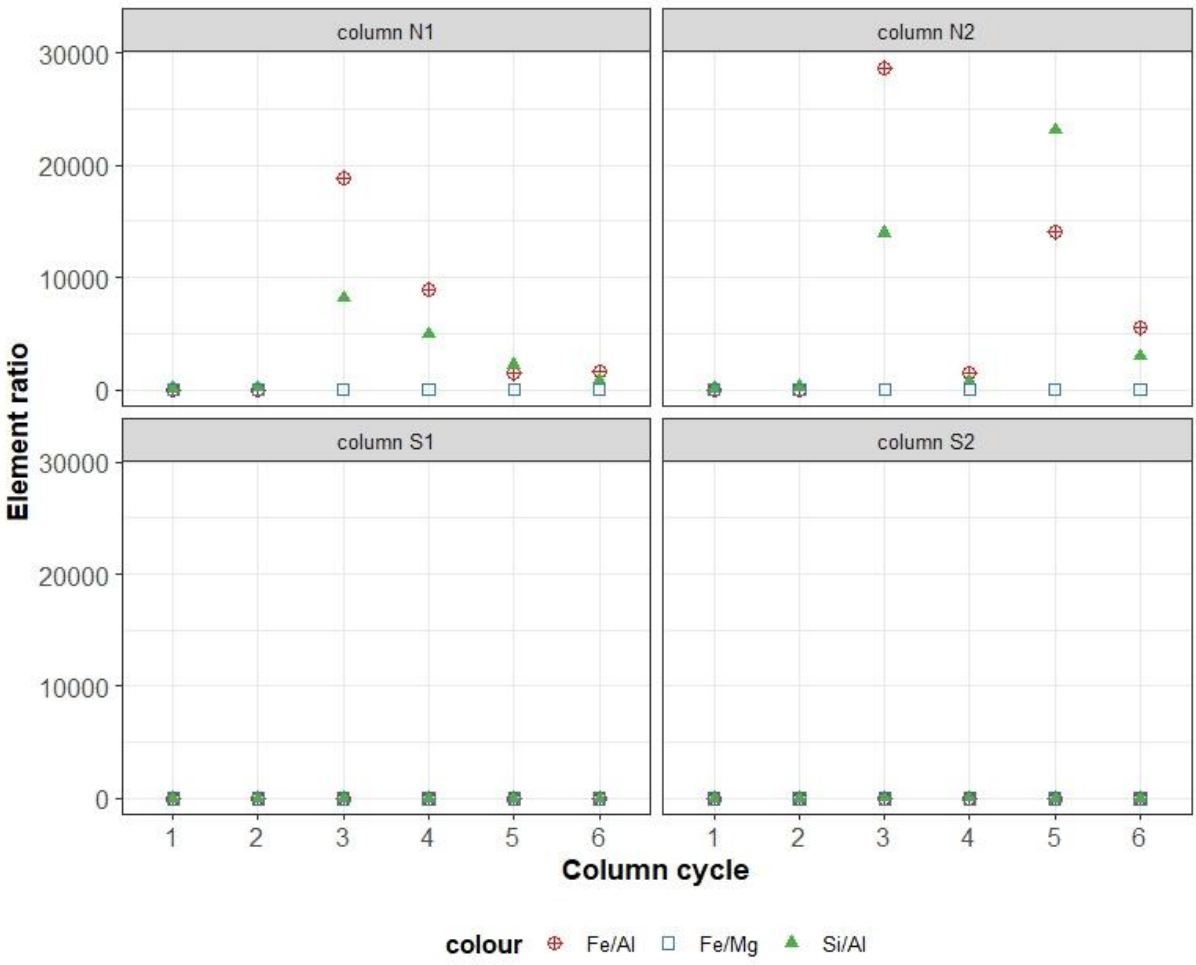

Figure 5. 13. *Ratios of Fe/Al, Fe/Mg and Si/Al from effluent concentrations over time from the NAu-2 and SWy-3 biological columns during Experiment 2 (1st treatment cycle).*

5.3.3.2 Summary

In summary, most Fe from the NAu-2 column experiments is lost during Experiment 2, with the only treatment cycle in Experiment 1 losing at least an 1 order of magnitude less than any of the treatment cycles in Experiment 2. This loss could be due to several factors:

1. increased solubilisation of the NAu-2 clay during dissimilatory Fe reduction in the clay activation phase of the treatment cycle, which is well recognised [REF]. The reduction extents of the NAu-2 columns (up to 24.5% Fe^{2+}) were greater than the SWy-3 columns, suggesting that more dissolution of the clay mineral may have occurred within the column.
2. not repacking the NAu-2 columns could have given rise to greater microbial activity within the column and prolonged exposure of the column sediments to extracellular

polymeric substances (EPS), which also possibly increasing the rate of clay mineral dissolution.

The results presented here suggest that microbial clay activation is sustainable over at least three treatment cycles for all clays tested in these experiments. In the longer term, however, the loss of Fe from this microbially-driven treatment system may not follow a linear trend and predicting clay mineral integrity, which is critical to the success of Fe redox-cycling, and the lifespan of this clay-based AOP could be challenging.

5.3.4 Microbiology

To gain a better understanding of the role of the microbial community in the biological treatment experiments, the 16S rRNA sequencing data sets for column porewaters and sediments were examined. The specific goals of this work were to identify (if possible) which microbes were responsible for clay activation through microbial Fe-reduction and which microbes were able to survive the treatment process and/or potentially affect it. Sequence read depth was found not to be of adequate quality for some time-series samples, so selected data is shown to support hypotheses proposed.

5.3.4.1 Understanding the diversity and richness of microbial communities in the clay columns

First, ordination plots using Principal Component Analysis (PCoA) based on Bray-Curtis dissimilarity were used to explore community diversity between clay types in sediments and column porewaters from Experiments 1 and 2, to identify whether the same microbial communities were likely to be responsible for clay activation during the treatment experiments.

Community relationships between column sediments were explored using cDNA results to indicate communities that were active at the time of sampling (Figure 5.14). The first two axes of the ordination explain 7.7% of the variance each, which indicates that the ordination captures a modest amount of the higher dimensional differences between samples. Ideally a statistical test such as PERMANOVA would be used to assess these differences and this is recognised as further work. At this level it is not possible to confidently comment on relationships between the two clay types, although samples taken from the NAu-2 live control column (NCx) during Experiment 1, showed the greatest community diversity within a single sediment column (Figure 5.14). Otherwise, the relatively small number of sediment

samples collected means that no other correlations between samples can be observed at this scale.

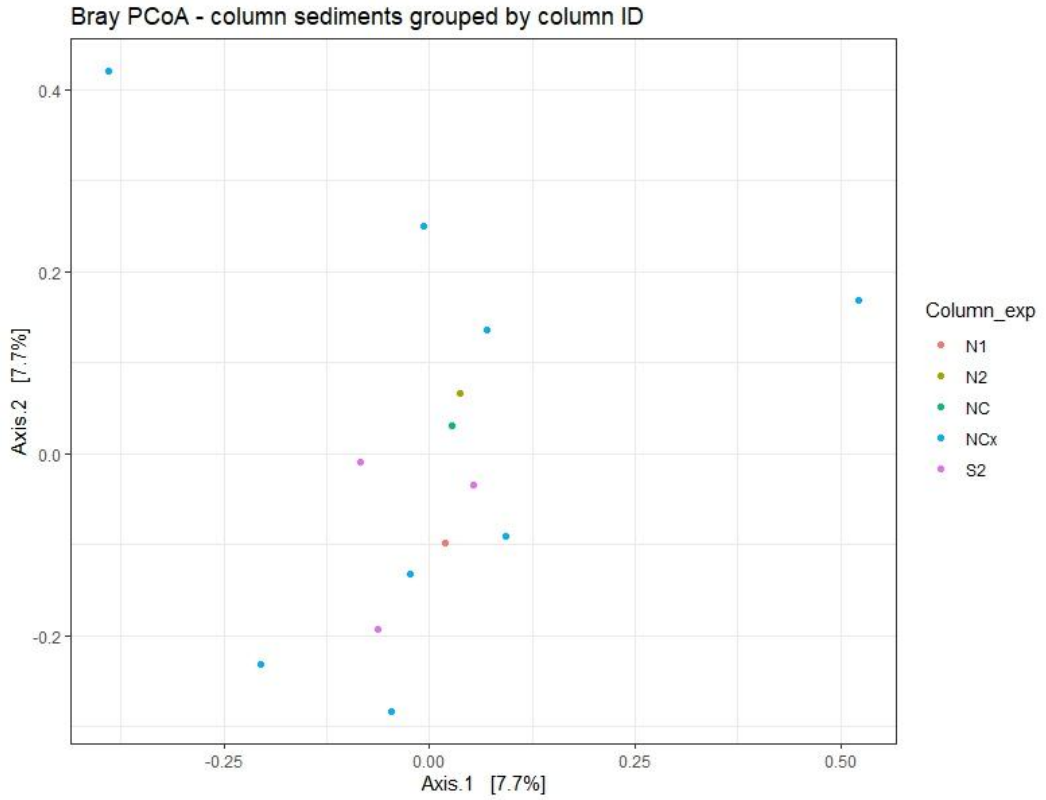

Figure 5. 14. *Principal Coordinates Analysis (PCoA) ordination of 16S cDNA data for all sediments sampled from the NAu-2 and SWy-3 biological columns during Experiments 1 and 2.*

cDNA results for porewater samples across the experiments showed different trends to the sediments, with ordination explaining a small amount of variance (3.6% on the first two axes). When grouped together, the majority of porewaters from the SWy-3 and NAu-2 columns sampled during Experiment 1 showed little diversity as a group (Figure 5.15), suggesting that porewaters may influence the microbial community composition more than clay type. Within this sphere, porewaters from within the NAu-2 column sets (N1, N2 and NCx) showed more community diversity than the SWy-3 porewaters through Experiments 1 and 2 (Appendix C, Figure C.13), despite the N series porewaters being in contact with the same clay. For this part of the study, NCx was considered as a live test column due to having been contaminated at an early stage in the Experiment.

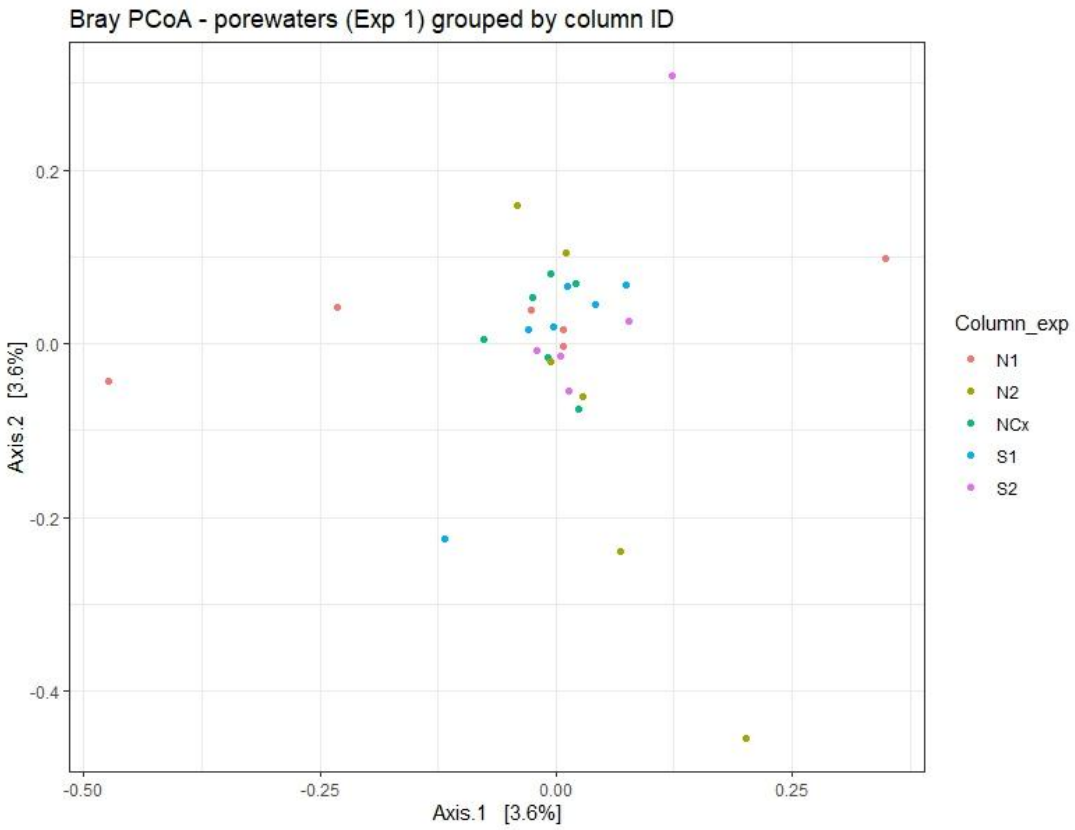

Figure 5. 15. *Principal Coordinates Analysis (PCoA) ordination of 16S cDNA data for all porewaters sampled during Experiment 1 show little diversity in community composition overall.*

5.3.4.2 Survival of microbial communities through the treatment process

To explore whether alpha diversity in columns and porewaters changed over time (and with ongoing treatment cycles) the Shannon and Simpson diversity measures were used. The Simpson diversity measure shown here is specifically the *Simpson Index of Diversity* (1-D) where relative abundance is less influenced by rare species than the Shannon index. cDNA data sets from porewaters collected during both experiments 1 and 2 were grouped according to clay type as a function of time (and ongoing treatment. cDNA data was used here over DNA in order to elucidate microbes active during sampling, *e.g.,* therefore those most likely to survive •OH exposure during treatment cycle(s). Due to having the greatest sample numbers, cDNA for porewaters in Experiment 2 (only) is shown on Figure 5.16. For both alpha diversity metrics, the differences between clay types, which were not large to begin with, grew closer over time as the communities underwent multiple treatment cycles (marked by red stars on Figure 5.16).

This trend can be a typical adaptive community response to long term habitation within a confined bioreactor (Valentín-Vargas et al., 2012), as microbes within a given environment

adapt to common stimuli, including operation and ecological factors. Additionally, for both alpha diversity metrics and for both clay types, there was an initial drop followed by an increase. This pattern is more apparent for Shannon diversity, which less influenced by highly dominant species, compared to the Simpson index. Although the change in the Simpson index is slight, it is clear. Notably, the Simpon index was always very close to its maximum value, indicating high diversity likely dominated by a few highly abundant taxa. The initial drop and recovery may be explained by the inoculum adapting to the new environment (Section 5.3.4.3). To further explore the nature of these changes, the starting composition of column inoculum, porewaters and sediments were characterised from cDNA data and discussed next.

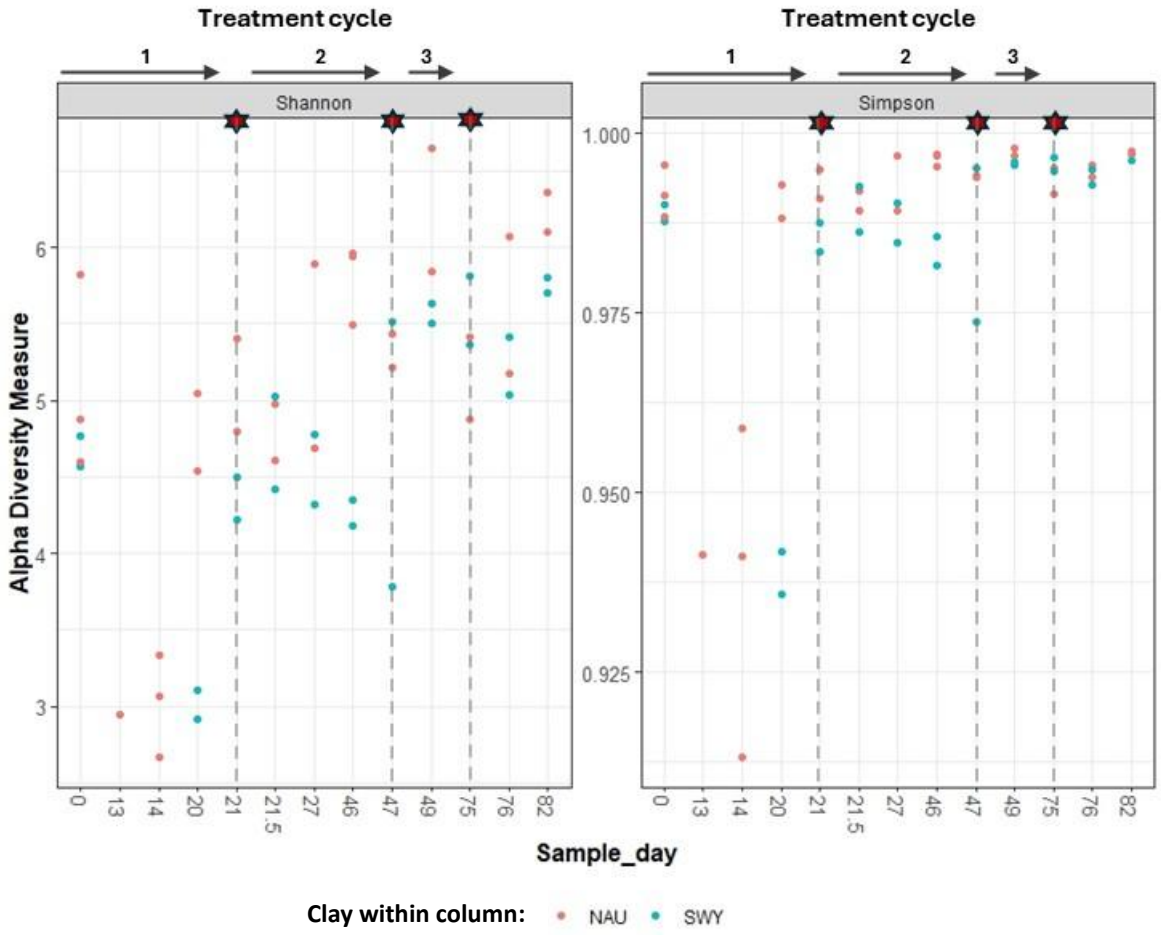

Figure 5. 16. *Alpha diversity for porewaters sampled from NAu-2 (NAU, red dots) and SWy-3 (SWY, blue dots) biological columns in Experiment 2. Contact with BA occurred during the three treatment cycles (T1, T2 and T3) within Experiment 2, on days 21 (T1), 47 (T2) and 75 (T3), shown by grey dashed lines and red stars.*

5.3.4.3 Microbes active during 'clay activation' (microbial Fe-reduction)

Initially, commonalities were explored between the starting inoculum and porewaters sampled during the early stages of clay activation (Appendix C, Figures C.14, C.15). Due to low read counts, no data is available for the native (untreated) sediments samples. Results show that at phylum level, the pondwater and pondwater + NPK feed mix (Appendix C, Figures C.14) may have impacted the microbiology of all column porewaters through addition of (in order of approximate abundance) Proteobacteria, Firmicutes (mainly from the pondwater), Bacteroidota, Actinobacteriota and Cyanobacteria (primarily from the pondwater + NPK feed mix), alongside minor contributions of Planctomycetota and Verrumicrobiota (Appendix C, Figures C.14). These microorganisms are found in a diverse range of terrestrial and aquatic environments, including sediments and the aquatic subsurface and have various roles, including plant biomass degradation (Bacteroidota), carbon cycling (Cynobacteria), digestive processes in animals and human (Actinobacteriota; Binda et al., 2018), and in marine environments, e.g. Planctomycetota (a phytoplankton metaboliser) and Verrumicrobiota (a Gram-negative bacteria).

Midway through the clay activation stage (day 17), compositional differences in sediment samples at phylum level show that the Proteobacteria dominate all columns irrespective of clay type, followed by Firmicutes and Bacteroidota in Appendix C (Figure C.16). This is not unexpected given that the Proteobacteria are considered the largest group of Gram-negative bacteria with an extreme metabolic diversity and are of medical, veterinary, industrial and agricultural interest (Kersters et al., 2006). The relative abundance of Proteobacteria is greater in NAu-2 columns than in SWy-3 but in the latter, Phylum Firmicutes, which form a dominant component of the human microbiome (e.g. in the digestive tract) and are gram-positive (Davey et al., 2016), has a greater relative abundance (Figure 5.17). Other less abundant phylum present in the NAu-2 and SWy-3 sediments can be seen in bar plots in Appendix C (Figure C.16) but will not be discussed here further.

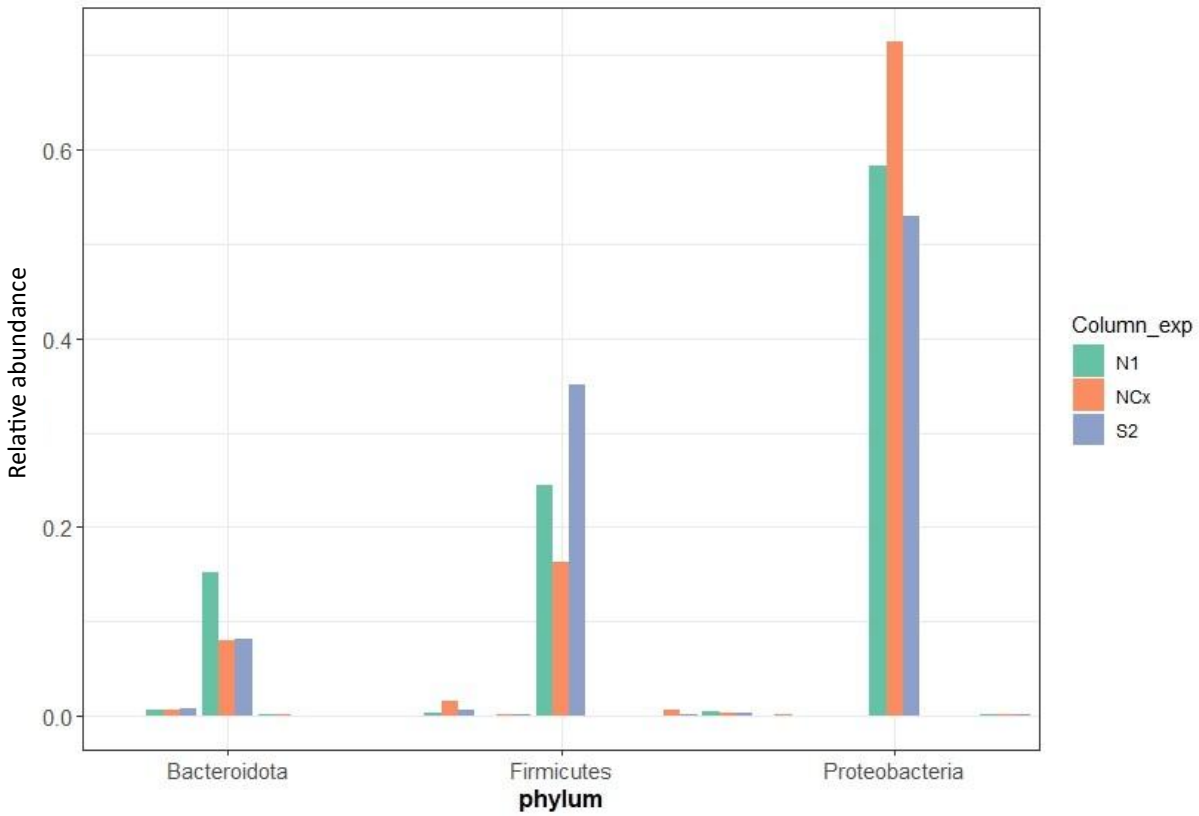

Figure 5. 17. *Bar plots showing relative abundances of major phyla present in column sediments NAu-2 (N1, NCx) and SWy-3 (S2) before the start of biological Experiment 1 (cDNA data shown).*

Comparing the microbiome in pondwater and sediments from the same experiment (Exp. 1, day 17) shows that the same three phyla (Figure 5.18) still tend to dominate both types of sample during clay activation and Fe reduction: Proteobacteria, Firmicutes and Bacteroidota. According to comparable literature studies, Proteobacteria is commonly detected during operating bioreactors and often alongside Firmicutes (Tang et al., 2014), so the presence of these two major groups could be expected. There are strong commonalities between sediments and porewater microbiomes within the same columns, sampled on the same day (Figures 5.18, Appendix C, Figure C.17), as might be expected, however, the porewater samples have greater numbers of family-level taxa within these main phyla (i.e. higher evenness) than the sediment samples do. This is likely why changes in the microbial community with time are easily to identify in the sediment samples.

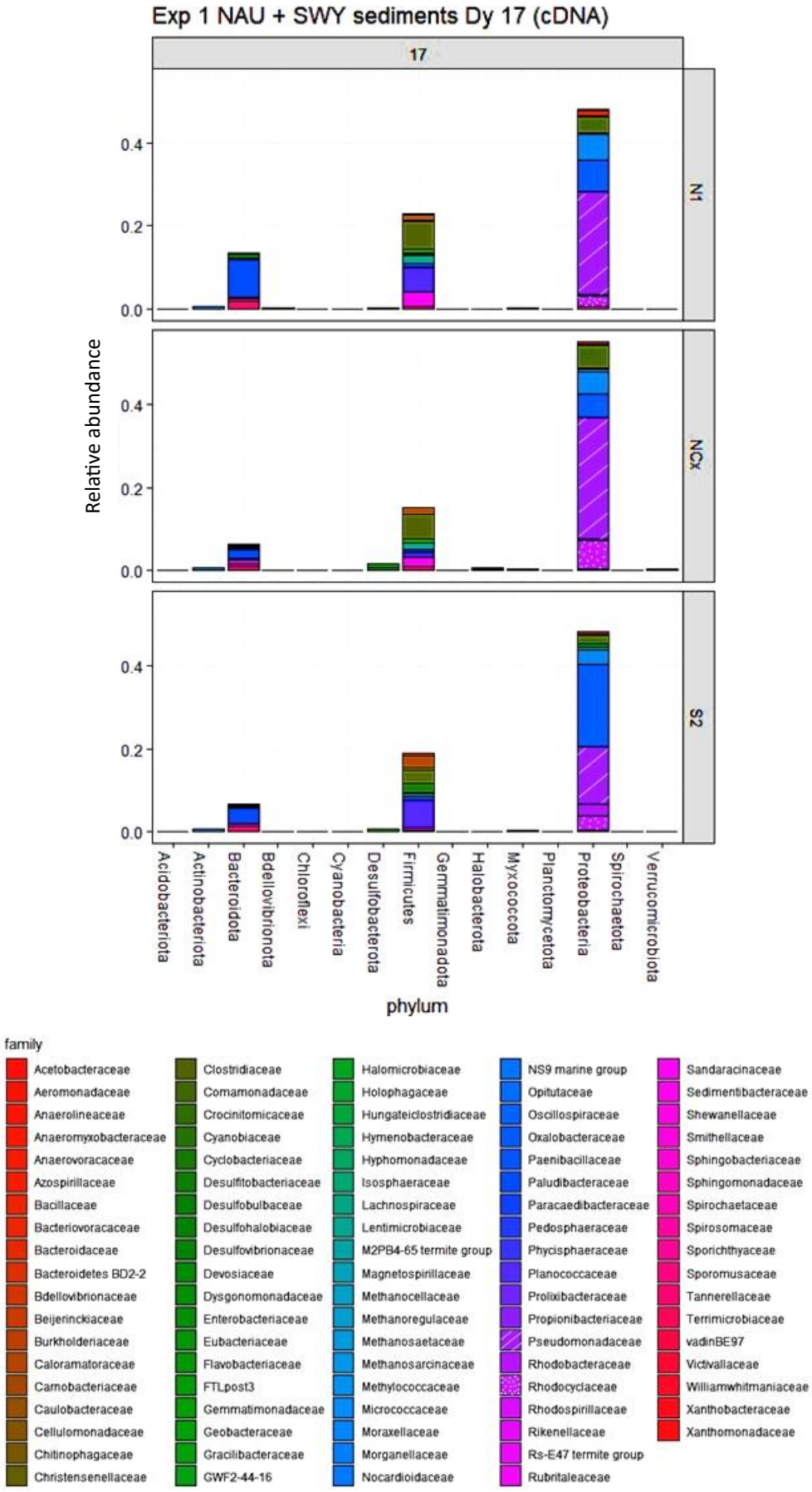

Figure 5. 18. *Bar plots showing major phyla (with family subdivisions) in NAu-2 (N1, NCx) and SWy-3 (S2) column sediments during the mid-stages of clay activation (Fe-reduction), before the start of the first treatment cycle in biological Experiment 1 (cDNA data shown).*

At family level, Figure 5.18 shows the dominant taxa in NAu-2 column sediments (Exp. 1, day 17) in order of (approximate) relative abundance include Pseudomonodaceae, Rhodocyclaceae (both phylum Proterbacteria), Comamonadaceae, Burkholderiaceae (phylum Firmicutes) and Sphingomonadaceae (phylum Bacteroidota). Families Pseudomonodaceae and Rhodocyclaceae are also common to the SWy-3 column sediments but in lower abundance than the NAu-2 column sets. Figure 5.18 shows that the SWy-3 column sediments' microbiomes are dominated instead by Oxalobacteraceae, Pseudomonodaceae (phylum Proteobacteria), Comamonadaceae and Burkholderiaceae (phylum Firmicutes). This suggests that although commonalities exist, the different clays supported slightly different microbiomes during clay activation and Fe-reduction.

Family groups that include dissimilatory Fe-reducers and that were identified in both of the clay sediment types in this PhD include Pseudomonadaceae and Comamonadaceae. Laboratory experiments by (Gates et al., 1998) showed that a mixed culture of Pseudomonas could reduce up to 69% Fe^{3+} in montmorillonite clay, so within the context of this PhD the presence of Pseudomonas is not unexpected. (Silva et al., 2007) reports that some strains Pseudomonas can degrade 4-hydroxybenzoic acid (salicylic acid) and this potentially has significant implications for treatment performance monitoring of this novel AOP system. Further study is needed to confirm whether this is an issue.

Within family Comamonadaceae, Rhodoferax is a known dissimilatory Fe-reducer (Zhuang et al., 2011) although to date, there are no reports in the literature of clay mineral Fe reduction by Rhodoferax, nor is there identification of the genus in the column experiments. Further molecular work could confirm this.

5.3.4.4 Survival of microbial communities through the treatment process

Using cDNA data from one of the NAu-2 column replicates, 60 days after the completion of the single treatment cycle during Experiment 1, the total number of family groups decreased within the dominant phyla identified. As previously cited, this may be expected in a confined reactor as no further flow was used in this experiment after the only treatment cycle (after day 20). Post-treatment, the family groups that were active in this column during clay activation on Day 17 (Figure 5.18) have significantly increased in relative abundance (e.g. phyla Proteobacteria and Firmicutes) and also new phyla have appeared (Figure 5.19), e.g. Bacteroidota, Actinabacteriota, Desulfobacterota and Myxococcota. This relative increase

could be quantified for comparison with literature. Of note is the appearance of phylum Desulfobacterota, which indicates that sulphate-reducing bacteria were active. Sulphur was detected in column effluents although in relatively low concentrations (mean of 14.4 mg/L, range =0.02-36.9 mg/L). Some sulphate-reducers are able to respire Fe^{3+} (Muyzer & Stams, 2008) but can also be strict anaerobes, so with time as the confined column environment likely became more reducing, sulphate-reducers may have thrived over other microbial groups. It is noted that much further study could be carried out to look at the functionality of the different bacterial groups with the columns.

The increase in abundance of these taxa with time and after treatment suggests survival of exposure to •OH and other reactive oxygen species (ROS) during treatment of benzoic acid (BA), and adaptation of the column microbiome to a less diverse but resilient community. In an experimental study by (Ma et al., 2019), exposure of biologically-active sediments to ROS during clay mineral Fe^{2+} oxygenation initially inactivated microbes, with the relative abundance of Geobacteraceae decreasing but that of Anaerolineaceae increasing from ~15-~30%. Interestingly, family Anaerolineaceae was also observed to appear as a new group after exposure to ROS, in the NAu-2 duplicate sampled during dy 90 of Exp. 1 (Figure 5.18).

Further study is needed for a robust interpretation of cDNA data for column Experiment 2, which represents NAu-2 and SWy-3 column microbiomes after three complete treatment cycles, 123 days after initial inoculation and approximately 30 days after the third complete treatment cycles (Figure 5.20). However, with time, there is a considerable change in the community composition for both columns, since the first treatment cycle and compared to the sterile control column (Appendix C, Figure C.18). Microbial communities in both the NAu-2 and SWy-3 columns have become less diverse and appears to be dominated by the stricter anaerobic groups. Proteobacteria has a higher relative abundance in the SWy-3 column than in the NAu-2 column, whereas Desulfobacterota is relatively more abundant in the NAu-2 column. Anaerolineaceae also persists in the NAu-2 column but not in the SWy-3 column. At this later stage in Experiment 2, new additions to both the column microbiomes include phylum Halobacterota, which are strict anaerobes with optimal growth conditions under high extreme salinity (Ng et al., 2000), suggested up to 10 ten times that of seawater. The appearance of this phylum after three treatment cycles may have implications for the success of the sustainable AOP tested as part of this PhD, as future treatment cycles may not successful if insufficient oxygenation occurs within the column.

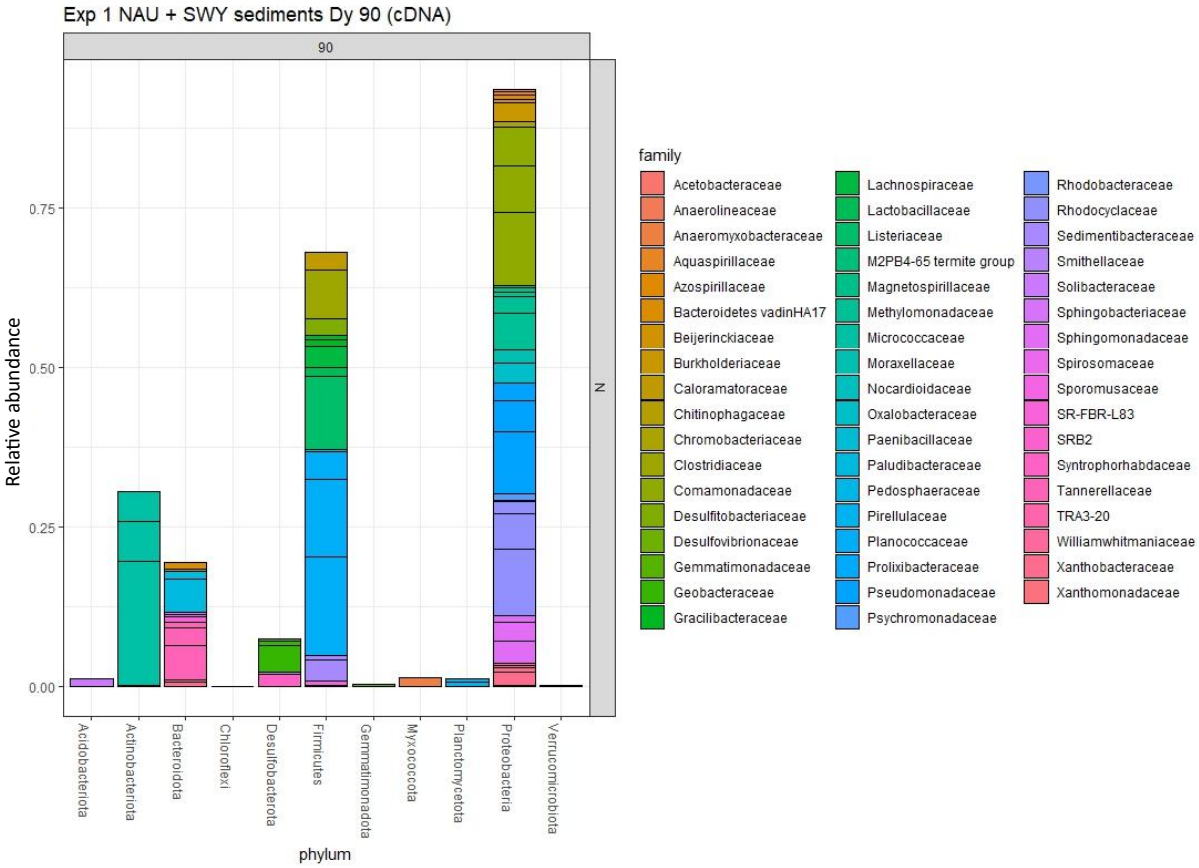

Figure 5. 19. *Bar plots showing major phyla (with family subdivisions) in NAu-2 (N1) column sediments, after a single treatment cycle (90 days after the start of Experiment 1; cDNA data shown).*

To this end, the formation and role of biofilms and associated secretion EPS in the sediment columns may be important in terms of treatment success in addition to influencing competition between microbes (Jayathilake et al., 2017). The role of biofilms in either inhibiting or promoting electron transfer has been studied extensively in the context of bioreactor performance and affect on electron transfer processes, e.g. (Hu et al., 2021). Some species of microbe will function as an electron shuttle most effectively as a biofilm rather than in planktonic form, e.g. *Geobacter sulfurreducens*, whilst the functionality of other species may be unaffected , e.g. *Shewanella oneidensis* (Hu et al., 2021). Biofilm formation was not investigated in this study but could provide key insight into the extent of clay dissolution that may be expected through dissimilatory Fe reduction, and subsequent loss of Fe under flow conditions.

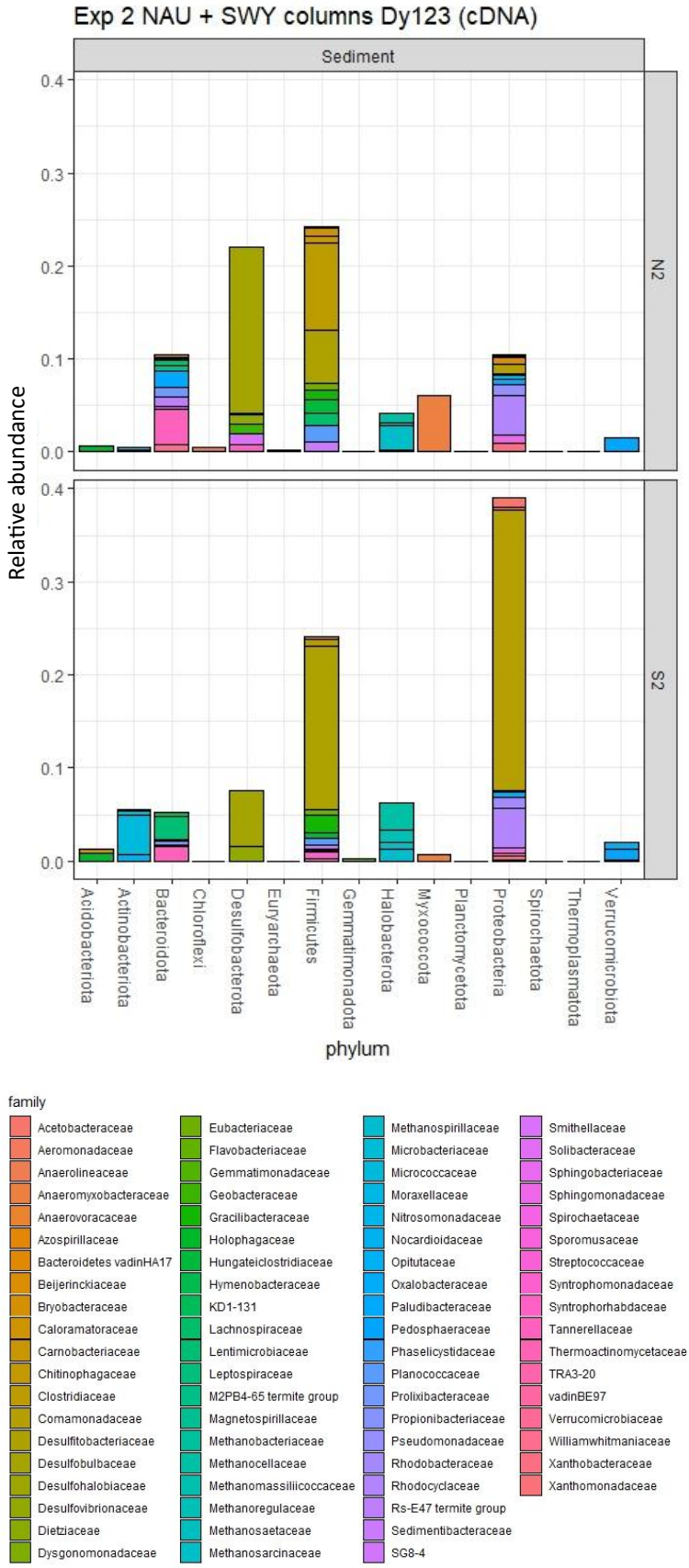

Figure 5. 20. *Bar plots showing relative abundance of major phyla (with family subdivisions) in NAu-2 (N1) and SWy-3 (S2) column sediments following three complete treatments cycle, 123 days after the start of biological Experiment 2 (cDNA data shown).*

5.3.4.5 Comparison of bacterial communities with environmental factors

To identify any significant relationships between the microbial communities and selected environmental and operational parameters, bacterial communities were compared using the 'manyglm' command in the R package 'mvabund' (Wang et al., 2012) with a Poisson error family and Montecarlo resampling.

Where P<0.05, bacterial communities were found to have statistically significant relationships to the various experimental variables and their interactions. Clay, sample type, treatment cycle, experiment number and sample day were all found to be related (Table 5.5). There were also many significant taxon-specific relationships (Table C.3).

Table 5. 6. *Multivariate generalized linear model comparing bacterial communities against column and experiment parameters and their pairwise interactions. Significant ($p \leq 0.05$) univariate results are given in Appendix C, Table C.3.*

Variable	Results
Clay	Dev = 944.32, df = 1, 102, p = 0.001
Sample type	Dev = 1273.103, df = 2, 100, p = 0.001
Treatment cycle	Dev = 8941.974, df = 16, 84, p = 0.001
Experiment number	Dev = 1135.477, df = 1, 83, p = 0.001
Sample day	Dev = 2774.607, df = 12, 71, p = 0.001
Treatment cycle: Experiment number	Dev = 0.097, df = 2, 69, p = 0.004
Clay: Sample type: Sample day	Dev = 4884.163, df = 41, 28, p = 0.001
Clay: Sample type: Treatment cycle	Dev = 0.001, df = 4, 56, p = 0.001

5.4 Conclusions

In conclusion, a local pondwater community was found to be effective at activating clay mineral structural Fe, through microbial Fe reduction, in flow-through benchtop column experiments. The NAu-2 columns were reduced to 24.5% (n=2) and 11% (n=2);

During the three treatment cycles tested in the experiment here, •OH was be generated *in situ* through oxygenation of the activated Fe-clay minerals, NAu-2 and SWy-3, within the same column experiments. Over both treatment experiments, •OH yields for the NAu-2 columns ranged from 18-40 µmol/g Fe^{2+} and for the SWy-3 columns, 9-27 µmol/g Fe^{2+}, which

are all within the range of literature values of 0.8 µmol/g Fe^{2+} (Ma et al., 2019) to 123 µmol/g Fe^{2+} (Tong et al., 2016).

Concentrations of 4-HBA were highest in the NAu-2 columns during the first treatment cycle in Experiment 1 (maximum of 26 µM) and lower for the other three cycles in Experiment 2. The NAu-2 columns always generated more 4-HBA overall, during the three treatment cycles (Experiment 2), although this was not reflected in a significantly higher treatment efficiency when compared to the SWy-3 clays, considering the additional Fe available in the NAu-2 column. Limiting factors to further treatment cycles could be (i) continued loss of total Fe from the column due to microbial Fe reduction and subsequent loss in the form of dissolved Fe, during column flow, (ii) the consumption of 4-HBA by microbes meaning that the •OH yield was underestimated, if determining •OH by quantitative trapping of BA, or (iii) the presence of humic compounds which may inhibit the production of •OH by 30-40%.

The use of cDNA for microbiology analysis allowed the active column microbiomes to be characterised. Microbes responsible for Fe-reduction were likely Pseudomonas, Rhodoferax and Geobacter, once lower oxygen levels were established. With time and after three treatment cycles, different groups of sulphate reducers dominated the both of the clay columns, although the community diversification at least at family-level had already begun during earlier clay activation/Fe-reduction phases. Richness plots suggested that whilst evenness always remained fairly high in column porewaters, after exposure to three cycles of treatment, sediment microbiomes had become less diverse and community had changed. Likely this was adaptation to environmental factors such as exposure to ROS during the treatment process but also adaptation to the confinement of the column environment, where strict anaerobes were more suited to the low oxygen conditions, over other facultative microbes. Of interest was the appearance of microbes within phylum Halobacter, which thrive in high-salinity environments. Their appearance in the treatment columns at a late stage in has implications for the effectiveness of further treatment cycles and poses questions about the effectiveness of oxygenation during each cycle when the model micropollutant was introduced into the column in oxygenated pondwater.

Mass balance calculations show that although measurable amounts of Fe were transported out of the column during flow, Fe loss from the columns was extremely low during the first treatment cycle in Experiment 1, from each clay column (≤1% loss). For Experiment 2, approximations of Fe loss per treatment cycle are approximately 1/3 of the figure reported in

Table 5.5 for each column, indicating that the maximum Fe loss from column N1 during Experiment 2 would have been around 1.4%. This gives promise to the longevity of this AOP treatment system, providing factors affecting Fe availability and •OH can be constrained further.

6. Conclusions and Further Work

6.1 Introduction

This thesis set out to achieve nine objectives across two research themes. The following sections conclude on how the objectives have been met within each theme. The later section of this chapter discusses practical recommendations for directions in which the research could be continued.

6.1.1 Theme 1 conclusions: Wastewater treatment efficiency and sustainability

Theme 1 concerned monitoring the performance of the novel AOP over time and over several treatment (redox) cycles at mesocosm scale, using the oxygen saturation level of water to cycle between reducing and oxidising environments.

6.1.1.1. Design and test a mesocosm treatment system to operate under realistic conditions

As described in Chapter 3, a series of large benchtop mesocosm (column) experiments were successfully designed and fabricated in-house and tested for use in medium- to -long-term water treatment experiments. The final column design was achieved through optimisation using a series of preliminary flow and sediment packing tests with different sizes of smaller test column and different build materials. Following this design work, a prototype benchtop column was tested for overall performance under flow and different redox conditions during a test treatment cycle, whilst a working monitoring and sampling scheme were developed.

6.1.1.2. Monitor the chemical and biological activity of the treatment system over time and through at least three treatment cycles;

The Chapters 4 and 5 describe the methods used to monitor and analyse samples and data collected from the chemical and biological column experiments, respectively. In summary, these methods included:

- geochemical and/or microbiological analysis of all column influents used to achieve initial clay activation, e.g. the chemical reductant or the pondwater inoculum;
- *in-situ* monitoring of oxygen saturation within the column environment during the treatment cycle (later biological and chemical experiments only), to confirm that low oxygen conditions were being achieved during the clay activation phase;

- time-series sampling of sediments and porewaters through treatment cycles for characterisation of column microbial communities (biological columns only);
- times-series sampling of column effluent geochemistry to measure:
    - BA and 4-HBA concentrations and from which to calculate •OH production, as indicators of treatment success level;
    - Fe, Al and Si loss from the columns, as indicators of clay loss or dissolution.

Aside from the measurement of the model micropollutant BA and its hydroxylation product, 4-HBA, key findings from time-series sampling of all experiments were that Fe was lost during and following the clay activation phase of the treatment, during each treatment cycle. For the chemical column experiments, batch experiments showed most of the Fe available in the column sediments is from the nontronite (contributing > 85% Fe^{TOT} in the reactive layer sediments). Mass balance calculations based on Fe concentrations measured in column effluents during treatment cycles of both the chemical and biological column experiments showed that only a small proportion of the total Fe available in the column was lost from either of the treatment flow experiments. For the chemical column (containing clay this was approximately 1.7% loss over 4 treatment cycles and for biological column this approximately 1.4% over 3 treatment cycles, for the equivalent NAu-2 clay column.

Both chemical and biological activation of the clay minerals appeared to some level of mineral dissolution through either chemical Fe reduction or microbially mediated Fe reduction. Further study is recommended to measure the Fe reduction extent during the clay activation phase of every treatment cycle performed, perhaps through the use of smaller sacrificial columns (discussed below) in order to confirm the exact reduction extent achieved. It was not possible to measure this during every cycle performed in this study although with the use of oxygen probes, it was possible to confirm that low oxygen saturation environments inside the column were achieved (<1%; Chapter 4) during the clay activation phase.

6.1.1.3. Analyse the results to determine whether hydroxyl radicals generated during clay mineral iron oxygenation can efficiently remove target pollutants from a synthetic WW under flow (treatment) conditions, and to what extent

The •OH yields generated from Fe^{2+} oxygenation of the combined clay and sand sediment during the chemical treatment experiments ranged from 0.07-0.12 µmol/g Fe^{2+} (using NAu-2

clay). The calculated •OH yield per unit Fe^{2+} for the biological treatments was: Experiment 1, 35-40 µmol/g Fe^{2+} (NAu-2); 15-16 µmol/g Fe^{2+} (SWy-3), and Experiment 2, 19-36 (NAu-2) and 9-27 (SWy-3). These were all within the range of literature values reported in similar studies (0.8-123 µmol/g Fe^{2+}; Ma et al., 2019; Tong et al., 2016, respectively).

As a micropollutant treatment system, the novel biological AOP tested in this thesis had, overall, a low treatment efficiency of BA that ranged from 0.3-0.7% in the NAu-2 columns and 0.2-0.5% in the SWy-3 columns. There was no discernible different in treatment performance in these experiments except that the SWy-3 clay columns performed better than the NAu-2 columns towards the end of Experiment 2. It is suggested that because the NAu-2 columns were not repacked between Experiments 1 and 2, long-term exposure to a microbial community (i.e. a biofilm) may have impacted the integrity of the clay mineral ahead of Experiment 2 and caused a degree of dissolution or weakening of clay mineral edges. Proportionally more Fe was measured in NAu-2 column effluents during flow phases of the treatment experiment, compared to SWy-3. Although the presence of biofilm may have enhanced bioreduction, the availability of Fe^{2+} for oxygenation and OH production may have be lessened. The chemical experiments produced more consistent, but still low, treatment efficiencies of 0.25-0.55%, with the first cycle generating the most •OH per g of Fe^{2+} oxygenated.

Further research is needed to optimise the treatment system for better performance and in addition, to clarify the influence of pondwater constituents, e.g. redox-active species such as humic acids, and microbiology on the fate of BA, e.g. (Elder & Kelly, 1994). This is an area where further work is warranted to constrain the factors involved and is addressed later in this chapter.

Iron was detected in column effluents during all treatment cycles in both column experiments, either during or following the clay activation phase when Fe reduction occurred. It is likely that Fe reduction through chemical and biological pathways caused the solubilisation of Fe^{2+} derived from sand-associated Fe(oxy)hydroxides in addition to Fe^{2+} coordinated clay mineral edge sites and in column flow conditions, this was then removed from the column as soluble Fe^{2+}. The loss of Fe^{2+} is expected to have a direct impact on •OH production due to limiting Fe^{2+} availability for oxygenation. Further study is needed here to quantify this loss and effect on treatment further.

6.1.1.4. Determine the number of effective treatment cycles

The target micropollutant, benzoic acid (BA), was degraded to its degradation product, 4-hydroxybenzoic acid (4-HBA) through each of the 3 treatment cycles in the biological column experiments and through each of the 4 treatment cycles in the chemical column experiments. The efficiency of the chemical and biological treatment columns was consistently <1% in all treatment experiments. NAu-2 and SWy-3 columns, with the SWy-3 columns becoming slightly more efficient with time compared to the NAu-2 columns. In summary at least three effective treatment cycles were possible in the biological column experiments and four with the chemical column experiments. There is good reason to suggest that more cycles would be achievable although a low treatment efficiency would be expected, as with the experiments performed as part of this thesis.

6.1.2 Theme 2 conclusions: Characterisation of microbial community

Theme 2 concerned gaining a deeper understanding of the microbial community responsible for driving iron reduction during the treatment process.

6.1.2.1. Determine which communities are active and driving iron reduction during the treatment process and elucidate how the microbiology in the treatment system is changing over time with treatment cycles.

The use of cDNA for microbiology analysis allowed the active column microbiomes to be characterised and indicated which groups of microbes at family-level were responsible for Fe-reduction during clay activation. Using the lowest taxa assignments possible whilst maintaining data quality, Fe-reducers were likely Pseudomonas, Rhodoferax and Geobacter, once lower oxygen levels were established. With time and after three treatment cycles, different groups of sulphate reducers dominated the both of the clay columns, although the community diversification at least at family-level had already began during the clay activation/Fe-reduction phase. Data suggested that whilst the spread and number of species always remained fairly high in column porewaters, after exposure to three cycles of treatment, sediment microbiomes became less diverse and the community changed. Of note were that phylum Firmicutes, which is a large group of gram-positive bacteria with resilient cell walls, tended to dominate initially and later (after treatment) still maintain a presence in the SWy-3 columns. Links between clay mineralogy and propensity to support particular

groups of microbes was not investigated in detail here but could provide useful information in the long term to support a nature-based treatment system.

Changes in the column sediment communities in both clay columns were likely adaptations to environmental factors such as exposure to ROS during the treatment process but also adaptation to the confinement of the column environment, where strict anaerobes were more suited to the low oxygen conditions, over other facultative microbes. Of interest was the appearance of microbes within phylum Halobacter, which thrive in high-salinity environments. Their appearance in the treatment columns at a late stage in has implications for the effectiveness of further treatment cycles and poses questions about the effectiveness of oxygenation during each cycle when the model micropollutant was introduced into the column in oxygenated pondwater.

Mass balance calculations show that although measurable amounts of Fe were transported out of the column during flow, Fe loss from the columns was extremely low during the first treatment cycle in Experiment 1, from each clay column (≤1% loss). For Experiment 2, approximations of Fe loss per treatment cycle are approximately 1/3 of the figure reported in Table 5.5 for each column, indicating that the maximum Fe loss from column N1 during Experiment 2 would have been around 1.4%. This gives promise to the longevity of this AOP treatment system, providing factors affecting Fe availability and •OH can be constrained further.

6.2 Recommendations and Further Work

There are many areas of further study that could improve both the design, understanding and practical operation of the novel AOP tested in this PhD and several points will be addressed below.

1. the use of smaller but a greater number of sacrificial columns tests would allow higher resolution sampling to occur in the during treatment episodes and allow for easier handling and operation of the columns. Although large columns were designed to ensure that adequate sample volumes could be obtained, this led to limitations in sediment sample collection due to transporting the larger columns into the glovebox

whilst full of sediment. Furthermore, concerns over disrupting the redox environment inside the column during sampling mid-experiment;

2. development of additional aeration methods for column sediments during the oxic BA treatment stage, when Fe^{2+} is oxygenated to form •OH production;
3. direct measurement of •OH through effluent and rapid storage of samples ahead of either electron spin resonance (ESR, e.g. Tong et al., 2016) or the modification of a low sensitivity photometric method;
4. alternate to the above, use of mass spectrometry, e.g. LC-MS, to measure model micropollutants and potentially low concentration degradation products. An HPLC method was optimised for this PhD study due to the large sample numbers generated and for appropriation to the project topic, which was to develop an inexpensive water treatment technology suitable for low- to middle-income countries. However, the background corrections needed to resolve peaks in pondwater matrices was challenging and other analytical techniques may be more suited to develop this work further;
5. it was outside the scope of this study to test the effects of hydraulic retention time (HRT) on BA degradation enough detail to make effective improvements to experiments. Increasing the HRT of BA inside the column may improve •OH yields, providing the hydraulic head is sufficient for the hydraulic conductivity of the clay-containing columns;
6. biological microcosm batch experiments would be beneficial in testing the capability of a pondwater community to degrade comparable concentrations of BA, to that supplied to the column. A photosynthetic bacterium *Rhodopseudomonas palustris* has been reported to be capable of BA degradation along with several forms of anaerobic denitrifying pseudomonas microorganisms (Elder & Kelly, 1994). In addition to some additional measure of BA sorption onto the PVC column surface, microbiology batch experiments would allow a mass balance to be calculated for the BA.

The practical issues of upscaling this nature-based AOP to large pilot or field test scale could be challenging at this stage. Further work is required to optimise this proof-of-concept AOP as the low efficiency of BA treatment observed during this PhD would not currently attract significant interest or investment by the water industry. Effectively managing different redox

environments in a water treatment plant could also be challenging, and may require additional infrastructure and space, in order to maximise clay surface area for optimal reaction completeness. Through dissimilatory Fe-reduction and secretion of biofilm-associated EPS, the partial or complete dissolution of clay mineral and any associated Fe (oxyhydr)oxides, together with physical mass transport during flow, may eventually result in the loss of significant quantities of Fe. This may render the treatment system ineffective.

In summary, effective and long-term treatment options for micropollutants are limited and successful economically viable, low-carbon AOPs are not yet routinely available in field-based engineered systems, or elsewhere. Other nature-based solutions such as riverbank filtration and constructed wetlands (Toro-Vélez et al., 2016; Sacher & Brauch, 2002; Oberleitner et al., 2020), have been shown to effectively removal micropollutants from water although more rapid and space-efficient alternatives that are sustainable, are required for implementation in less rural areas. This study has shown that there is mileage in sustainable radical-based advanced oxidation for water treatment. A future thought is to supplement these low-carbon, nature-based treatment solutions with renewable energy, to enhance radical production for example, and provide greater efficiency and return.

7. References

Allen, J.M., Lucas, S. & Allen, S.K. (1996) 'Formation of hydroxyl radical (·OH) in illuminated surface waters contaminated with acidic mine drainage'. Environmental toxicology and chemistry 15 (2) p.pp. 107–113.

Amonette, J.E. & Charles Templeton, J. (1998) 'Improvements to the quantitative assay of nonrefractory minerals for Fe(II) and total Fe using 1,10-phenanthroline', *Clays and Clay Minerals*, 46(1), pp. 51–62.

Anjum, N.A., Gill, S.Singh. & Tuteja, Narendra. (2017) *Enhancing cleanup of environmental pollutants. Volume 1, Biological approaches*. Vol. 1.

Balmer, M.E. & Sulzberger, B. (1999) 'Atrazine degradation in irradiated iron/oxalate systems: Effects of pH and oxalate', *Environmental Science and Technology*, 33(14), pp. 2418–2424.

Banzhaf, S. & Hebig, K.H. (2016) 'Use of column experiments to investigate the fate of organic micropollutants - A review', *Hydrology and Earth System Sciences*, 20(9), pp. 3719–3737.

Banzhaf, S., Nödler, K., Licha, T., Krein, A. & Scheytt, T. (2012) 'Redox-sensitivity and mobility of selected pharmaceutical compounds in a low flow column experiment', *Science of the Total Environment*, 438pp. 113–121.

Baresel, C., Ek, M., Ejhed, H., Allard, A.S., Magnér, J., Dahlgren, L., Westling, K., Wahlberg, C., Fortkamp, U., Söhr, S., Harding, M., Fång, J. & Karlsson, J. (2019) 'Sustainable treatment systems for removal of pharmaceutical residues and other priority persistent substances', *Water Science and Technology*, 79(3), pp. 537–543.

Bedfordshire Geology Group (2011) *The Lower Greensand: for geologists*, 2011(07/20).

Bernhardt, E.S., Rosi, E.J. & Gessner, M.O. (2017) 'Synthetic chemicals as agents of global change', *Frontiers in Ecology and the Environment*, 15(2), pp. 84–90.

Binda, C., Lopetuso, L.R., Rizzatti, G., Gibiino, G., Cennamo, V. & Gasbarrini, A. (2018) 'Actinobacteria: A relevant minority for the maintenance of gut homeostasis'. Digestive and Liver Disease 50 (5) p.pp. 421–428.

Bishop, M.E., Glasser, P., Dong, H., Arey, B. & Kovarik, L. (2014) 'Reduction and immobilization of hexavalent chromium by microbially reduced Fe-bearing clay minerals', *Geochimica et Cosmochimica Acta*, 133pp. 186–203.

Buchner, D. (2023) *RNA cleanup with magnetic beads*.

Buxton, G. V., Greenstock, C.L., Helman, W.P. & Ross, A.B. (1988) 'Critical Review of rate constants for reactions of hydrated electrons, hydrogen atoms and hydroxyl radicals (·OH/·O− in Aqueous Solution', *Journal of Physical and Chemical Reference Data*, 17(2), pp. 513–886.

Callahan, B.J., McMurdie, P.J., Rosen, M.J., Han, A.W., Johnson, A.J.A. & Holmes, S.P. (2016) 'DADA2: High-resolution sample inference from Illumina amplicon data', *Nature Methods*, 13(7), pp. 581–583.

Cama, J. & Ganor, J. (2015) ‘Chapter 4 - Dissolution Kinetics of Clay Minerals’, in Christophe Tournassat, Carl I Steefel, Ian C Bourg, & Faqpza Bergaya (eds.) *Developments in Clay Science*. [Online]. Elsevier. pp. 101–153.

Caporaso, J.G., Lauber, C.L., Walters, W.A., Berg-Lyons, D., Huntley, J., Fierer, N., Owens, S.M., Betley, J., Fraser, L., Bauer, M., Gormley, N., Gilbert, J.A., Smith, G. & Knight, R. (2012) ‘Ultra-high-throughput microbial community analysis on the Illumina HiSeq and MiSeq platforms’, *ISME Journal*, 6(8), pp. 1621–1624.

Carey, G.R., McBean, E.A. & Feenstra, S. (2018) ‘Estimating transverse dispersivity based on hydraulic conductivity’, *Environmental Technology and Innovation*, 10pp. 36–45.

Chen, L. (2017) *INVESTIGATING THE SUSTAINABILITY OF A NOVEL ADVANCED OXIDATION PROCESS*. [Online]. Newcastle University, Newcastle upon Tyne, UK.

Chen, N., Fang, G., Liu, G., Zhou, D., Gao, J. & Gu, C. (2019) ‘The degradation of diethyl phthalate by reduced smectite clays and dissolved oxygen’, *Chemical Engineering Journal*, 355pp. 247–254.

Chen, N., Fang, G., Liu, G., Zhou, D., Gao, J. & Gu, C. (2018) ‘The effects of Fe-bearing smectite clays on [rad]OH formation and diethyl phthalate degradation with polyphenols and H 2 O 2’, *Journal of Hazardous Materials*, 357pp. 483–490.

Chen, R., Liu, H., Zhang, P., Zhao, L., Ding, K. & Yuan, S. (2019) ‘Attenuation of Fe(III)-reducing bacteria during table fluctuation of groundwater containing Fe2+’, *Science of the Total Environment*, 694p. 133660.

Cheng, D., Yuan, S., Liao, P. & Zhang, P. (2016) ‘Oxidizing Impact Induced by Mackinawite (FeS) Nanoparticles at Oxic Conditions due to Production of Hydroxyl Radicals’, *Environmental Science and Technology*, 50(21), pp. 11646–11653.

Chitra, S., Paramasivan, K., Cheralathan, M. & Sinha, P.K. (2012) ‘Degradation of 1,4-dioxane using advanced oxidation processes’, *Environmental Science and Pollution Research*, 19(3), pp. 871–878.

Cihan, A., Petrusak, R., Bhuvankar, P., Alumbaugh, D., Trautz, R. & Birkholzer, J.T. (2022) ‘Permeability Decline by Clay Fines Migration around a Low-Salinity Fluid Injection Well’, *Groundwater*, 60(1), pp. 87–98.

Clarizia, L., Russo, D., Di Somma, I., Marotta, R. & Andreozzi, R. (2017) ‘Homogeneous photo-Fenton processes at near neutral pH: A review’, *Applied Catalysis B: Environmental*, 209pp. 358–371.

Davey, L., Halperin, S.A. & Lee, S.F. (2016) ‘Thiol-Disulfide Exchange in Gram-Positive Firmicutes’, *Trends in Microbiology*, 24(11), pp. 902–915.

Deng, Y. & Zhao, R. (2015) ‘Advanced Oxidation Processes (AOPs) in Wastewater Treatment’, *Current Pollution Reports*, 1(3), pp. 167–176.

Ding, Y. (2017) *COMPARING THE EFFICIENCY OF IRON-BASED ADVANCED OXIDATION PROCESSES*. [Online]. Newcastle University, Newcastle upon Tyne, UK.

Domenico, P.A. & Schwartz, F.W. (1997) *Physical and Chemical Hydrogeology*. 2nd Edition. Wiley.

Dong, H., Jaisi, D.P., Kim, J. & Zhang, G. (2009) '1505-1519 Microbe-clay mineral interactions'. American Mineralogist 94 (11–12) p.pp. 1505–1519.

Elder, D.J.E. & Kelly, D.J. (1994) 'The bacterial degradation of benzoic acid and benzenoid compounds under anaerobic conditions: Unifying trends and new perspectives', *FEMS Microbiology Reviews*, 13(4), pp. 441–468.

Entwistle, J., Latta, D.E., Scherer, M.M. & Neumann, A. (2019) *Abiotic Degradation of Chlorinated Solvents by Clay Minerals and Fe(II): Evidence for Reactive Mineral Intermediates*, (Ii), .

Ernstsen, V., Gates, W.P. & Stucki, J.W. (1998) 'Microbial reduction of structural iron in clays - A renewable source of reduction capacity', *Journal of Environmental Quality*, 27(4), pp. 761–766.

Evans, D.M., Kitson, J.J.N., Lunt, D.H., Straw, N.A. & Pocock, M.J.O. (2016) 'Merging DNA metabarcoding and ecological network analysis to understand and build resilient terrestrial ecosystems', *Functional Ecology*, 30(12), pp. 1904–1916.

Evans, D.M., Pocock, M.J.O. & Memmott, J. (2013) 'The robustness of a network of ecological networks to habitat loss', *Ecology Letters*, 16(7), pp. 844–852.

Fialips, C.I., Cooper, N.G.A., Jones, D.M., White, M.L. & Gray, N.D. (2010) 'Reductive degradation of p,p'-DDT by Fe(II) in nontronite NAu-2', *Clays and Clay Minerals*, 58(6), pp. 821–836.

Finck, N., Schlegel, M.L. & Bauer, A. (2015) 'Structural iron in dioctahedral and trioctahedral smectites: a polarized XAS study', *Physics and Chemistry of Minerals*, 42(10), pp. 847–859.

Gandiglio, M., Lanzini, A., Soto, A., Leone, P. & Santarelli, M. (2017) 'Enhancing the energy efficiency of wastewater treatment plants through co-digestion and fuel cell systems', *Frontiers in Environmental Science*, 5(October), pp. 1–21.

Gates, W.P., Jaunet, A.-M., Tessier, D., Cole, M.A., Wilkinson, H.T. & Stucki, J.W. (1998) 'Swelling and Texture of Iron-Bearing Smectites Reduced by Bacteria', *Clays and Clay Minerals*, 46(5), pp. 487–497.

Gates, W.P., Stucki, J.W. & Kirkpatrick, R.J. (1996) 'Structural properties of reduced Upton montmorillonite', *Physics and Chemistry of Minerals*, 23(8), pp. 535–541.

Glaze, W.H., Kang, J.-W. & Chapin, D.H. (1987) 'The Chemistry of Water Treatment Processes Involving Ozone, Hydrogen Peroxide and Ultraviolet Radiation', *Ozone: Science & Engineering*, 9(4), pp. 335–352.

Gligorovski, S., Strekowski, R., Barbati, S. & Vione, D. (2015) 'Environmental Implications of Hydroxyl Radicals (•OH)', *Chemical Reviews*, 115(24), pp. 13051–13092.

von Gunten, U. (2018) 'Oxidation Processes in Water Treatment: Are We on Track?', *Environmental Science & Technology*, 52(9), pp. 5062–5075.

Haber, F. & Weiss, J. (1932) 'Über die Katalyse des Hydroperoxydes', *Die Naturwissenschaften*, 20(51), pp. 948–950.

Han, R., Lv, J., Huang, Z., Zhang, Suhuan & Zhang, Shuzhen (2020) 'Pathway for the Production of Hydroxyl Radicals during the Microbially Mediated Redox Transformation of Iron (Oxyhydr)oxides', *Environmental Science & Technology*, 54(2), pp. 902–910.

Han, R., Wang, Z., Lv, J., Zhu, Z., Yu, G.H., Li, G. & Zhu, Y.G. (2022) 'Multiple Effects of Humic Components on Microbially Mediated Iron Redox Processes and Production of Hydroxyl Radicals', *Environmental Science and Technology*, 56(22), pp. 16419–16427.

Hao, F., Guo, W., Lin, X., Leng, Y., Wang, A., Yue, X. & Yan, L. (2014) 'Degradation of Acid Orange 7 in aqueous solution by dioxygen activation in a pyrite/H2O/O2 system', *Environmental Science and Pollution Research*, 21(10), pp. 6723–6728.

Hollender, J., Zimmermann, S.G., Koepke, S., Krauss, M., Mcardell, C.S., Ort, C., Singer, H., Von Gunten, U. & Siegrist, H. (2009) 'Elimination of organic micropollutants in a municipal wastewater treatment plant upgraded with a full-scale post-ozonation followed by sand filtration', *Environmental Science and Technology*, 43(20), pp. 7862–7869.

Hu, Y., Wang, Y., Han, X., Shan, Y., Li, F. & Shi, L. (2021) 'Biofilm Biology and Engineering of Geobacter and Shewanella spp. for Energy Applications'. Frontiers in Bioengineering and Biotechnology 9.

Huang, L., Feng, C., Jiang, H., Dong, H., Liu, Z., Zeng, Q., Wang, X. & Zhang, L. (2018) 'Reduction of structural Fe(III) in nontronite by thermophilic microbial consortia enriched from hot springs in Tengchong, Yunnan Province, China', *Chemical Geology*, 479pp. 47–57.

Hug, S.J. & Leupin, O. (2003) 'Iron-Catalyzed Oxidation of Arsenic(III) by Oxygen and by Hydrogen Peroxide: pH-Dependent Formation of Oxidants in the Fenton Reaction', *Environmental Science & Technology*, 37pp. 2734–2742.

Inter-Agency and Expert Group on SDG Indicators (2016) *Inter-Agency and Expert Group on SDG Indicators (IAEG-SDGs) 2016 – UN Sustainable Development Goals SDG6 website, https://sustainabledevelopment.un.org/sdg6.*

Intergovernmental Panel on Climate Change (2018) *Global Warming of 1.5°C. An IPCC Special Report on the impacts of global warming of 1.5°C above pre-industrial levels and related global greenhouse gas emission pathways, in the context of strengthening the global response to the threat of climate change*.

Intergovernmental Panel on Climate Change (2019) *Refinement to the 2006 IPCC Guidelines for National Greenhouse Gas Inventories. Report adopted and accepted during the 49th Session of the IPCC in May 2019, prepared Task Force on National Greenhouse Gas Inventories (TFI) in accordance with the decision taken*.

Jackson, M.L. (1969) 'Soil chemical analysis - advanced course: a manual of methods useful for instruction and research in soil chemistry, physical chemistry of soils, soil fertility, and soil genesis.' *2nd edition, Madison, Wisconsin.*

Jaisi, D.P., Dong, H. & Liu, C. (2007) 'Influence of biogenic Fe(II) on the extent of microbial reduction of Fe(III) in clay minerals nontronite, illite, and chlorite', *Geochimica et Cosmochimica Acta*, 71(5), pp. 1145–1158.

Jaisi, D.P., Dong, H. & Liu, C. (2007) 'Kinetic analysis of microbial reduction of Fe(III) in nontronite', *Environmental Science and Technology*, 41(7), pp. 2437–2444.

Jaisi, D.P., Kukkadapu, R.K., Eberl, D.D. & Dong, H. (2005) 'Control of Fe(III) site occupancy on the rate and extent of microbial reduction of Fe(III) in nontronite', *Geochimica et Cosmochimica Acta*, 69(23), pp. 5429–5440.

Jaisi, D.P., Liu, C., Dong, H., Blake, R.E. & Fein, J.B. (2008) 'Fe2+ sorption onto nontronite (NAu-2)', *Geochimica et Cosmochimica Acta*, 72(22), pp. 5361–5371.

Jarvis, A.P. (2020) *Personal communication*.

Jayathilake, P.G., Jana, S., Rushton, S., Swailes, D., Bridgens, B., Curtis, T. & Chen, J. (2017) 'Extracellular polymeric substance production and aggregated bacteria colonization influence the competition of microbes in biofilms', *Frontiers in Microbiology*, 8(SEP), .

Jia, M., Bian, X. & Yuan, S. (2017) 'Production of hydroxyl radicals from Fe(II) oxygenation induced by groundwater table fluctuations in a sand column', *Science of the Total Environment*, 584–585pp. 41–47.

Joe-Wong, C., Brown, G.E. & Maher, K. (2017) 'Kinetics and Products of Chromium(VI) Reduction by Iron(II/III)-Bearing Clay Minerals', *Environmental Science and Technology*, 51(17), pp. 9817–9825.

Kashefi, K., Shelobolina, E.S., Elliott, W.C. & Lovley, D.R. (2008) 'Growth of thermophilic and hyperthermophilic Fe(III)-reducing microorganisms on a ferruginous smectite as the sole electron acceptor', *Applied and Environmental Microbiology*, 74(1), pp. 251–258.

Keeling, J.L., Raven, M.D. & Gates, W.P. (2000) *G E O L O G Y A N D C H A R A C T E R I Z A T I O N OF T W O H Y D R O T H E R M A L N O N T R O N I T E S F R O M W E A T H E R E D M E T A M O R P H I C ROCKS AT THE U L E Y GRAPHITE MINE , S O U T H A U S T R A L I A*, 48(5), .

Keenan, C.R. & Sedlak, D.L. (2008) 'Ligand-enhanced reactive oxidant generation by nanoparticulate zero-valent iron and oxygen', *Environmental Science and Technology*, 42(18), pp. 6936–6941.

Kersters, K., De Vos, P., Gillis, M., Swings, J., Vandamme, P. & Stackebrandt, E. (2006) 'Introduction to the Proteobacteria', in Martin Dworkin, Stanley Falkow, Eugene Rosenberg, Karl-Heinz Schleifer, & Erko Stackebrandt (eds.) *The Prokaryotes: Volume 5: Proteobacteria: Alpha and Beta Subclasses*. [Online]. New York, NY: Springer New York. pp. 3–37.

Khan, N.A., Johnson, M.D., Kubicki, J.D., Holguin, F.O., Dungan, B. & Carroll, K.C. (2019) 'Cyclodextrin-enhanced 1,4-dioxane treatment kinetics with TCE and 1,1,1-TCA using aqueous ozone', *Chemosphere*, 219pp. 335–344.

Komadel, P., Lear, P.R. & Stucki, J.W. (1990) 'Reduction and Reoxidation of Nontronite: Extent of Reduction and Reaction Rates', *Clays and Clay Minerals*, 38(2), pp. 203–208.

Komadel, P., Madejová, J. & Stucki, J.W. (2006) 'Structural Fe(III) reduction in smectites', *Applied Clay Science*, 34(1–4), pp. 88–94.

Kostka, J.E., Dalton, D.D., Skelton, H., Dollhopf, S. & Stucki, J.W. (2002) 'Growth of Iron(III)-Reducing Bacteria on Clay Minerals as the Sole Electron Acceptor and Comparison of Growth Yields on a Variety of Oxidized Iron Forms', *Applied and Environmental Microbiology*, 68(12), pp. 6256–6262.

Kostka, J.E., Haefele, E., Viehweger, R. & Stucki, J.W. (1999) 'Respiration and dissolution of iron(III)-containing clay minerals by bacteria', *Environmental Science and Technology*, 33(18), pp. 3127–3133.

Kostka, J.E., Stucki, J.W., Nealson, K.H. & Wu, J. (1996) 'Reduction of Structural Fe(III) in Smectite by a Pure Culture of Shewanella Putrefaciens Strain MR-1', *Clays and Clay Minerals*, 44(4), pp. 522–529.

Kostka, J.E., Wu, J., Nealson, K.H. & Stucki, J.W. (1999) 'The impact of structural Fe(III) reduction by bacteria on the surface chemistry of smectite clay minerals', *Geochimica et Cosmochimica Acta*, 63(22), pp. 3705–3713.

Kotelnikov, N.A., Sokolova, T.A., Tolpeshta, I.I., Karavanova, E.I., Izosimova, Yu.G. & Zavgorodnyaya, Yu.A. (2022) 'The Content of Benzoic Acid in Podzolic Soil and Its Sorption on Montmorillonite', *Moscow University Soil Science Bulletin*, 77(1), pp. 30–36.

Kwon, S.C., Kim, J.Y., Yoon, S.M., Bae, W., Kang, K.S. & Rhee, Y.W. (2012) 'Treatment characteristic of 1,4-dioxane by ozone-based advanced oxidation processes', *Journal of Industrial and Engineering Chemistry*, 18(6), pp. 1951–1955.

Lee, J., Kim, J. & Choi, W. (2014) 'Oxidation of aquatic pollutants by ferrous-oxalate complexes under dark aerobic conditions', *Journal of Hazardous Materials*, 274pp. 79–86.

Lee, Y. & von Gunten, U. (2010) 'Oxidative transformation of micropollutants during municipal wastewater treatment: Comparison of kinetic aspects of selective (chlorine, chlorine dioxide, ferrateVI, and ozone) and non-selective oxidants (hydroxyl radical)', *Water Research*, 44(2), pp. 555–566.

Lewis, J. & Sjöstrom, J. (2010) 'Optimizing the experimental design of soil columns in saturated and unsaturated transport experiments', *Journal of Contaminant Hydrology*, 115(1–4), pp. 1–13.

Lewis, S.R., Datta, S., Gui, M., Coker, E.L., Huggins, F.E., Daunert, S., Bachas, L. & Bhattacharyya, D. (2011) 'Reactive nanostructured membranes for water purification', *Proceedings of the National Academy of Sciences*, 108(21), pp. 8577–8582.

Li, G.L., Zhou, C.H., Fiore, S. & Yu, W.H. (2019) 'Interactions between microorganisms and clay minerals: New insights and broader applications'. Applied Clay Science 177 p.pp. 91–113.

Liao, P., Yu, K., Lu, Y., Wang, P., Liang, Y. & Shi, Z. (2019) 'Extensive dark production of hydroxyl radicals from oxygenation of polluted river sediments', *Chemical Engineering Journal*, 368(March), pp. 700–709.

Liao, W., Yuan, S., Liu, X. & Tong, M. (2019) 'Anoxic storage regenerates reactive Fe(II) in reduced nontronite with short-term oxidation', *Geochimica et Cosmochimica Acta*, 257pp. 96–109.

Liu, F., Wang, Z., Liu, J., Latif, J., Qin, J., Yang, H., Jiang, W., Deng, Y., Yang, K., Ni, Z., Ding, Y., Xie, J., Wang, Y. & Jia, H. (2024) 'Seasonal and Spatial Fluctuations of Reactive Oxygen Species in Riparian Soils and Their Contributions on Organic Carbon Mineralization', *Environmental Science and Technology*, 58(16), pp. 7066–7077.

Liu, J., Zhu, C., Zhu, F., Sun, H., Wang, J., Fang, G. & Zhou, D. (2024) 'Strong Substance Exchange at Paddy Soil-Water Interface Promotes Nonphotochemical Formation of Reactive Oxygen Species in Overlying Water', *Environmental Science and Technology*, 58(17), pp. 7403–7414.

Liu, X., Yuan, S., Tong, M. & Liu, D. (2017) 'Oxidation of trichloroethylene by the hydroxyl radicals produced from oxygenation of reduced nontronite', *Water Research*, 113pp. 72–79.

Liu, X., Yuan, S., Zhang, P., Zhu, J. & Tong, M. (2020) 'Reduced nontronite-activated H2O2 for contaminants degradation: The beneficial role of clayed fractions in ISCO treatments', *Journal of Hazardous Materials*, 386.

Llanos, E.J., Leal, W., Luu, D.H., Jost, J., Stadler, P.F. & Restrepo, G. (2019) 'Exploration of the chemical space and its three historical regimes', *Proceedings of the National Academy of Sciences of the United States of America*, 116(26), pp. 12660–12665.

Lovley, D. (2006) 'Dissimilatory Fe(III)- and Mn(IV)-Reducing Prokaryotes', in Martin Dworkin, Stanley Falkow, Eugene Rosenberg, Karl-Heinz Schleifer, & Erko Stackebrandt (eds.) *The Prokaryotes: Volume 2: Ecophysiology and Biochemistry*. [Online]. New York, NY: Springer New York. pp. 635–658.

Lyngsie, G., Krumina, L., Tunlid, A. & Persson, P. (2018) 'Generation of hydroxyl radicals from reactions between a dimethoxyhydroquinone and iron oxide nanoparticles', *Scientific Reports*, 8(1), p. 10834.

Ma, S., Tong, M., Yuan, S. & Liu, H. (2019) 'Responses of the Microbial Community Structure in Fe(II)-Bearing Sediments to Oxygenation: The Role of Reactive Oxygen Species', *ACS Earth and Space Chemistry*, 3(5), pp. 738–747.

Margot, J., Kienle, C., Magnet, A., Weil, M., Rossi, L., de Alencastro, L.F., Abegglen, C., Thonney, D., Chèvre, N., Schärer, M. & Barry, D.A. (2013) 'Treatment of micropollutants in municipal wastewater: Ozone or powdered activated carbon?', *Science of the Total Environment*, 461–462pp. 480–498.

Margot, J., Rossi, L., Barry, D.A. & Holliger, C. (2015) 'A review of the fate of micropollutants in wastewater treatment plants', *Wiley Interdisciplinary Reviews: Water*, 2(5), pp. 457–487.

McMurdie, P.J. & Holmes, S. (2013) 'phyloseq: An R Package for Reproducible Interactive Analysis and Graphics of Microbiome Census Data', *PLOS ONE*, 8(4), pp. e61217-.

Mezyk, S.P., Rickman, K.A., McKay, G., Hirsch, C.M., He, X. & Dionysiou, D.D. (2011) 'Remediation of chemically-contaminated waters using sulfate radical reactions: Kinetic studies', *ACS Symposium Series*, 1071pp. 247–263.

Mierzwa, J.C., Rodrigues, R. & Teixeira, A.C.S.C. (2018) 'UV-Hydrogen Peroxide Processes', in *Advanced Oxidation Processes for Waste Water Treatment*. [Online]. Elsevier. pp. 13–48.

Minella, M., De Laurentiis, E., Maurino, V., Minero, C. & Vione, D. (2015) 'Dark production of hydroxyl radicals by aeration of anoxic lake water', *Science of the Total Environment*, 527–528pp. 322–327.

Mopper, K. & Zhou, X. (1990) 'Hydroxyl Radical Photoproduction in the Sea and Its Potential Impact on Marine Processes', *Science*, 250(4981), pp. 661–664.

Mueller, B. (2015) 'Experimental Interactions Between Clay Minerals and Bacteria: A Review', *Pedosphere*, 25(6), pp. 799–810.

Murad, E. (2006) 'Chapter 12.1 Mössbauer spectroscopy of clays and clay minerals'. Developments in Clay Science 1 (C) p.pp. 755–764.

Murray, K.E., Thomas, S.M. & Bodour, A.A. (2010) 'Prioritizing research for trace pollutants and emerging contaminants in the freshwater environment', *Environmental Pollution*, 158(12), pp. 3462–3471.

Muyzer, G. & Stams, A.J.M. (2008) 'The ecology and biotechnology of sulphate-reducing bacteria', *Nature Reviews Microbiology*, 6(6), pp. 441–454.

Myers, M.A., Johnson, N.W., Marin, E.Z., Pornwongthong, P., Liu, Y., Gedalanga, P.B. & Mahendra, S. (2018) 'Abiotic and bioaugmented granular activated carbon for the treatment of 1,4-dioxane-contaminated water', *Environmental Pollution*, 240pp. 916–924.

Neumann, A., B. Hofstetter, T., Skarpeli-Liati, M. & P. Schwarzenbach, R. (2009) 'Reduction of Polychlorinated Ethanes and Carbon Tetrachloride by Structural Fe(II) in Smectites', *Environmental Science and Technology*, 43(11), pp. 4082–4089.

Neumann, A., Hofstetter, T.B., Lussi, M., Cirpka, O.A., Petit, S. & Schwarzenbach, R.P. (2008) 'Assessing the Redox Reactivity of Structural Iron in Smectites Using Nitroaromatic Compounds As Kinetic Probes', *Environmental Science and Technology*, 42pp. 8381–8387.

Neumann, A., Petit, S. & Hofstetter, T.B. (2011) 'Evaluation of redox-active iron sites in smectites using middle and near infrared spectroscopy', *Geochimica et Cosmochimica Acta*, 75(9), pp. 2336–2355.

Neumann, A., Sander, M. & Hofstetter, T.B. (2011) 'Redox properties of structural Fe in smectite clay minerals', *ACS Symposium Series*, 1071 pp. 361–379.

Ng, W.V., Kennedy, S.P., Mahairas, G.G., Berquist, B., Pan, M., Shukla, H.D., Lasky, S.R., Baliga, N.S., Thorsson, V., Sbrogna, J., Swartzell, S., Weir, D., Hall, J., Dahl, T.A., Welti, R., Goo, Y.A., Leithauser, B., Keller, K., Cruz, R., et al. (2000) 'Genome sequence of Halobacterium species NRC-1', *Proceedings of the National Academy of Sciences*, 97(22), pp. 12176–12181.

Oberacker, P., Stepper, P., Bond, D.M., Höhn, S., Focken, J., Meyer, V., Schelle, L., Sugrue, V.J., Jeunen, G.-J., Moser, T., Hore, S.R., von Meyenn, F., Hipp, K., Hore, T.A. & Jurkowski, T.P. (2019) 'Bio-On-Magnetic-Beads (BOMB): Open platform for high-throughput nucleic acid extraction and manipulation', *PLOS Biology*, 17(1), p. e3000107.

Oberleitner, D., Schulz, W., Bergmann, A. & Achten, C. (2020) 'Impact of seasonality, redox conditions, travel distances and initial concentrations on micropollutant removal during riverbank filtration at four sites', *Chemosphere*, 250.

O'Reilly, S.E., Furukawa, Y. & Newell, S. (2006) 'Dissolution and microbial Fe(III) reduction of nontronite (NAu-1)', *Chemical Geology*, 235(1–2), pp. 1–11.

Oturan, M.A. & Aaron, J.J. (2014) 'Advanced oxidation processes in water/wastewater treatment: Principles and applications. A review', *Critical Reviews in Environmental Science and Technology*, 44(23), pp. 2577–2641.

Page, S.E., Kling, G.W., Sander, M., Harrold, K.H., Logan, J.R., McNeill, K. & Cory, R.M. (2013) 'Dark formation of hydroxyl radical in arctic soil and surface waters', *Environmental Science and Technology*, 47(22), pp. 12860–12867.

Page, S.E., Sander, M., Arnold, W.A. & McNeill, K. (2012) 'Hydroxyl radical formation upon oxidation of reduced humic acids by oxygen in the dark', *Environmental Science and Technology*, 46(3), pp. 1590–1597.

Pandis, P.K., Kalogirou, C., Kanellou, E., Vaitsis, C., Savvidou, M.G., Sourkouni, G., Zorpas, A.A. & Argirusis, C. (2022) 'Key Points of Advanced Oxidation Processes (AOPs) for Wastewater, Organic Pollutants and Pharmaceutical Waste Treatment: A Mini Review'. ChemEngineering 6 (1).

Patterson, S. (2020) *Personal communication*.

Pearson, J.C. (2017) *Development of a Sustainable Water Treatment Process for use in Developing Countries Based on Advanced Oxidation using Fe-bearing Clay Minerals*. [Online]. Newcastle University, Newcastle upon Tyne, UK.

Pham, A.L.T., Doyle, F.M. & Sedlak, D.L. (2012) 'Kinetics and efficiency of H2O2 activation by iron-containing minerals and aquifer materials', *Water Research*, 46(19), pp. 6454–6462.

Pham, H.T., Kitsuneduka, M., Hara, J., Suto, K. & Inoue, C. (2008) 'Trichloroethylene transformation by natural mineral pyrite: The deciding role of oxygen', *Environmental Science and Technology*, 42(19), pp. 7470–7475.

Pignatello, J.J., Oliveros, E. & MacKay, A. (2006) 'Advanced oxidation processes for organic contaminant destruction based on the fenton reaction and related chemistry', *Critical Reviews in Environmental Science and Technology*, 36(1), pp. 1–84.

Pocock, M.J.O., Evans, D.M. & Memmott, J. (2012) 'The robustness and restoration of a network of ecological networks', *Science*, 335(6071), pp. 973–977.

R Core Team. (2023) *_R: A Language and Environment for Statistical Computing_*. .

Rastogi, T., Mahmoud, W.M.M. & Kümmerer, K. (2018) 'Human and Veterinary Drugs in the Environment', in *Encyclopedia of the Anthropocene*. [Online]. Elsevier. pp. 263–268.

Rekhate, C. V. & Srivastava, J.K. (2020) 'Recent advances in ozone-based advanced oxidation processes for treatment of wastewater- A review'. Chemical Engineering Journal Advances 3.

Remucal, C.K. & Sedlak, D.L. (2011) 'The role of iron coordination in the production of reactive oxidants from ferrous iron oxidation by oxygen and hydrogen peroxide', *ACS Symposium Series*, 1071pp. 177–197.

Ribeiro, F.R., Fabris, J.D., Kostka, J.E., Komadel, P. & Stucki, J.W. (2009) 'Comparisons of structural iron reduction in smectites by bacteria and dithionite: II. A variable-temperature mössbauer spectroscopic study of garfield nontronite', *Pure and Applied Chemistry*, 81(8), pp. 1499–1509.

Romero, R., Contreras, D., Sepúlveda, M., Moreno, N., Segura, C. & Melin, V. (2020) 'Assessment of a Fenton reaction driven by insoluble tannins from pine bark in treating an emergent contaminant', *Journal of Hazardous Materials*, 382(April 2019), p. 120982.

Sacher, F. & Brauch, H.-J. (2002) *EXPERIENCES ON THE FATE OF ORGANIC MICROPOLLUTANTS DllRING RIVERBANK FILTRATION*.

Schaefer, M., Gorski, C. & Scherer, M. (2011) 'Spectroscopic Evidence for Interfacial Fe(II)-Fe(III) Electron Transfer in a Clay Mineral', *Environmental science & technology*, 45pp. 540–545.

Schwarzenbach, R.P., Egli, T., Hofstetter, T.B., von Gunten, U. & Wehrli, B. (2010) 'Global Water Pollution and Human Health', *Annual Review of Environment and Resources*, 35(1), pp. 109–136.

Schwarzenbach, R.P., Escher, B.I., Fenner, K., Hofstetter, T.B., Johnson, C.A., von Gunten, U. & Wehrli, B. (2006) 'The Challenge of Micropollutants in Aquatic Systems', *Science*, 313(5790), pp. 1072–1077.

Shelobolina, E.S., VanPraagh, C.G. & Lovley, D.R. (2003) 'Use of Ferric and Ferrous Iron Containing Minerals for Respiration by Desulfitobacterium frappieri', *Geomicrobiology Journal*, 20(2), pp. 143–156.

Silva, T.R., Valdman, E., Valdman, B. & Leite, S.G.F. (2007) 'Salicylic acid degradation from aqueous solutions using Pseudomonas fluorescens HK44: parameters studies and application tools', *Brazilian Journal of Microbiology*, 38(1), pp. 39–44.

Stamm, C., Räsänen, K., Burdon, F.J., Altermatt, F., Jokela, J., Joss, A., Ackermann, M. & Eggen, R.I.L. (2016) 'Unravelling the Impacts of Micropollutants in Aquatic Ecosystems: Interdisciplinary Studies at the Interface of Large-Scale Ecology', *Advances in Ecological Research*, 55pp. 183–223.

Stoeck, T., Pan, H., Dully, V., Forster, D. & Jung, T. (2018) 'Towards an eDNA metabarcode-based performance indicator for full-scale municipal wastewater treatment plants', *Water Research*, 144pp. 322–331.

Stucki, J.W. (2011) 'A review of the effects of iron redox cycles on smectite properties', *Comptes Rendus Geoscience*, 343(2), pp. 199–209.

Stucki, J.W. (1981) 'The Quantitative Assay of Minerals for Fe^{2+} and Fe^{3+} Using 1,10-Phenanthroline: II. A Photochemical Method', *Soil Science Society of America journal.*, 45(3), pp. 638–641.

Stucki, J.W., Golden, D.C. & Roth, C.B. (1984) 'Preparation and Handling of Dithionite-Reduced Smectite Suspensions.', *Clays and Clay Minerals*, 32(3), pp. 191–197.

Stucki, J.W., Komadel, P. & Wilkinson, H.T. (1987) 'Microbial Reduction of Structural Iron(III) in Smectites', *Soil Science Society of America Journal*, 51(6), pp. 1663–1665.

Tang, B., Zhang, Z., Chen, X., Bin, L., Huang, S., Fu, F., Yang, H. & Chen, C. (2014) 'Biodiversity and succession of microbial community in a multi-habitat membrane bioreactor', *Bioresource Technology*, 164pp. 354–361.

Tong, M., Yuan, S., Ma, S., Jin, M., Liu, D., Cheng, D., Liu, X., Gan, Y. & Wang, Y. (2016) 'Production of Abundant Hydroxyl Radicals from Oxygenation of Subsurface Sediments', *Environmental Science and Technology*, 50(1), pp. 214–221.

Toro-Vélez, A.F., Madera-Parra, C.A., Peña-Varón, M.R., Lee, W.Y., Bezares-Cruz, J.C., Walker, W.S., Cárdenas-Henao, H., Quesada-Calderón, S., García-Hernández, H. & Lens, P.N.L. (2016) 'BPA and NP removal from municipal wastewater by tropical horizontal subsurface constructed wetlands', *Science of the Total Environment*, 542pp. 93–101.

United Nations (2019) *Report of the Secretary-General, Special edition: progress towards the Sustainable Development Goals*.

Valentín-Vargas, A., Toro-Labrador, G. & Massol-Deyá, A.A. (2012) 'Bacterial Community Dynamics in Full-Scale Activated Sludge Bioreactors: Operational and Ecological Factors Driving Community Assembly and Performance', *PLOS ONE*, 7(8), pp. e42524-.

Vignola, M., Werner, D., Wade, M.J., Meynet, P. & Davenport, R.J. (2018) 'Medium shapes the microbial community of water filters with implications for effluent quality', *Water Research*, 129pp. 499–508.

Vione, D., Falletti, G., Maurino, V., Minero, C., Pelizzetti, E., Malandrino, M., Ajassa, R., Olariu, R.-I. & Arsene, C. (2006) 'Sources and Sinks of Hydroxyl Radicals upon Irradiation of Natural Water Samples', *Environmental Science & Technology*, 40(12), pp. 3775–3781.

Wang, W., Qu, Y., Yang, B., Liu, X. & Su, W. (2012) 'Lactate oxidation in pyrite suspension: A Fenton-like process in situ generating H 2O 2', *Chemosphere*, 86(4), pp. 376–382.

Wang, X., Dong, H., Zeng, Q., Xia, Q., Zhang, L. & Zhou, Z. (2017) 'Reduced Iron-Containing Clay Minerals as Antibacterial Agents', *Environmental Science and Technology*, 51(13), pp. 7639–7647.

Wang, Y., Naumann, U., Wright, S.T. & Warton, D.I. (2012) 'Mvabund- an R package for model-based analysis of multivariate abundance data', *Methods in Ecology and Evolution*, 3(3), pp. 471–474.

Wickham, H. (2016) *ggplot2: Elegant Graphics for Data Analysis*. Springer-Verlag New York.

Wong, M.K.-S., Nakao, M. & Hyodo, S. (2020) 'Field application of an improved protocol for environmental DNA extraction, purification, and measurement using Sterivex filter', *Scientific Reports*, 10(1), p. 21531.

Wright, E.S. (2016) *Using DECIPHER v2.0 to Analyze Big Biological Sequence Data in R*.

Wu, C., De Visscher, A. & Gates, I.D. (2017) 'Reactions of hydroxyl radicals with benzoic acid and benzoate', *RSC Advances*, 7(57), pp. 35776–35785.

Wu, J., Roth, C.B. & Low, P.F. (1988) 'Biological Reduction of Structural Iron in Sodium-Nontronite', *Soil Science Society of America Journal*, 52(1), p. 295.

Xie, W., Yuan, S., Tong, M., Ma, S., Liao, W., Zhang, N. & Chen, C. (2020) 'Contaminant Degradation by •oH during Sediment Oxygenation: Dependence on Fe(II) Species', *Environmental Science and Technology*, 54(5), pp. 2975–2984.

Yan, N., Zhong, H. & Brusseau, M.L. (2019) 'The natural activation ability of subsurface media to promote in-situ chemical oxidation of 1,4-dioxane', *Water Research*, 149pp. 386–393.

Yuan, S., Liu, X., Liao, W., Zhang, P., Wang, X. & Tong, M. (2018) 'Mechanisms of electron transfer from structrual Fe(II) in reduced nontronite to oxygen for production of hydroxyl radicals', *Geochimica et Cosmochimica Acta*, 223pp. 422–436.

Zeng, Q., Dong, H. & Wang, X. (2019) 'Effect of ligands on the production of oxidants from oxygenation of reduced Fe-bearing clay mineral nontronite', *Geochimica et Cosmochimica Acta*, 251pp. 136–156.

Zeng, Q., Dong, H., Wang, X., Yu, T. & Cui, W. (2017) 'Degradation of 1, 4-dioxane by hydroxyl radicals produced from clay minerals', *Journal of Hazardous Materials*, 331pp. 88–98.

Zeng, Q., Dong, H., Zhao, L. & Huang, Q. (2016) 'Preservation of organic matter in nontronite against iron redox cycling', *American Mineralogist*, 101(1), pp. 120–133.

Zepp, R.G., Holgne, J. & Bader, H. (1987) 'Nitrate-Induced Photooxidation of Trace Organic Chemicals in Water', *Environmental Science and Technology*, 21(5), pp. 443–450.

Zhang, J., Dong, H., Liu, D. & Agrawal, A. (2013) 'Microbial reduction of Fe(III) in smectite minerals by thermophilic methanogen Methanothermobacter thermautotrophicus', *Geochimica et Cosmochimica Acta*, 106pp. 203–215.

Zhang, N., Bu, X., Li, Y., Zhang, Y., Yuan, S., Wen, Z., Tong, M. & Lin, L. (2020) 'Water Table Fluctuations Regulate Hydrogen Peroxide Production and Distribution in Unconfined Aquifers', *Environmental science & technology*, 54(8), pp. 4942–4951.

Zhang, N., Liu, Y., Wan, Z., Zhang, Y., Xie, W., Zhang, P., Tong, M. & Yuan, S. (2024) 'Dependence of Biotic and Abiotic H2O2 and •OH Production on the Redox Conditions and Compositions of Sediment during Oxygenation', *Environmental Science and Technology*, 58(8), pp. 3849–3857.

Zhang, P., Huang, W., Ji, Z., Zhou, C. & Yuan, S. (2018) 'Mechanisms of hydroxyl radicals production from pyrite oxidation by hydrogen peroxide: Surface versus aqueous reactions', *Geochimica et Cosmochimica Acta*, 238pp. 394–410.

Zhang, P., Liu, J., Yu, H., Cheng, D., Liu, H. & Yuan, S. (2023) 'Kinetic models for hydroxyl radical production and contaminant removal during soil/sediment oxygenation', *Water Research*, 240.

Zhang, P. & Yuan, S. (2017) 'Production of hydroxyl radicals from abiotic oxidation of pyrite by oxygen under circumneutral conditions in the presence of low-molecular-weight organic acids', *Geochimica et Cosmochimica Acta*, 218pp. 153–166.

Zhang, P., Yuan, S. & Liao, P. (2016) 'Mechanisms of hydroxyl radical production from abiotic oxidation of pyrite under acidic conditions', *Geochimica et Cosmochimica Acta*, 172pp. 444–457.

Zhang, S., Zheng, H. & Tratnyek, P.G. (2023) 'Advanced redox processes for sustainable water treatment', *Nature Water*, 1(8), pp. 666–681.

Zhang, X., Zhang, C., Sun, X., Yang, J. & Zhu, C. (2019) 'Mechanism and kinetic study of the reaction of benzoic acid with OH, NO3 and SO4- radicals in the atmosphere', *RSC Advances*, 9(33), pp. 18971–18977.

Zhang, Y., Tong, M., Yuan, S., Qian, A. & Liu, H. (2020) 'Interplay between iron species transformation and hydroxyl radicals production in soils and sediments during anoxic-oxic cycles', *Geoderma*, 370p. 114351.

Zhao, G., Wu, B., Zheng, X., Chen, B., Kappler, A. & Chu, C. (2022) 'Tide-Triggered Production of Reactive Oxygen Species in Coastal Soils', *Environmental Science and Technology*, 56(16), pp. 11888–11896.

Zhao, L., Dong, H., Kukkadapu, R., Agrawal, A., Liu, D., Zhang, J. & Edelmann, R.E. (2013) 'Biological oxidation of Fe(II) in reduced nontronite coupled with nitrate reduction by Pseudogulbenkiania sp. Strain 2002', *Geochimica et Cosmochimica Acta*, 119pp. 231–247.

Zhao, L., Dong, H., Kukkadapu, R.K., Zeng, Q., Edelmann, R.E., Pentrák, M. & Agrawal, A. (2015) 'Biological redox cycling of iron in nontronite and its potential application in nitrate removal', *Environmental Science and Technology*, 49(9), pp. 5493–5501.

Zhou, X. & Mopper, K. (1990) 'Determination of photochemically produced hydroxyl radicals in seawater and freshwater*'. Marine Chemistry 30.

Zhuang, K., Izallalen, M., Mouser, P., Richter, H., Risso, C., Mahadevan, R. & Lovley, D.R. (2011) 'Genome-scale dynamic modeling of the competition between Rhodoferax and Geobacter in anoxic subsurface environments', *The ISME Journal*, 5(2), pp. 305–316.

Zhuang, Y.F., Fialips, C.I., White, M.L. & Perez Ferrandez, D.M. (2012) 'New redox-active material for permeable water remediation systems', *Applied Clay Science*, 59–60pp. 26–35.

Zuorro, A., Fidaleo, Marco, Fidaleo, Marcello & Lavecchia, R. (2014) 'Degradation and antibiotic activity reduction of chloramphenicol in aqueous solution by UV/H2O2 process', *Journal of Environmental Management*, 133pp. 302–308.

Zuorro, A. & Lavecchia, R. (2014) 'Evaluation of UV/H 2 O 2 advanced oxidation process (AOP) for the degradation of diazo dye Reactive Green 19 in aqueous solution', *Desalination and Water Treatment*, 52(7–9), pp. 1571–1577.

Appendix A

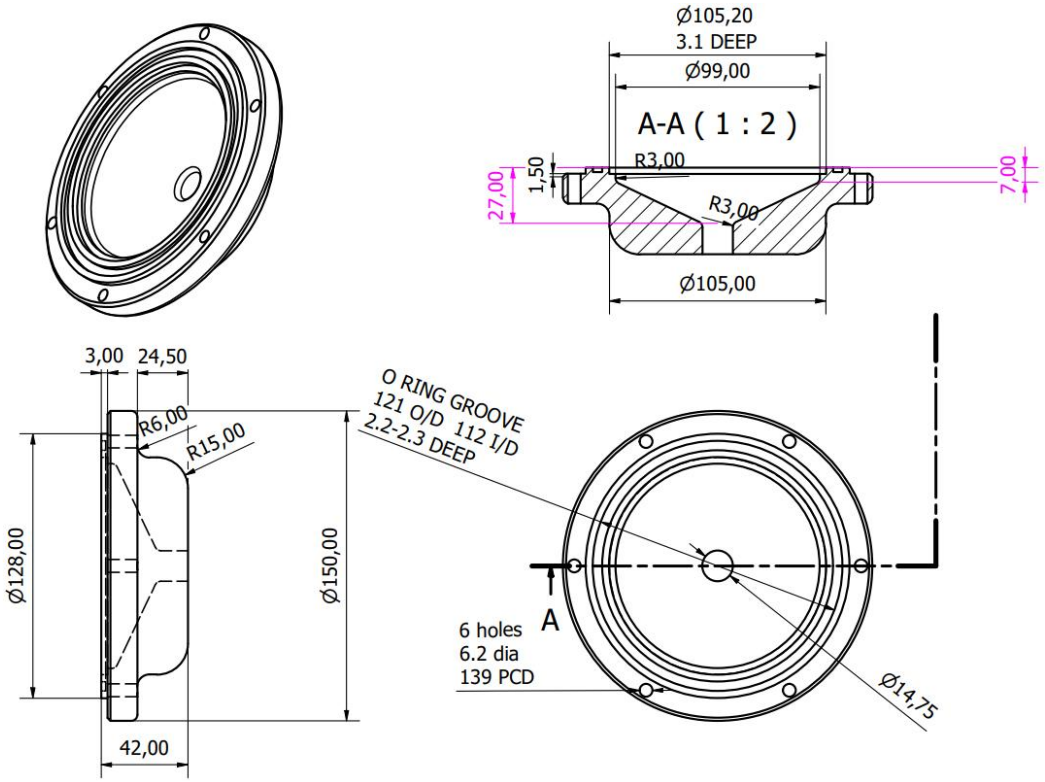

Figure A. 1 *Technical drawing of the HDPE base for each experimental column. The base is internally chamfered to promote laminar fluid flow and also to prevent build up of fines.*

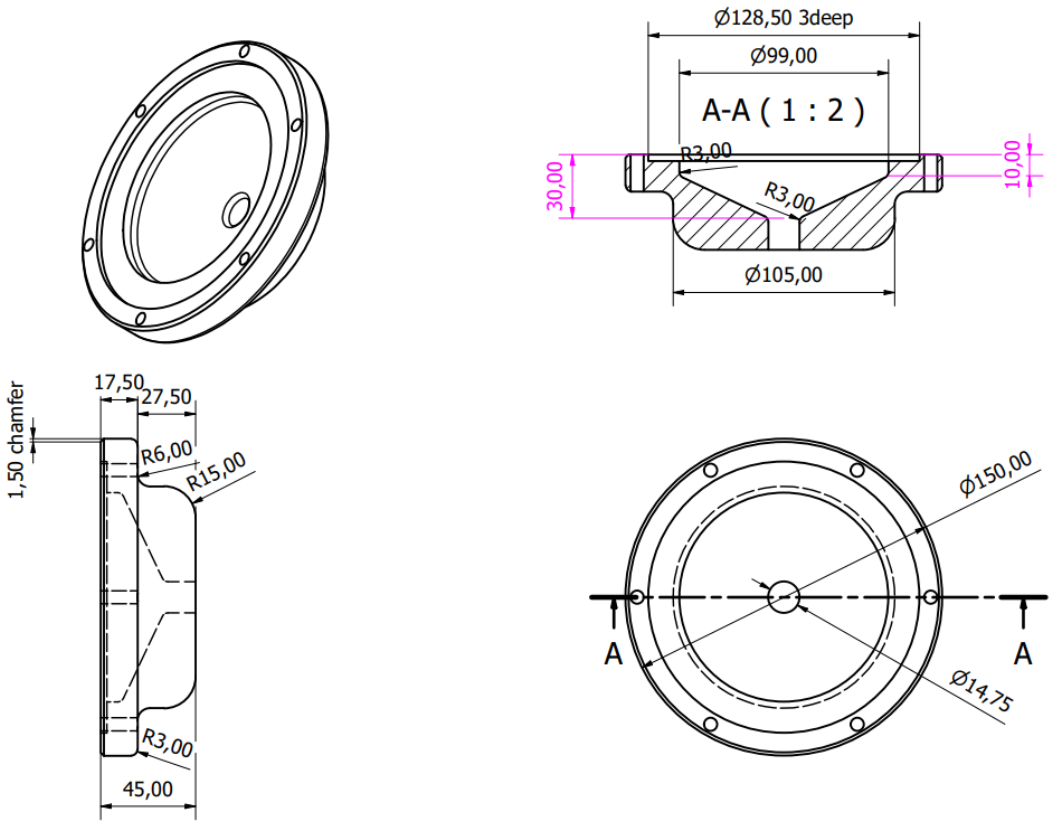

Figure A. 2 *Technical drawing of top of experimental column, with internal chamfer for laminar fluid flow. The top if secured to the collar and column shaft with 6X 4" screw nuts.*

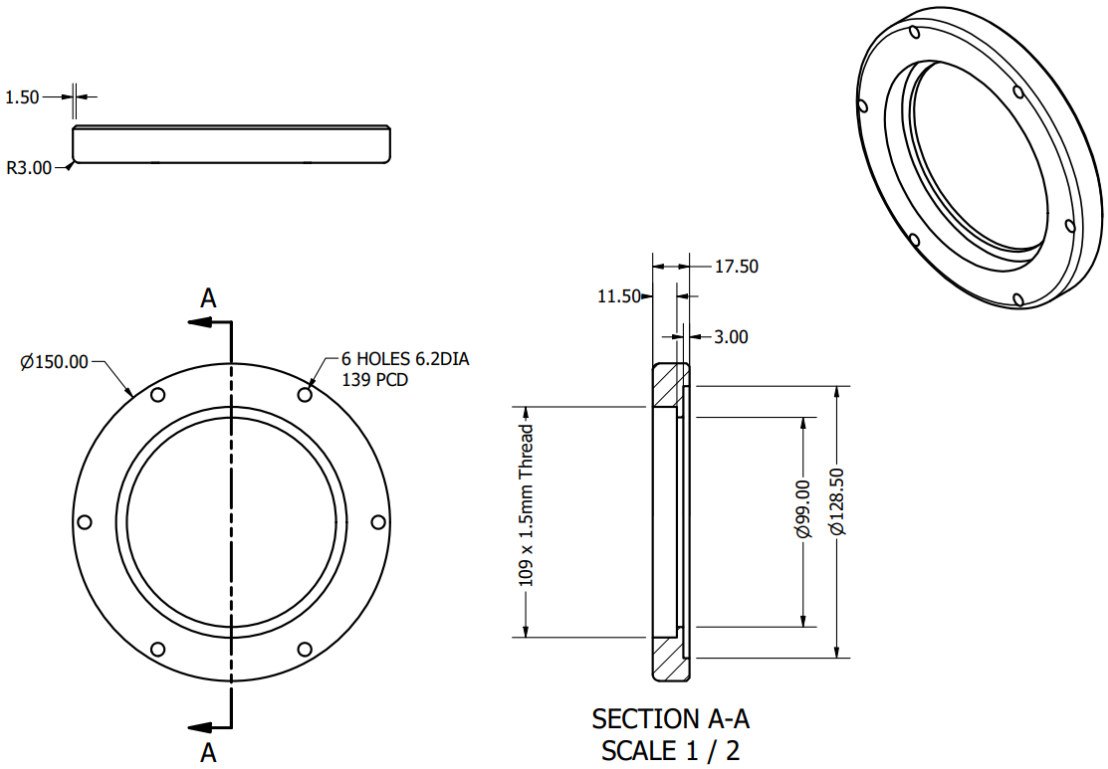

Figure A. 3 *Technical drawing of one of two HPDE screw-thread collars used to secure column shaft to top and base of experimental column.*

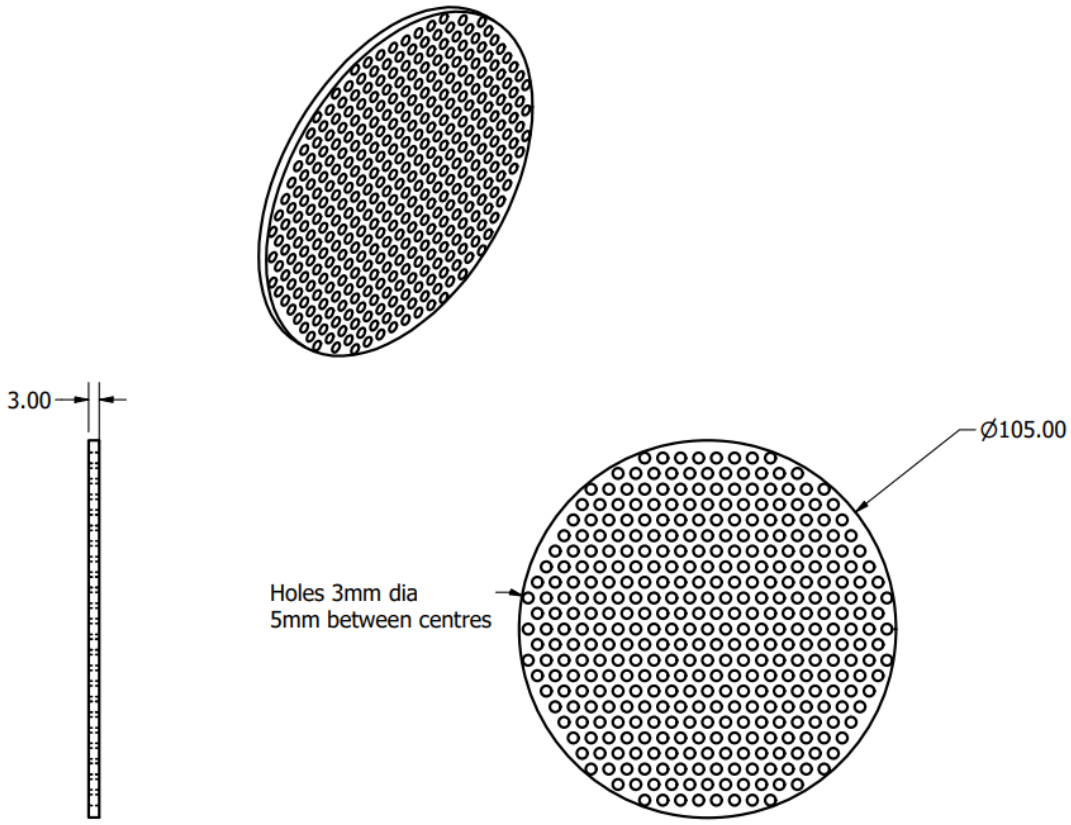

Figure A. 4 *Technical drawing of one of two rigid HPDE mesh layers, installed at the base and top of each experimental column to support geotextile layers whilst allowing influent and effluent flow.*

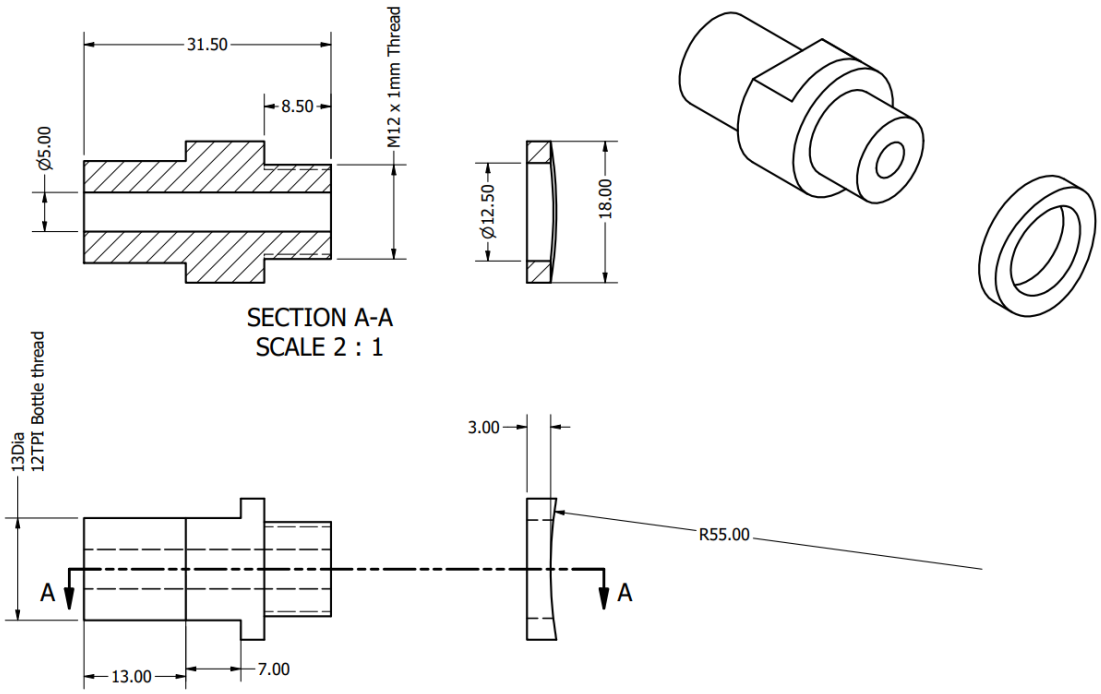

Figure A. 5 *Technical drawing of a column sampling port. Three sampling ports were installed on the long side of each experimental column.*

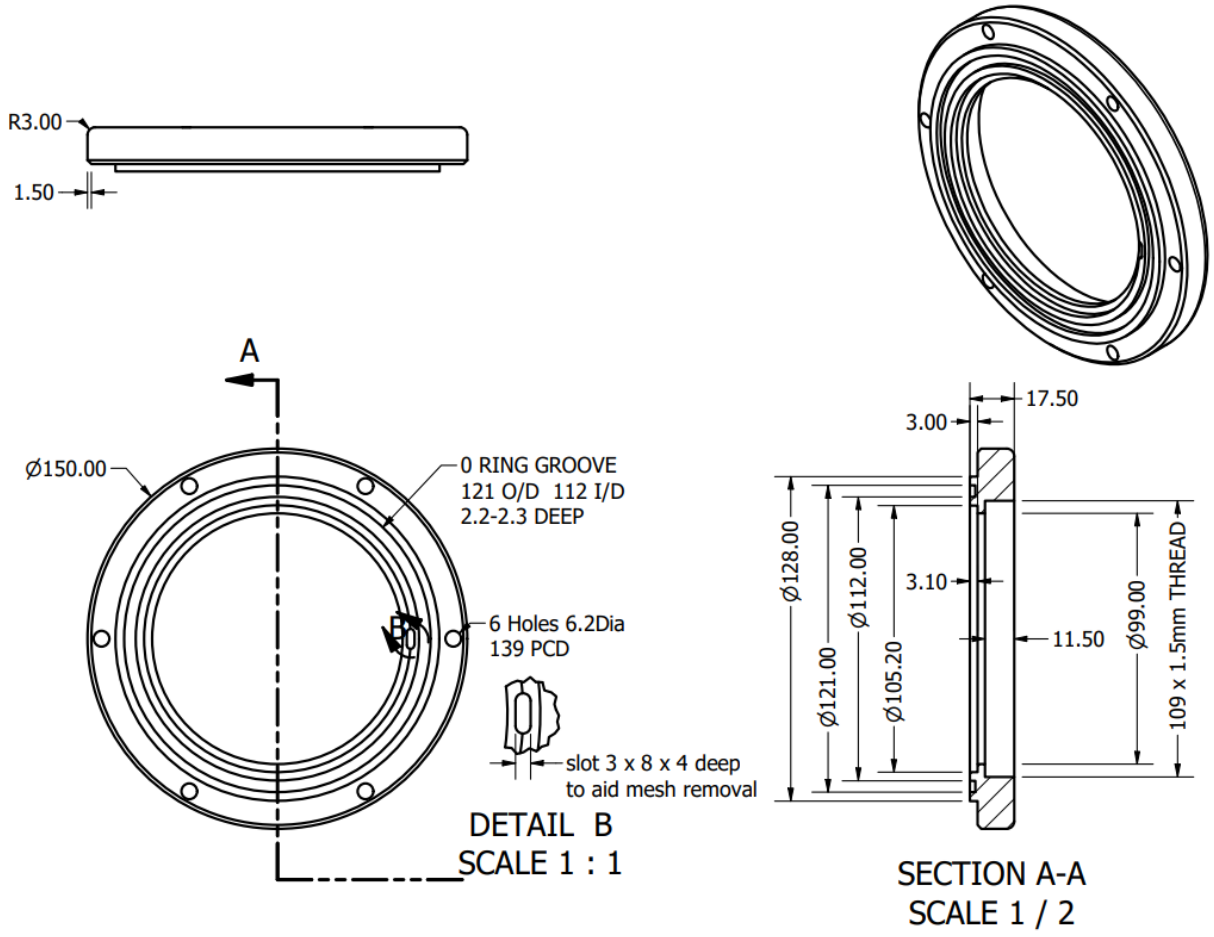

Figure A. 6 *Technical drawing of second HPDE screw-thread collars used to secure column shaft to top and base of experimental column.*

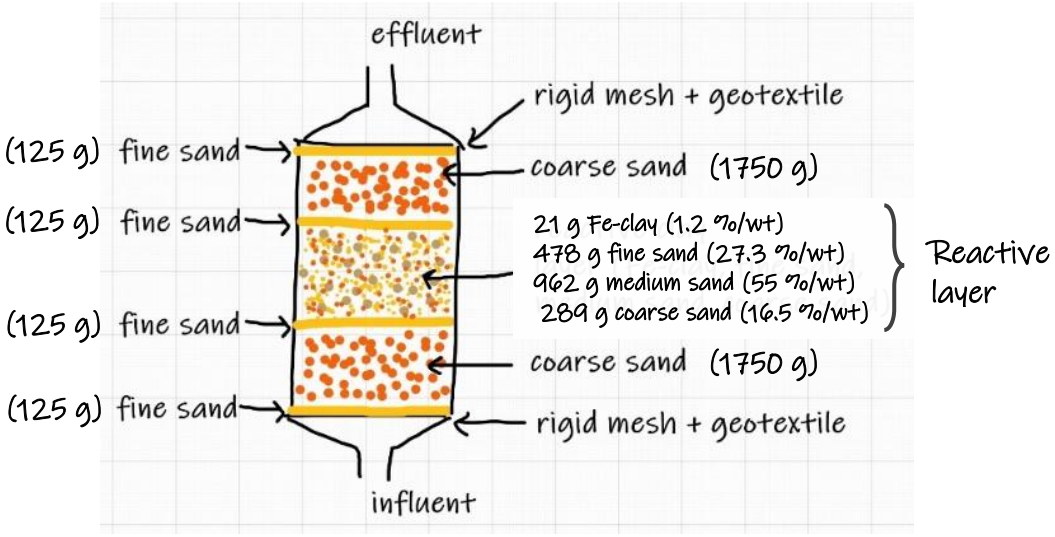

Figure A. 7 *Sketch showing final packing regime of benchtop experimental columns containing SWy-2. Fine, medium and coarse sand fractions are packed in layers of known mass and vertically encapsulate a 'reactive' clay and sand layer in the central section of the column.*

Appendix B

B.1 Microcosm batch experiments: further information

Mixtures of nontronite clay and sand plus sand-only microcosm batches (Table B.1) were activated by sodium dithionite reduction to the same target Fe^{2+} levels (19% and 38%; Chapter 4, Table 4.3) as the chemical column treatment experiments (Chapter 4, Table 4.2) under O_2-free conditions. Fe^{2+}/Fe^{TOT} ratios within the nontronite and sand mixtures obtained by the methods described in Chapter 4, Section 4.2.7 were used to provide estimates of the reduction extent in the chemical columns' reactive layers after the first and subsequent treatment cycles, where target Fe^{2+} reduction extents were 19% and 38%, respectively.

***Table B.* 1.** *Inventory of clay and sand sediment masses used in microcosm batch experiments.*

Sediment type	**Mass* in microcosm**	
	Clay + sand	Sand only
Nontronite <2 µm	0.4 g (1.5%)	-
fine sand	7.1 g (26.9%)	7.3 g
medium sand	14.3 g (53.7%)	14.5 g
coarse sand	4.8 g (17.9%)	4.8 g
Total mass substrates (g)	26.6 g (100%)	26.6 g

* dry weight % also shown for clay + sand microcosms

Table B. 2. *Estimate of lowest quantification limits for elements measured on ICP-OES, based on 10X standard deviations on 10 blank measurements.*

Element		Element detection limit (10 X stdev on blank samples)
Aluminium	Al	0.0059
Arsenic	As	0.0087
Barium	Ba	0.0001
Calcium	Ca	0.0192
Cadmium	Cd	0.0003
Chromium	Cr	0.0008
Copper	Cu	0.0011
Iron	Fe	0.0027
Potassium	K	0.0822
Magnesium	Mg	0.0116
Manganese	Mn	0.0002
Sodium	Na	0.3026
Nickel	Ni	0.0014
Lead	Pb	0.0154
Sulphur	S	0.2257
Silicon	Si	0.0537
Strontium	Sr	0.0005
Zinc	Zn	0.0008

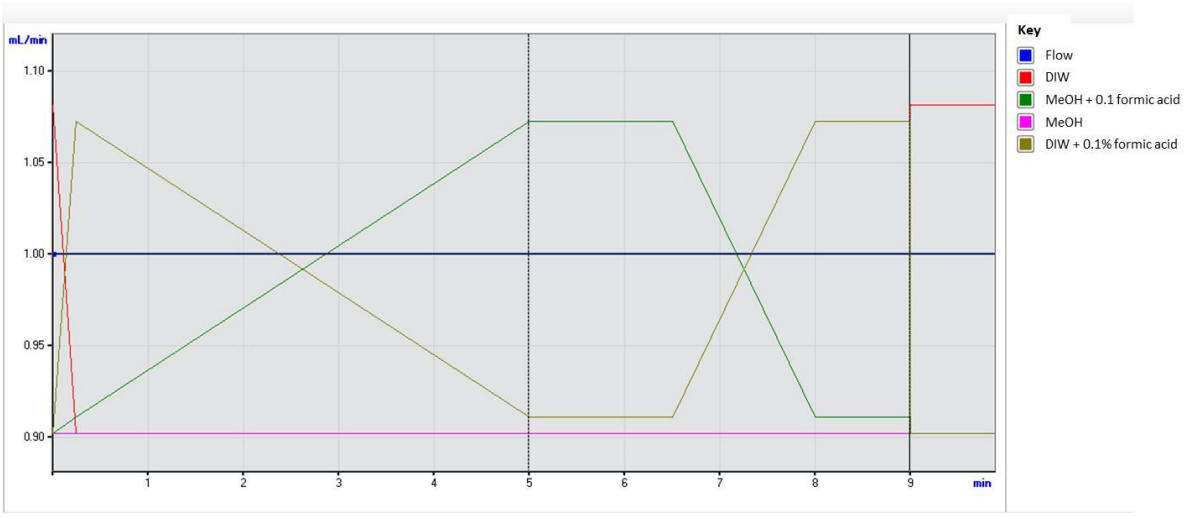

Figure B. 1. *Illustration of 9 min HPLC gradient program used for measurement of BA and 4-HBA in chemical column samples using MeOH and de-ionised water (H_2O) as mobile phases, both amended with formic acid (FA) to buffer pH to 2.3-2.5. Peak separation and organic elution were optimised using an increasing MeOH/H_2O ramp (5/95 to 95/5) over 5 min with a 1.5 min hold, with a second MeOH/H_2O ramp (95/5 to 5/95) over 1.5 min with a 1 min hold, to wash inorganic salts from the column before the next sample injection.*

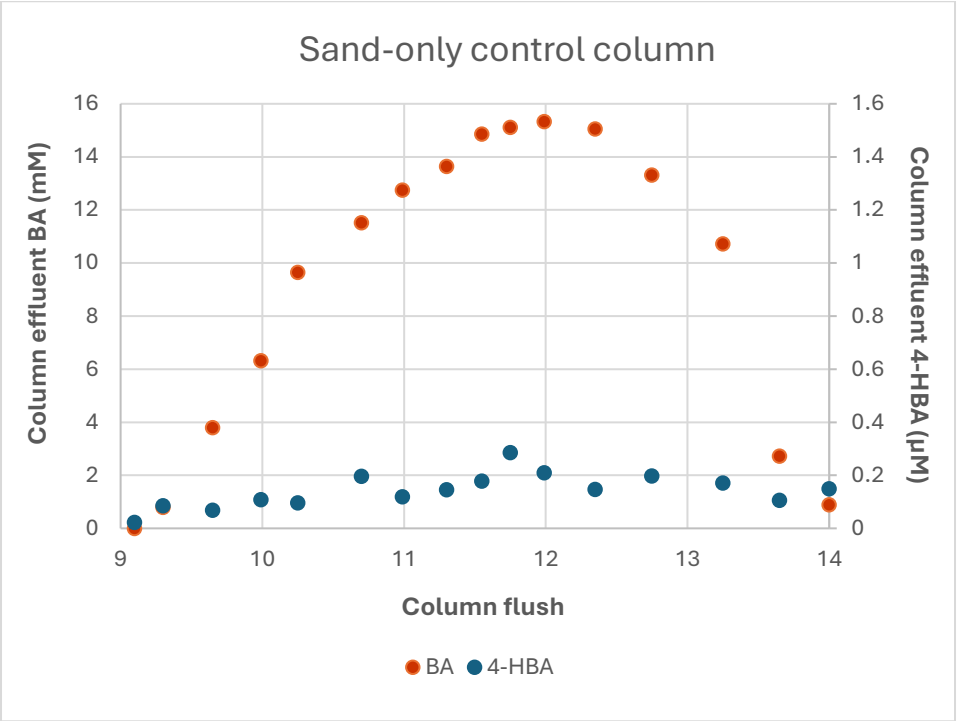

Figure B. 2*. Typical concentration profiles of benzoic acid and 4-hydroxybenzoic acid in the effluent of the sand-only chemical control column experiment, over the last 5 column flushes of a typical treatment cycle.*

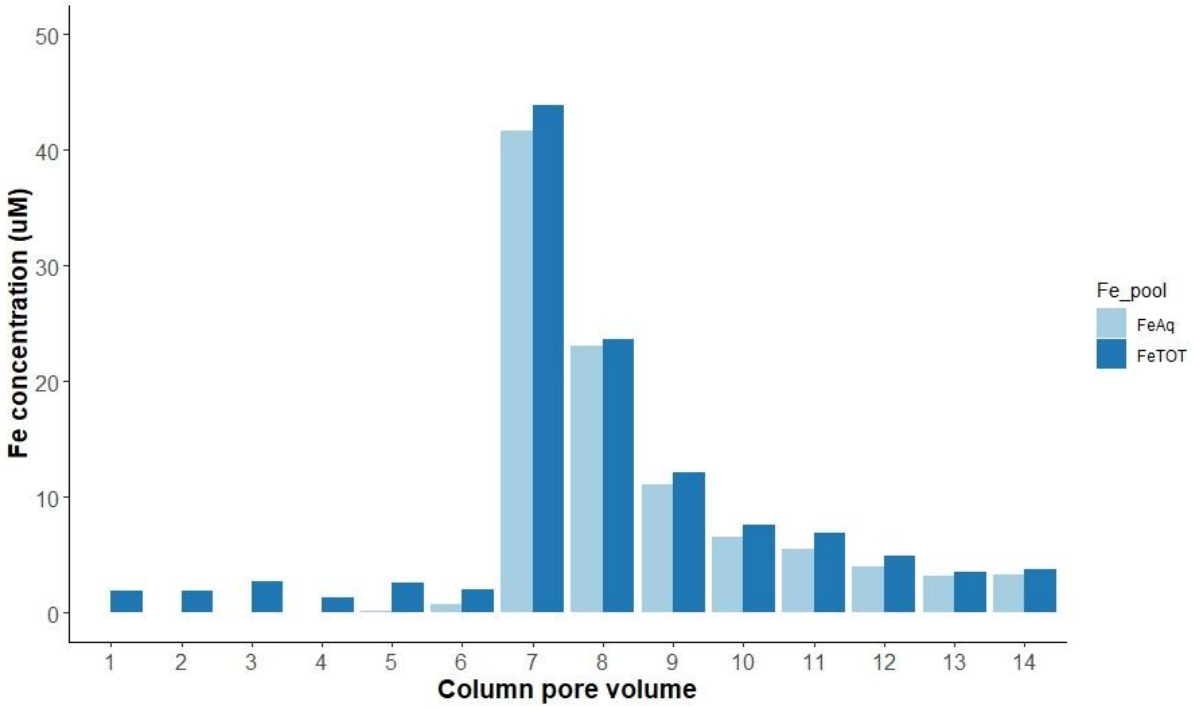

Figure B. 3. *Plot of iron pools across column cycles during sand-only chemical (control) column experiment.*

Figure B. 4. *Spearman's correlation matrix (for non-parametric data) for major cations measured in chemical column effluents during every column flush and during each treatment cycle. Cation data from control effluents were not included in this test.*

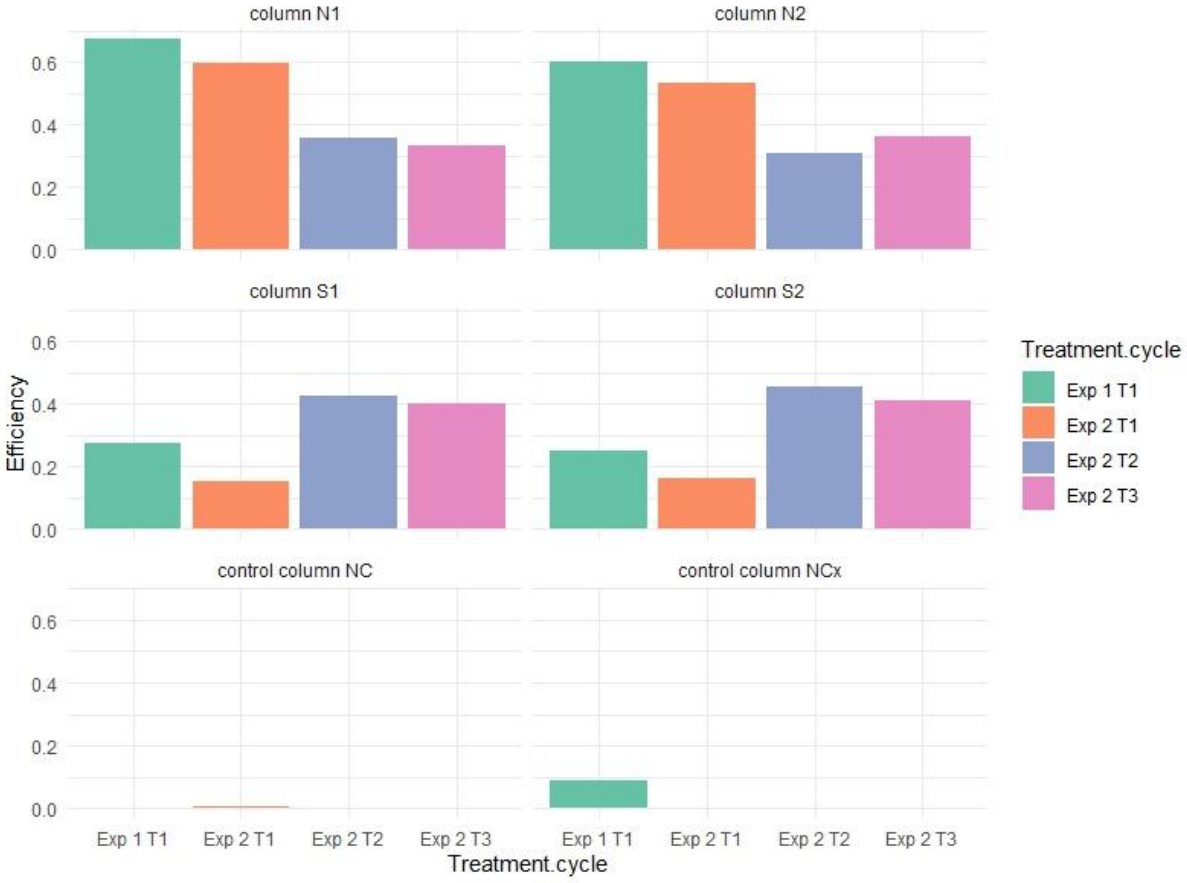

Figure B. 5. *Bar plots showing treatment efficiency of biological column Experiments 1 and 2.*

Appendix C

Table C. 1. *Physico-chemical parameters of Leazes Park pondwater (measured within 1 hour of collection during June 2022 and March 2023) in addition to combinations of live and sterile pondwater with NPK fertliser and/or benzoic acid used as column inoculants.*

Sample	pH	T°C	Conductivity µS	TDS mg/L	O_2 mg/L	% O_2 saturation	COD mg/L
Live pondwater	8.1 ± 0.4 n=8	17.3 ± 1.8 n=3	489.3 ± 9.2 n=4	339.2 ± 6.1 n=5	9.9 ± 0.1 n=2	-	42.9 ± 4.7 n=2
Live pondwater + NPK	6.1 ± 0.4 n=2	18.7 ± 2.1	1872	1308	9.95	-	1191 ± 2.1 n=2
Sterile pondwater	8.2	21.8	432	299	equilibrated to 9.98	-	-
Sterile pondwater + NPK	6.9 ± 0.3 n=3	23.2	1756	1290	equilibrated to 9.98	97	1128.5
Sterile pondwater + BA	8.2	23.2	1259	1009	equilibrated to 9.98	97.5	-

Table C. 2. *COD measurements of biological column porewaters pondwater (Experiment 1), 10 days after inoculation with live pondwater and NPK fertiliser.*

	Column				
	N1	**N2**	**S1**	**S2**	**control**
COD mg/L	1190	1183	1173	1174	1168

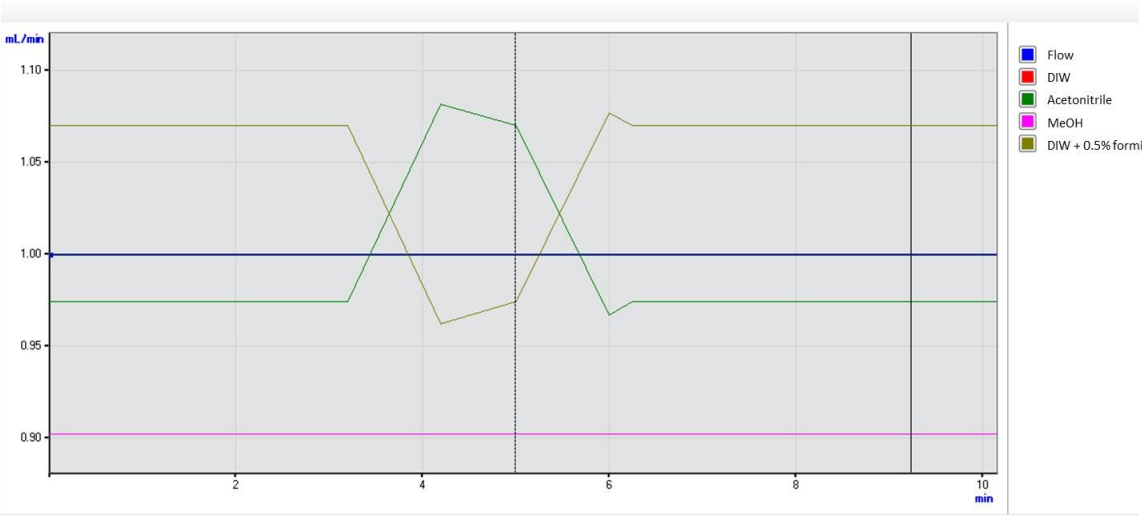

Figure C. 1. *Illustration of 10 min HPLC gradient program used for measurement of BA and 4-HBA in biological column samples using mobile phases of acetonitrile (AcN) and de-ionised water (H_2O) amended with 0.5% formic acid (FA) to buffer pH to 2.2-2.4. Peak separation and organic elution were optimised using an increasing AcN/H2O ramp (5/95 to 95/5) over 5 min with a 1.5 min hold, with a second AcN/H_2O ramp (95/5 to 5/95) over 1.5 min with a 1 min hold, to wash inorganic salts from the column before the next sample injection.*

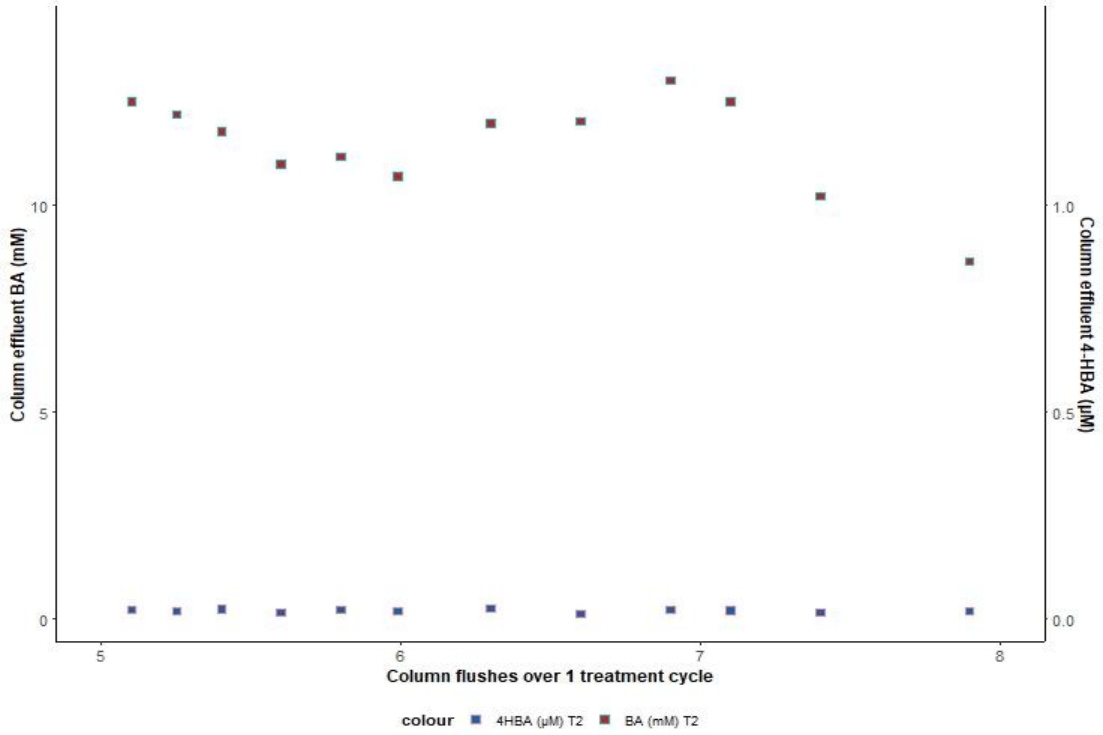

Figure C. 2*. Concentration profiles of BA and 4-HBA in biological column effluent across the single treatment cycle performed for the control column NC (NAu-2 clay), using data from Experiment 2. Data plotted as a function of column flush, where flush #4 is the start of BA treatment and flush #8 (after #7) marks the end of the treatment cycle.*

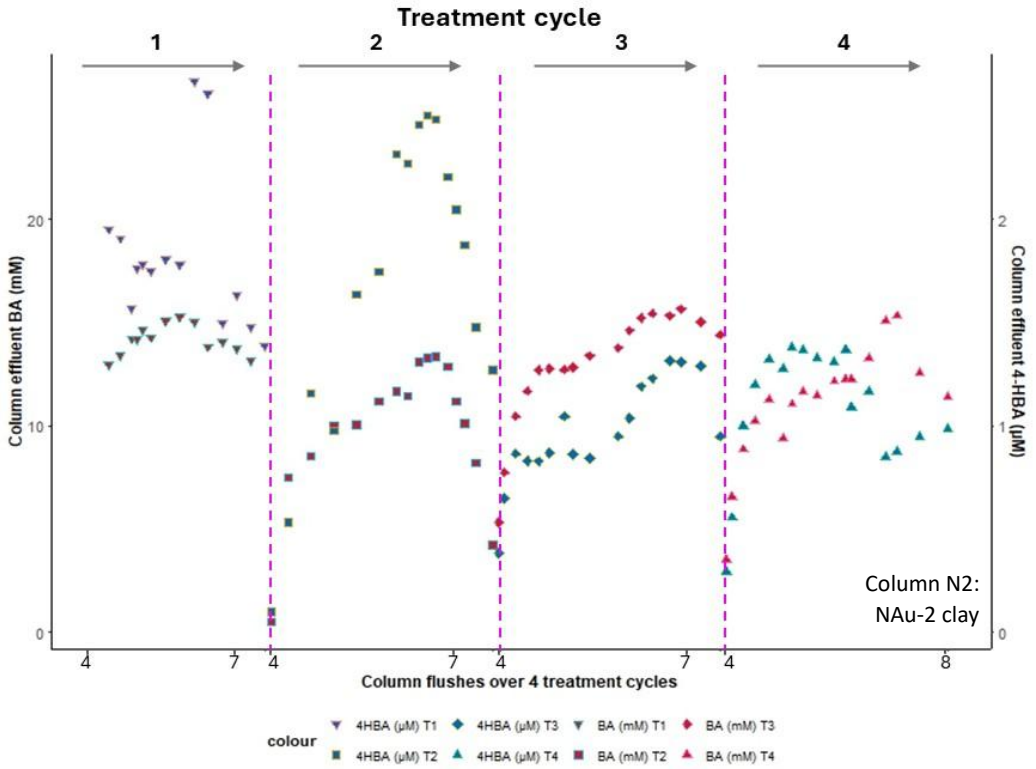

***Figure C. 3**. Concentration profiles of BA and 4-HBA in biological column effluents across all 4 treatment cycles, for column N2 (NAu-2 clay), using data from Experiments 1 and 2. Data plotted as a function of column flush, where flush #4 is the start of BA treatment and flush #8 (after #7) the end of each treatment cycle.*

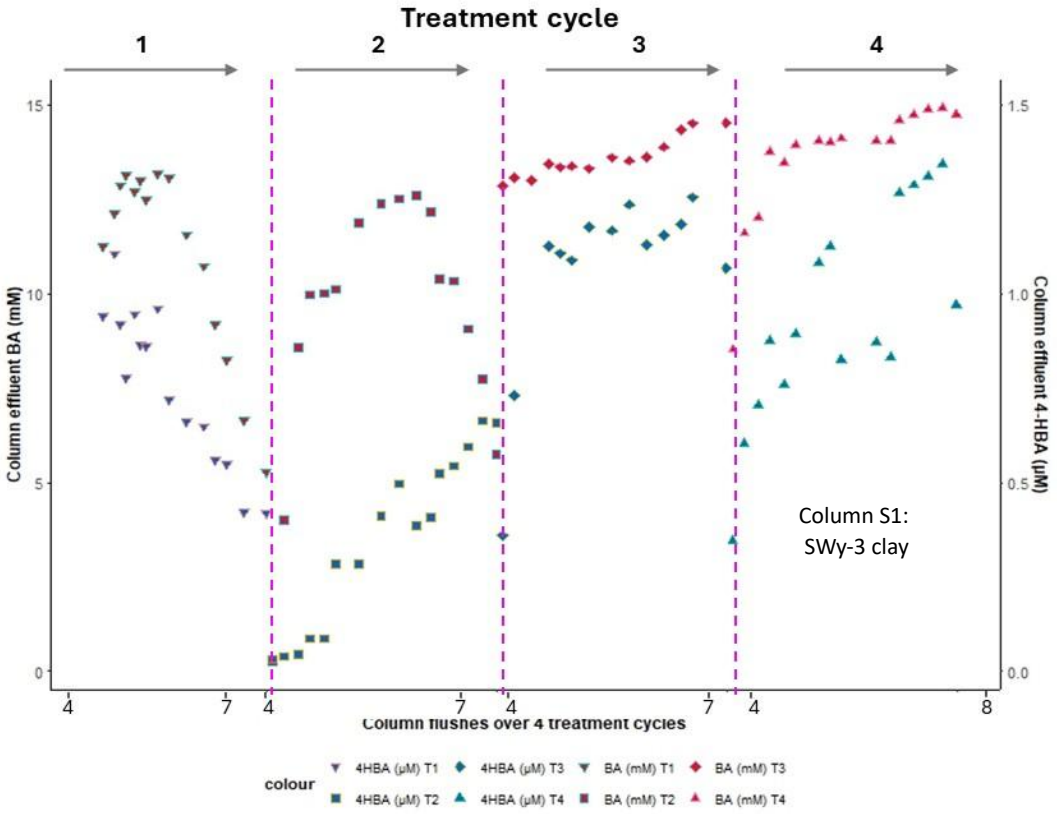

***Figure C. 4**. Concentration profiles of BA and 4-HBA in biological column effluents across all 4 treatment cycles, for column S1 (SWy-3 clay), using data from Experiments 1 and 2. Data plotted as a function of column flush, where flush #4 is the start of BA treatment and flush #8 (after #7) the end of each treatment cycle.*

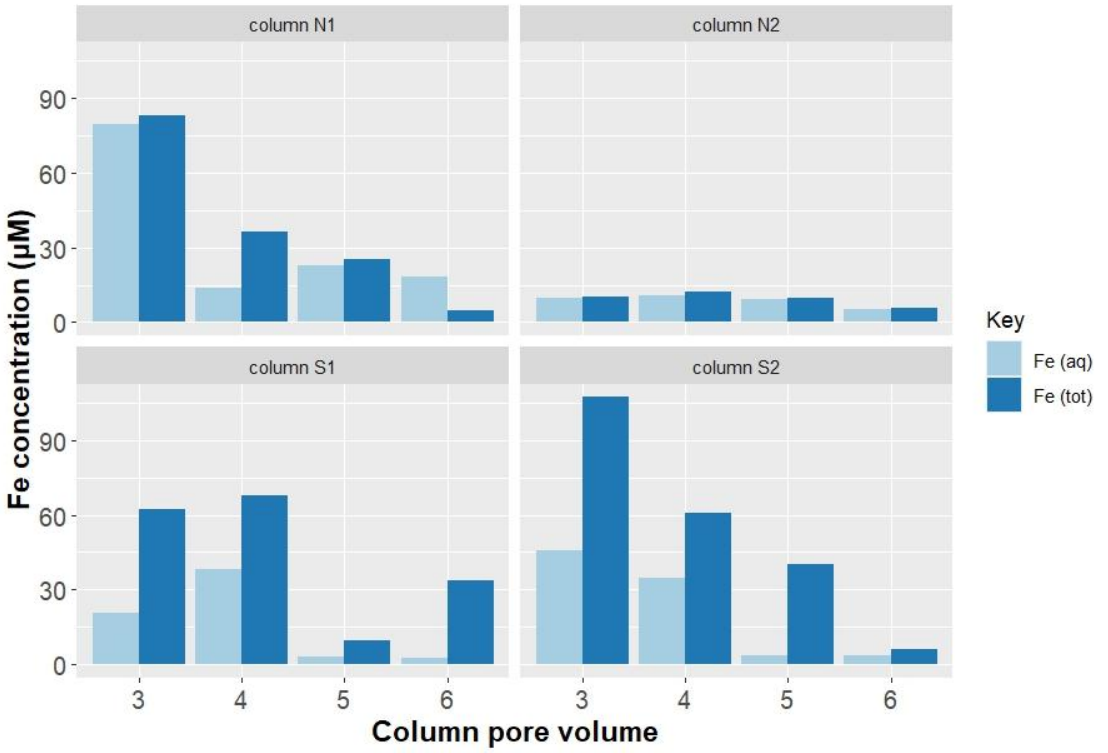

Figure C. 5. *Filtered and total Fe sampled from control column effluents in biological column Experiment 1, treatment cycle 1.*

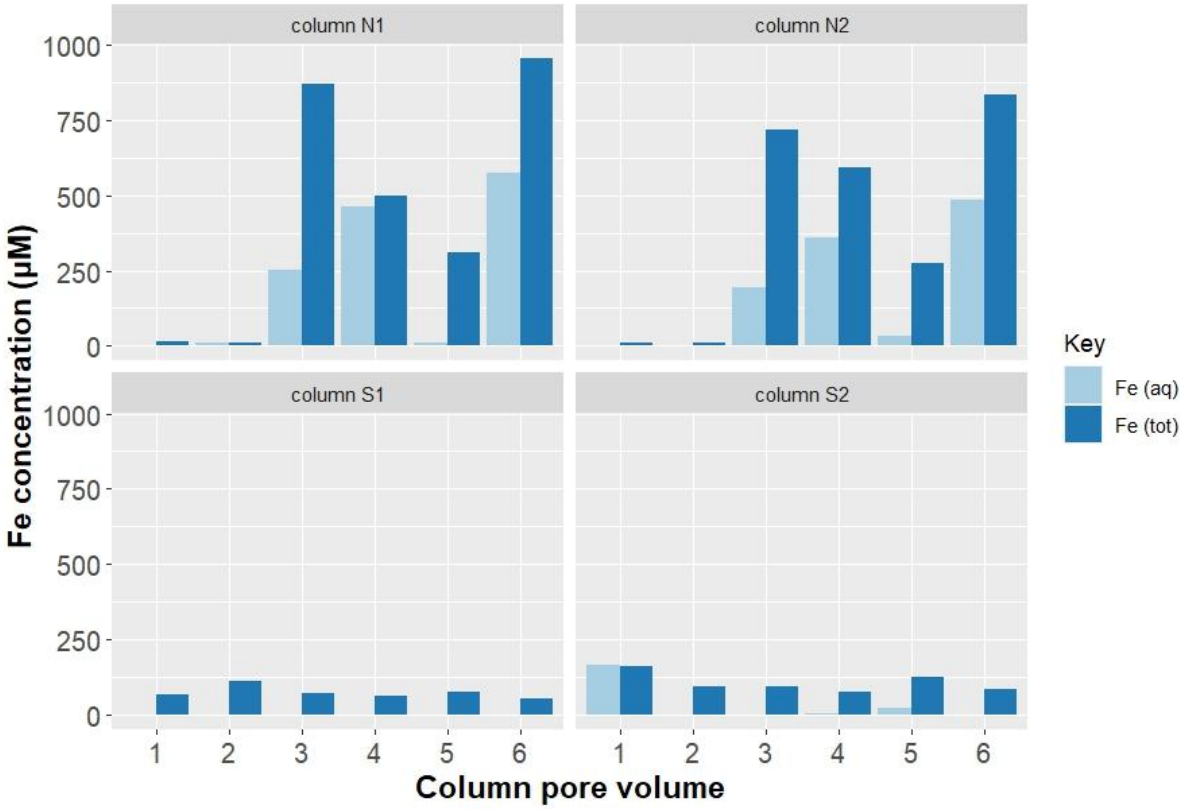

Figure C. 6. *Filtered and total Fe sampled from control column effluents in biological column Experiment 2, treatment cycle 1.*

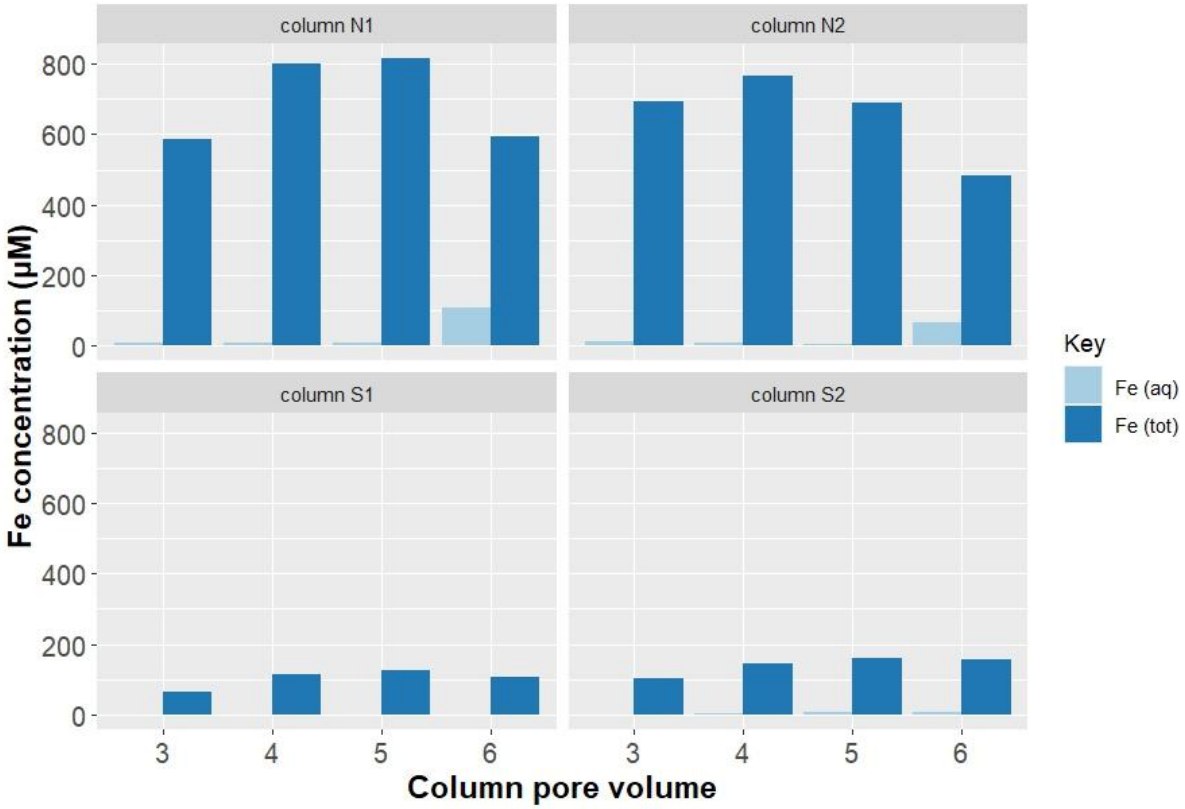

Figure C. 7. *Filtered and total Fe sampled from control column effluents in biological column Experiment 2, treatment cycle 2.*

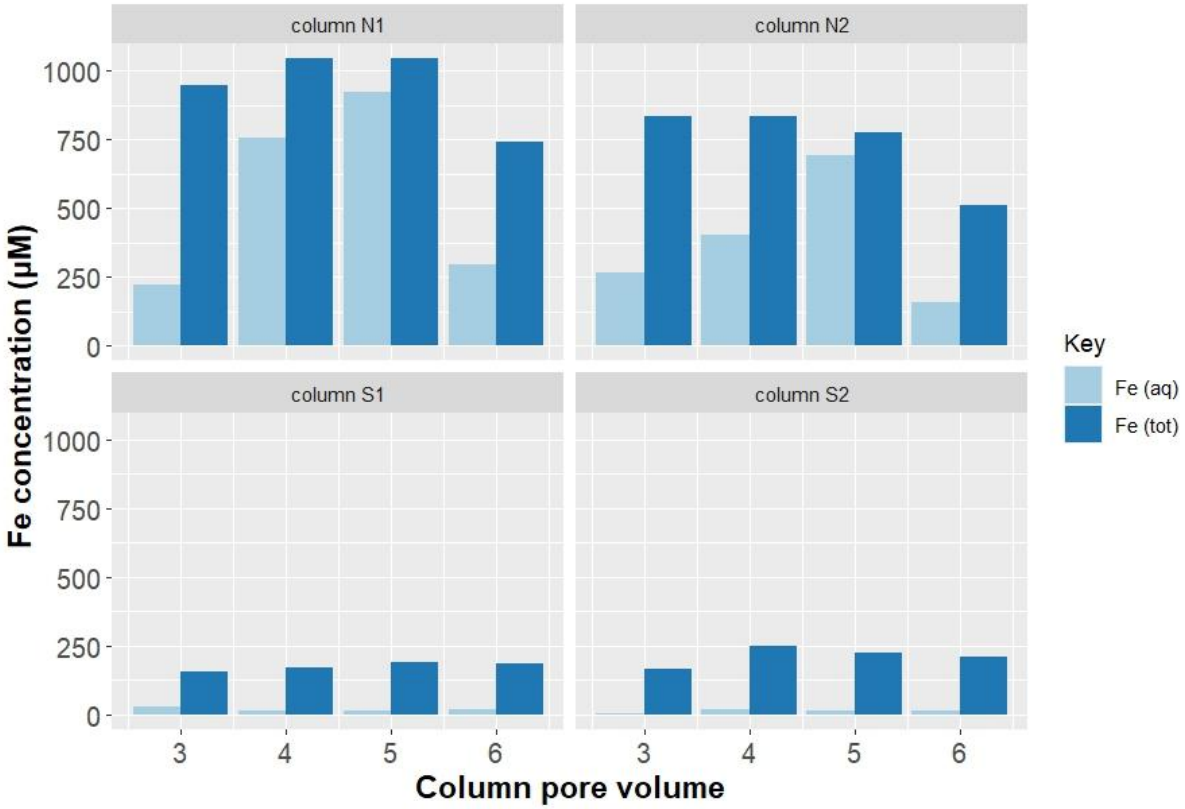

Figure C. 8. *Filtered and total Fe sampled from control column effluents in biological column Experiment 2, treatment cycle 3.*

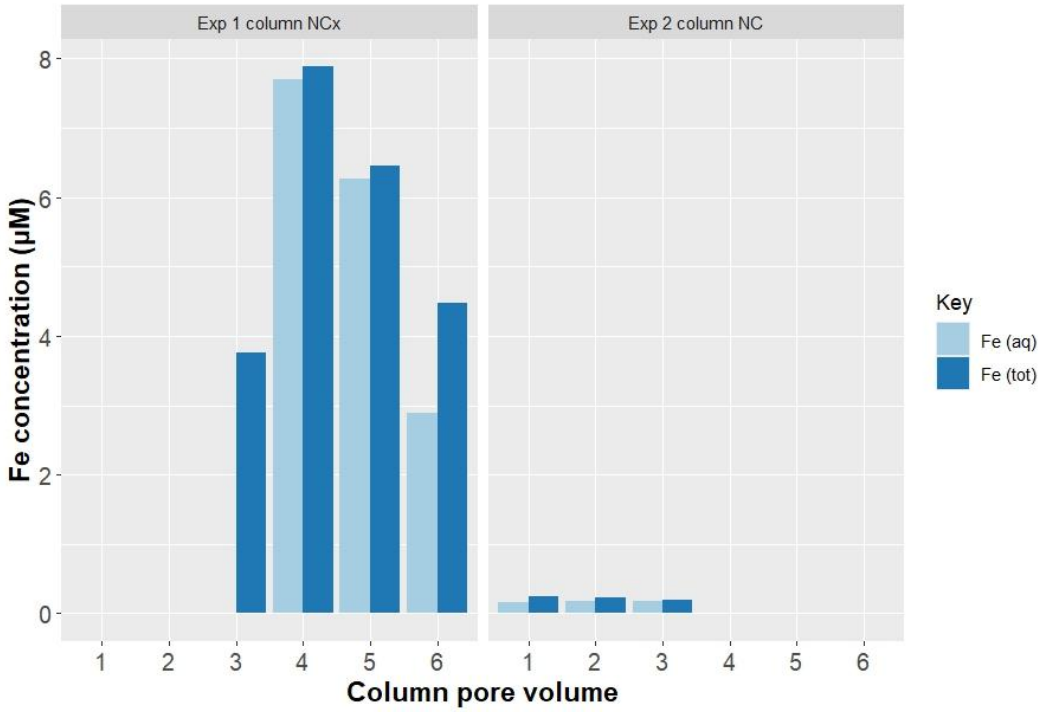

Figure C. 9. *Filtered and total Fe sampled from control column effluents in biological column Experiments 1 (column NCx) and 2 (column NC).*

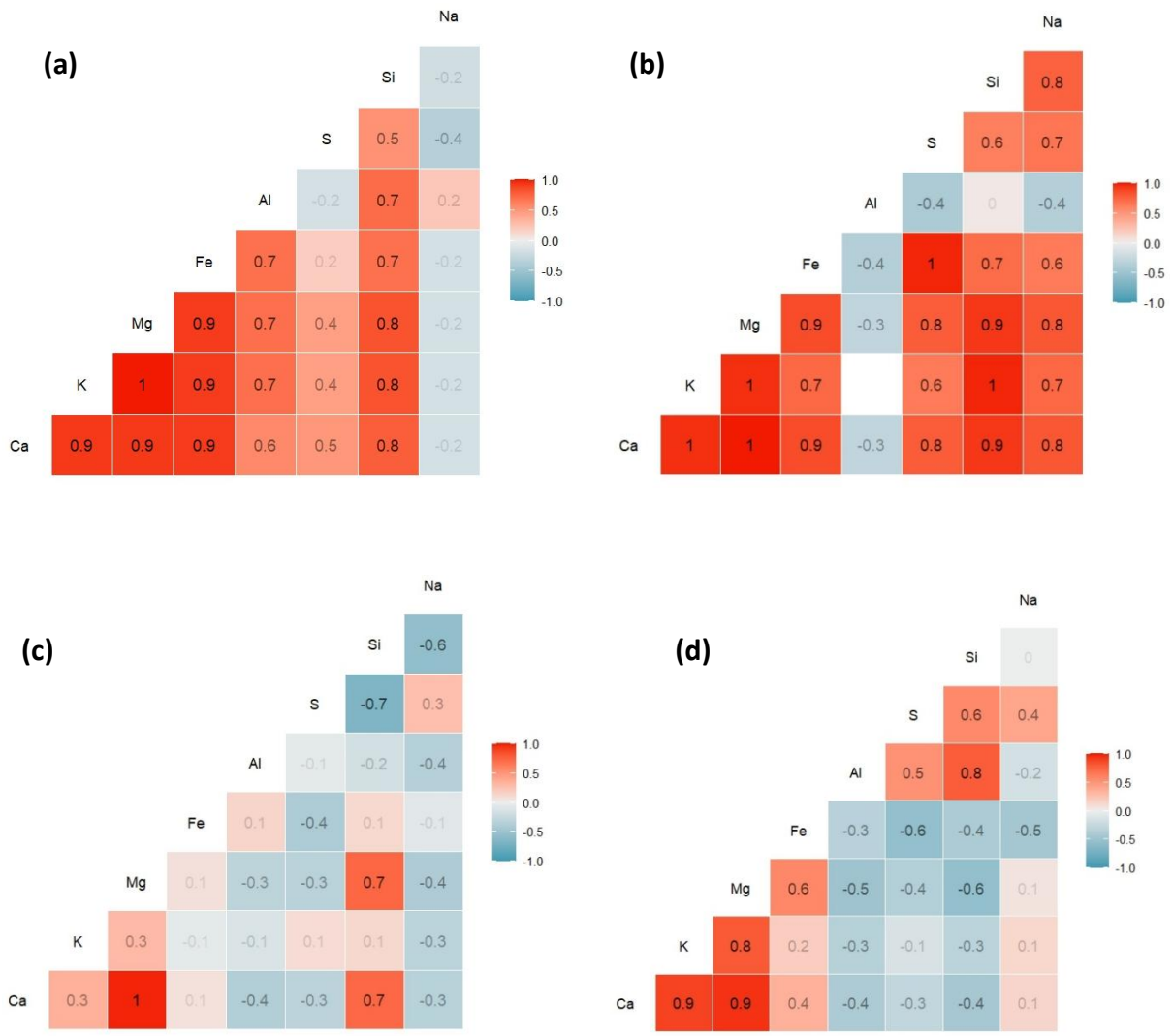

Figure C. 10. *Heatmaps showing Spearman's rank correlation matrices for major cations in biological column effluents from (a) all NAu-2 effluents sampled in Experiment 1 (all treatment cycles), (b) all SWy-3 effluents sampled in Experiment 1, (c) all NAu-2 effluents sampled in Experiment 2, and (d) all SWy-3 effluents sampled in Experiment 2.*

-

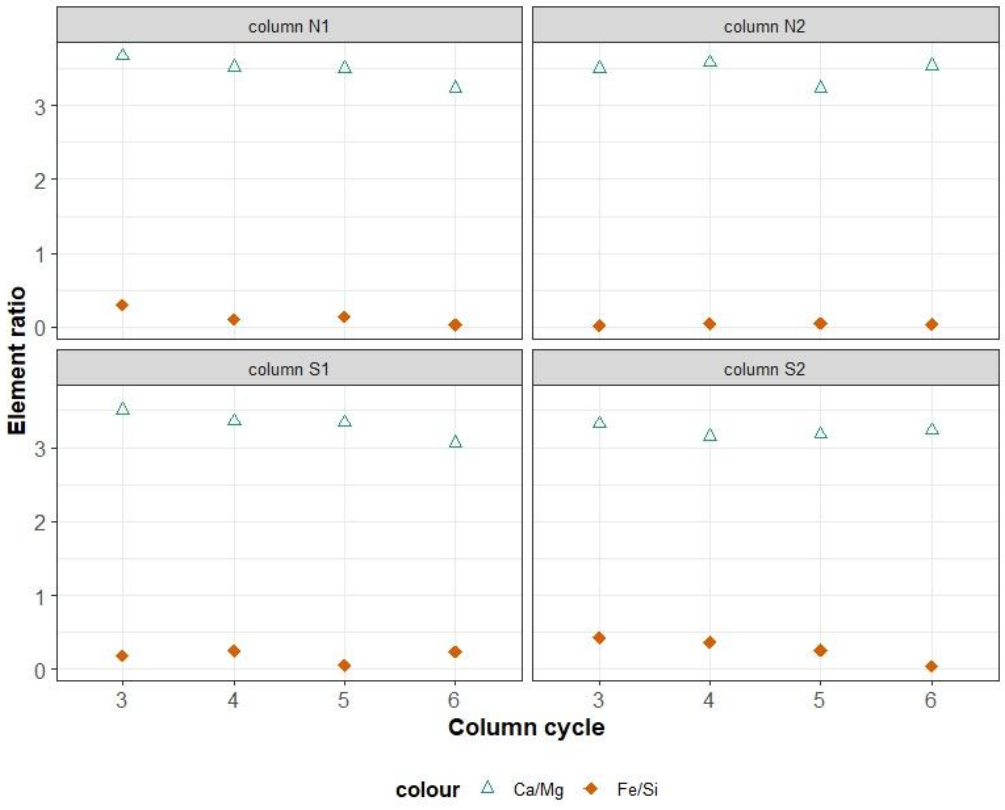

Figure C. 11. *Ratio of Ca and Mg in effluent concentrations during the first treatment cycle of biological Experiment 1 (effluent data from NAu-2 and SWy-3 treatment columns shown).*

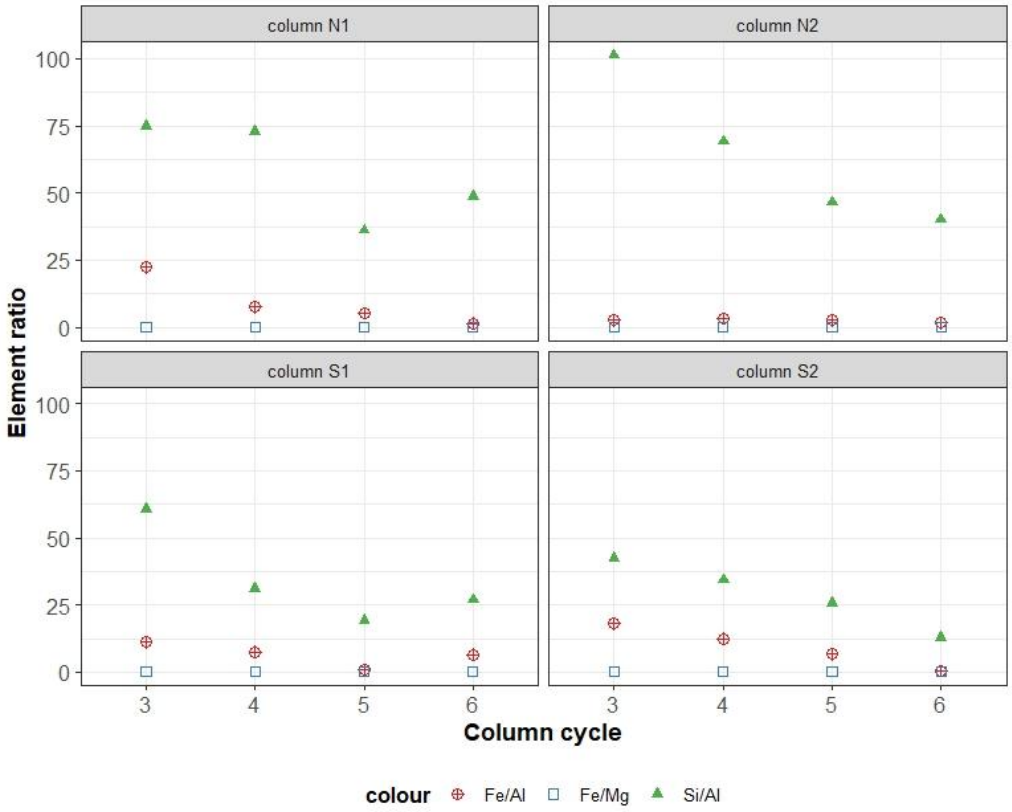

Figure C. 12. *Ratios of Fe/Al, Fe/Mg and Si/Al in effluent concentrations during the first treatment cycle of biological column Experiment 1 (effluent data from NAu-2 and SWy-3 treatment columns shown).*

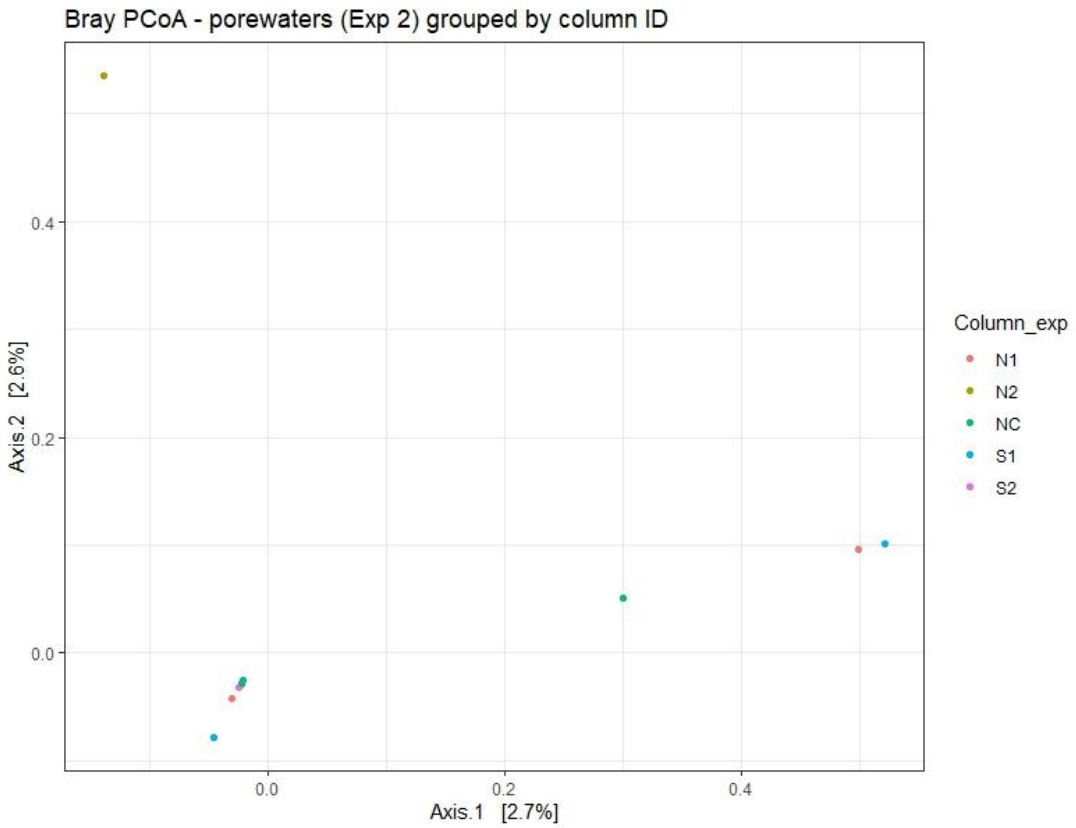

Figure C. 13. *Principal Coordinates Analysis (PCoA) ordination of 16S cDNA data for all porewaters sampled during biological column Experiment 2, grouped by column ID.*

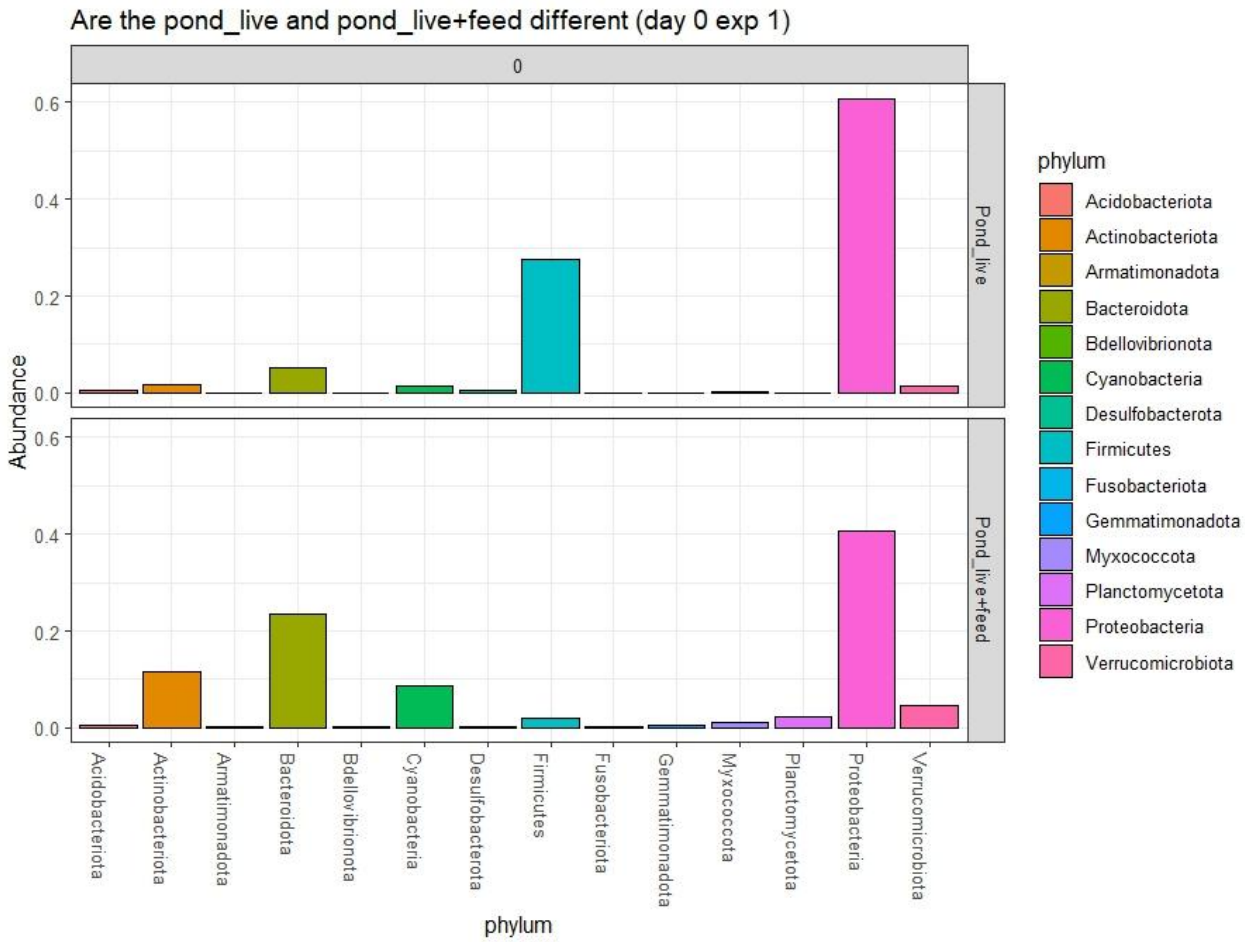

Figure C. 14. *Starting inoculants supplied to all biological treatment columns on Dy 0 of Experiment 1 (cNDA data).*

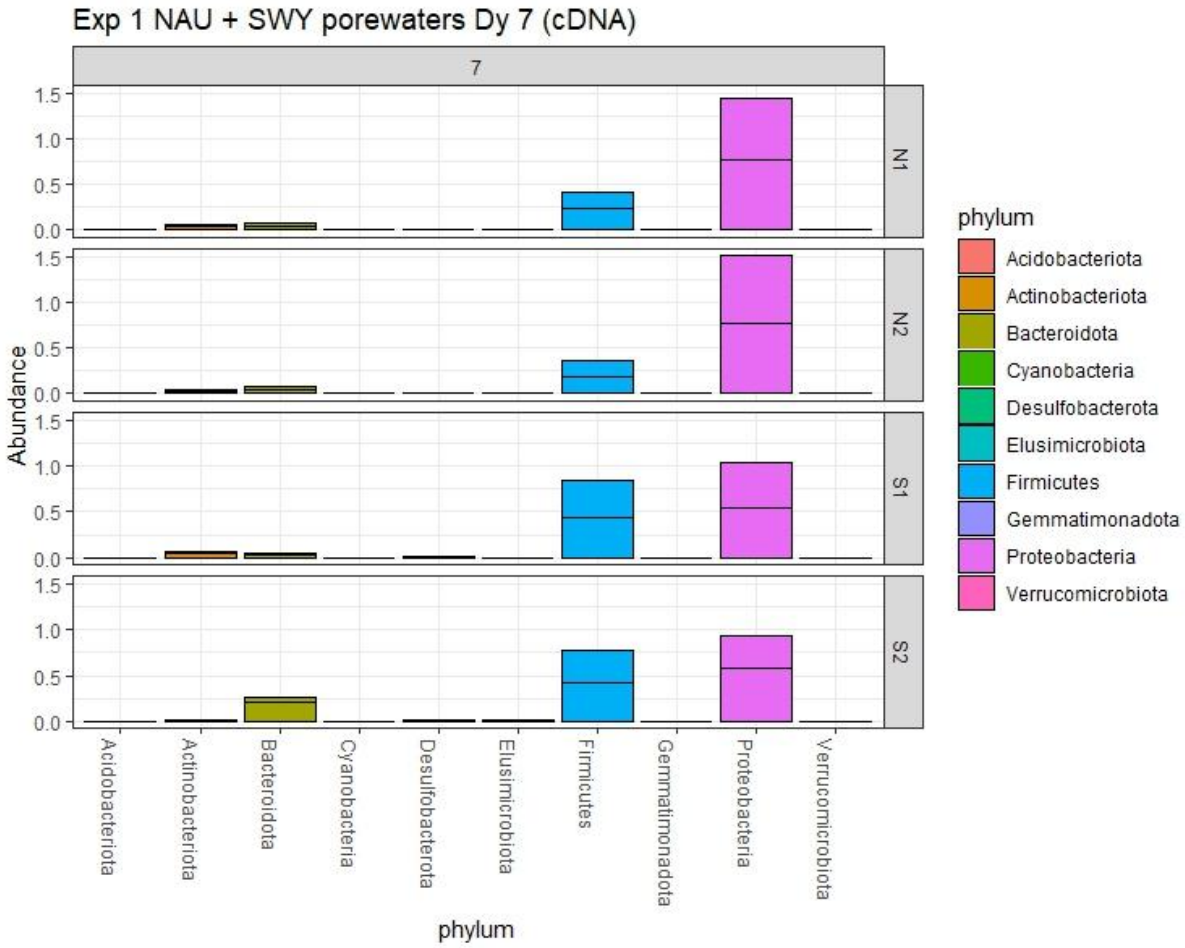

Figure C. 15. *Column porewaters from NAu-2 and SWy-3 biological columns from Experiment 1, day 7 (cNDA data). Two samples of cDNA are shown per column, leading to a (cumulative) relative abundance >1 on the y axis.*

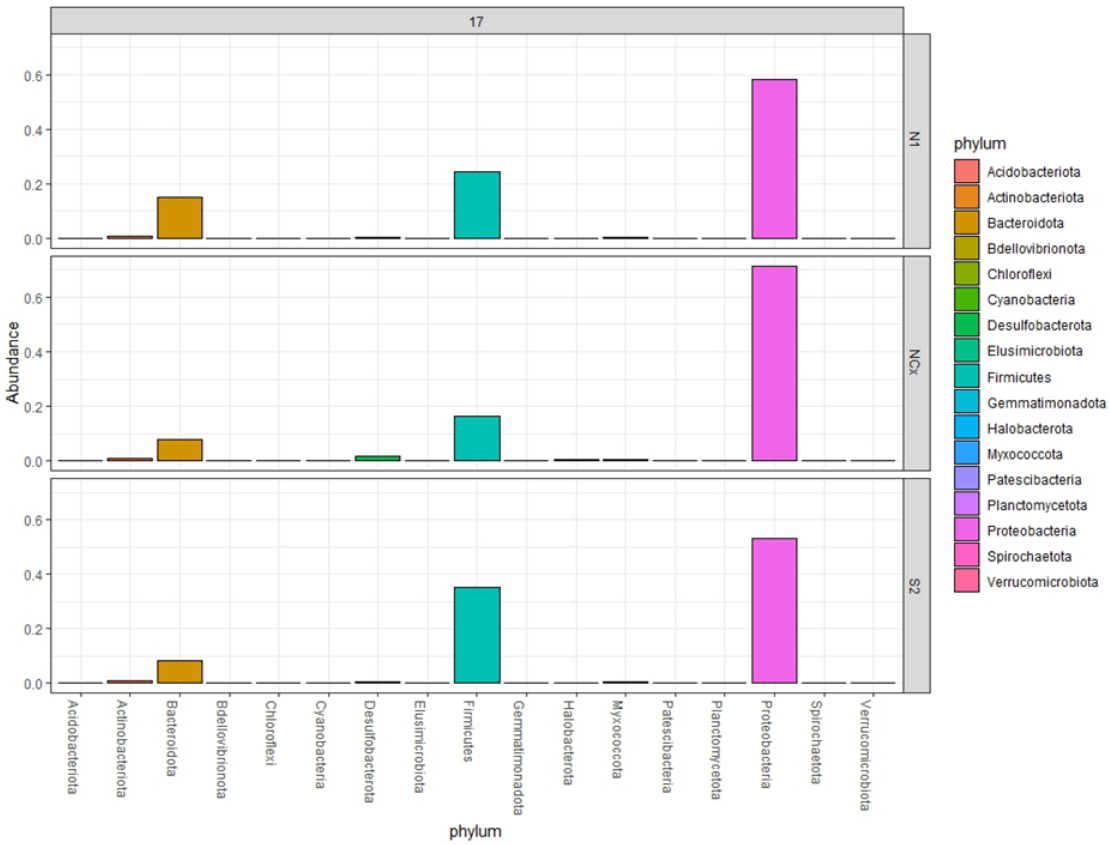

Figure C. 16. *Bar plots showing major phyla present in NAu-2 and SWy-3 biological column sediments during the mid-stages of clay activation (Fe-reduction), before the start of the first treatment cycle in Experiment 1 (cDNA data shown).*

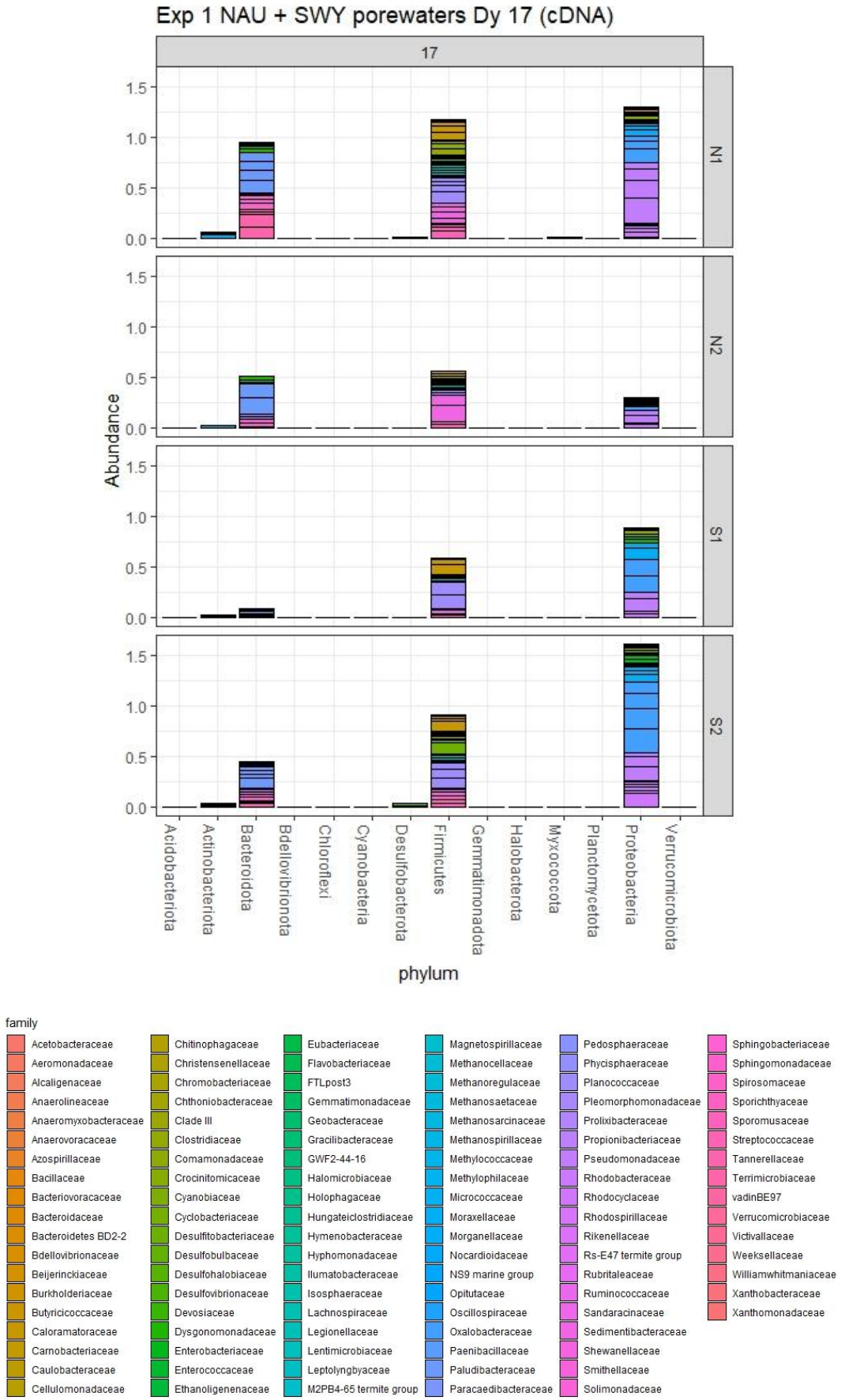

Figure C. 17. *Bar plots showing major phyla (with family subdivisions) in NAu-2 and SWy-3 biological column porewaters during the mid-stages of clay activation (Fe-reduction), before the start of the first treatment cycle in Experiment 1 (cDNA data shown).*

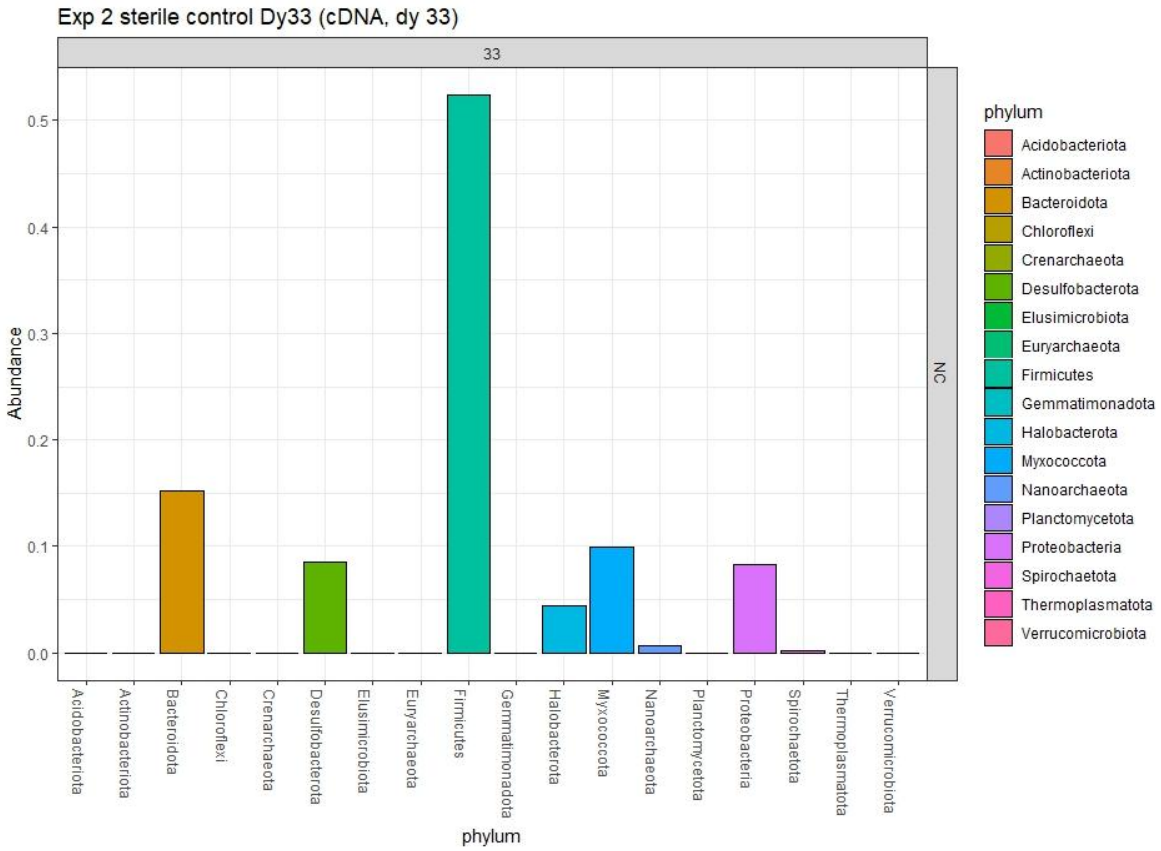

Figure C. 18. *Bar plots showing major phyla (with family subdivisions) in autoclaved NAu-2 biological control column, 33 days after inoculation with a dead pondwater and after one complete treatment cycle at the start of Experiment 2 (cDNA data shown).*

Table C. 3. *Univariate results from the multivariate generalized linear model comparing bacterial communities against biological column and experiment parameters and their pairwise interactions. Only significant ($p \leq 0.05$) results are given. Multivariate results are given in Table 5.5.*

Taxon	Clay: Sample type: Treatment cycle	Clay	Sample day	Treatment cycle	Treatment cycle: Experiment number	Sample type	Clay: Sample type: Sample day	Experiment number
Absconditabacteriales..SR1.	Dev = 0, p = 0.011							
Acetivibrio		Dev = 15.5, p = 0.029						
Acetobacterium			Dev = 38.398, p = 0.006	Dev = 60.273, p = 0.006	Dev = 0, p = 0.033			
Acetobacteroides						Dev = 20.406, p = 0.005		
Acinetobacter							Dev = 53.088, p = 0.003	Dev = 13.602, p = 0.039
ADurb.Bin063.1	Dev = 0, p = 0.001				Dev = 0, p = 0.039			

Anaerocella								Dev = 13.444, p = 0.04
Anaerofustis					Dev = 0, p = 0.028			
Anaerolineaceae				Dev = 46.079, p = 0.018				
Anaeromyxobacter						Dev = 19.863, p = 0.009		
Anaerovoracaceae				Dev = 43.756, p = 0.036				
Anaerovorax							Dev = 42.452, p = 0.039	
Arcticibacter				Dev = 55.237, p = 0.006				
Azospirillum								Dev = 23.079, p = 0.002
Bacillales							Dev = 41.073, p = 0.047	
Bacilli			Dev = 30.6, p = 0.011	Dev = 55.358, p = 0.006				
Bacteria							Dev = 55.707, p = 0.001	Dev = 17.42, p = 0.007
Bacteroidales		Dev = 16.735, p = 0.016						Dev = 14.218, p = 0.032
Bacteroides								Dev = 14.596, p = 0.028
Bacteroidetes.BD2.2				Dev = 42.724, p = 0.049				
Bacteroidetes.vadinHA17				Dev = 44.372, p = 0.033				
Bacteroidia			Dev = 27.975, p = 0.013					
Blvii28.wastewater.sludge.group				Dev = 48.528, p = 0.01				
Burkholderiales						Dev = 20.061, p = 0.008		
Candidatus.Falkowbacteria				Dev = 48.804, p = 0.01				
Citrifermentans		Dev = 15.867, p = 0.026						
Clostridia							Dev = 57.462, p = 0.001	Dev = 40.627, p = 0.001
Clostridium.sensu.stricto.10				Dev = 52.195, p = 0.006			Dev = 44.736, p = 0.018	
Clostridium.sensu.stricto.12				Dev = 43.959, p = 0.034				

Clostridium.sensu.stricto.8							Dev = 47.494, p = 0.006	
Comamonadaceae			Dev = 52.216, p = 0.003				Dev = 42.053, p = 0.039	Dev = 13.416, p = 0.041
D8A.2				Dev = 45.493, p = 0.025	Dev = 0, p = 0.034			
Dechloromonas				Dev = 49.134, p = 0.01				
Desulfitobacteriaceae				Dev = 95.611, p = 0.006			Dev = 53.133, p = 0.003	
Desulfitobacterium			Dev = 26.476, p = 0.016					
Desulfobulbus			Dev = 32.523, p = 0.008	Dev = 56.017, p = 0.006			Dev = 52.083, p = 0.003	
Desulfosporosinus								Dev = 13.786, p = 0.036
Desulfotomaculum			Dev = 28.797, p = 0.013				Dev = 42.377, p = 0.039	
Desulfovibrio			Dev = 36.153, p = 0.006	Dev = 61.239, p = 0.006				
Desulfuromonadia	Dev = 0, p = 0.001						Dev = 61.426, p = 0.001	
Enterobacterales			Dev = 35.809, p = 0.006				Dev = 49.263, p = 0.004	
Enterobacteriaceae				Dev = 50.122, p = 0.007			Dev = 46.426, p = 0.008	Dev = 17.325, p = 0.007
Firmicutes							Dev = 50.678, p = 0.003	
Flavobacterium			Dev = 32.793, p = 0.007					Dev = 13.401, p = 0.042
Fonticella							Dev = 72.531, p = 0.001	Dev = 24.603, p = 0.002
Gammaproteobacteria							Dev = 54.892, p = 0.001	
Geothrix				Dev = 58.87, p = 0.006				
Gracilibacter							Dev = 46.85, p = 0.007	
Gracilibacteraceae			Dev = 36.923, p = 0.006					
GWE2.42.42				Dev = 70.797, p = 0.006				

GWF2.44.16			Dev = 31.553, p = 0.009					Dev = 15.554, p = 0.016
Hungateiclostridiaceae	Dev = 0, p = 0.042				Dev = 0.096, p = 0.004			
Hypnocyclicus				Dev = 46.971, p = 0.014	Dev = 0, p = 0.042			
Ignavibacteriales				Dev = 43.066, p = 0.045				
KD1.131				Dev = 52.004, p = 0.006				
Lachnospiraceae							Dev = 74.273, p = 0.001	Dev = 31.652, p = 0.001
Lentimicrobium			Dev = 30.4, p = 0.011				Dev = 48.855, p = 0.004	
Lineage.IV							Dev = 46.43, p = 0.008	
M2PB4.65.termite.group				Dev = 50.598, p = 0.007				
Macellibacteroides			Dev = 31.797, p = 0.009				Dev = 65.992, p = 0.001	
Magnetospirillum			Dev = 24.729, p = 0.03	Dev = 59.034, p = 0.006			Dev = 55.171, p = 0.001	
Massilia			Dev = 45.653, p = 0.003	Dev = 45.817, p = 0.023			Dev = 46.696, p = 0.007	
Methanobacterium				Dev = 65.854, p = 0.006				
Methanocellaceae				Dev = 46.249, p = 0.017				
Methanoregula				Dev = 74.587, p = 0.006				
Methanosaeta				Dev = 77.228, p = 0.006				
Methanosarcina				Dev = 102.76, p = 0.006				
Methylobacter								Dev = 23.145, p = 0.002
Micrococcaceae			Dev = 25.031, p = 0.027	Dev = 61.803, p = 0.006				
MVP.15				Dev = 45.171, p = 0.026				
OPB41				Dev = 79.59, p = 0.006				
Oxalobacteraceae						Dev = 18.179, p = 0.018	Dev = 55.278, p = 0.001	Dev = 19.432, p = 0.006

Paenibacillus								Dev = 13.627, p = 0.039
Paludibacter			Dev = 59.208, p = 0.003					Dev = 15.68, p = 0.013
Paludibaculum				Dev = 51.615, p = 0.007				
Pedobacter							Dev = 48.89, p = 0.004	Dev = 19.35, p = 0.006
Pedosphaeraceae				Dev = 73.389, p = 0.006			Dev = 42.802, p = 0.036	
Phaselicystis				Dev = 47.075, p = 0.014				
Planococcaceae							Dev = 81.823, p = 0.001	
Propionibacteriaceae				Dev = 52.091, p = 0.006				
Pseudomonadaceae			Dev = 28.644, p = 0.013					
Pseudomonas			Dev = 46.273, p = 0.003	Dev = 74.709, p = 0.006				Dev = 17.267, p = 0.007
RBG.16.49.21				Dev = 48.189, p = 0.01				
Rhodobacteraceae							Dev = 44.67, p = 0.019	
Rhodocyclaceae			Dev = 44.523, p = 0.003	Dev = 42.447, p = 0.049			Dev = 49.162, p = 0.004	
Rhodopseudomonas				Dev = 65.772, p = 0.006				
Rice.Cluster.I	Dev = 0, p = 0.001			Dev = 75.051, p = 0.006				
Ruminiclostridium							Dev = 53.072, p = 0.003	
Sedimentibacter			Dev = 29.625, p = 0.012				Dev = 48.671, p = 0.004	Dev = 31.264, p = 0.001
Smithella	Dev = 0, p = 0.001							
Sphingobacteriales				Dev = 44.795, p = 0.03				
Sporomusa							Dev = 42.498, p = 0.039	Dev = 26.395, p = 0.002
Syntrophomonas				Dev = 75.993, p = 0.006				
Syntrophorhabdus				Dev = 51.082, p = 0.007				
Treponema				Dev = 44.104, p = 0.033				

WCHB1.32			Dev = 54.762, p = 0.003				Dev = 42.479, p = 0.039	